Supramolecular Multivalency

Zur Erlangung des akademischen Grades eines
Doktors der Naturwissenschaften
(Dr. rer. nat.)
von der Fakultät für Chemie
der Technischen Universität Dortmund
angenommene

DISSERTATION

von

Diplom-Chemikerin
Marion K. Müller
aus Mainz

Dekan:	**Prof. Dr. Heinz Rehage**
1. Gutachter:	**Prof. Dr. Herbert Waldmann**
2. Gutachter:	**Prof. Dr. Ir. Luc Brunsveld**

Tag der mündlichen Prüfung: 27. April 2009

Die vorliegende Arbeit wurde unter Anleitung von Prof. Dr. Herbert Waldmann und Prof. Dr. Ir. Luc Brunsveld am Fachbereich Chemie der Technischen Universität Dortmund und am Max-Planck-Institut für molekulare Physiologie, Dortmund in der Zeit von März 2005 bis März 2009 angefertigt.

Meinen Geschwistern Martin und Mareike
und meinen Eltern

„Ich bin immer noch verwirrt, aber auf einem höheren Niveau.“
Enrico Fermi

Table of Contents

1 Introduction

A majority of biological signaling and interactions is based on recognition of a ligand by its corresponding receptor.[1, 2] Understanding these binding events is crucial for the understanding of many diseases such as bacterial and viral infections, auto-immune diseases or metastasis of tumor cells.[3, 4] In most cases a single ligand-receptor interaction is weak and the ligand dissociates from the receptor rapidly. Binding strengths are increased by simultaneous multiple ligand-receptor interactions.

1.1 The Phenomenon of Multivalency

1.1.1 Multivalency in Nature

Multivalency or polyvalency denominates the phenomenon of simultaneous binding of multiple ligands on one entity to multiple receptors on another entity. The valency of one unit thereby is defined as its number of ligands of the same kind. Figure 1 illustrates bivalent or polyvalent binding compared to a monovalent interaction. Multivalent binding leads to enhanced binding strength, stabilization of the interaction and enhancement of receptor selectivity, amongst others.[1]

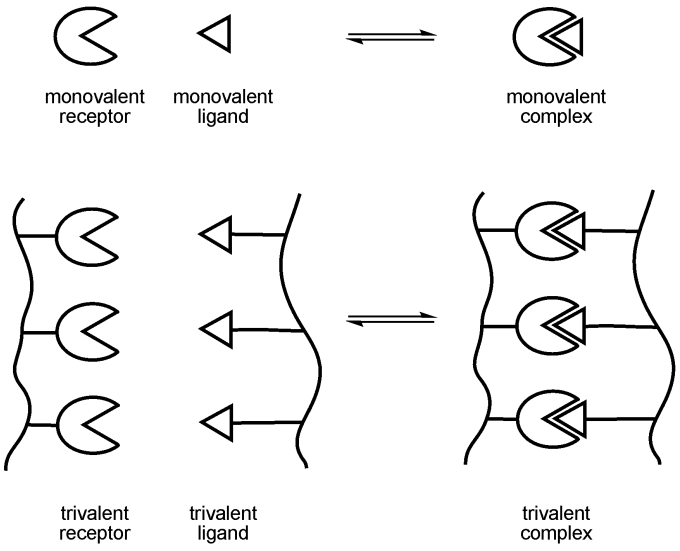

Figure 1. Illustration of multivalent (trivalent) interaction and monovalent binding.[1]

Multivalent scaffolds in nature range from molecules of low valency, like antigens, to those of high valency supramolecular assemblies such as receptors in cell membranes. Examples of synthetic scaffolds with different valencies are discussed in Chapter 1.2. Nature takes advantage of multivalency to enhance numerous originally weak interactions, mainly carbohydrate-carbohydrate, carbohydrate-protein and protein-protein interactions.[1] This includes, amongst others, key-steps in cell-cell, cell-bacterium, cell-virus or antibody-antigen recognition (Figure 2). One prominent example is the infection of cells with the influenza virus, mediated through the multivalent interaction of the hemagglutinin-receptors on the virus with the sialic acid motif on glycoprotein receptors of the host cell.[5] Furthermore, *E. coli* attach *via* multivalent binding of their P fimbrae to a disaccharide motif on lectins of endothelial urethral cells.[6] Neutrophil tethering on endothelial cells or antibody-antigen recognition by macrophages are two examples in which multivalent recognition plays an essential role in human immune response.[7] Due to its key role in diverse fundamental interactions, understanding and strengthening or inhibiting multivalent interactions provides promising targets for interference with and control over essential biological phenomena.

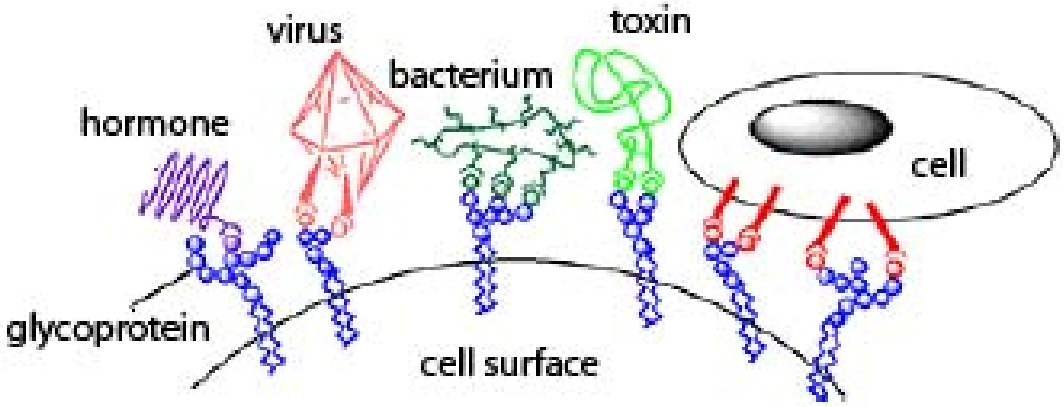

Figure 2. Examples of multivalent interactions in nature.[8]

1.1.2 Cooperativity and Multivalent Binding

Multivalent binding can result in binding affinities that are stronger than the equivalent monovalent interaction by magnitudes. Kinetic calculations show

that the energy gained by formation of the multivalent binding complex can be higher than the sum of the single energetic contributions of the ligand-receptor binding.[9] The binding strength increases approximately exponentially with the number of possible multivalent binding events.[1] Enhanced binding strength, compared to the corresponding monovalent interaction, arises from thermodynamic advantages and ligand stabilization due to different mechanisms of ligand binding in multivalent interactions.[10]

Regarding the nature of the receptor and its scaffold, four main multivalent binding mechanisms can be described, summarized in Figure 3.

A) Simultaneous binding of a scaffold with multiple ligands to receptors, that themselves are oligomeric, can result in chelation. In case of chelation, merely the first receptor-ligand contact needs to afford the energy for translational entropy whereas every subsequent binding interaction can proceed without additional penalties.[9] Thus this effect favors the bound ligand-receptor complex.

B) Some receptors have more than one binding pocket which results in so called subsite binding possibilities. These subsites can either bind to the same recognition element as the main site or to a different one. Binding energy of multivalent interactions can be gained by additional binding to subsites[11] of the receptor.

C) The probably most significant feature of multivalent binding is steric stabilization of the ligand-receptor-complex. For example, multivalent interaction can result in clustering of glycoproteins, anchored in the membrane, which in result stabilize their assembly through additional interactions.[12] Multivalent complexes enable steric stabilization and thus adjust the ligand-receptor-binding equilibrium to the bound state.

D) Furthermore, multivalent binding increases the probability of statistical rebinding. The presence of a large amount of ligands in proximity of the receptor leads to a high probability of subsequent rebinding to the next ligand once one interaction dispersed.

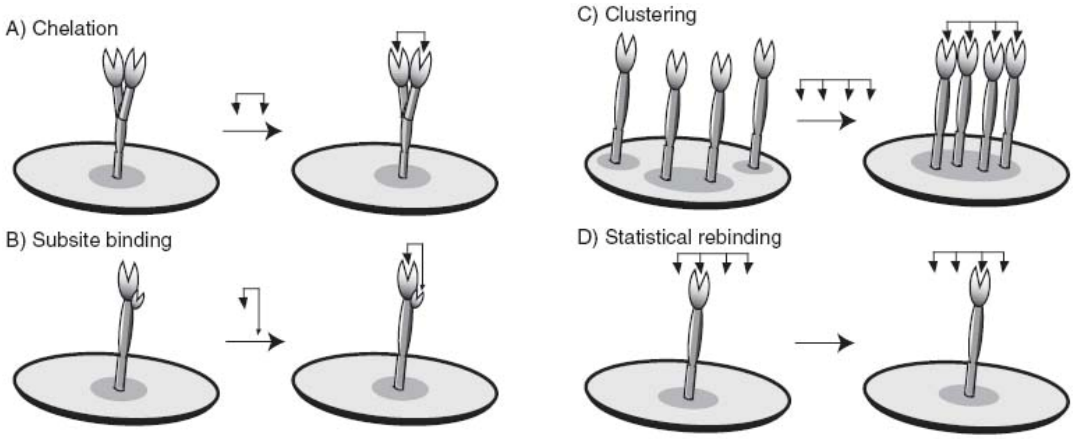

Figure 3. Multivalent mechanisms to enhance ligand-receptor binding strength.[10]

Steric stabilization of the ligand-receptor complex typically comes with inter- and intramolecular cooperative effects.[13] After the first intramolecular binding to a multivalent entity occurred, subsequent binding of more ligands of the same scaffold leads to a multivalent complex. On the other hand, binding of a second scaffold to the same multivalent entity leads to the formation of an intermolecular aggregate (Figure 4). Ligand-receptor interactions are depending on equilibrium constants of their binding. After the initial binding of one ligand on a multivalent scaffold to one receptor takes place, subsequent binding events are not concentration dependent anymore. Figure 5 illustrates the increase in effective ligand concentration around a multivalent entity after the first binding to a scaffold with multivalent ligands. The overall concentration of ligands in solution, though, remains constant. Depending on the system under study, the local proximity induced by the first binding event can either lead to positive, none or negative influence on subsequent binding events. For example, steric hindrance, due to inflexible scaffolds and insufficient possibilities for adjustment of ligand-receptor binding, typically leads to negative contributions. In that case the negative binding effect weakens the overall strength of the multivalent interaction. Furthermore, cooperativity effects are to be taken into account.[14] Ungaro *et al.* describe cooperativity as the “influence of the binding of one ligand on the receptor’s affinity toward further binding.” Cooperativity effects are highly dependent on the type of interaction and the character of the interaction partners. Although multivalency

is often associated with cooperativity, this effect is extremely difficult to determine in multivalent systems. The complexity of the determination of cooperativity effects in multivalent systems is mainly because the models for calculation are limited to monovalent ligands. [9, 13]

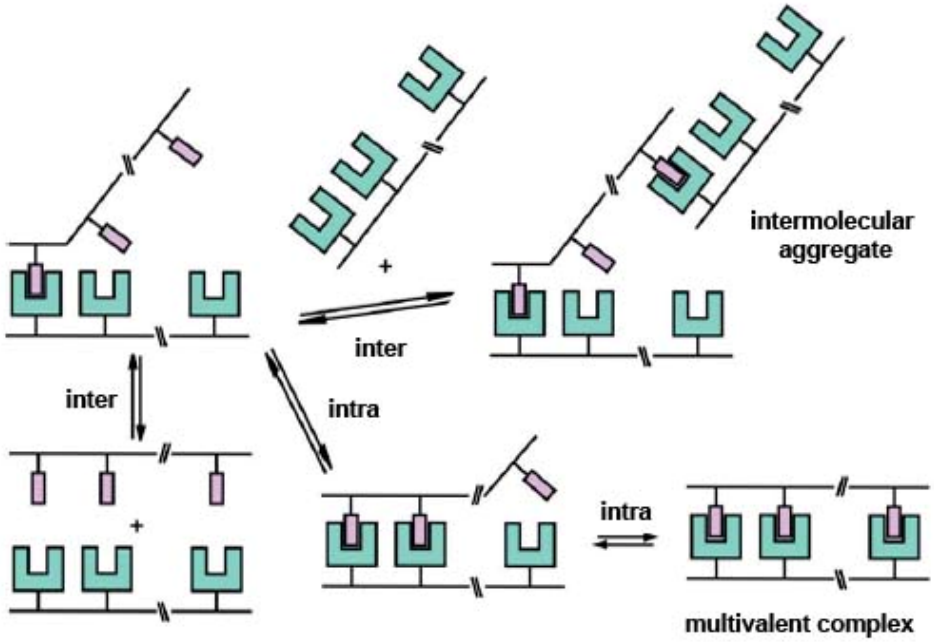

Figure 4. Cartoon illustrating inter- and intramolecular binding, which lead to a multivalent complex or an intermolecular aggregate.[15]

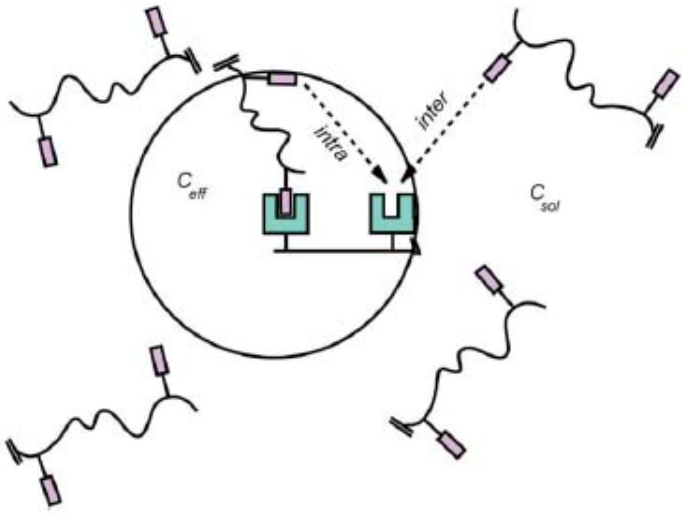

Figure 5. Cartoon illustrating the increase in the effective ligand concentration (c_{eff}) in proximity of the multivalent surface after the first binding event. The overall concentration of ligands in solution (c_{sol}) remains constant.[15]

1.2 Synthetic Scaffolds with Multivalent Focus

1.2.1 Multivalent compounds

The significant enhancement of ligand-receptor binding affinity *via* multivalent interactions has put the design and synthesis of synthetic multivalent compounds into research focus. A large variety of multivalent scaffolds has been examined with regard to shape, backbone flexibility, linker length and valency. Scaffold classes based on structures such as aromatic compounds, peptides, dendrimers, polymers or solid supports have been exploited as multivalent scaffolds.[16, 17] However, the mechanisms with which the multivalent compounds bind remain essentially unknown.[18]

Biological interactions targeted with synthetic multivalent compounds are numerous. Examples span from lectin and agglutin inhibition to surface recognition of proteins. To provide a flavor of the different constructs and their features with respect to multivalency and possible binding properties, some examples are described briefly in this chapter (Figure 6). For a complete overview on the design of multivalent compounds, compound classes employed for multivalent tasks and multivalent systems targeted with synthetic multivalent substances, the reader is referred to the literature.[1, 17, 19-23]

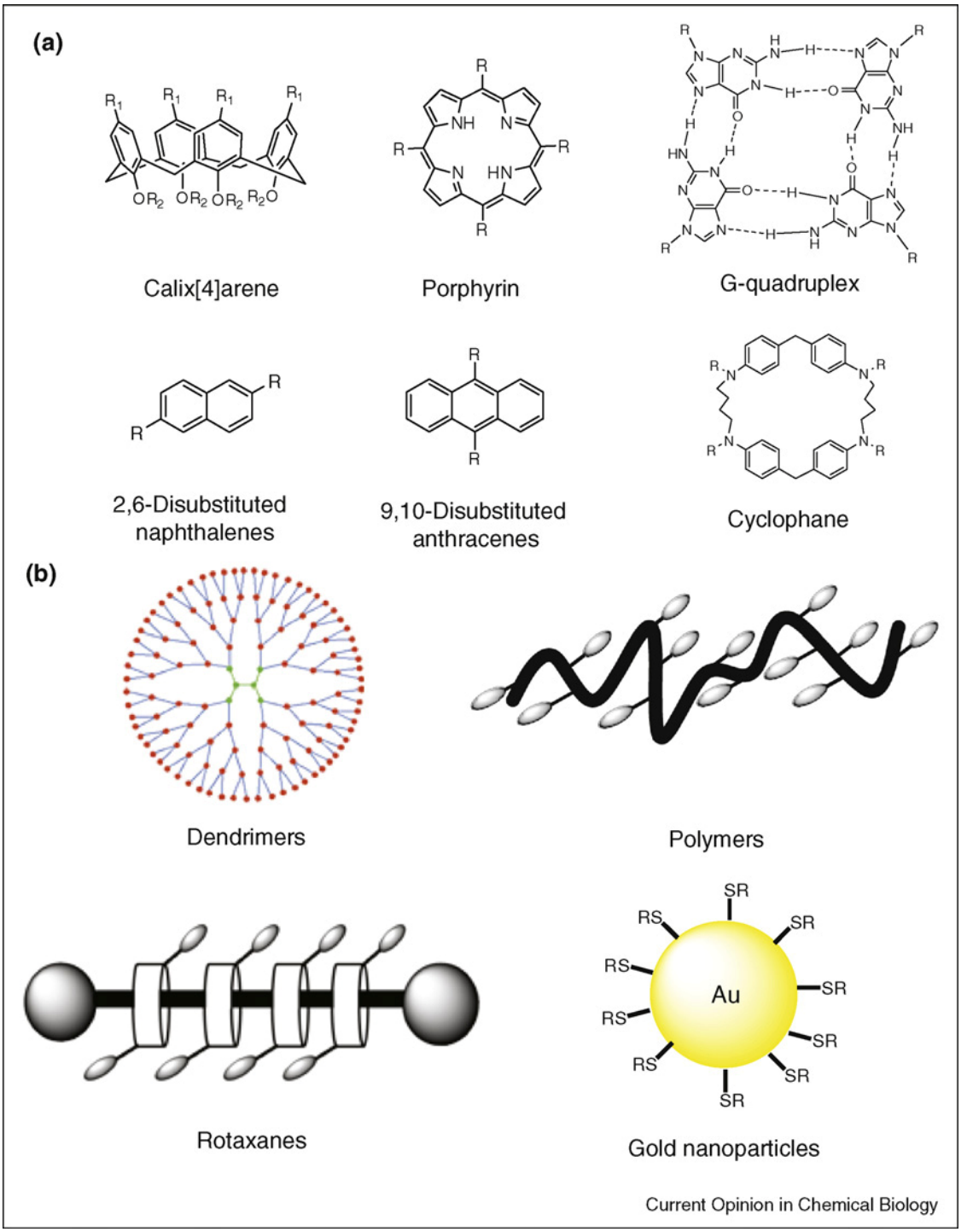

Figure 6. Examples of multivalent scaffolds.[19] a) low-valency and b) high-valency scaffolds.

Scaffolds of lower valency ranging up to ten ligands have been reported numerously. In order to provide an idea of the scope of low valency scaffolds, examples of calix[*n*]arenes are discussed here.[15, 24, 25] The compound class of the calix[*n*]arenes, both charged and neutral, is based on aromatic scaffolds. Calix[4]arenes have been well studied regarding their backbone flexibility and

binding properties to diverse multivalent surfaces.[15] They can be present in a variety of distinct conformations (Figure 7) and therefore are considered to be rather flexible compared to other small valency scaffolds.

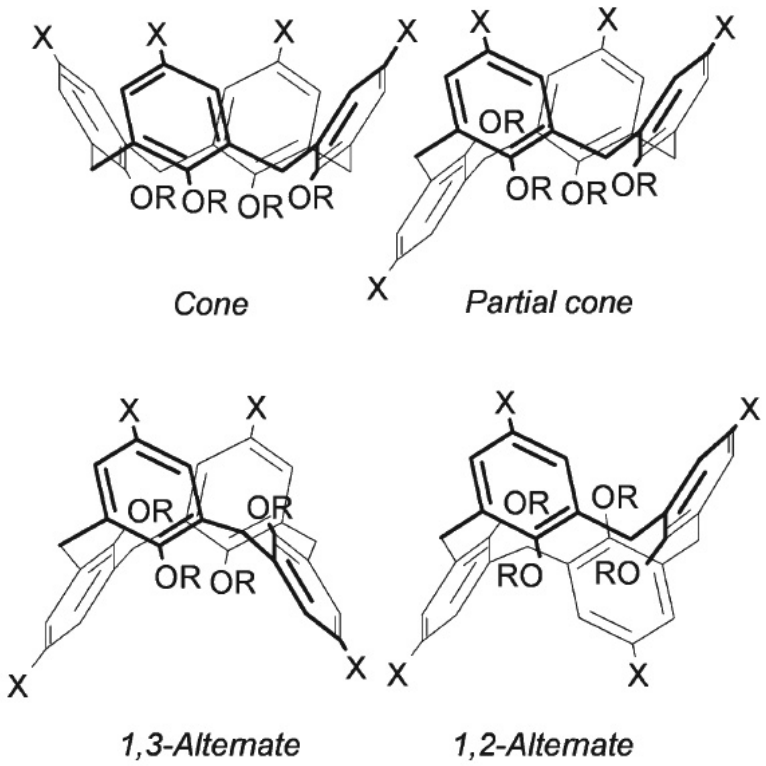

Figure 7. The four conformations of calix[4]arenes. Ligands for multivalent interactions can be attached in R- and X-position.[15]

Calix[4]arenes carrying glycosidic ligands have been well studied with regard to their multivalent interaction with bacteria, lectins and toxins.[15] Studies regarding the influence of shape and flexibility of the calixarene scaffold in carbohydrate-protein interaction has been performed by Sgarlata and coworkers.[26] A cone-blocked tetraminocalix[4]arene and a conformational mobile octaminocalix[8]arene (Figure 8) were decorated with multiple copies of *N*-acetyl-D-glucosamin and their multivalent properties were studied employing an haemagglutination inhibition assay with wheat germ agglutinin. All compounds tested showed much lower minimum inhibitory concentrations than *N*-acetyl-D-glucosamin. Interestingly all multivalent compounds based on the cone-blocked calix[4]arene turned out to have a higher inhibitory potency than the conformationally mobile calix[8]arene. Furthermore tetravalent

calix[4]arene scaffolds had the highest potency even when compared to the corresponding octavalent calix[4]arenes. Increase in valency or enhanced mobility of the calixarene backbone decreased the inhibitory abilities of the compounds in this haemagglutination assay. Apparently, the flexibility of the mobile octaminocalix[8]arene does not enable induced fit of the ligands to the glycoprotein but seems to result in steric constraints that decrease the overall binding potency. Furthermore, the decrease in binding potency obtained by increasing the number of ligands per calix[4]arenes scaffold from four to eight might result in steric crowding of the ligands on the scaffold. Crowding most probably also leads to steric hindrance and causes the decrease in binding potency.

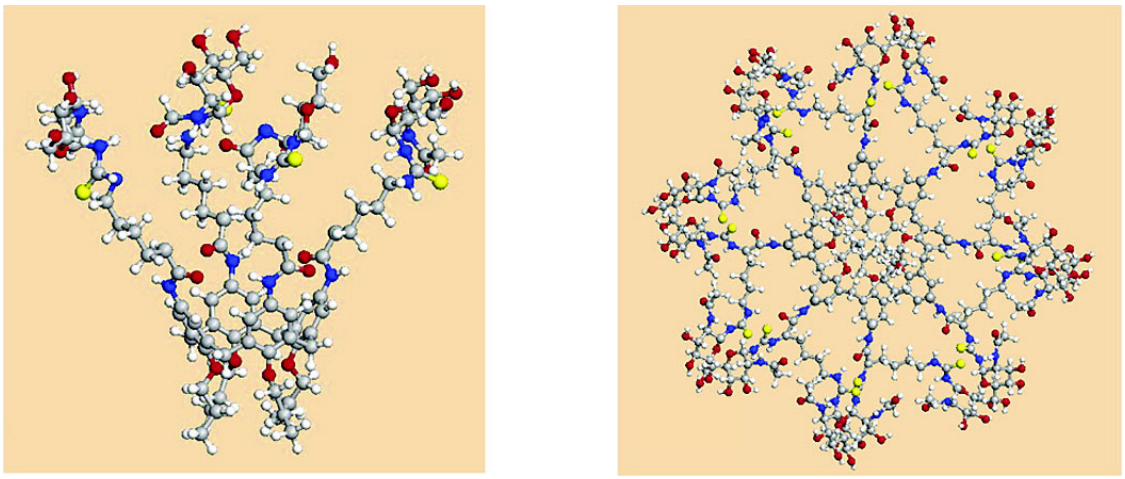

Figure 8. Examples of different calix[4]arenes provided with gallactose, glucose or lactose.[26]

Other low-valent compound classes such as porphyrins, cyclophanes, resorcinarenes and a large variety of small glycomimetics have been examined as multivalent scaffolds with decorated glycosides regarding their interaction to glycoside-binding proteins.[27] A general tendency in all studies is that all multivalent compounds feature much higher activities than their monovalent control compounds.[28] In terms of saccharide binding to carbohydrate binding proteins, the effect of enhanced multivalent binding is referred to as the “cluster glycoside effect”.[22, 27, 29] On the other hand, the magnitude of improvement achieved with the multivalent interaction was highly dependent on the assay reported. Development of new, more efficient

multivalent low valency scaffolds mainly focuses on the optimization of backbone flexibility and linker length to achieve 'induced fit' to the multivalent receptor.[8, 25, 30, 31] However, low valency scaffolds are highly limited in the number of multivalent ligands that can be attached to them and in terms of backbone flexibility.

To obtain compounds of higher valency, various platforms have been developed such as linear polymers, dendrimers, nano particles like beads or gold surfaces and self-assembling monolayers (SAMs) (Figure 6).[19, 20, 23] In order to provide an idea of the abilities and perspectives of high valency scaffolds, one example of dendrimers is discussed at this point. Dendrimers are macromolecular branched compounds and have been extensively studied as multivalent framework for different applications by various groups. [32-37]
In the group of Cloninger, dendrimers provided with mannose ligands of generation 1 to 6 were synthesized and systematically evaluated concerning their ability to inhibit the lectin concanavalin A (con A).[38, 39] The valencies of the dendrimers reached from low valency of 8 ligands per scaffold in the generation 1 dendrimer up to valencies over 200 mannose ligands per scaffold in the generation 6 dendrimer. Compared to methyl mannose as control substance generation 1 (8 mannose ligands) and generation 2 (16 mannose ligands) dendrimers did not show any increase in activity toward con A. Binding of generation 3 dendrimers was enhanced by the factor of two whereas biding of generation 4-6 dendrimers was increased by two orders of magnitude.[40] These results indicate that generation 1 and 2 dendrimers bind to lectins in a monovalent fashion. As could be expected, their scaffolds are not large enough to enable spanning of the multiple binding sites of con A. The authors suggest that the small increase in binding of generation 3 dendrimers probably results from glycoside clustering. Higher generation dendrimers, however, are able to span multiple binding sites on one lectin. Apparently, the multivalent binding leads to formation of dendrimer-lectin clusters and thus to a strong increase in binding. The different binding motifs and their effects on binding strength are illustrated in Figure 9. Further studies on dendrimer generations 4 to 6 showed that the activity per sugar ligand is dependent on

the area each sugar has on the surface of the dendrimer scaffold.[41] Below a value of approximately 800 $Å^2$ the activity per mannose ligand decreased significantly compared to the same scaffold with less mannose ligands. These studies emphasize the need for high valency compounds with an optimized spatial distribution of ligands that does not result in steric crowding of the binding motifs on the scaffold.

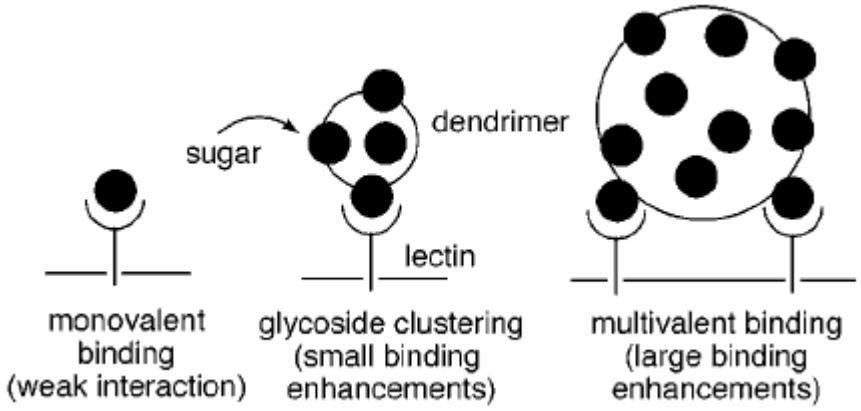

Figure 9. The different binding motifs suggested for generation 1 to 6 dendrimers. Small binding enhancements are achieved of generation 3 dendrimers presumably due to glycoside clustering. Generation 4 to 6 dendrimers apparently bind in a multivalent manner.

A wide range of polymer backbones has been examined as multivalent scaffolds with similar biological targets and comparable results to those of the dendrimers shown above.[10, 27, 42-44] In general, compared to compounds with lower valency, high valency scaffolds exhibit highly efficient inhibition and competition due to their ability to bind in different multivalent manners (Figure 3 and Figure 4).[28] However, high multivalent compounds with polymer-like backbones possess limited properties to adapt their molecular structure to the requirements of their target. Thus, valency corrected binding does not necessarily increase with higher valency as was explained above for the dendrimer example. Regardless of the compound class used as covalent scaffold for multivalent tasks, the issue of backbone flexibility and optimal linker length, to achieve optimal ‘induced fit’ to the multivalent system targeted, is still essentially unsolved.

1.3 Self-Assembling Supramolecular Architectures

Compounds that might be able to overcome the current limitations of synthetic multivalent systems, such as insufficient flexibility, are self assembling supramolecules. Self-assembling supramolecular architectures are systems that occur widely in nature. Examples are the bilayer membranes of cells, DNA or the tobacco mosaic virus. Synthetic self-assembling supramolecular polymers are of great current interest in chemistry, materials science and in biology.[45-48] Reported self-assembled systems range from capsules to linear polymers to nanostructures such as micelles, vesicles and nanotubes. Advantages of self assembling supramolecular architectures are plentiful. Self-assembling supramolecules possess features such as diverse topology, composition, and assembly dynamics. The supramolecules are formed from the monomers through specific non-covalent interactions for instance hydrogen bonding, π-π stacking or ion pairing. These architectures possess well defined shapes and highly organized structures with distinct molecular surfaces. Self-assembled materials are close to the thermodynamic minimum and acquire high thermodynamic and kinetic stability. The reversibility of their non-covalent binding enables self-repairing of structural defects. Furthermore most supramolecular assemblies are responsive to their environment. Variation of the pH, solvent and temperature enables external control to some extent.

The field of self assembling supramolecular architectures is vast. In this chapter examples of self assembling supramolecular architectures are given to provide an idea of the current research focus. Examples mentioned here have been used for biology related purposes and concern supramolecular assembly in aqueous solution. For more detailed information on the examples or reviews on supramolecular polymers the reader is referred to the literature.[21, 49-55]

1.3.1 Self assembling Supramolecules with Multivalent Focus

In order to overcome existing problems with insufficient flexibility of multivalent polymeric scaffolds, a limited set of self-assembling architectures has been evaluated concerning their potential to enhance multivalent interactions. Self

assembling architectures built up macromolecular structures that are able to respond to external factors and, when provided with the corresponding ligands, can interact with biological material. The usage of dynamic systems as multivalent scaffolds is promising, because highly flexible scaffolds have the potential to feature fewer steric constraints in ligand-receptor binding.

Only few groups developed approaches to employ self-assembling systems as multivalent scaffolds taking advantage of dynamic supramolecular nanostructures. One example of self-assembling supramolecular, multivalent architectures are the pseudopolyrotaxanes[56] (Figure 6), engaged as multivalent interaction partner of galectin-1 by the group of Stoddart.[57] The synthesis of these supramolecules is based on a self assembly protocol leading to cyclodextrines threaded on a polyviologen string (Figure 10). The cyclodextrines decorated with lactosides are able to spin around the chain and can move forth and backwards on the polymer string. As illustrated in Figure 10, these lactoside pseudorotaxanes are big and flexible enough to bind galectin-1 in a multivalent fashion and span its binding sites.[57] Rotation of the lactoside ligands furthermore enables intermolecular binding to several galectins.

In principle, the ability to rotate and move along the polymer axis should allow orientation of the ligand in the most favorable manner for maximal binding interaction with the receptors. Nevertheless, subsequent studies revealed that these multivalent systems based on pseudopolyrotaxanes seemed to bind in a negatively cooperative fashion presumably due to steric hindrance and electrostatic repulsion.[58, 59] Additionally, another fact should be taken into account at this point: although the pseudopolyrotaxanes display a highly flexible multivalent polymer, the order of the cyclodextrins on the string is set after the assembly. Threading on the chain locks the sorting of the cyclodextrins and does not allow later rearrangement.

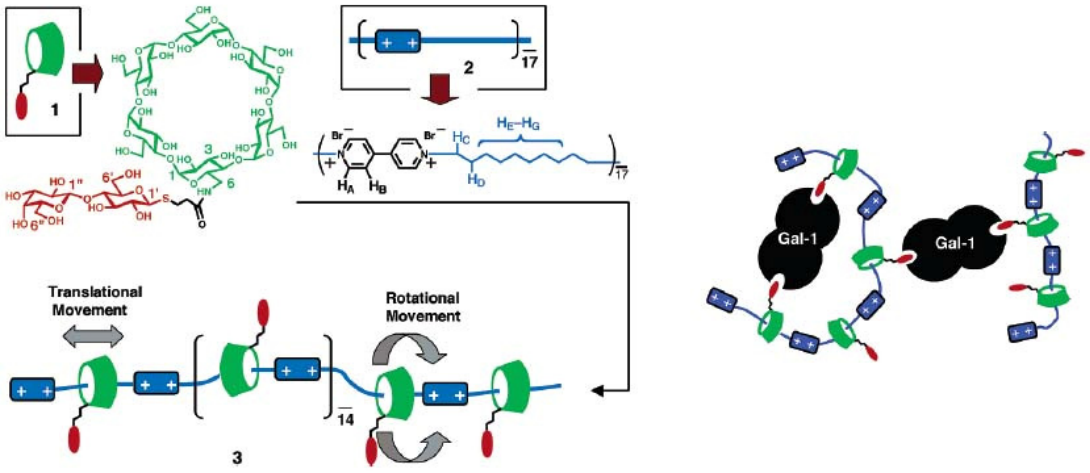

Figure 10. Self-assembly of lactoside cyclodextrines and a polyviologen string resulting polyrotaxanes. Polyrotaxanes allow rotation and flexible movement of cyclodextrins along the string.[57]

Another important class of self-assembling supramolecular architectures are nanomaterials such as micelles and vesicles. Stupp and coworkers significantly contributed to the field of self-assembling nanostructures and the application of nanomaterials in biological systems.[60, 61]. The group designed peptide amphiphiles, which form *via* hydrophobic collapse and promote *in vivo* growth of blood vessels.[62] Self-assembled positively charged peptide nanofibers bind negatively charged heparin chains. Interaction of the heparin-amphiphile complex with FGF-2 and FGF receptors results in stimulation of growth of blood vessels (Figure 11).

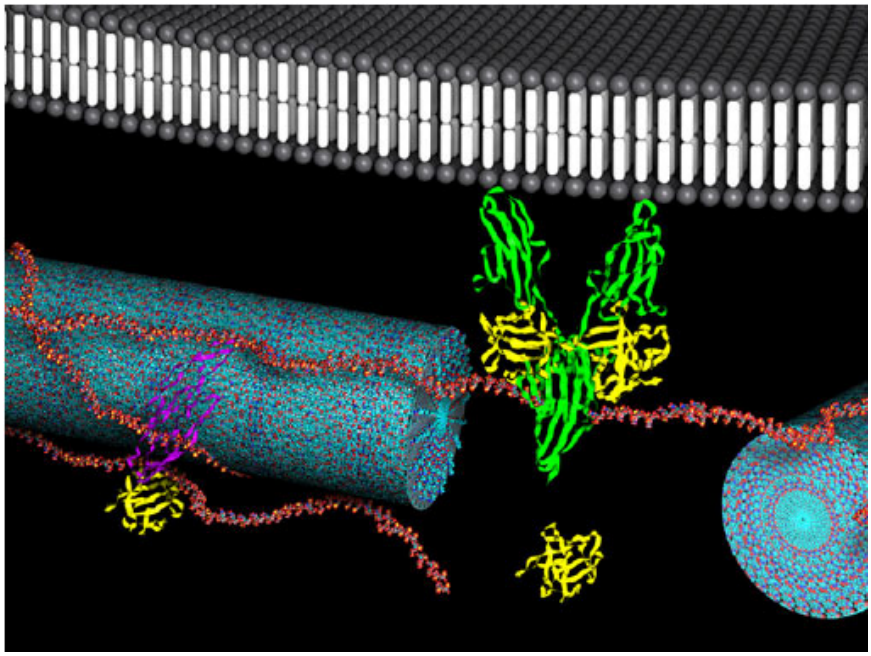

Figure 11. Self-assembled positively charged peptide nanofibers (blue) bind negatively charged heparin chains (red). Subsequent interaction of that complex to FGF-2 (yellow) and FGF (green) receptors results in stimulation of growth of blood vessels.[62]

Lee and coworkers synthesized aromatic amphiphiles decorated with mono saccharides for multivalent interaction.[63, 64] In aqueous solution the supramolecules self-assemble into carbohydrate coated nanofibers and transform into micellular structures upon addition of the guest molecule Nile Red (Figure 12). Studies on lectin binding showed that both objects, fibers and micelles, function as multivalent inhibitors. Interestingly, in motility studies on *E. coli* Lee and coworkers found that motility inhibition with the spherical micelles was significantly lower than with the nanofibers. Strength and efficiency of multivalent interactions are dependent on the shape and the surface properties of the interaction system. Apparently, multivalent interactions increase with the potential of the multivalent scaffold to adapt to the receptors surface.

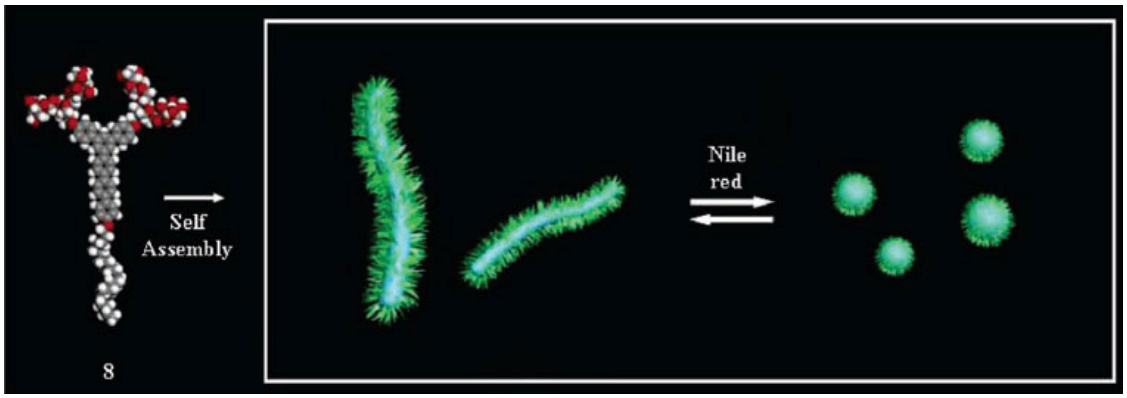

Figure 12. Self-assembly of carbohydrate coated aromatic amphiphilies. The supramolecules self-assemble into carbohydrate coated nanofibers and transform into micellular structures upon addition of the guest molecule Nile Red. The aromatic amphiphilies decorated with mono saccharides exhibit strong binding to FimH receptors of *E.coli*.[63]

The above sketched fields and challenges emphasize the need for new, highly flexible multivalent architectures, which are able to adapt themselves to the multivalent surface in the most ideal mode. In a very recent review on the topic of supramolecular multivalent scaffolds Martos *et al.*[19] concluded: "…multivalency has demonstrated that precise design and strong individual interactions are not necessary if recognition to a protein surface is to be achieved. The sum of weaker contacts in a flexible context around a central scaffold can be much more efficient and even selective. Future directions should include the use of supramolecular (reversible) contacts around a platform that might allow the system to optimize the choice of ligands, linkers and geometries to better complement the binding sites of the protein, …" Without question, there is a need for new supramolecular synthetic systems, with diverse topology, composition, and assembly dynamics which serve as multivalent scaffolds.

2 Aim of the Thesis

The question, how to design and synthesize a macromolecule that optimally mimics and matches the arrangement of its multiple targets in the membrane and adapts itself to the dynamics of these targets, is essentially still unsolved. Synthetic supramolecular systems are self-assembling and dynamic scaffolds that could provide an entry to target the natural supramolecular polyvalent assemblies more effectively.

There is a need for new, highly flexible multivalent scaffolds with diverse topology and mechanisms to flexibly control polymer composition and dynamics. Self-assembling supramolecular polymers were envisaged as a new compound class for multivalent tasks. The design, synthesis, and biological evaluation of a biocompatible, auto-fluorescent, polyvalent supramolecular polymer was planned.

We meant to modify the reported synthesis of self-assembling discotics to enable subsequent attachment of ligands in the last step of the synthesis. To study the applicability of self-assembling polymers in terms of multivalent interactions, easily accessible ligands with well studied biological interactions were thought to be attached to the discotics. For example, the discotic monomers were foreseen to be functionalized with glycosidic residues to induce multivalent binding to lectins and agglutins. Furthermore, mixtures of functionalized and unfunctionalized discotics should be studied to examine the use of unfunctionalized discotic monomers as spacer between the functional groups. Mixtures of different functionalized discotics were foreseen to provide easy access to heterovalent assemblies. Synthesis of heterovalent compounds is highly challenging and controlled ligand ratios are not accessible so far.

Furthermore, the applicability of the discotic polymers as modulator for protein assembly and interactions was to be evaluated. Therefore discotics were planned to be decorated with ligands that enable subsequent protein ligation. Discotic monomers linked to proteins were envisaged to induce the assembly of these proteins in aqueous solution through self assembly of the discotic monomers to their supramolecular polymer. The unfunctionalized discotic monomer was foreseen to serve as modulator to control the space between

the discotic monomers, ligated to a protein, in a concentration dependent manner. Self assembling supramolecules are a compound class with highly promising features concerning multivalent interactions and protein modulation.

3 Results and Discussion

3.1 Synthesis of Discotic Scaffolds

Biological systems that undergo polyvalent recognition interactions typically are dynamic supramolecular assemblies, with the recognition partners in a self-reorganizing environment such as the cell-membrane. Induction or inhibition of these types of interactions provides entry to targeting diseases and infections related to them.[1, 2] The question how to design and synthesize a macromolecule that optimally mimics and matches the arrangement of its targets in the membrane and adapts itself to the dynamics of these targets is essentially unsolved.[63-67] Critical issues are, amongst others, the difficulty to control exact ligand placing, backbone folding of synthetic polymers and the generation of systems that actively adjust their ligand positioning in response to the dynamic rearrangement of the biological interaction partners. Synthetic supramolecular systems[51, 52] are self-assembling and dynamic scaffolds that could enable targeting the natural supramolecular polyvalent assemblies more effectively.

3.1.1 Design of Supramolecules for Biological Tasks

In order to design a new class of dynamic, supramolecular polymers for multivalent interaction and control over the assembly of biomacromolecules, the synthesis of a self-assembling supramolecular scaffold was planned. The supramolecular system ideally features properties such as self-assembly into polymer structures in water, and a strong fluorescence signal of the assemblies, useful for detection in biological studies.

So called ‘discotics’ feature these advantages. Discotics build up highly ordered, unique architectures in aqueous solution, even at very dilute concentrations.[68] The large aromatic cores of the discotic monomers induce self assembly into columnar structures up to the size of biomacromolecules.

Additionally, the discotic scaffold exhibits a strong fluorescence signal owing to its aromatic core.

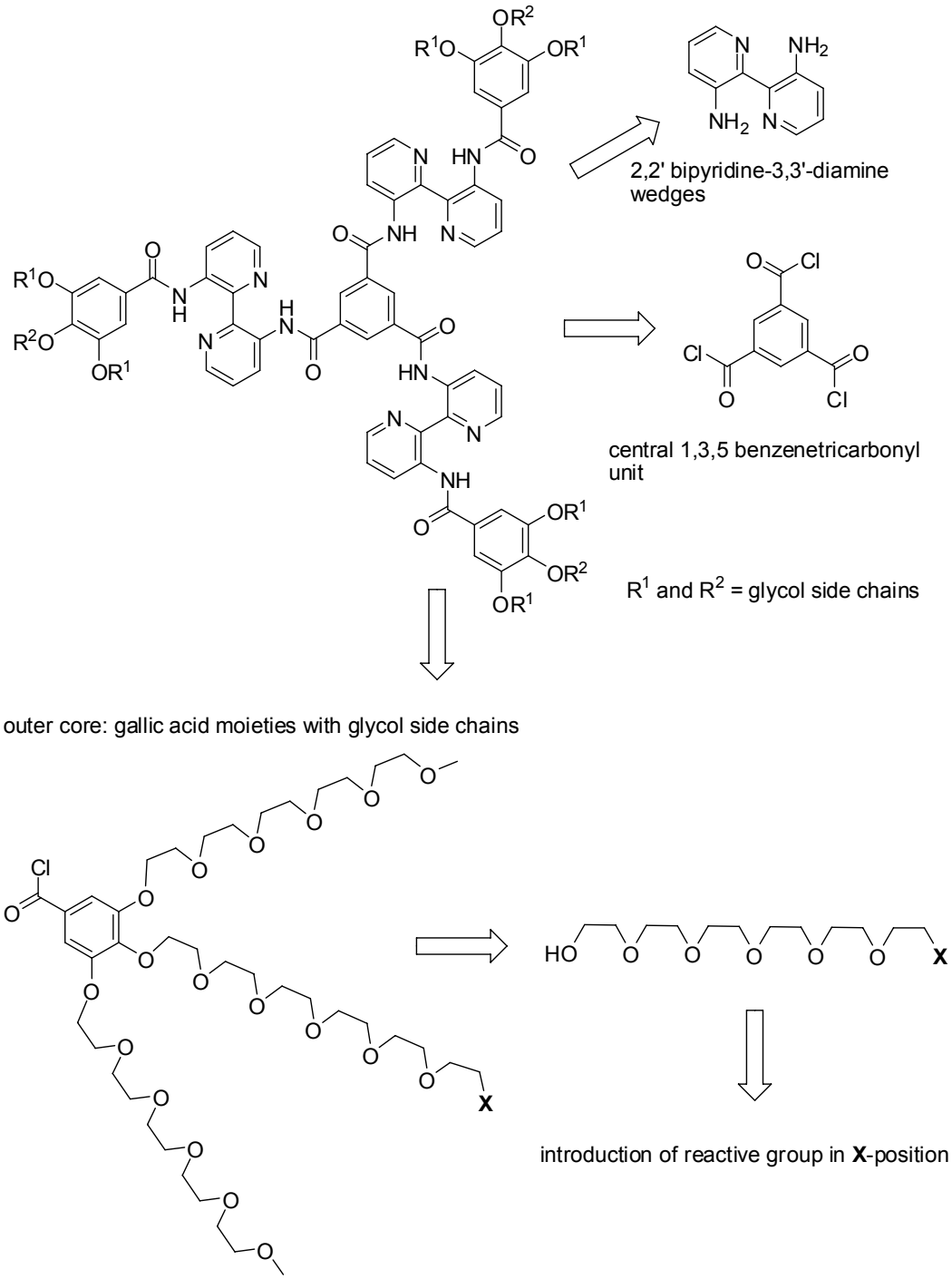

Scheme 1. Retrosynthetic approach for the introduction of functional groups for subsequent modification of the discotic with ligands.

The aromatic core is surrounded by glycol side chains which enable water solubility and guarantee biological inertness of the discotic scaffold.

Furthermore, the glycol side chains of the discotics provide an ideal building block to modify the discotic monomers with ligands. Due to their unique properties, discotics were selected to develop a flexible platform for multivalent interactions and as a modulator of protein assembly.
The discotics are built up from three main building blocks: a central 1,3,5-benzenetricarbonyl unit, three 2,2'-bipyridine-3,3'-diamine wedges and the outer core consisting of three gallic acid moieties provided with glycol side chains (Scheme 1) which guarantee water solubility.

In order to be able to use this scaffold for biological applications, it had to be made possible to modify the discotic with diverse biological ligands in the last step of the synthesis. Therefore we needed to introduce a functional group in the outer core of the discotic, which would allow subsequent synthetic modification of the scaffold. The functional groups were supposed to be introduced on the termini of the glycol side chains. Furthermore, only the *para*-positioned side chain of the gallic acid was supposed to be modified. Although a gallic acid derivative with three equal side chains is easier accessible, three functionalizable groups per gallic acid would result in nine groups on the final discotic. In this case, one monomeric discotic would already be an interaction partner with high polyvalent potential. Studying the polyvalent effects of the supramolecular columns with those discotics would most probably be difficult due to the high valency of the monomers. Besides this, assembly of discotic monomers with nine ligands would most probably result in crowding of the ligands at the periphery of the supramolecular columns. Crowding would complicate the functionalisation of the discotic with ligands and could lead to negative cooperative effects in multivalent binding. For these reasons we envisaged to synthesize symmetrical trivalent discotics with elongated side chains carrying functionalized groups on the termini of the side chains in *para*-position of the gallic acid moieties. We planned to elongate the functionalized side chain in *para*-position by one glycol unit. Thus, the ligands could be attached to the longer chain and stitch out of the glycol periphery of the discotic. This should avoid possible sterical constraints in the interaction between the functionalized discotics and the corresponding biological system.

Discotics, equipped with reactive groups at the end of the side chains in *para*-position of the gallic acid moiety, were envisaged to enable subsequent functionalisation of the discotic scaffold with specific ligands. In order to be flexible in terms of attachment of ligands we chose to design two differently functionalized discotic scaffolds. One discotic scaffold was proposed to be provided with an amine functionality. Many biological interesting ligands either carry or can be decorated with acids and thus could be attached to an amine modified discotic by acylation. Furthermore we planned to introduce an azide functionality to the discotic scaffold. Ligands provided with a propargylic residue could be attached by Huisgen [2+3] cycloaddition.[69, 70] This reaction is highly selective and widely used for attachment of ligands in aqueous solutions.[71] These two functionalized discotics were envisaged as key building blocks to a variety of discotics carrying different ligands.

3.1.2 Synthesis of the Inert Discotic

Synthesis of disc-shaped molecules based on trimesic acid and bis-acetylated diaminobipyridines has been reported in the literature.[51, 52, 72] According to the strategies, discotics were built up with a central 1,3,5-benzenetricarbonyl unit, surrounded by three 2,2'-bipyridine-3,3'-diamine wedges attached to gallic acid scaffolds provided with glycol side chains in the outer core.

We first set out to synthesize achiral unfunctionalized discotics as reported. These discotics carry equal glycol side chains, capped with methoxy-groups, in *meta*- and *para*-position of the wedges (Scheme 2). They possess no reactive groups for further synthetic modification and were meant to serve as control scaffolds and as biologically inert spacers in supramolecular polymers as described in Chapters 3.3 and 3.4.

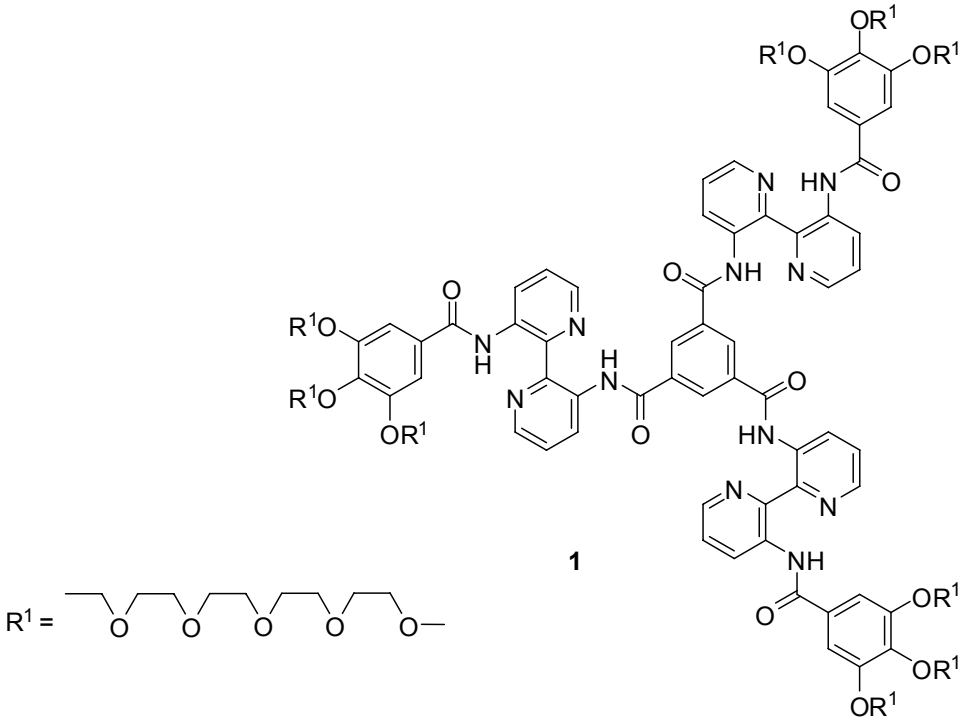

Scheme 2. The inert discotic scaffold **1**, built up by linking three 2,2'-bipyridine-3,3'-diamine wedges to a central 1,3,5-benzenetricarbonyl unit. Glycol side chains ensure water solubility.

Disc-shaped molecules **1** (Scheme 2) were synthesized by a convergent approach. The molecules were built up by linking three *N*-monoacylated 2,2'-bipyridine-3,3'-diamine wedges to a central 1,3,5-benzenetricarbonyl unit. The synthesis of 2,2'-bipyridine-3,3'-diamine **4** (Scheme 3) has been described previously.[73, 74] In our hands Ullmann coupling of 2-chloro-3-nitropyridin (**2**) to the bipyridine **3** and subsequent reduction of the nitro-groups was performed in 25% yield over two steps.

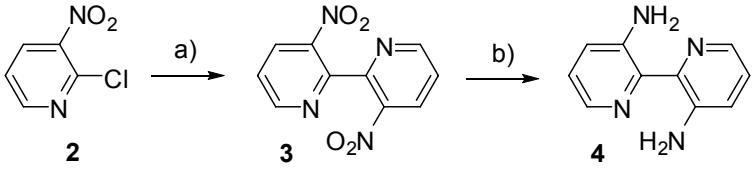

Scheme 3. Synthesis of the 2,2'-bipyridine-3,3'-diamine a) Cu, DMF, 110 °C, 34%; b) $SnCl_2$, HCl, 72%.

Pentaethylene glycol-monomethylether (**10**) was prepared according to Scheme 4 from the corresponding commercially available glycols **5** and **7**.

Monobenzylated diethylene glycol **6** was alkylated with tosyl-activated triethylene glycol-monomethylether **8** to yield pentaethylene glycol-monomethylether **10** after debenzylation in 88% yield. The yield is comparable to the previously reported coupling of tetraethylene glycol-monomethylether to activated benzyl monoethylene glycol (85%).[68] Nevertheless, the starting material triethylene glycol-monomethylether is cheaper than the corresponding tetraethylene glycol-monomethylether.

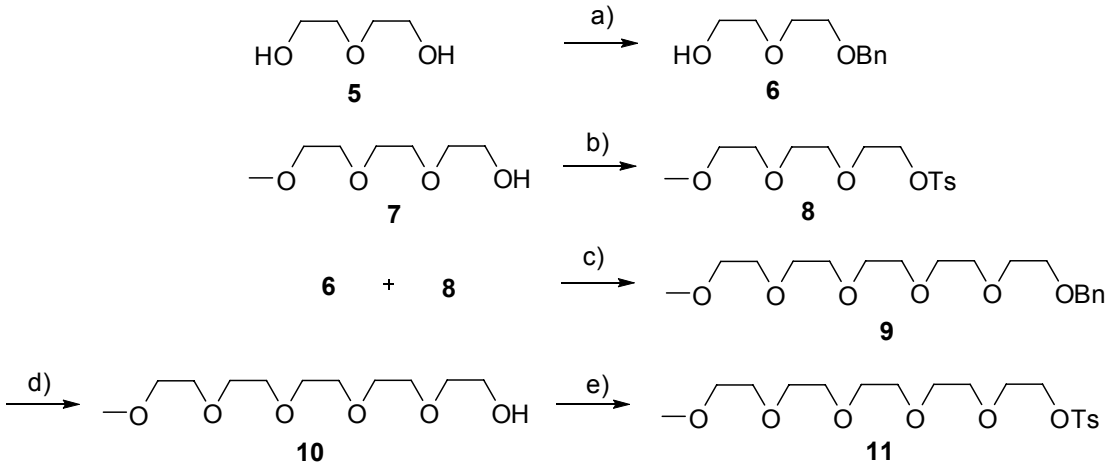

Scheme 4. Synthesis of the pentaethylenglycol-monomethylether side chain. a) BnBr, NaH, THF, 16 h, 80 °C, 73%; b) tosyl chloride, NaOH, THF/water, 5 h, 0 °C, 65%; c) KOH, THF, 12 h, 100 °C, 88%; d) H_2 (50 bar), Pd/C, HCl, ethanol/water, 12 h, quant.; e) tosyl chloride, TEA, CH_2Cl_2, 12 h, 72%.

Pentaethylene glycol-monomethylether (**10**) was activated to its tosylate **11** and introduced threefold on the gallic acid by alkylation of the commercially available methyl 3,4,5-trihydroxybenzoate in 81% yield (Scheme 5). The methylester of **13** was saponified under basic conditions at 100 °C. The free acid **14** was activated to its acid chloride **15** with oxalyl chloride and a catalytic amount of DMF. To avoid radical chlorination of the aromatic core the reaction was carried out in the absence of light. The crude acid chloride **15** was used directly for the subsequent step.

The synthesis of **1** is based on the consecutive selective acylation of the two amino groups of 2,2'-bipyridine-3,3'-diamine **4** (Scheme 5). The condensation to the monoacylated bipyridine **16** was carried out by adding a dilute solution of the acid chloride **15** to an ice-cooled and dilute solution (both about 0.1 mM) of 2,2'-bipyridine-3,3'-diamine **4** and triethylamine (TEA) to obtain a high

degree of monoacylation. Monoacylated and diacylated compounds were separated by column chromatography. In the final step **16** was attached to benzene-1,3,5-tricarbonyl trichloride (**17**). A slight excess of **16** was used to ensure complete threefold reaction of the inner core. The crude compound was thoroughly purified by column chromatography using silica gel and size exclusion chromatography. Due to the assembly of the discotics in various organic solvents[68], chloroform or CH_2Cl_2 were used for chromatographic purification, because the discotics do not assemble in these solvents. Compound **1** was isolated in reasonable yields (37% over three steps).

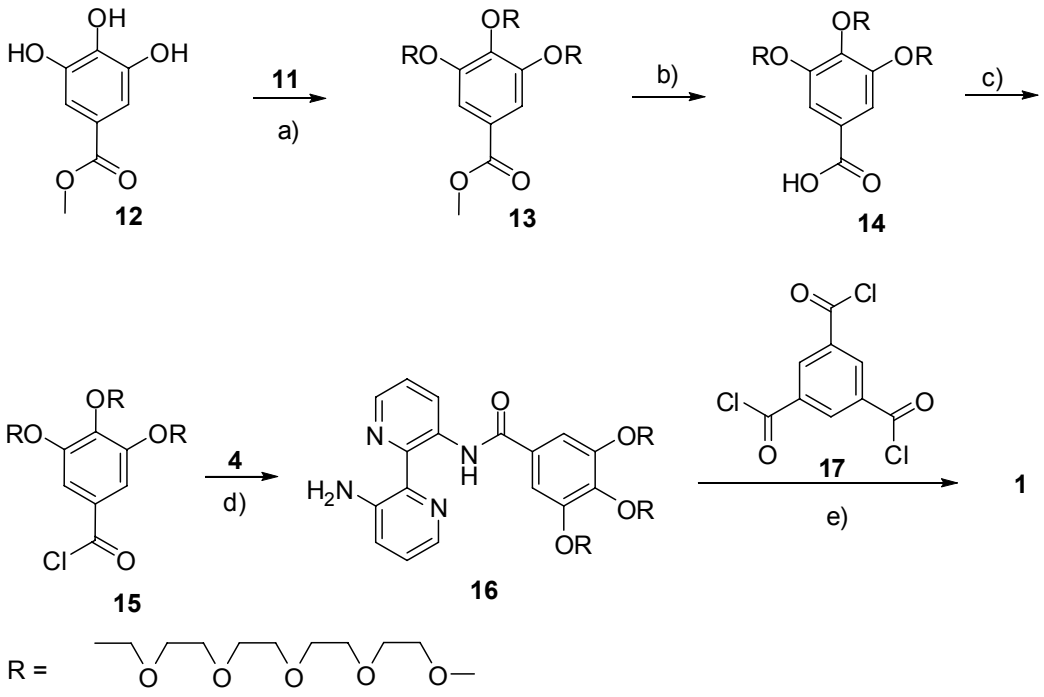

Scheme 5. Synthesis of the inert discotic **1**. a) **11**, K_2CO_3, DMF, 12 h, 70 °C, 81%; b) KOH, ethanol/water, 100 °C, 82%; c) $(CO)_2Cl_2$, DMF, CH_2Cl_2, 12 h, 62%; d) 4, TEA, CH_2Cl_2, 5 h, 5°C; e) TEA, CH_2Cl_2, 59% over 2 steps.

3.1.3 Synthesis of the Azide- and Amine Functionalized Discotics

We set out to generate derivatives of **1** that would allow facile modification with ligands. As already mentioned in Chapter 3.1.1, we planned to introduce amine or azide functionalities on the discotic scaffold. The amine functionality was envisaged to be decorated with ligands *via* acylation with an acid. This reaction gives access to many biologically interesting substances such as peptides and for example dyes provided with acid-linkers. On the other hand, [2+3] cycloaddition of the azide functionality opens the door to highly selective attachment of compounds with propargyl residues. This reaction can be carried out selectively, even with ligands carrying unprotected other reactive groups.

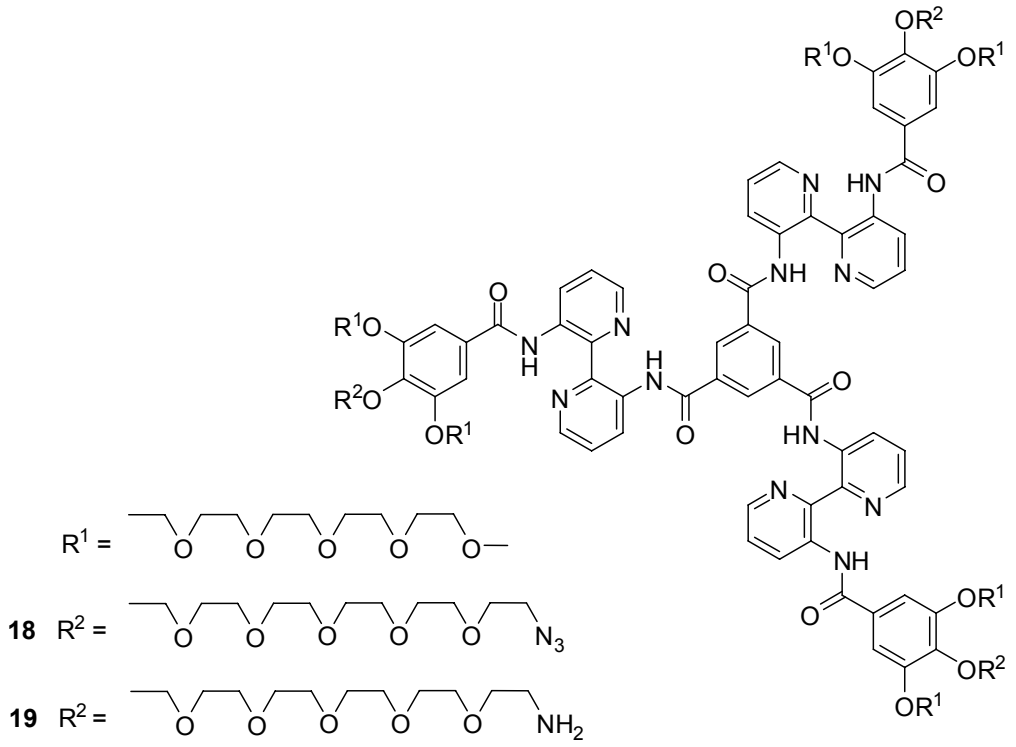

Scheme 6. Discotic scaffold with functional groups at the side chain termini in R^2 position offer a flexible access to functionalized discotic scaffolds. **18** azide discotic; **19** amine discotic.

Compounds **18** and **19** were designed featuring three selectively introduced azide or amine functionalities at the periphery of the molecule. Discotic scaffolds **18** and **19** were envisaged to provide a flexible platform for

modifications with biological ligands in the final step of the synthesis (Scheme 6). Compounds **18** and **19** were synthesized in a multistep approach in a convergent fashion, resulting in a discotic molecule provided with six inert ethylene glycol-monomethylether side chains and three azide- or amine-functionalized side chains.

The glycol side chain **22** with an azide functionality was derived from hexaethylene glycol (**20**) in two steps by mono-tosylation and subsequent substitution (Scheme 7). Mono-tosylation was carried out using a threefold excess of **20** compared to the tosyl chloride to avoid double tosylation. The desired compound **21** was isolated in 80% yield, while 30-50% of starting material **20** was recovered. Reaction with sodium azide to generate **22** proceeded in 85% yield.

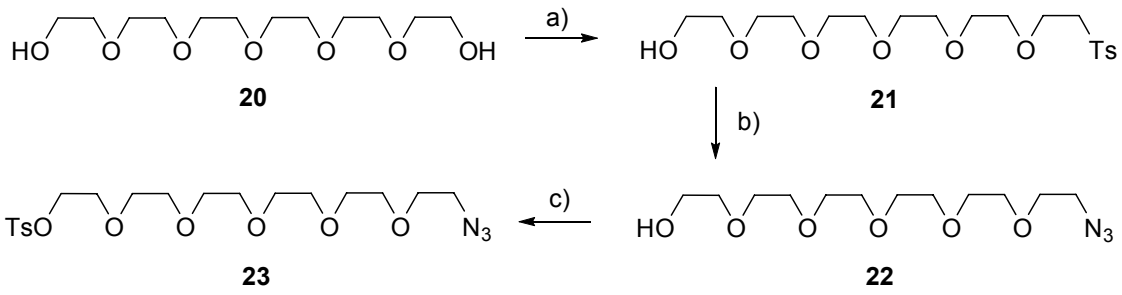

Scheme 7. Synthesis of the azido-hexaethyleneglycol side chain. a) tosyl chloride, TEA, THF, 12 h, 80%; b) NaN_3, DMF, 6 h, 85%; c) tosyl chloride, TEA, CH_2Cl_2, 12 h, 66%.

Hydrogenation of the azide, catalyzed by palladium on charcoal, was performed in high yields. However, Boc-protection of the free amine appeared to be less straightforward. First trials of the protection with Boc-anhydride in presence of base seemed to result in amine double Boc protection, according to NMR and mass-spectrometry. Slow addition of a slight excess (less than 1.2 equiv.) of Boc-anhydride at 0 °C, addition of base only after 3 h and long reaction times of up to 1 d finally yielded the desired hexaethylene glycol **25** with mono-protected amine functionality in reasonable yield (Scheme 8). Compounds **22** and **25** were activated to their respective tosylates (**23** and **26**).

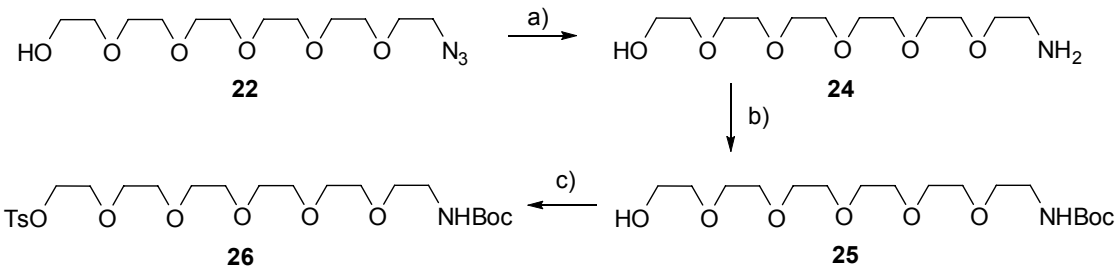

Scheme 8. Synthesis of the amino-hexaethylene glycol side chain. a) H_2 (10 bar), Pd/C, ethanol/water, 48 h, 96%; b) Boc_2O, dioxane, 0 °C-rt, 27 h, 61%; c) tosyl chloride, TEA, THF, 12 h, 62%.

In order to selectively introduce modified glycol side chains to the discotic scaffold, methyl 3,4,5-trihydroxybenzoate was orthogonally protected at the 4-position (Scheme 9). Therefore, methyl 3,4,5-trihydroxybenzoate was allowed to react with acetic anhydride under basic conditions to yield the per-acetylated compound **27** as colorless crystals. **27** was mono-benzylated in *para*-position with benzyl bromide, in presence of potassium carbonate and potassium iodide, to yield **28**.[75] Hydrolysis of the acetyl groups gave compound **29**, selectively protected at the 4-position. Alkylation with activated pentaethylene glycol-monomethylether **11** yielded **30**. Subsequent debenzylation in an autoclave under hydrogen atmosphere gave **31** in 20% total yield over five steps. Gallic acid derivative **31** could now be provided with the glycol side chains carrying functional groups. Activated glycol chains **23** or **26** were introduced on **31** by alkylation under basic conditions at 70 °C, to provide scaffolds **32** and **33** as modified outer cores of the discotic in 70% and 90% yield respectively.

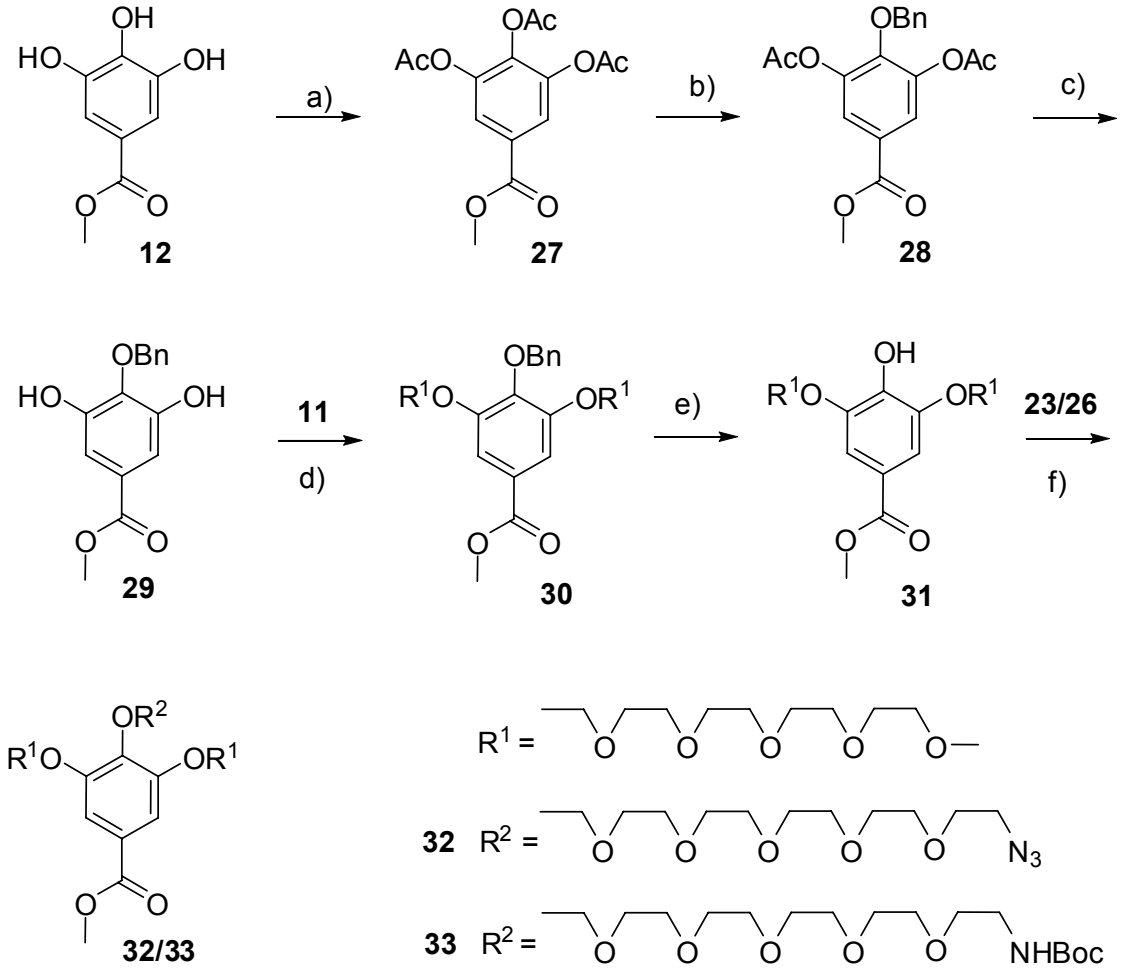

Scheme 9. Synthesis of the gallic acid derivatives **32** and **33** with amine- or azide-functionalisation. a) Ac_2O, pyridine, 12 h, 80%; b) BnBr, K_2CO_3, KI, Acetone, 57%; c) K_2CO_3, methanol/water, 70%; d) K_2CO_3, DMF, 70 °C, 61%; e) H_2, Pd/C, HCl, ethanol/water, 94%; f) K_2CO_3, DMF, 70 °C, 70% for **32** and 90% for **33.**

Compounds **32** and **33** were saponified under basic conditions at 100 °C (Scheme 10). The free acids **34** and **35** were activated to their acid chlorides. These reactions were carried out in the absence of light to avoid radical chlorination of the aromatic core. Subsequent reaction of **4** with the acid chlorides **36** or **37** at 0 °C afforded mono-*N*-acylated bipyridines **38** and **39** in 62% and 52% yield, respectively. Pure **38** was obtained after thorough purification by column chromatography with silica gel, size exclusion chromatography and column chromatography again. However, purification of **39** turned out to be much more difficult than it had been in case of **16**. Purification by column chromatography with silica gel, size exclusion chromatography and column chromatography again resulted in the desired

product **39** containing an impurity of approximately 10%, according to LC/MS. However, high purities at this stage were absolutely required for both compounds (**38** and **39**), because the following threefold reaction with trimesic acid generates the self-assembling discotics, from which impurities are only very difficult removed. Impurities, leading to side reactions in this last step, resulting in compounds of similar weight as the discotic product, could most probably not be separated from the desired molecules. Thus the crude of **39** was isolated by preparative LC/MS in fractions of 60 mg to finally result pure **39**.

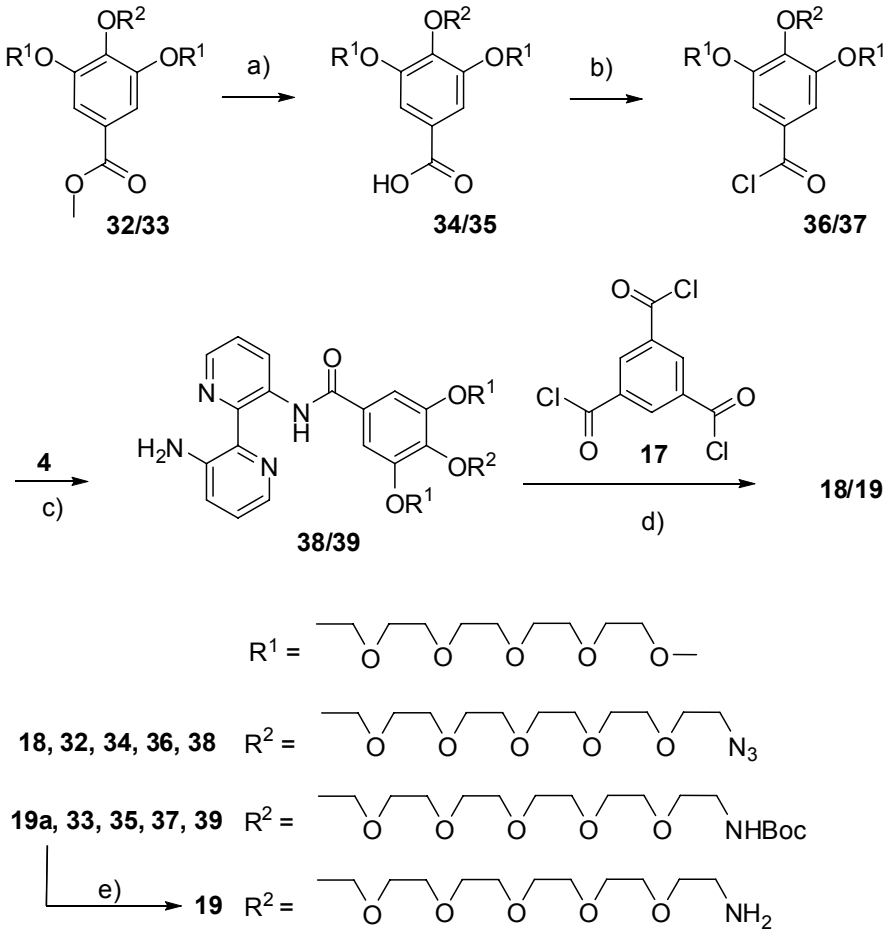

Scheme 10. Synthesis of the discotic scaffold with amine- or azide-functionalisation. a) KOH, ethanol/water, 100 °C, quant. for **34** and 94% for **35** ; b) $C_2O_2Cl_2$, DMF, CH_2Cl_2, 12 h; c) TEA, CH_2Cl_2, 5 h, 5 °C, 62% for **38** and 52% for **39**; d) TEA, CH_2Cl_2, 39% for **18** and 57% for **19a**; e) TFA, CH_2Cl_2, 30 min, quant.

In the final step, threefold reaction of trimesic chloride (**17**) with pure **38** gave target compound **18** in reasonable 39% yield, after purification by column chromatography over silica gel and size exclusion chromatography.

Acylation of **39** with trimesic chloride gave **19a** in 57% yield. Pure **19a** was also obtained after purification by column chromatography with silica gel followed by size exclusion chromatography. Deprotection of **19a** under acidic conditions proceeded fast. Purification by size exclusion chromatography separated **19** from molecules of low molecular weight. Discotic **19** with free amine functionalities was isolated quantitatively (Scheme 6). Having compounds **18** and **19** in hand, we could now set out to decorate the discotics with ligands for biological studies.

3.2 Ligand-functionalisation of Discotics

Compounds **18** and **19** provide flexible scaffolds for modifications with biological ligands. Introduction of ligands is possible for example by acylation of **19** or by copper catalyzed [2+3] cycloaddition of **18** with alkynes. In this chapter the synthesis of a set of functionalized discotics will be described.

3.2.1 Preparation of a Glycoside Modified Discotics

Mannose was envisaged to be attached to the azide discotic **18** by [2+3] cycloaddition as ligand for the interaction with bacterial agglutins and lectins[3]. Mannose was chosen, because of its property to bind to the FimH receptors of *E. coli* - an easily accessible bacterial system to study polyvalency as described in Chapter 3.3. Furthermore, the corresponding galactose and glucose modified discotics were planned to be prepared as well. Galactose also targets FimH receptors though with lower affinity than mannose. Glucosyl-ligands do not bind to these receptors, but are involved in immune response.
To explore the feasibility of this approach, 1-propargyl-α-D-mannopyranoside **42** was first prepared in three steps (Scheme 11).[76] 1,2,3,4,6-Penta-*O*-acetyl-α-D-mannopyranosid **40** was obtained by acetylation of mannose in 93% yield. The propargyl residue was introduced, employing the tin tetrachloride catalyzed glycosidation procedure.[76] 1-Propagyl-2,3,4,6-tetra-*O*-acetyl-α-D-manno-pyranosid **41** was isolated in 54% yield. Deprotection proceeded quantitatively. 1-Propargyl-glucopyranosid (**48**) and 1-propargyl-galactopyranosid (**45**) were prepared accordingly in 50% and 48% respective total yield over three steps.

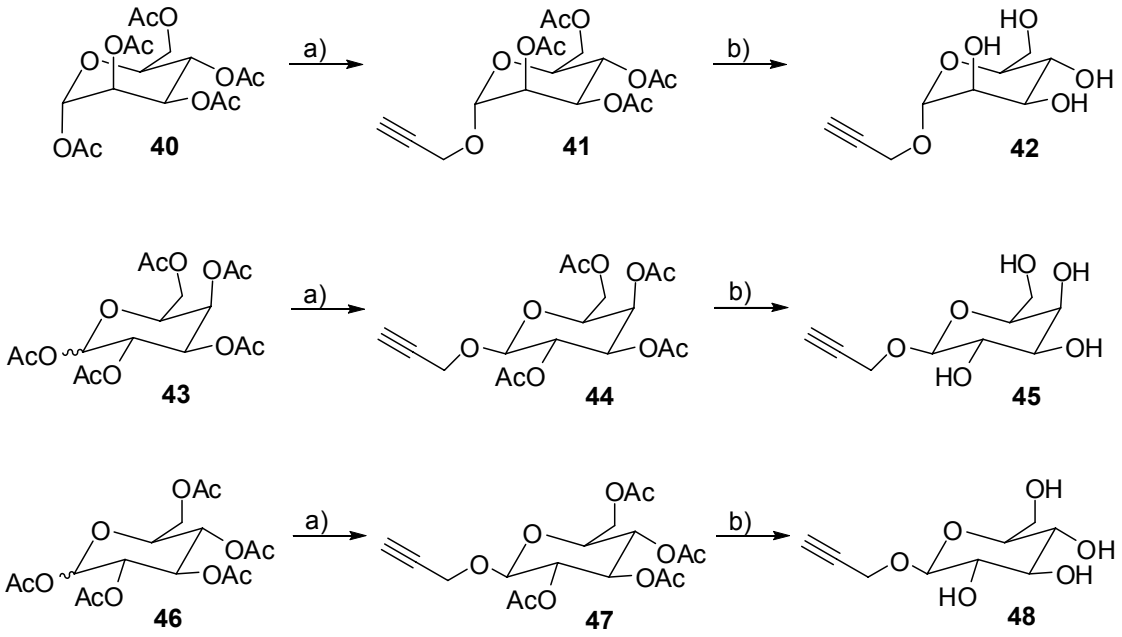

Scheme 11. Synthesis of 1-propargyl-α-D-mannopyranosid **42** (above), 1-propargyl-β-D-galactopyranosid **45** (middle) and 1-propargyl-β-D-glucopyranosid **48** (below); a) 2-propargyl-alcohol, $SnCl_4$, CH_2Cl_2, 46-54%; b) NaOMe, methanol/water, 96-100%; The penta-acetylated compounds **40**, **43** and **46** were prepared from the corresponding glycosides in 90-97% yield, using acetic anhydride and pyridine.

For the threefold modification of **18** with this mannose derivative, standard conditions of 2 mol-% $CuSO_4$, 5 mol-% of sodium ascorbate, and 15 equiv. of 1-propargyl-mannose per azide residue in a water/*t*-butanol mixture were applied (Scheme 12).[77] In contrast to many previous reports on the copper catalyzed azide-alkyne cycloaddition for sugars,[71] the modification of **18** to **49** *via* this reaction was relatively slow. Approximately 30% of the azide functionalities reacted rapidly within the first hours, but the complete functionalization of all groups required longer times. MALDI-TOF MS spectra (Figure 13) show the progression of the [2+3] addition over time. After 4 h the mass peak of the mono addition appeared. Nevertheless after 2 weeks there was still some starting material left and mono-, di-, and tri-addition products were detected. Only after 3 weeks the main mass peak corresponded to the desired product. After 4 weeks full conversion to the desired compound **49** was detected. Neither addition of the glycoside nor increase of copper catalyst or sodium ascorbate seemed to have influence on reaction times.

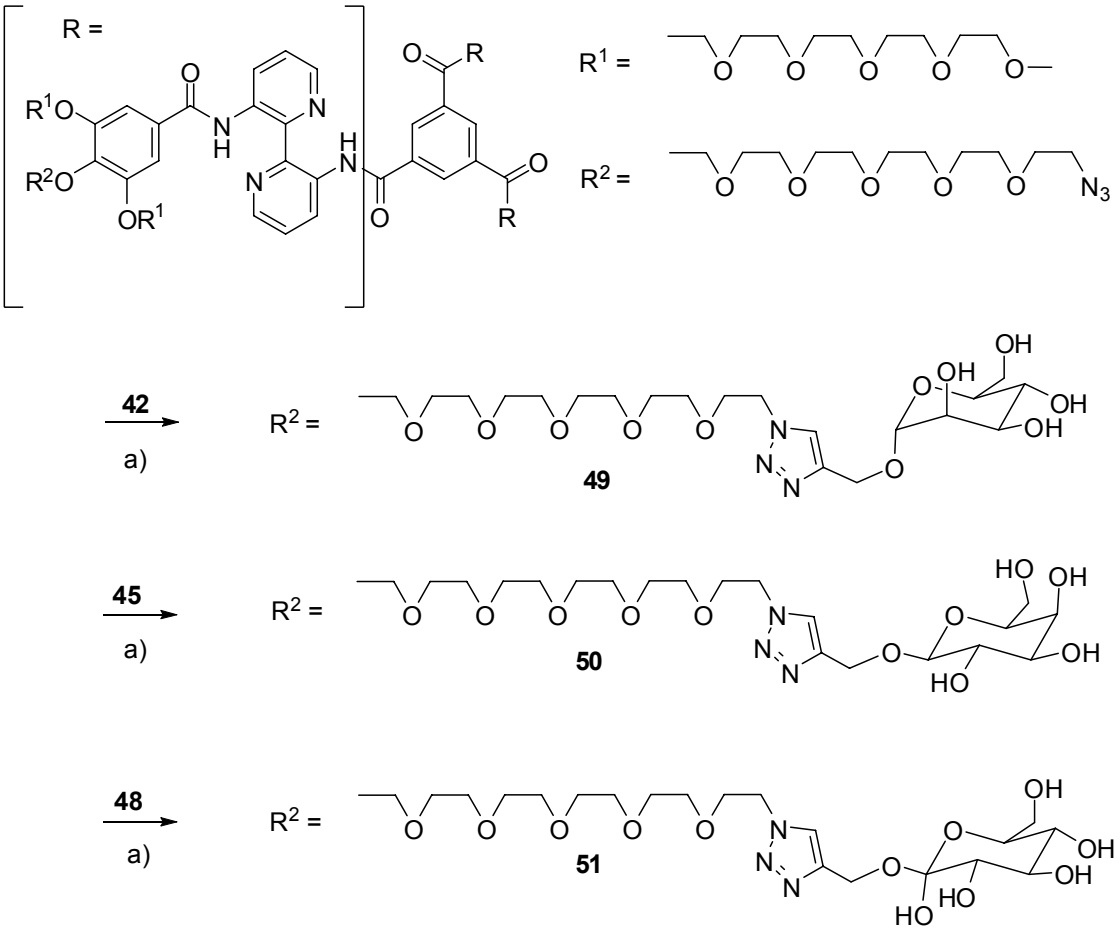

Scheme 12. Synthesis of the glycoside discotics **49**, **50** and **51** from azide discotic **18.** a) Na-ascorbate, $CuSO_4$, *t*-butanol/water.

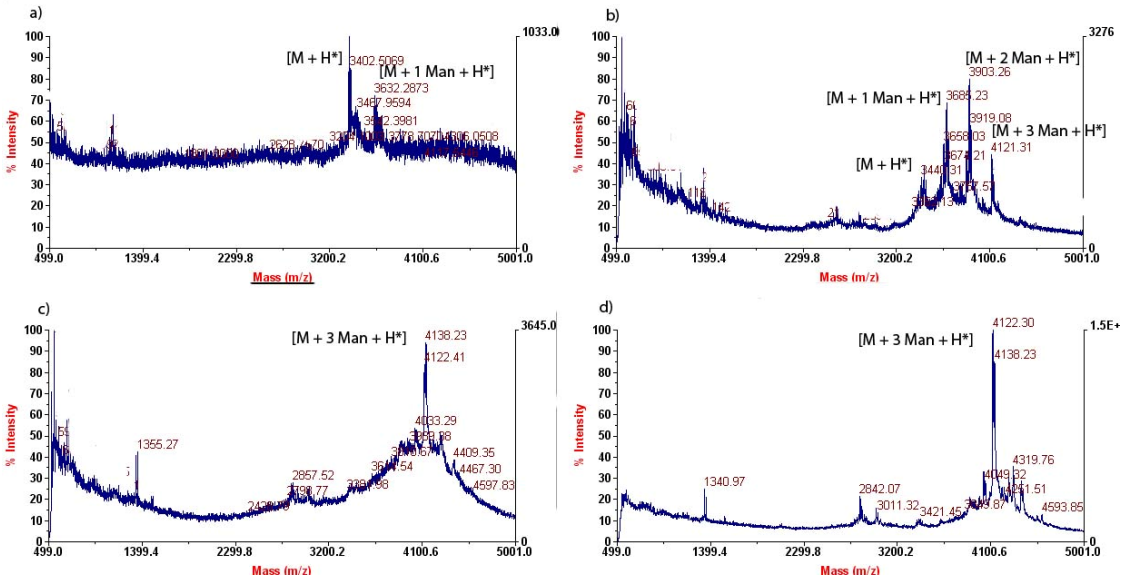

Figure 13. MALDI-TOF MS Spectra of mannose coupling to azide discotic **18** after a) 4 h, b) 2 weeks, c) 3 weeks and d) 4 weeks. After 4 weeks all azides were converted.

One possible explanation for the slow reaction is the coordination of copper to the bipyridin core. Thus, decrease of the amount of free copper in solution could lead to slow reaction times. Nevertheless, we think that this is not the case here. To be able to coordinate copper, a bipyridine core needs to have both heterocyclic nitrogens in one plane. The bulky moieties of the bipyridine wedges in the discotic would most likely not allow rotation of the bipyridines and thus prevent the coordination of copper. This assumption is supported by the fact that a copper adduct of the product or side products in MALDI-TOF MS has never been detected and that the discotics remain fluorescent during the reaction.

Apparently the high degree of supramolecular polymerization of **18**/**49** at the reaction conditions in water results in molecular crowding (*vide infra*) of the reactive functionalities. Crowding then causes sterical hindrance and prevents further reaction of free azides. The dynamic rearrangement of the discotics nevertheless allows full conversion of the free azide groups over time, probably at the chain-ends of the supramolecular polymer. The pure product **49** could be isolated in 80% yield after size exclusion chromatography to remove the excess of mannose. Unlike the other discotic scaffolds **1**, **18** and

19 the mannose modified discotic did not dissolve in CH_2Cl_2 and had to be purified in DMF *via* size exclusion chromatography.

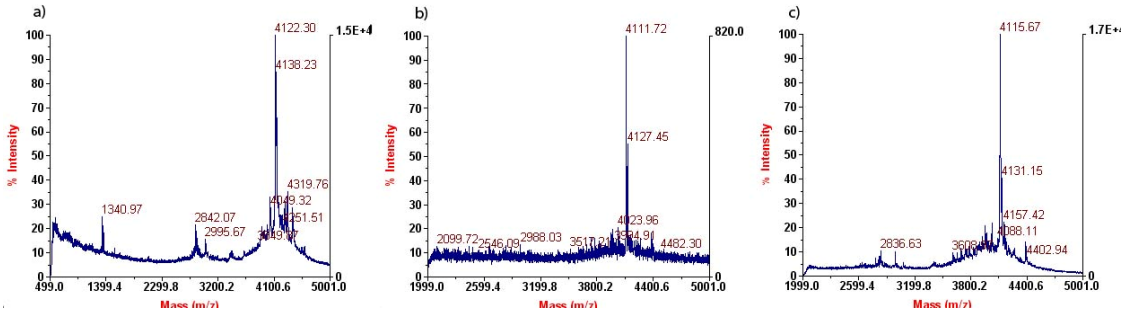

Figure 14. MALDI-TOF MS Spectra of a) mannose discotic **49** b) galactose modified discotic **50** and c) glucose modified discotic **51** after 4 weeks reaction time.

Click reactions with the corresponding galactose- and glucose-derivatives were carried out in the same timeframe. The isolated yields were 72% for the galactose modified discotic **50** and 65% for the glucose modified discotic **51**. Mass spectra of **49**, **50** and **51**, each after 4 weeks reaction time are shown in Figure 14.

In order to prove the hypothesis of molecular crowding on the surface of the supramolecular polymers, future experiments could be performed in chloroform (monomer state) using a copper catalyst compatible with organic solvents.[70] Furthermore mixtures of **1** and **18** could be employed for the reaction in water. Compound **1** should serve as spacer in the supramolecular columns and could prevent molecular crowding.

3.2.2 Preparation of a Texas Red Discotic

Heterovalent supramolecular assembly with differently functionalized discotics is one anticipated advantage of dynamic supramolecular columns employed for interaction with biological systems. Heterovalent polymers could be easily accessed by simple mixing of the desired modified discotic scaffolds. In order to be able to study the properties of discotic mixtures, a fluorescent dye was attached to the scaffold. The dye was meant to provide an independent

possibility of detection in binding studies when using mixtures of differently functionalized discotics and the discotic attached to the dye. Texas Red was chosen with regard to its fluorescent properties such as small Stokes shift and an excitation wavelength around 590 nm, avoiding interference with the fluorescence of the discotic scaffold.

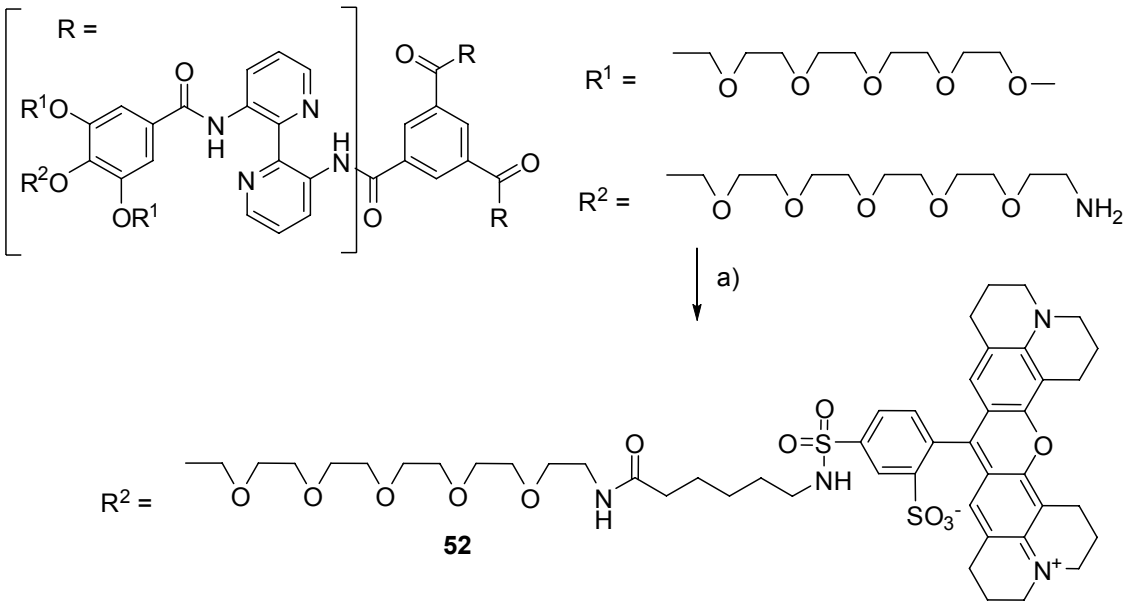

Scheme 13 . Synthesis of the Texas Red discotic **52** *via* the amine discotic **19**. a) Texas Red-X-NHS, TEA, CH_2Cl_2, 2 weeks.

The amine disc **19** was allowed to react with an excess of Texas Red®-X, activated as its succinimidyl ester, readily available from Invitrogen, for 2 weeks (Scheme 13). The reaction was monitored by MALDI-TOF MS (Figure 15). After 12 h **19** had reacted at either one or two of the three free amine positions per scaffold (Figure 15). Only little starting material was left. However, the reaction seemed not to have continued any further after 3 more days. No mass signal of the desired product **52** could be detected. Addition of base and more Texas Red succinimide led to further conversion with the main fraction of the product consisting of tri-functionalized discotic after 10 days of reaction. Unfortunately, unlike the modification of **18** with mannose, complete conversion of all starting material could not be achieved. Neither addition of extra dye or base nor dilution or concentration of the reaction mixture resulted

in further conversion of the mono- and di-functionalized side products over a period of another week. Through repeated work up by size exclusion chromatography enrichment of the tri-functionalized Texas Red discotic could be achieved, but complete isolation from its side products was not possible. Separation by preparative affinity chromatography over silica or alumina under various conditions was not successful either. Furthermore, no optimized conditions for purification of the Texas Red discotic could be found using preparative Gel Permeation Chromatography. The difficultness of the purification probably lies in the ionic charges of the Texas Red molecule which lead to broadening of the fractions during chromatographic purification. Nevertheless, each discotic features at least one fluorescent Texas Red molecule and thus subsequent studies, described in chapter 3.3, with Texas Red discotic **52** were carried out using the mixture containing mono- and di-Texas Red modified discotic.

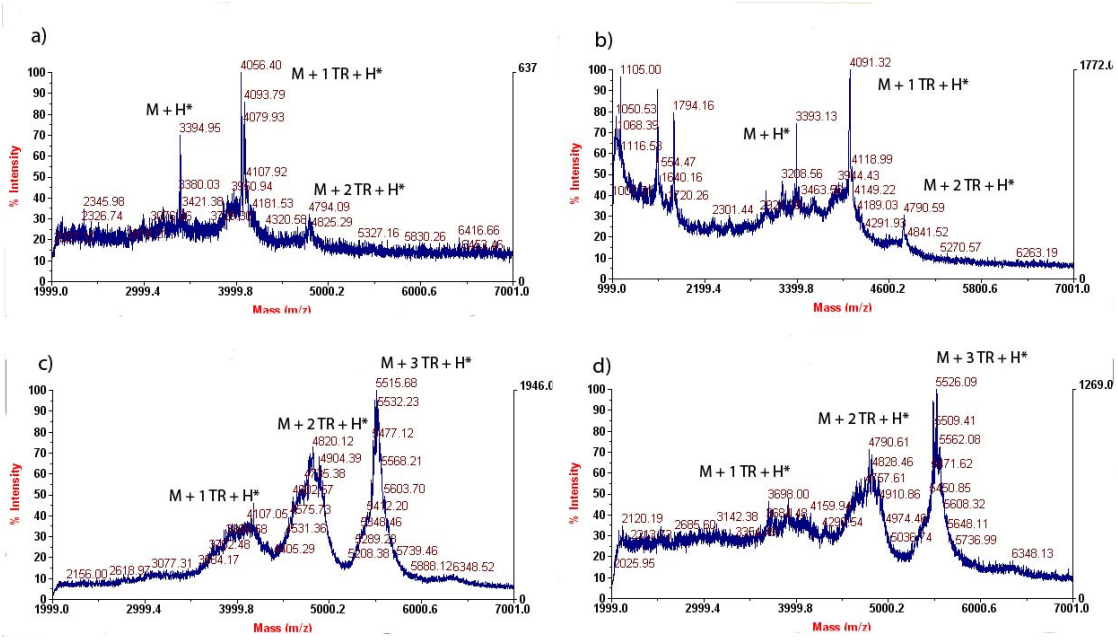

Figure 15. MALDI-TOF MS MS Spectra of Texas Red coupling to amine disc **19** after a) 12 h, b) 3 d, c) 10 d and d) 14 d. After 10 d no further progress in the reaction can be seen.

Again, the quick conversion of all discotics to the mono-functionalized intermediate gives rise to the assumption that sterical hindrance causes the stagnation in the reaction process. However, the supramolecules do not

assemble in CH_2Cl_2 (monomeric state). Thus, overcrowding of ligands on the supramolecular periphery of the columns is not likely. Nevertheless, charges of the Texas Red ligand might generate some kind of aggregation, which leads to sterical hindrance and prevents further conversion of free amines. In case of Texas Red coupling no full conversion over time could be achieved, like it was in case of mannose coupling. Nevertheless, the product consists of a compound mixture in which all discotics carry at least one Texas Red dye.

3.2.3 Preparation of a Biotin Discotic

Another ligand that was selected for attachment to the discotic scaffold was biotin. Biotin was chosen as ligand because of its well-studied binding properties to streptavidin.[78] First trials to modify **19** with biotin were performed using *N*-hydroxysuccinimidyl biotin with a short alkyl spacer, but did not result in acylation of any of the three amine functionalities of **19**, most probably because of the insufficient solubility of the biotin derivative in CH_2Cl_2. Thus, two water soluble biotin substances with glycol side chains spacers, supplied as *N*-hydroxysuccinimide ester, were used in the following reactions. BiotinPEO_4-X-NHS was coupled to the amine discotic **19** as illustrated in Scheme 14. MALDI-TOF MS analysis (Figure 16) was performed on the reaction mixture after 4 h, 12 h, 3 d and on the product after purification. Already after 4 h the main peak found corresponded to the tri-acylated product while only some starting material was left. The reaction was stopped after 3 d and the crude product was purified by size exclusion chromatography. Compound **53** was isolated in 65% yield.

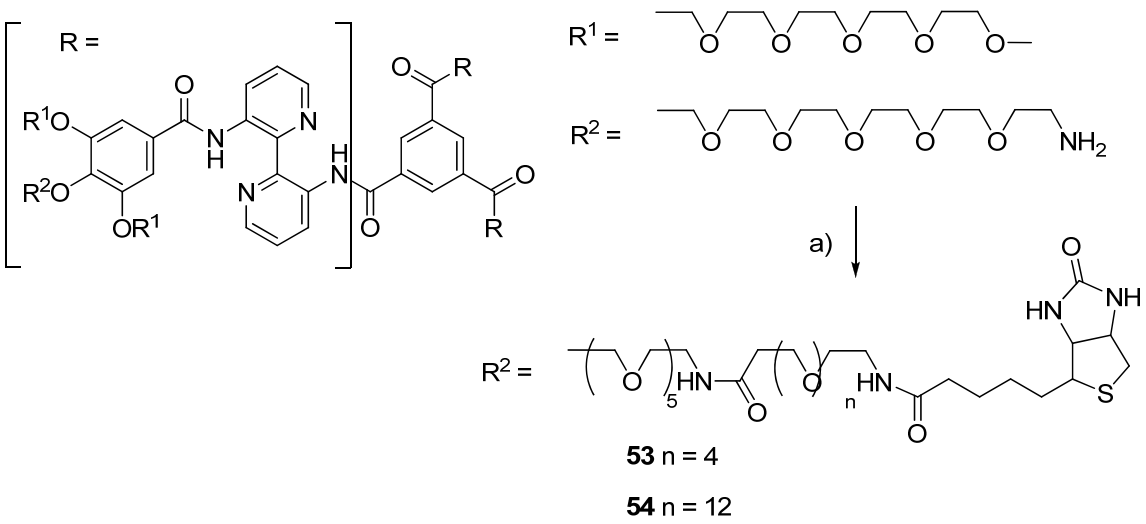

Scheme 14. Synthesis of the Biotin discotics **53** and **54** via the amine discotic **19**. a) n = 4: BiotinPEO$_4$-X-NHS or n = 12: BiotinPEO$_{12}$-X-NHS, TEA, CH_2Cl_2, 4 d, rt.

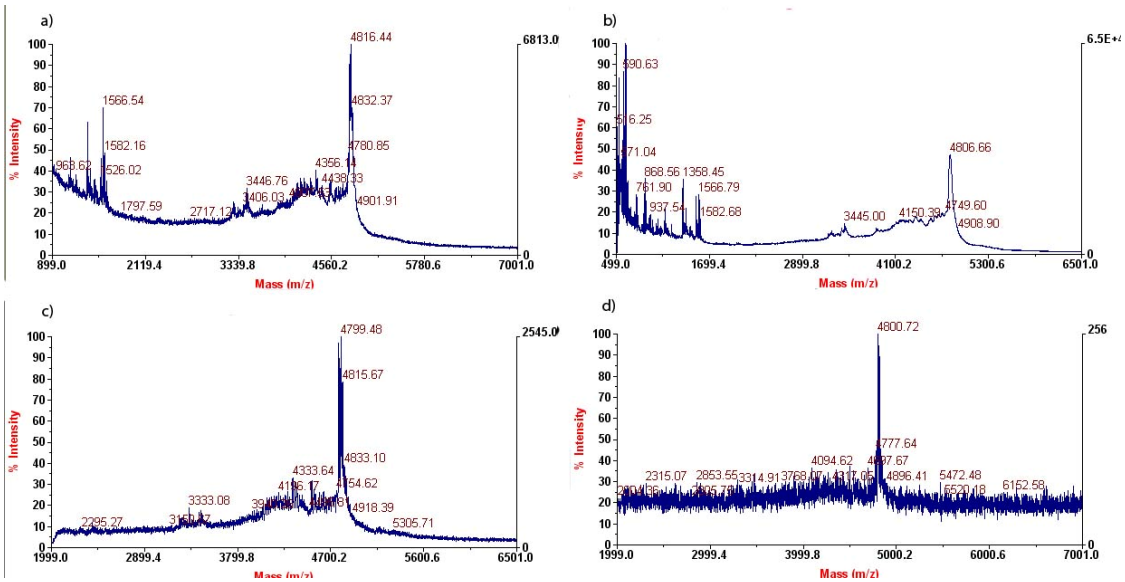

Figure 16. MALDI-TOF MS Spectra of Biotin-Disc **53** after a) 4 h, b) 12 h, c) 3 d and d) size exclusion chromatography.

Whereas BiotinPEO$_4$-X-NHS – carrying a glycol spacer of four units and a length of approximately 16 Å – reacted relatively fast, coupling of the corresponding BiotinPEO$_{12}$-X-NHS – with about 50 Å length – was not complete even after several weeks of reaction. The reaction proceeded within the first 2 d and resulted in a main mass peak of the desired product and

significant amounts of di-acylated and mono-acylated discotics while no starting material **19** was left (Figure 17). After 3 d and 7 d, both additional activated ester and base were added but this led to no further conversion. After 9 d of total reaction time, the reaction mixture was split into three batches. The first portion was stirred like before. To the others either DIC/DMAP or HATU/DIPEA were added. The reactions were monitored for another 12 d. As shown in Figure 17 addition of coupling reagents did not lead to further conversion of free amines.

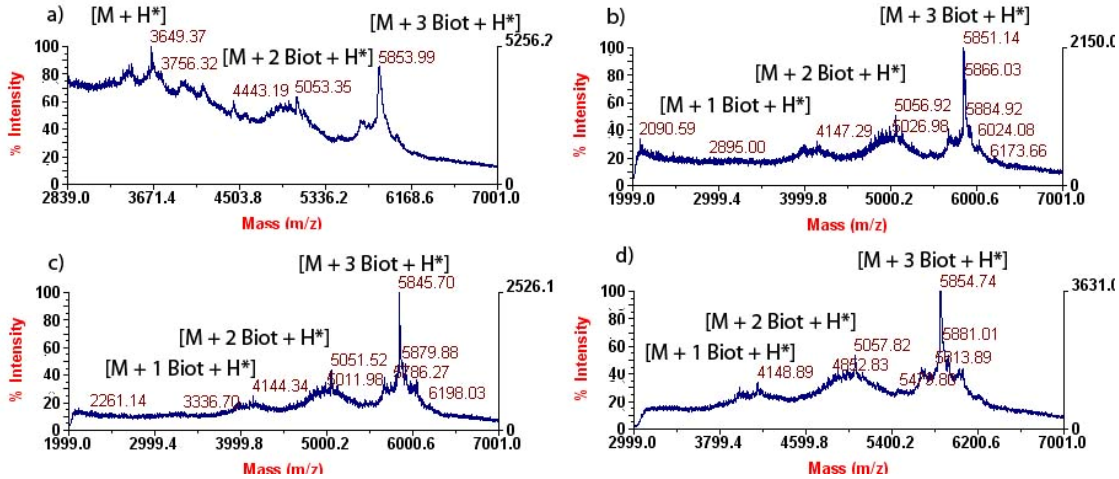

Figure 17. MALDI-TOF MS Spectra of biotin-Disc **54** after a) 1 d, b) 4 d c) 7 d, addition of biotin and base plus 2 d reaction time, d) addition of HATU/DIPEA.

The difference between the two biotin derivatives in terms of completion of the coupling reaction is another indication of steric crowding. Thus, overcrowding might also occur on the isolated molecule. As assumed in case of Texas Red coupling already (Chapter 3.2.2), not the stacking of the discotic but interaction of the attached ligand might cause aggregation even in CH_2Cl_2.

These results indicate that overcrowding is an essential limitation for ligand attachment. This problem could be overcome by designing a non-symmetrical discotic with only one reactive amine or azide group. The synthesis would afford two inert and one functionalized wedge in the outer core of the discotic and is not within the scope of this thesis. Nevertheless, functionalisation of these monovalent discotics then should prevent overcrowding.

3.2.4 Preparation of a Cysteine Discotic

N-Boc- and *S*-trityl-protected cysteine was attached as ligand to the discotic to provide a possible reaction partner for native chemical ligation of, for example, proteins to the supramolecular scaffold. The amino acid was activated as *N*-hydroxy-succinimid ester and allowed to react with the amine discotic **19** under basic conditions (Scheme 15). After 4 h only traces of diacylated compound were left, whereas most free amines had reacted. Coupling of the protected cysteine to the amine discotic **19** was complete after 12 h. After size exclusion chromatography 85% of cysteine discotic **55** were isolated.

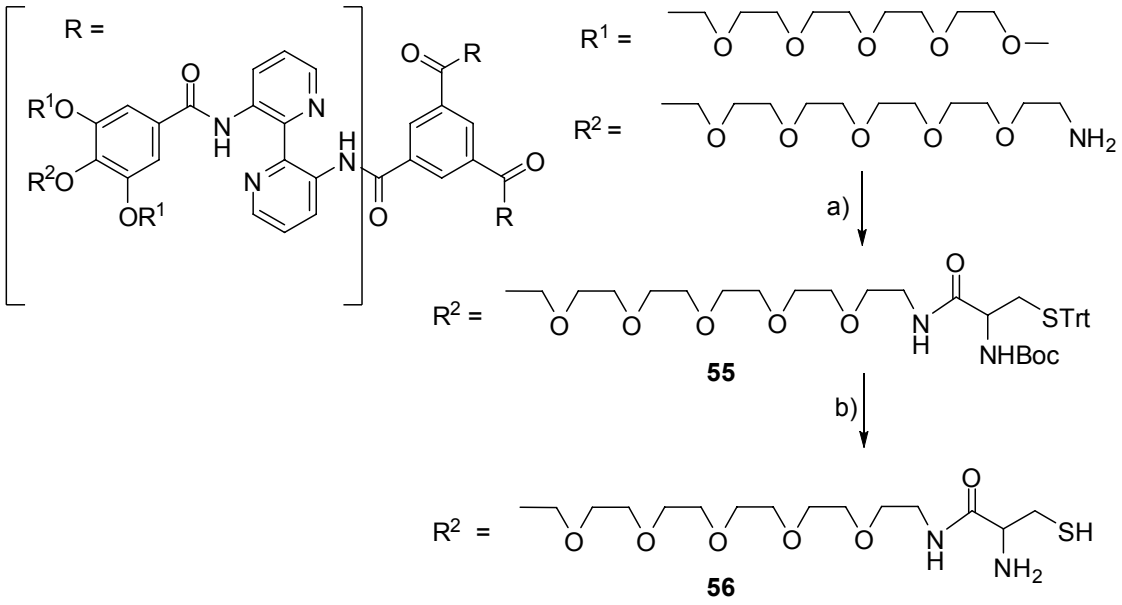

Scheme 15. Synthesis of the cysteine discotic **56** *via* the amine discotic **19**. a) Boc-Cys-(Trt)-NHS,CH_2Cl_2, 4 h; b) TES, TFA, CH_2Cl_2, 2h, rt.

Deprotection of the cysteines under acidic conditions with 20% TFA in CH_2Cl_2 proceeded quantitatively within 2 h (Figure 18). In order to remove molecules of small molecular weight the compound was purified by size exclusion chromatography. The deprotected cysteine discotic was stored at -20 °C to prevent disulfide formation. Prior to ligation reactions **56** was stirred in presence of *tris*(2-carboxyethyl)phosphine (TCEP) for 30 min to reduce potential disulfides.

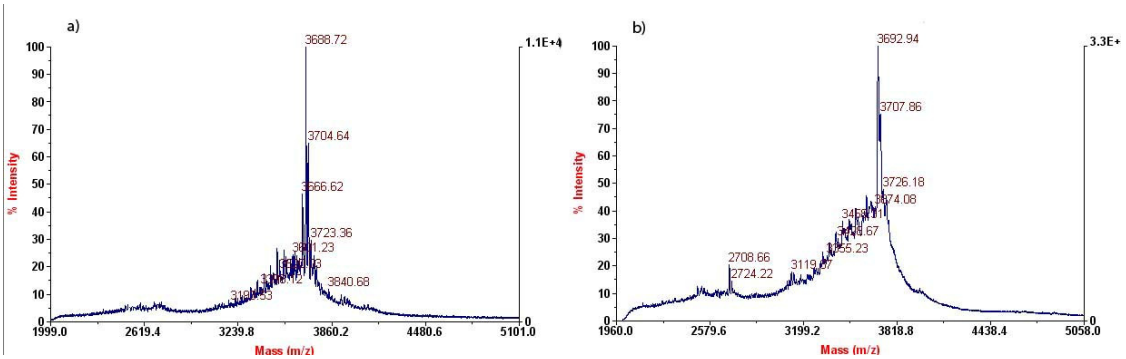

Figure 18. MALDI-TOF MS Spectra of cysteine disc **56** after a) size exclusion chromatography and b) 2 h reaction time.

3.2.5 Column Formation

All discotic compounds dissolve readily in water and form supramolecular polymers. It has been shown before that the degree of polymerization is dependent on the solvent.[79] Whereas glycol modified discotic compounds form supramolecular columns in water, they are in the monomer state when dissolved in chloroform. Column formation leads to a red shift in the UV-Vis and a strong increase in fluorescence of the polymer compared to the monomer. Thus absorption and emission spectra of **49** and **1** were recorded in both water (supramolecular polymer state) and chloroform (monomer state). In both cases fluorescence intensity in water was roughly a factor of four higher than in chloroform (Figure 19). Additionally the red shift in the UV-Vis spectra of the local maximum of about 3 nm indicates column formation (Figure 20).

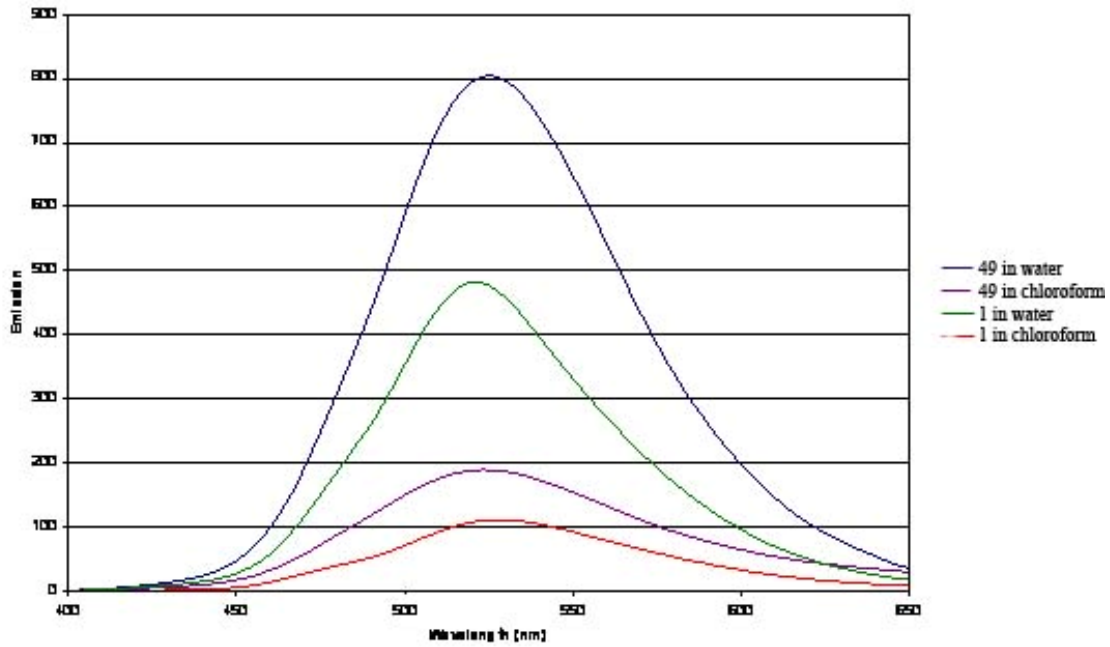

Figure 19. Fluorescence spectra of **1** and **49** in water and chloroform. Spectra were taken at an excitation wavelength of λ_{ex} = 340 nm.

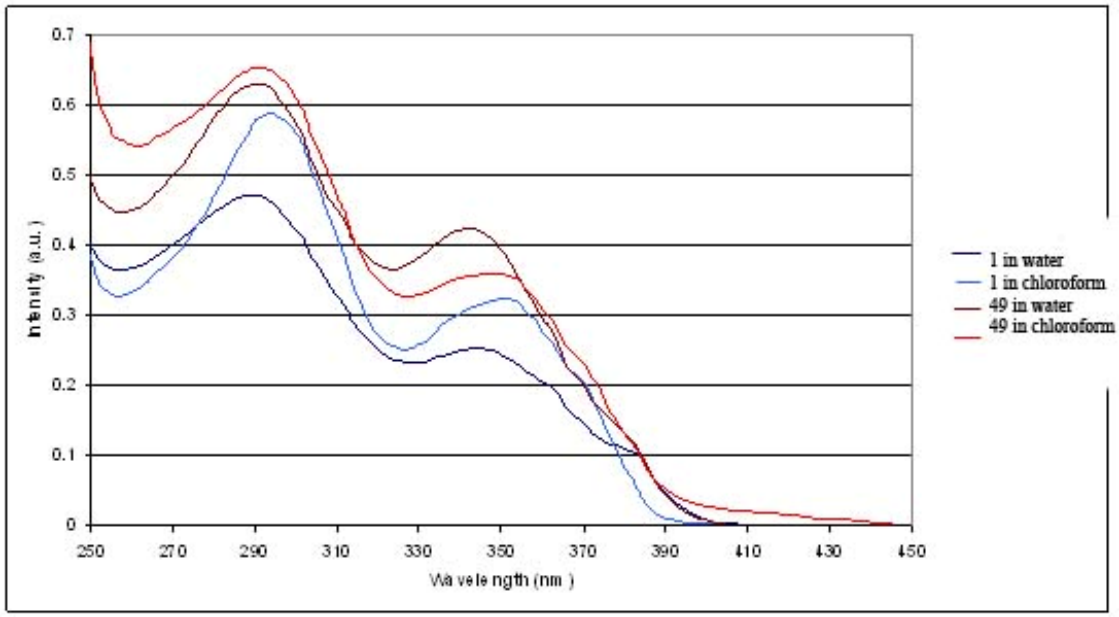

Figure 20. UV-Vis spectra of **1** (dark blue/indigo) and **49** (red/orange) in water (red/blue) and chloroform (green/purple).

3.3 Polyvalent Properties of Discotics

Mannose and mannose containing polymers are known to bind to the *E. coli.* FimH receptor.[3] The development of molecules with flexible polyvalent properties has been the subject of various studies.[38, 80] Prominent examples include glycodendrimers, -polymers, -copolymers and other compounds provided with mannose as polyvalent scaffold.[8, 15, 30, 31, 39, 81]
Multivalent architectures based on dynamic supramolecular discotics are studied here extensively for polyvalent tasks on bacterial surfaces, on streptavidin covered beads and on lectins.

3.3.1 Bacterial Assays

3.3.1.1 Binding of Mannose Discotic to BL 21α

The binding of polyvalent supramolecular polymers built up by **1** or **49** and mixtures thereof to bacteria was investigated *via* microscopy studies with the *E. coli* strain BL 21α. The bacteria were cultivated in LB media, washed, resuspended and incubated with either nonfunctionalized discotic **1**, mannosylated discotic **49**, or with water, for 1 h at room temperature.[42] The total concentration of discotic monomers **1** and **49** was kept highly dilute at 10^{-7} M. After washing and mounting on glass slides, binding to the bacteria was evaluated with a fluorescent microscope, taking advantage of the strong auto-fluorescence of the discotics when present as supramolecular polymer[68, 79] Images were taken both in brightfield and in fluorescence mode at an excitation wavelength of 360 nm and emission of 490 nm. Only when the bacteria were incubated with mannose modified discotic **49** a strong fluorescence of the bacterial aggregates could be observed, colocalizing with the brightfield image (Figure 21). Both the control experiments with non-functionalized scaffold **1** and with water did not show fluorescence. These results show that the polyvalent supramolecular polymers formed by **49** bind to the bacteria and that there is no unspecific binding of supramolecular polymers of **1** to the bacteria.

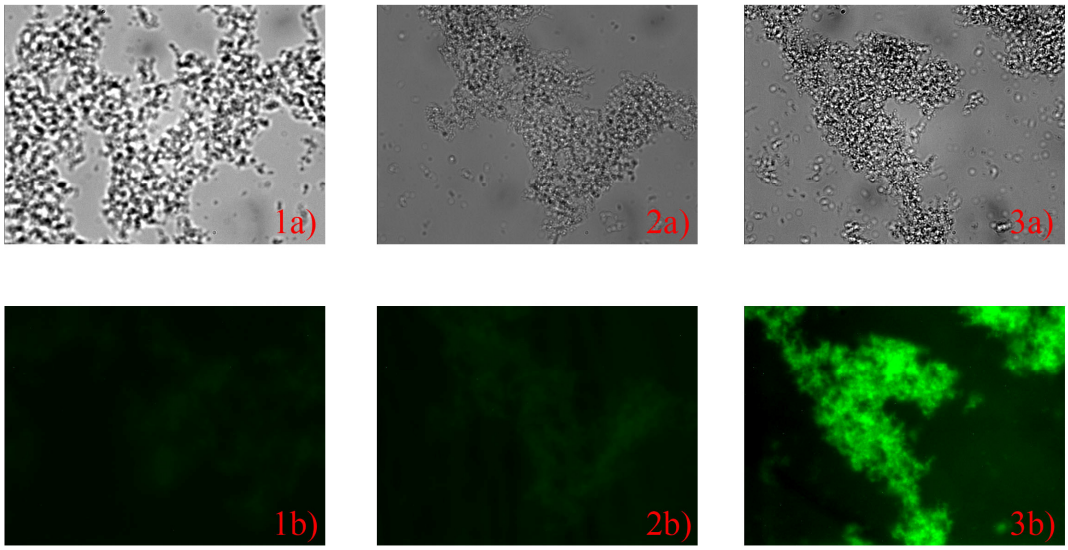

Figure 21. Microscopy pictures in a) brightfield and b) fluorescence (λ_{ex} = 360 nm, λ_{em} = 490 nm) mode on *E. coli* incubated with 1) water, 2) inert discotic **1**, 3) mannose discotic **49**.

3.3.1.2 Colocalization Studies with Auto-fluorescent E. coli

E. coli strain BL 21 α, transfected with a plasmid coding for pECFP, was used in order to perform exact fluorescence colocalization studies of the bacteria and the discotic compound. This bacterial strain expresses Cyan Fluorescent Protein (CFP) and therefore can be localized utilizing the fluorescent features of the protein. The assay was carried out following the procedure described above. In this case microscopy pictures were taken with brightfield, excitation wavelength of 360 nm and filters for CFP. Results are summarized in Figure 22 illustrating the colocalization of the discotic scaffold **49** (green) and the bacteria (blue). Control experiments with water and **1** do not result in a fluorescent response using filters for the discotic scaffold but show bright cyan auto-fluorescence of the bacteria (Figure 22; 1 and 2). Pictures taken after incubation of the *E. coli* with **49** convincingly demonstrate the co-localization of the green discotic fluorescence and the auto-fluorescence of the bacteria (Figure 22; 3).

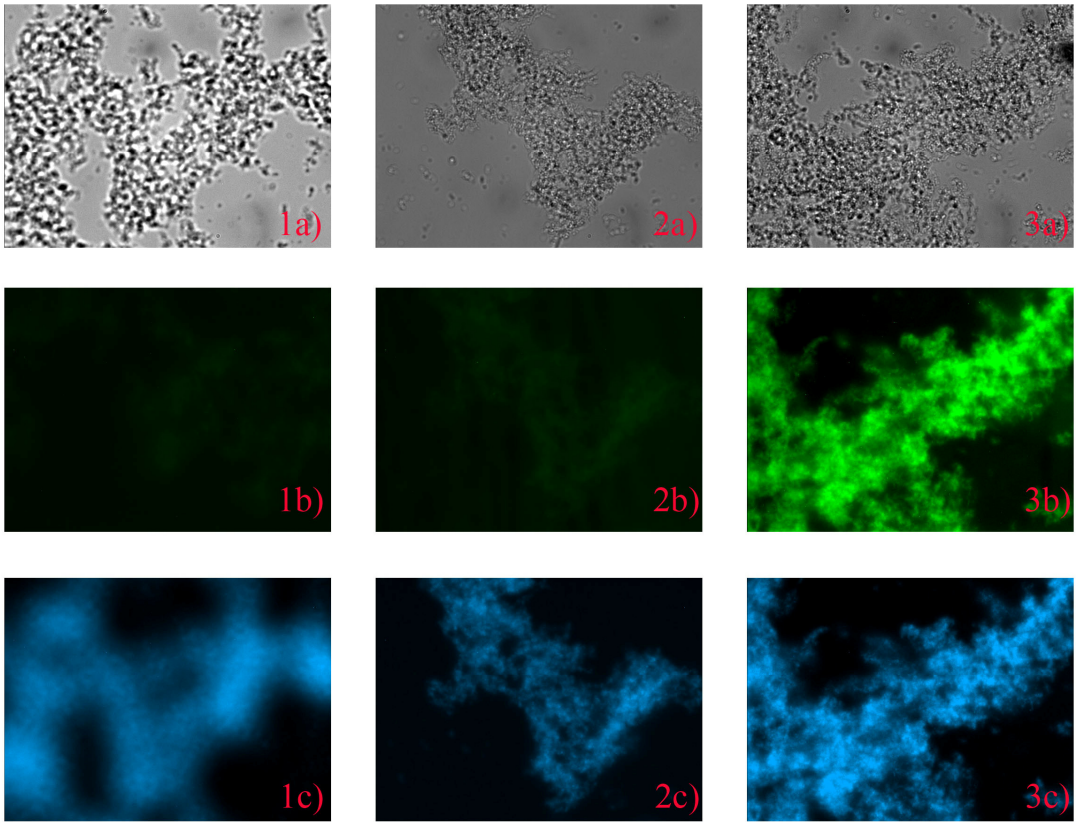

Figure 22. Microscopy pictures in a) brightfield and b) fluorescence (λ_{ex} = 360 nm, λ_{em} = 490 nm) mode c) fluorescence (CFP optical filter) on *E. coli* incubated with 1) water, 2) inert discotic **1**, 3) mannose discotic **49**.

3.3.1.3 Specificity of FimH Interaction

The specificity of the interaction of supramolecular polymers of **49** with the mannose binding FimH receptors on the bacterial surface was evaluated via binding studies to two *E. coli* strains ORN178 and ORN208[82]. These strains differ in their mannose-binding-properties due to the over-expression (ORN178) or suppression (ORN208) of the FimH receptor respectively.[82] Mixtures of **49** and ORN178 featured a strong fluorescence response where the bacteria were located, whereas no binding of **49** to ORN208 could be detected (Figure 23). These experiments show that the supramolecular polymers do not induce any unspecific binding and bind to the bacteria via the mannose-FimH receptor interaction selectively.

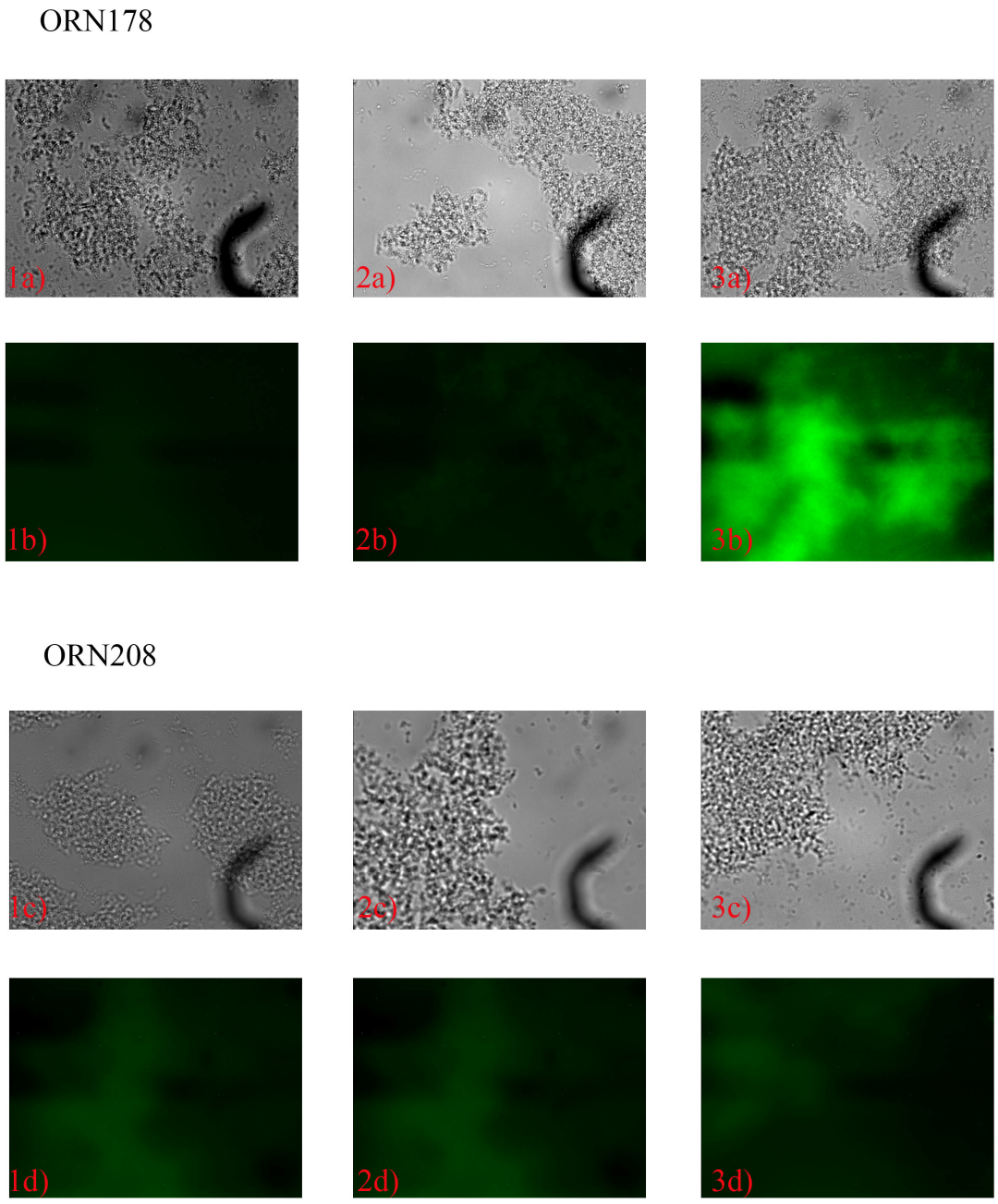

Figure 23. Studies on selective binding of **49** to FimH with *E. coli* strains ORN178 (overexpressed FimH) and ORN208 (no FimH); a) brightfield and b) fluorescence (optical filters at λ_{ex} = 360 nm, λ_{em} = 490 nm); *E. coli* incubated with 1) water, 2) inert discotic **1**, 3) mannose discotic **49**. A strong green fluorescence of the discotic scaffold is only detected on ORN178 incubated with **49** indicating that binding of **49** occurs selectively to FimH.

3.3.1.4 Bacterial Aggregation Studies

The influence of the supramolecular polymers on the clustering behavior of bacteria was further investigated. Only polyvalent molecules of sufficient size are able to interact with several bacteria at a time and induce clustering as indicated in Figure 24. Thus aggregation of bacteria serves as indication of columnar polyvalency.

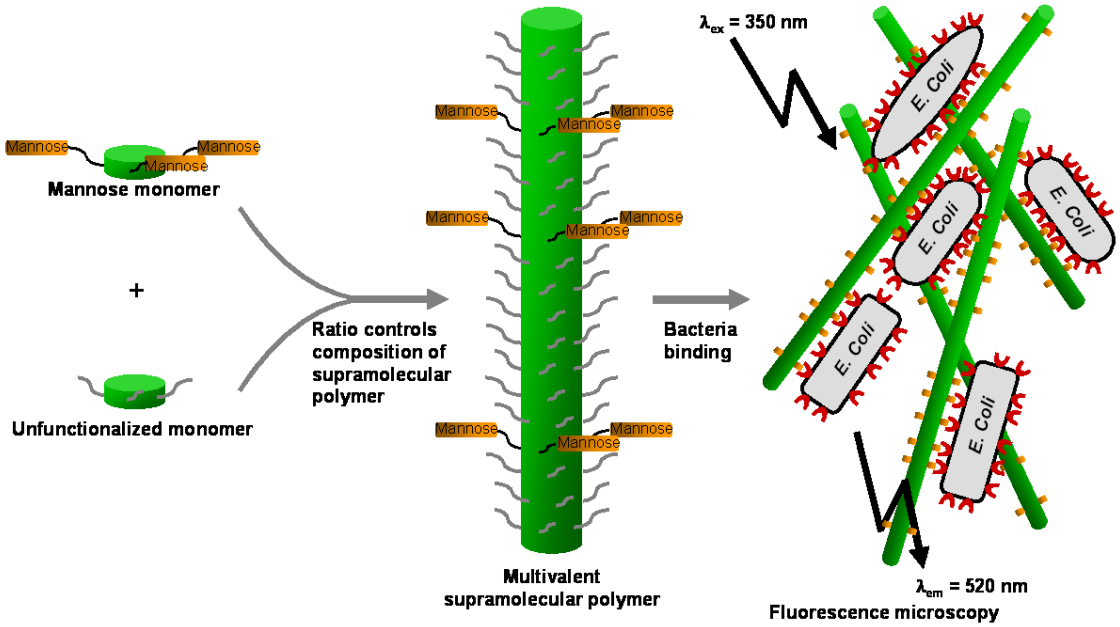

Figure 24. Schematic representation of the formation of polyvalent columnar supramolecular polymers, with control over ligand density *via* mixing of monomers, and the binding, clustering, and detection of bacteria with these polymers.

The polyvalent effect was evaluated on bacterial samples with dilute bacteria concentrations, at which the bacteria are present in non-aggregated state. When the bacteria were incubated with **49** the bacteria clustered and a colocalized fluorescence of the bacteria could be observed. Control experiments with either **1** or water only showed dispersed bacteria (Figure 24). This result demonstrates that the polyvalent supramolecular polymers induce the formation of bacterial aggregates by virtue of their polyvalent nature. Apparently the supramolecular polymers are long enough to function as crosslinking scaffolds for the bacteria, just like conventional polymers.[52] The outcome is especially interesting, considering that the concentration of

discotics is highly dilute at 10^{-7} M. That concentration corresponds to an average column length in water of approximately 7 supramolecules (degree of polymerization DP = 2 x √(K x concentration) with K_{ass} = 1 x 10^8 L x mol^{-1} at 20 °C and c = 10^{-7} mol x L^{-1}).[68] The interaction with the bacteria apparently brings the single supramolecular columns in local proximity and thus enables formation of longer columns even at this high dilution. Finally these supramolecular architectures are large enough to interact with several bacteria at a time.

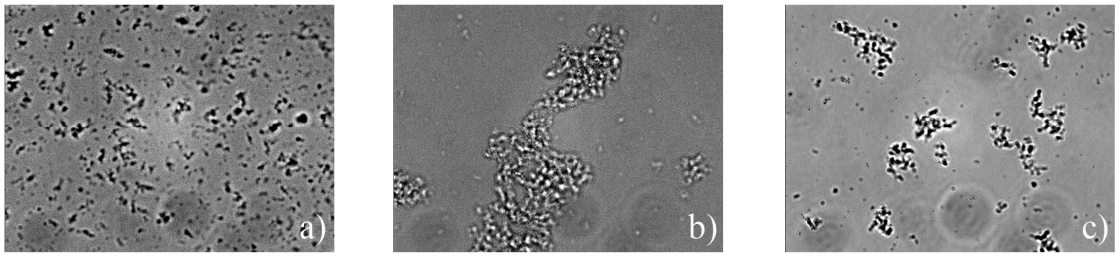

Figure 25. Microscopy pictures in brightfield mode on dilute bacterial samples incubated with a) 100% **1**, b) 99/1 **1/49** and c) 100% **49**.

In order to evaluate the influence of ligand density, supramolecular polymers consisting of mixtures of both **1** and **49** were generated and similarly evaluated at dilute bacteria concentrations. These supramolecular copolymers were inducing bacterial aggregation at all monomer compositions evaluated (Figure 25 and Figure 26). A functional monomer percentage of **49** as low as 1% still resulted in the formation of bacterial aggregates. Evidently, only a limited number of mannose functionalities at the periphery of the supramolecular polymer are required to induce clustering of the bacteria around the columnar architecture. Furthermore, the supramolecular polymers are sufficiently long to bridge the distances between the diluted functional monomers **49** to induce bacterial cross-linking (Figure 25). Interestingly, the aggregates observed for the supramolecular polymers diluted with non-functionalized discotic **1** were typically larger than those induced by polymers consisting of **49** only. This indicates that optimal binding to bacteria occurs when only a limited number of mannose functionalized monomers is present, surrounded by non-functionalized monomers. Apparently, overcrowding of the supramolecular

polymer with ligands results in sub-optimal binding. The dynamic and flexibility of mixed supramolecular columns consisting of **49** and **1**, on the other hand, facilitate optimal binding to the receptors. The unique supramolecular nature of the polymers thus allows easy adjustments and optimization of the monomer composition.

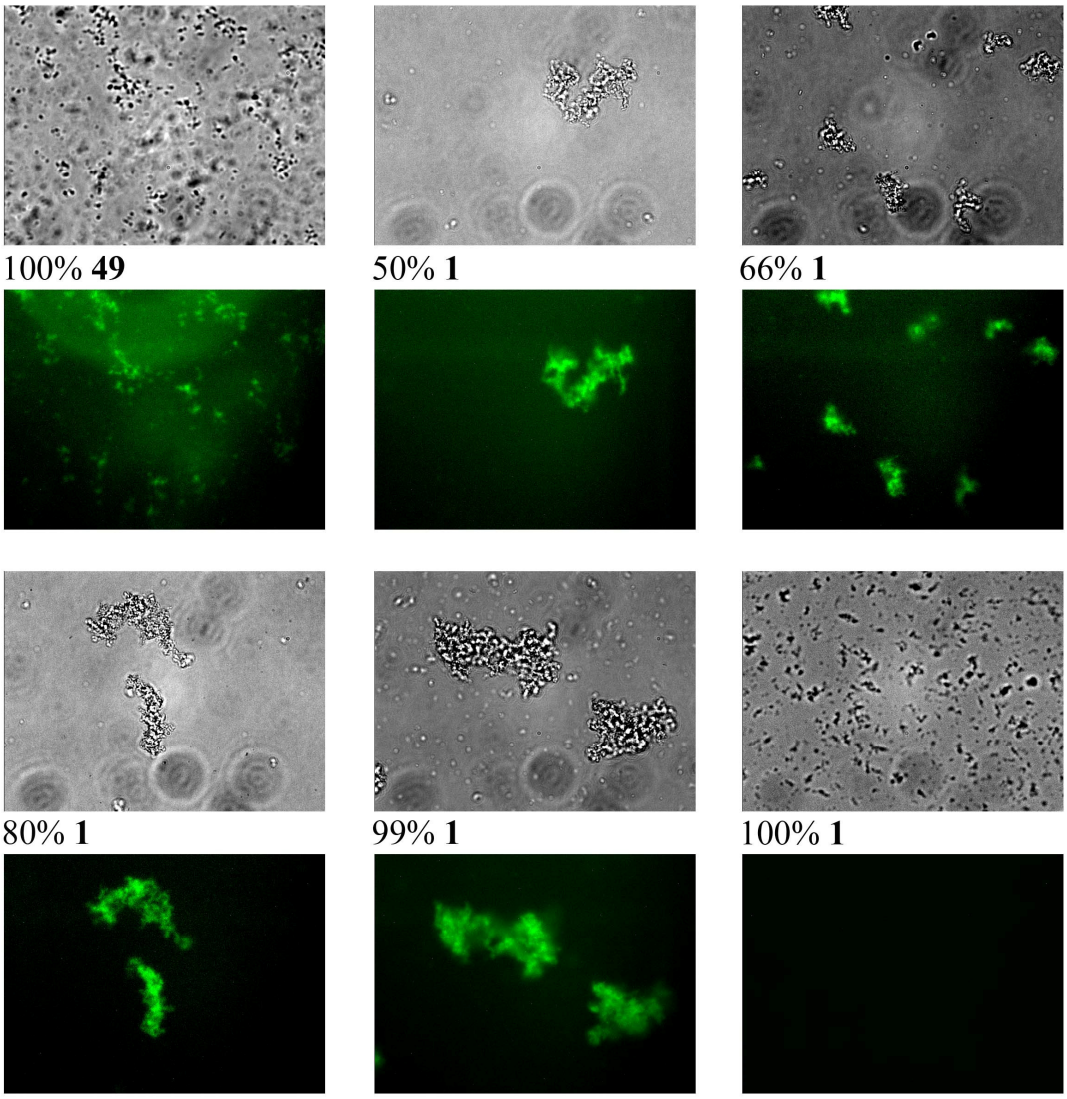

Figure 26. BL 21 α after incubation with varying mixtures of inert discotic **1** and mannose discotic **49**. Pictures were taken in brightfield (above) and fluorescence mode (optical filters λ_{ex} = 360 nm, λ_{em} = 490 nm) (below). No bacterial aggregation is induced by compound **1**, but mixtures of **1** and **49** and compound **49** alone strongly induce bacterial aggregation.

3.3.1.5 Mannose Competition Assay

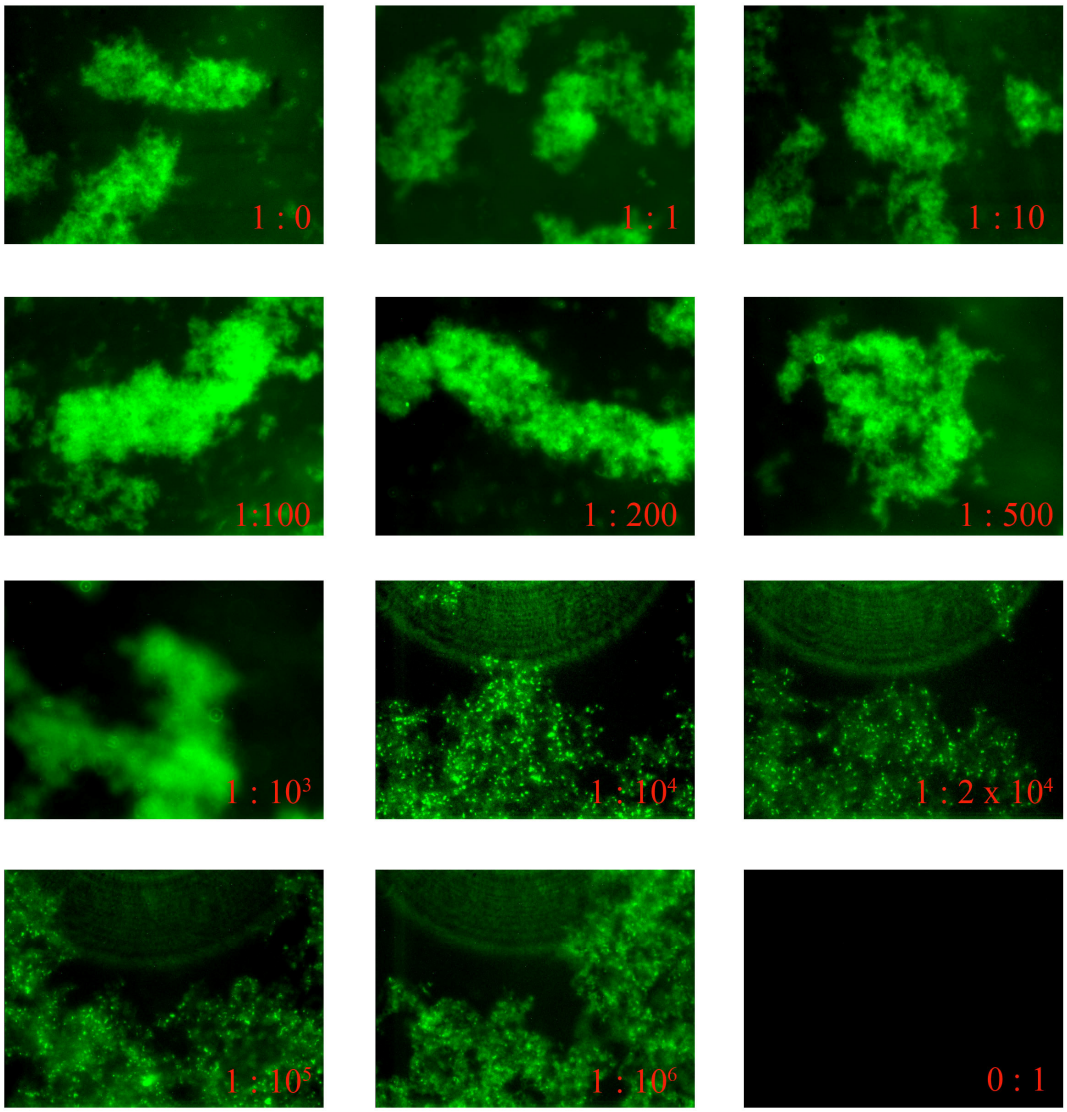

Figure 27. Mannose competition assay; Excess of mannose compared to **49** ranging from 1:1 to 1:10^6; 100% **49** (1:0) and 100% (0:1) mannose were measured as control experiments; fluorescence pictures were taken with optical filters at λ_{ex} = 360 nm, λ_{em} = 490 nm.

A competition experiment between the supramolecular polymers formed by **49** and mannose on bacteria binding was performed to examine the strength of the polyvalent binding of the supramolecular polymer. In order to allow the most effective competition by the mannose, the bacteria were first incubated with different concentrations of mannose for ten minutes, after which discotic **49** was added, again at the dilute concentration of 10^{-7} M (Figure 27). The

bacteria remained fluorescent over the whole concentration range studied. Even at a 10^6-fold excess of free mannose the bacteria were still highly fluorescent and there was no indication that the binding of **49** to the *E. coli* cell surfaces was diminished. These results show that there is a highly efficient polyvalent binding of the supramolecular polymers to the bacteria, significantly stronger than the monovalent binding of mannose.

3.3.1.6 Influence of the Mannose Discotic on Bacterial Growth

The microscopic pictures imply that the supramolecular architectures cover the bacterial cell surface. It can be expected that this artificial coat influences bacterial metabolism and cell division. This could be shown by an experiment in which bacteria were grown overnight, washed and resuspended in LB media to reach an OD_{600} of 0.5. Subsequently either water, **1** or **49** was added and the cells were incubated for 4 h at 37 °C after which the OD_{600} was measured again. Averages over three experiments are summarized in Table 1. Results show that only in case of interaction of the supramolecules with the *E. coli* bacterial cell growth was decelerated approximately twofold. Thus the mannose functionalized discotics coat the *E. coli* and influence their metabolism efficiently.

Table 1. Influence of **49** on bacterial cell growth. OD_{600} 4 h after incubation. Mean over three experiments.

	Mean ± standard deviation
OD_{600} (water)	1.98 ± 0.12
OD_{600} (**1**)	1.92 ± 0.09
OD_{600} (**49**)	1.14 ± 0.08

3.3.2 Polyvalent Binding to Lectins

A wide range of assays has been developed to evaluate the protein-carbohydrate binding constants.[28] Typically, the outcome is highly dependent on the type of assay, and thorough revision of the results in the context of the multivalent interaction is essential. The four most widely used techniques are the hemagglutination inhibition assay (HIA),[83] enzyme linked lectine assay (ELLA),[84] isothermal titration microcalorimetry (ITC)[85] and surface plasmon resonance assay (SPR)[86, 87]. HIA is often used to determine aggregation and precipitation properties of multivalent polymers, but high aberration in IC_{50} values only allow rough classification of binding affinity. On the other hand, ELLA does not involve aggregation but is based on inhibition and polyvalent effects. IC_{50} values are relatively precise, as determined by curve fitting. Therefore, ELLA was chosen for our studies on protein-carbohydrate binding.

In order to quantify the polyvalent binding of the supramolecular polymers of **49**, an enzyme linked lectine assay (ELLA)[28], a variation of the enzyme-linked immunosorbant assay (ELISA),[84] was performed. Mannose coated polyvalent structures are known to inhibit Concanavalin A (Con A) binding to the yeast cell surface receptor mannan competitively. Con A is a tetramer at neutral pH, containing four spatially well separated binding sites (6.5 nm) for oligosaccharides.[88]

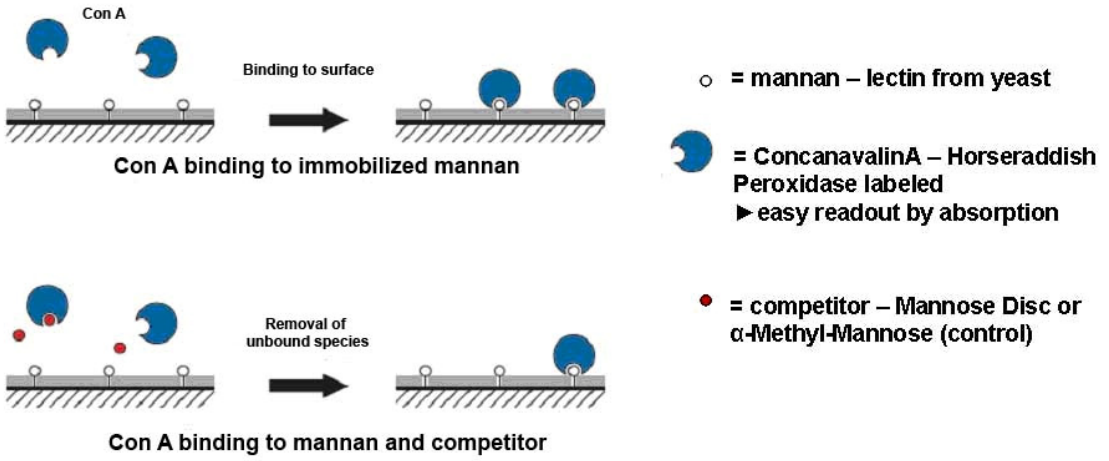

Figure 28. Cartoon to illustrate Con A binding to immobilized mannan and inhibition of binding by an inhibitor.

Experiments using horseradish peroxidase labeled Con A (HRP-Con A) as the lectin and yeast mannan as surface fixed ligand were carried out in 96-well plates, as illustrated in Figure 28. Optimal concentration of Con A was evaluated prior to the inhibition experiments. After pre-incubation with different concentrations of **49**, binding of HRP-Con A to mannan was measured photospectrometrically. Methyl-α-D-mannopyranoside served as reference compound. The inhibition of lectin binding was measured in three independent experiments and the IC_{50} values were determined from the corresponding inhibition curves (Figure 29). Typically, complete inhibition of lectin binding to mannan in the ELLA is seldom observed and maximum inhibition occurs at less than 100%.[28] A strong inhibition for **49** compared to α-D-methyl-mannopyranoside could be observed.

Control experiments with inert discotic **1** did not indicate unspecific binding or other interference of the discotic scaffold. The IC_{50} value for the methyl-glycoside was in our assay around 3 mM and the IC_{50} value for **49** around 120 µM (360 µM, valency-corrected). The relative valency corrected binding of **49** was 8.3 times stronger than the reference compound (24.9 per molecule **49**), showing the polyvalent effect of the supramolecular polymers.

Typically, small trivalent ligands do not show significant valency corrected enhancement effects to higher valency in specific lectin–ligand assays, such as the ELLA assay, as they cannot span the distances between the binding sites on the Con A. [89, 90] For these small individual scaffolds higher valencies improve the total potency, but do not improve valency corrected potency, which results merely from the 'cluster glycoside effect'.[22, 28] The supramolecular polymers formed by **49**, however, allow effective polyvalent binding up to high valencies and show high potency per ligand. Apparently, because of the polymeric nature of **49**, the compounds are capable of spanning the distance between the mannose binding sites on Con A.

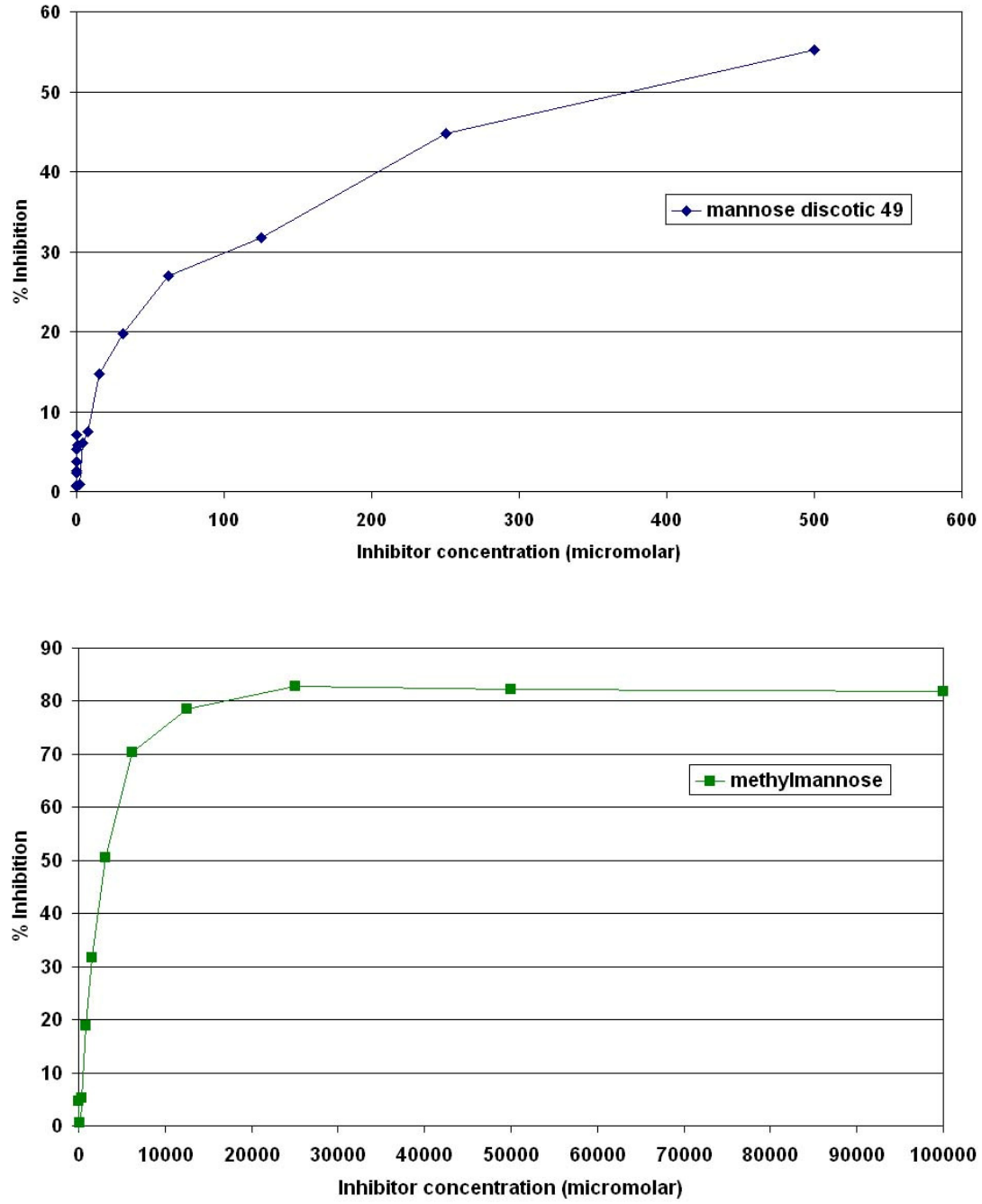

Figure 29. Inhibition curves of mannose modified discotic **49** (above) and methyl-α-D-mannopyranoside (below) for determination of the IC_{50}. Inhibitor concentrations are valency corrected.

In order to investigate the scope of the spanning properties of our supramolecular system, the assay was repeated using different mixtures of **49** with **1**. Mixtures with **49/1** ratios of 1/0, 1/1, 1/2, 1/5 and 1/10 were prepared 12 h prior to the experiments. Controls using **1** alone did not show any

unspecific interference of the inert scaffold. In each dilution series the same total amount of discotic was used (c[**49**] + c[**1**] = constant). Thus the maximum amount of inhibitor **49** was different in each case. Figure 30 shows the different inhibition curves. On the x-axis the absolute percentage of 49 at each determined data point was plotted. The highest amount of inhibitor, with a concentration of about 120 µM, was therefore set as 100%. The inhibition values plotted on the y-axis of Figure 30 can be directly correlated to the amount of inhibitor (c[**49**]) present at this data point. Thus, data points with the same percentage of **49** (= same concentration of **49**), but different total amounts of discotic mixtures (c[**49**] + c[**1**]) illustrate enhanced or decreased binding properties of the inhibitor **49** in presence of **1**. Pure **49** reached a maximum inhibition of about 50% when having 100% inhibitor in solution, about 40% inhibition with 50% inhibitor (~60 µM) and about 25% inhibition with 33% (~40 µM) inhibitor. Maximum of the 1/1 mixture was 53% inhibition with 50% (~60 µM) inhibitor and the maximum of the 1/2 mixture reached 37% inhibition with 33% (~40 µM) inhibitor. 1/5 and 1/10 mixtures were too low in inhibitor concentration and did not reach a value high enough in range for comparison. Unexpectedly, the inhibition curves of the 1/1 and 1/2 mixtures cross the curve of pure **49**. This indicates that, with a relative percentage higher than 33% of **49**, inhibition is more effective in presence of spacer **1**. Below this value the pure discotic **49** is the better inhibitor.

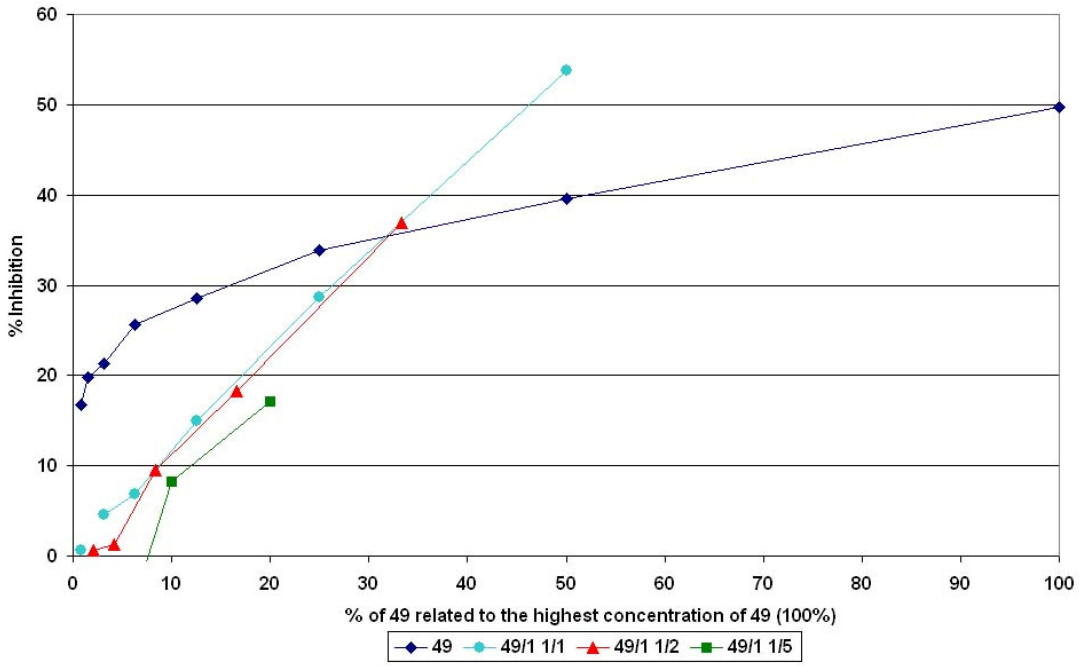

Figure 30. Inhibition curves of mannose modified discotic **49** (blue) and mixtures of **49** and **1** 1/1 (purple); 1/2 (green) and 1/5 (red).

These results give rise to the assumption that below a certain concentration of 33% inhibitor (~40 µM), the spatial proximity of the different mannose ligands enhances the binding abilities of the supramolecules. Above that value sufficient inhibitor is present. This leads to the conclusion that there might be a maximum in polyvalency for ideal inhibition of Con A binding.

These results are most probably due to the nature of the protein-carbohydrate interaction. As mentioned before, results from protein-carbohydrate binding and inhibition studies are highly dependent on the assay performed. In this ELLA, the multivalent interaction is based on inhibition of Con A binding to mannan. We suggest, that the high potency of Con A inhibition of **49** probably results from the ability of the supramolecular columns to span different binding sites of the lectins. Furthermore, we assume that interaction with the lectin results in stabilization of the columnar structures in proximity of the protein due to the cluster glycoside effect.

In case of mixtures of the different supramolecules **1**/**49** this stabilization does not take place at all concentrations. Most probably this is due to the size dependence of the columns according to their concentration. At high

concentrations (≥ 40 µM) the mixed supramolecular structures form columns of more than 100 supramolecules per polymer.[68] In case of 1/1 and 1/2 mixtures the supramolecules are big enough to feature sufficient mannose ligands on their periphery and probably are able to span the distances between binding pockets. Thus, mixtures of **1** and **49** enhance relative binding potency per mannose moiety at higher concentrations.

On the other hand, ligand concentration on the mixed supramolecular columns in dilute solutions (< 40 µM) is low. In this case, we assume that no, or much less column stabilization is induced by the interaction with the protein. The columnar structures apparently cannot span the distance between two binding sites at the protein. Thus the relative decrease of glycoside on the multivalent structures leads to decreased inhibition.

Unlike the results of discotic mixtures applied to multivalent bacterial surfaces, which were apparently able to provide steric advantages that led to cross linkages of columns between bacteria, in this lectine inhibition assay steric flexibility seemed to be of limited advantage for enhanced inhibition. These results show that also in case of our supramolecules the outcome of the polyvalent interaction is highly dependent on the type of biological polyvalency that is assessed. Aggregation in the bacterial assay led to an enhanced cluster glycoside effect in case of discotic mixtures. The ELLA is not based on aggregation and thus appeared to be concentration dependent when performed with discotic mixtures.

Overall, these results indicate that in case of ELLA, introduction of **1** as spacer for ideal spatial rearrangement enhances inhibition properties of the mannose discotic at concentrations higher than 40 µM.

3.3.3 Studies on Heterovalency

In order to investigate heterovalent properties of the supramolecular polymers, the mannose discotic **49** was mixed with Texas Red discotic **52**. The red dye provides the possibility to study the behavior of supramolecular scaffolds modified with different ligands through independent detection. As illustrated in Figure 31, the discotic with the mannose ligand (**49**) serves as targeting element for the discotic with the Texas Red ligand (**52**). Such a system could be applied to any combination of ligands attached to the discotic scaffold.

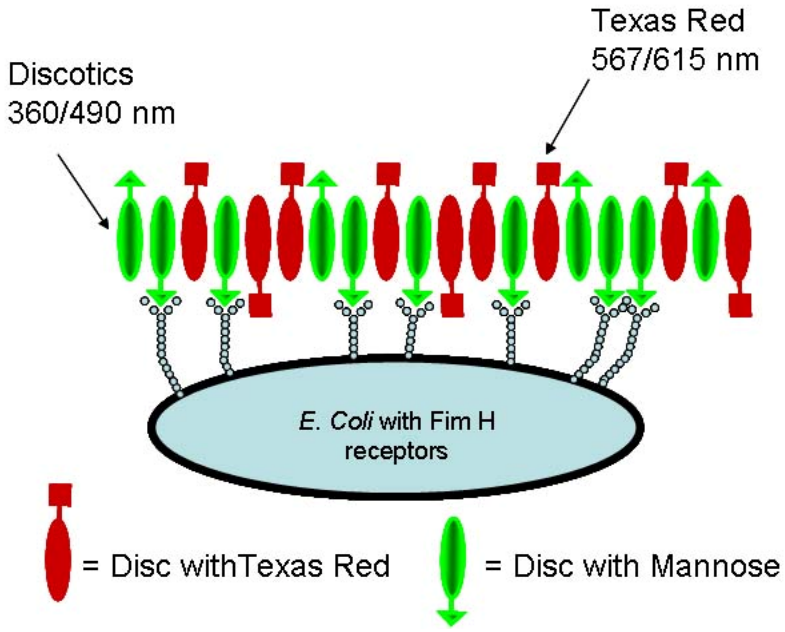

Figure 31. Cartoon demonstrating the localization of Texas Red Discotic at the interaction surface of the mannose discotic **49**. **49** serves as targeting element for **52**.

Mixtures (1/1 and 99/1) of **49** and **52** were prepared four hours prior to the experiments to ensure the formation of a random mixture of the two differently functionalized discotics in the columns. Bacteria were incubated at a total discotic concentration of 10^{-7} M. Microscopy pictures were taken in brightfield and in fluorescence mode with either a filter for the discotic scaffold (λ_{ex} = 360 nm, λ_{em} = 490 nm) or a filter for the Texas Red dye (λ_{ex} = 569 nm, λ_{em} = 620 nm). Control experiments were carried out using pure **49** and pure **52**.

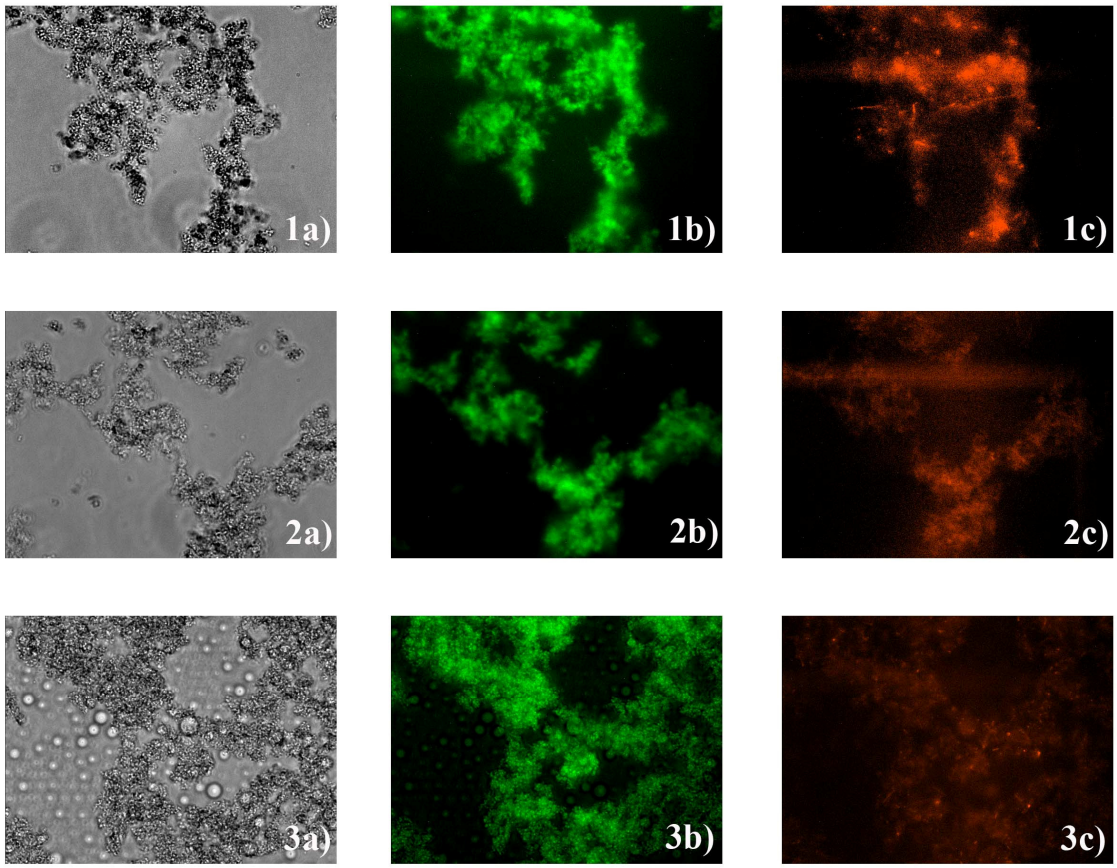

Figure 32. BL 21 α after incubation with varying mixtures of mannose discotic **49** and **52**. 1) **49/52** 1/1, 2) **49/52** 99/1, 3) **52**; Pictures were taken in a) brightfield, b) fluorescence (λ_{ex} = 360 nm, λ_{em} = 490 nm) mode and c) fluorescence (λ_{ex} = 569 nm, λ_{em} = 620 nm) mode. Control experiments 3b)-c) show unspecific binding of **52** to *E. coli*.

As shown in Figure 32, incubation with the discotic mixtures of 1/1 and 99/1 in both cases led to a fluorescent response of the discotic and the Texas Red dye on the bacterial cell surface. However, control experiments carried out with pure Texas Red discotic **52** also showed fluorescence of Texas Red to the bacteria and thus indicate unspecific binding of the pure Texas Red discotic **52** to *E. coli* as illustrated in Figure 32; 3c). The strong discotic fluorescence is still detected on the bacterial cell surface even if incubated with pure **52** only. Though the intensity of Texas Red is decreasing from picture 1c) to 3c), change of fluorescence filters from Texas Red filters to the wavelength of the discotic shows no change in response of the discotic fluorescence on the cells in presence or absence of **49**. At these concentrations the Texas Red discotic

apparently binds unspecific to *E. coli*. Reliable quantification of the amount of discotics binding to the bacteria in experiments 1-3 was not possible.
The decrease of the Texas Red intensity detected from experiment 1-3 nevertheless leads to the assumption that the presence of **49** increases the localization of **52** on the bacteria cell surface.

3.3.3.1 Polyvalent Binding to Streptavidin coated Beads

We decided to evaluate the heterovalent binding of the supramolecular system taking advantage of the strong biotin-streptavidin interaction. Binding studies of mixtures of Texas Red discotic **52** with biotin discotic **53** to a different surface were carried out.
In order to broaden the scope of the supramolecular interaction to a different polyvalent surface, a model system based on streptavidin coated beads[91] was investigated. The binding of biotin discotic **53** to magnetic streptavidin beads was tested. The beads were incubated with **53** and **1** at concentrations of 10^{-7} M. Magnetism of the beads guaranteed comfortable handling and washing. The beads were assembled as a pellet on the bottom of the vial with help of a magnet and the washing solution was removed carefully with a pipette. Subsequently, the beads were mounted on glass slides and fluorescent pictures were evaluated. Only when the beads were incubated with biotin modified discotic **53** a strong fluorescence of the single beads could be observed, colocalizing with the brightfield image (Figure 33; 1). Unspecific binding of the discotic scaffold **1** to the beads did not occur (Figure 33; 2).

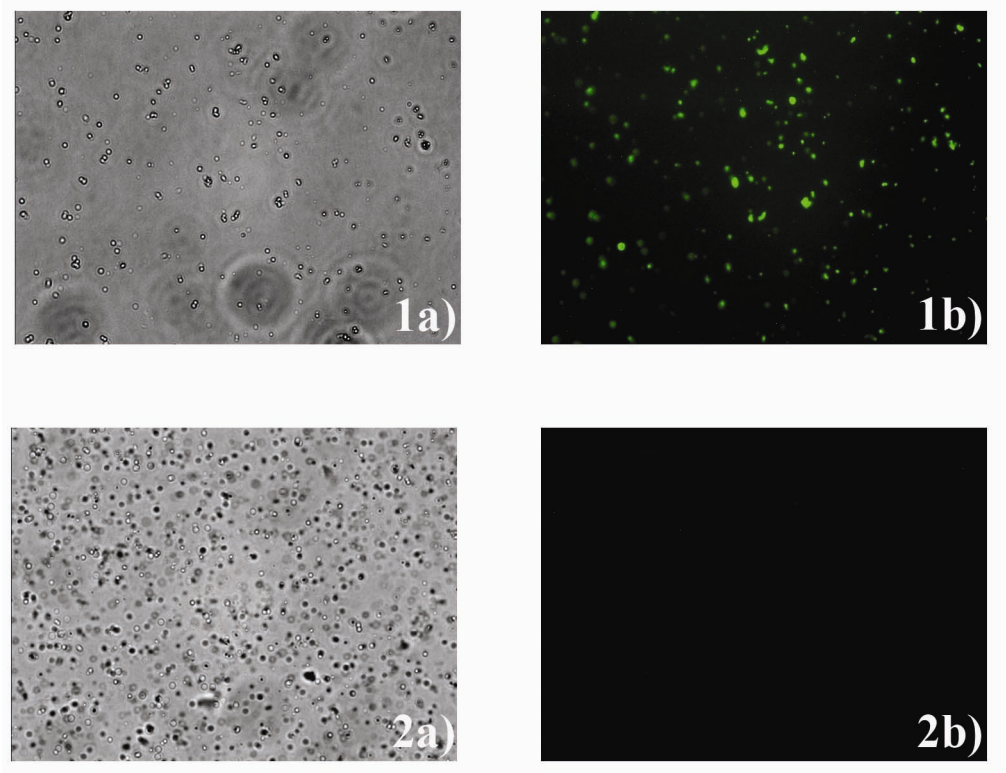

Figure 33. Magnetic Streptavidin beads after incubation with 1) mannose discotic **49** and 2) inert discotic **1**; pictures were taken in a) brightfield, b) fluorescence (λ_{ex} = 360 nm, λ_{em} = 490 nm) mode. Control experiments 2a) and b) indicate no unspecific binding of **1** to streptavidin.

Using this polyvalent streptavidin surface, heterovalency experiments with the Texas Red discotic **52** were carried out. A mixture of **53** and **52** (1/1) was prepared twelve hours prior to the experiments to ensure a complete random mixture of the two differently functionalized discotics in the columns. Beads were incubated with a mixture of **53** and **52** at total concentrations of 10^{-7} M washed and fixed on glass slides. Pure **53** and pure **52** served as controls. Microscopy pictures, summarized in Figure 34, were taken in brightfield mode and in fluorescent mode, with a filter for the discotic scaffold (λ_{ex} = 360 nm, λ_{em} = 490 nm) and a filter for the Texas Red dye (λ_{ex} = 569 nm, λ_{em} = 620 nm). Incubation of the streptavidin beads with the mixtures resulted in strong fluorescence response of both, the discotic scaffold and the Texas Red dye, on the bead surface (Figure 34; 2). Control experiments indicate no unspecific binding of the pure Texas Red discotic **52** to the Streptavidin beads (Figure 34; 3). Control studies with the pure biotin discotic **53** prove that the discotic

scaffold was not excited at the **52** excitation wavelength (Figure 34; 1). These results demonstrate that the differently functionalized discotics form randomized columns. The biotin discotic thus serves as interaction partner with the Streptavidin surface and at the same time as transport system for the Texas Red discotic. The flexibility of the system therefore provides convenient access to polyvalent supramolecules featuring different ligands. As shown in this experiment the supramolecular approach gives rise to new highly flexible polyvalent substances. Polyvalent scaffolds with multiple ligands of choice for different purposes and interactions can be easily prepared by simple mixture of the corresponding discotics.

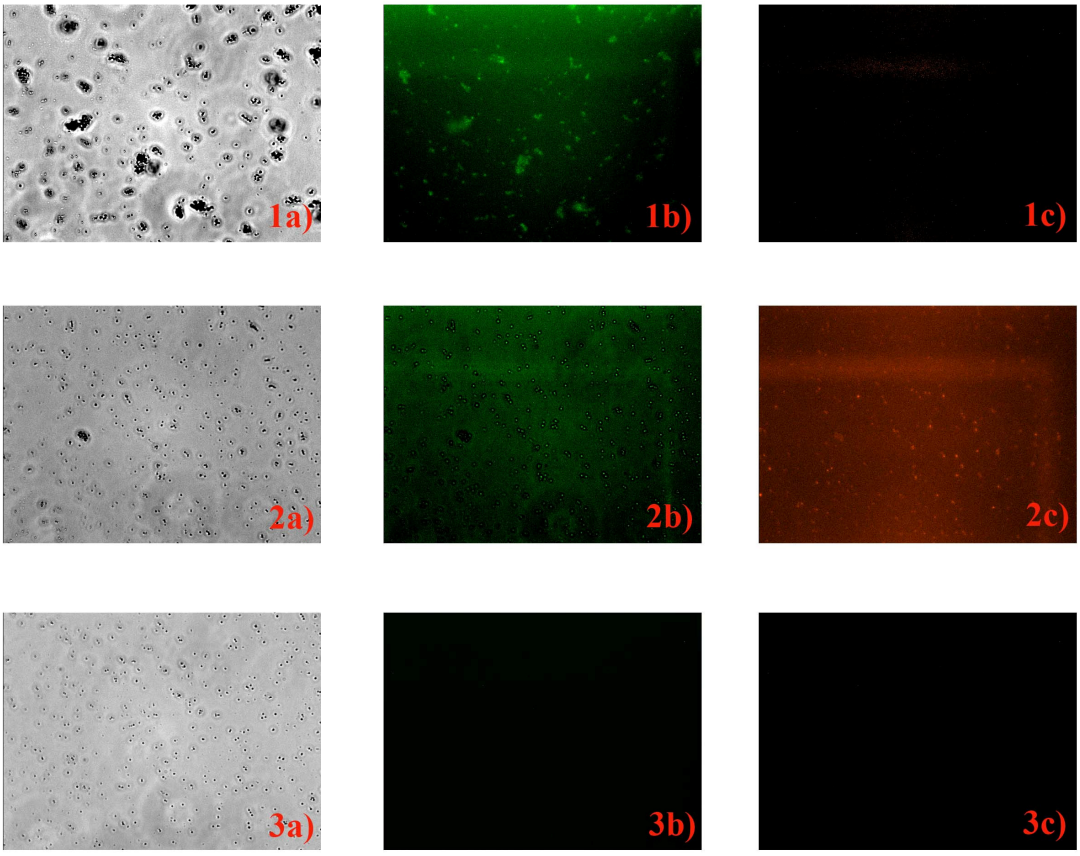

Figure 34. Microscopy pictures in a) brightfield, b) fluorescence (λ_{ex} = 360 nm, λ_{em} = 490 nm) mode and c) fluorescence (λ_{ex} = 569 nm, λ_{em} = 620 nm) mode on magnetic streptavidin seads incubated with 1) **53**, 2) **53/52** 1/1, 3) **52**.

3.4 Supramolecular Modulation of Protein Assembly

Supramolecular chemistry has allowed the development of self-assembling systems whose drive to assemble and disassemble is controlled by the reversible interactions of specific control elements that are tunable through external factors such as light, environment, and exogenous ligands.[54] In chemical biology, control over protein localization and assembly and the resulting activation and deactivation has been exploited with supramolecules for the study of, for example, signal transduction,[92, 93] tubulin stabilization,[94] and transcription factors.[95-97] Typically these studies included the use of small-molecular tools and their interaction with specific protein domains. Synthetic supramolecular constructs have been used to act as binding elements to protein substructures.[98-101] The use of synthetic supramolecular control elements like cyclodextrin hosts and steroid ligands to effect protein localization or function has successfully been applied.[102]

The use of supramolecular non-covalent recognition by synthetic supramolecular elements for the control of protein assembly and subsequent inhibition of assembly with an exogenous molecule has been reported by our group previously.[102] In this context, concentration dependent self-assembling supramolecular discotics provide excellent properties to serve as control elements for protein assembly.

3.4.1 Protein-Assembly Controlled by Supramolecular Polymers

Self-assembling supramolecular discotics are a new class of promising multivalent scaffolds (Chapter 3.3). We showed that mixtures of functionalized and inert discotics are able to arrange themselves to a multivalent receptor functionalized surface in an optimized manner due to the ability to rearrange monomers in the supramolecules. In a next step discotics were envisaged to serve as platform for control over protein assembly. Discotics were planned to be ligated to different proteins and use the self-assembly of the discotics to induce the assembly of these proteins. Attachment of the proteins was envisaged to be performed using the cysteine discotic **56**, which enables

native chemical ligation to the protein. Subsequent to protein coupling, the supramolecular system was envisaged to modulate the interaction of two proteins by varying the concentration of protein-discotics in solution. As an additional tool to adjust the protein assembly, inert discotics were foreseen to serve as spacer increasing the distance between the protein-functionalized discotics. In order to establish the concept of protein assembly along the supramolecular polymers a model system based on two proteins that feature fluorescence energy transfer, when brought together, was studies.

The non-radiative transfer of energy, after light absorption by one fluorescent substance to another is called Foerster resonance energy transfer (FRET). FRET between two fluorescent partners takes place, if the emitted wavelength of one fluorescent dye overlaps with the excitation wavelength of a second dye. If the two interaction partners are in close proximity (less than 100 Å), the energy of the FRET-donor can be transferred non-radiatively to the FRET-acceptor and emission of the acceptor can be detected.[103]

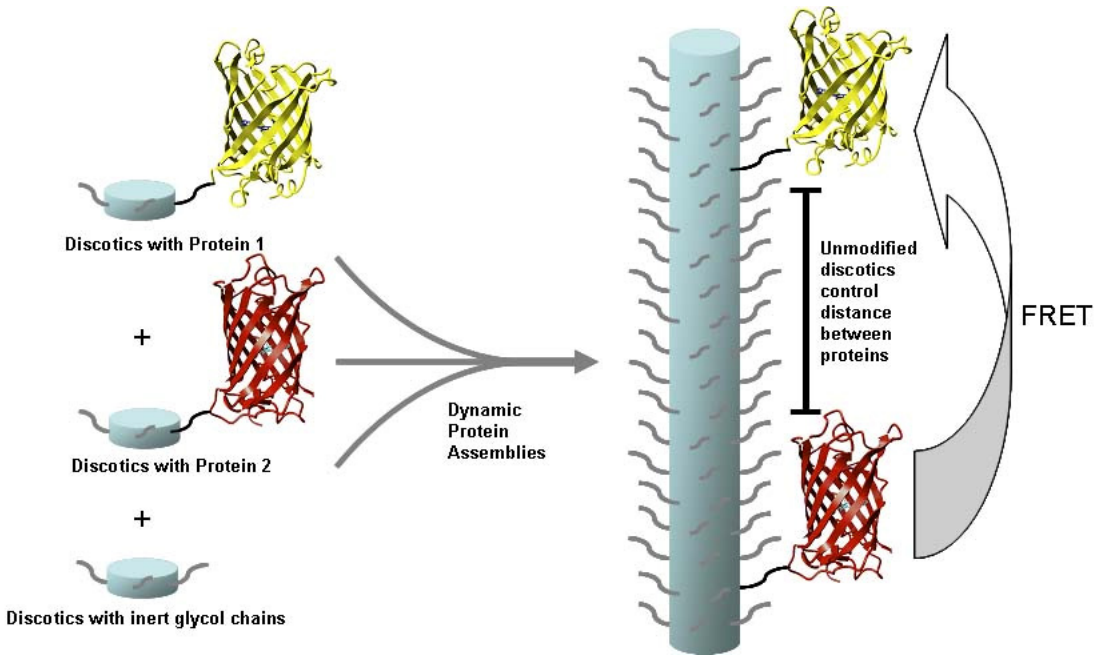

Scheme 16. Concept of supramolecular polymers as scaffold to control protein-protein interactions. The spatial distance of the proteins is controlled *via* concentration change of inert discotics.

This principle is used here to study the supramolecular assembly of protein interaction and is based on a FRET pair attached to different discotics. The concept is illustrated in Scheme 16. The FRET donor (red) is excited and transfers its energy to the acceptor (yellow). The unmodified discotics control the distance between the proteins. Thus, the FRET pair should be influenced by the concentration of the dye-carrying discotics and by the amount of inert discotics given to the system.

3.4.2 Modification of the Discotic with Yellow Fluorescent Protein

The influence on modulation of proteins with supramolecular polymers was first to be investigated with the protein model system of cyan fluorescent protein (CFP) / yellow fluorescent protein (YFP). These two proteins are a well known FRET-pair.[104] This property provides excellent conditions to investigate control over protein interaction by fluorescence readout. CFP and YFP were envisaged to be attached to the discotic scaffold **56** provided with cysteines (Chapter 3.2.4) *via* native chemical ligation.

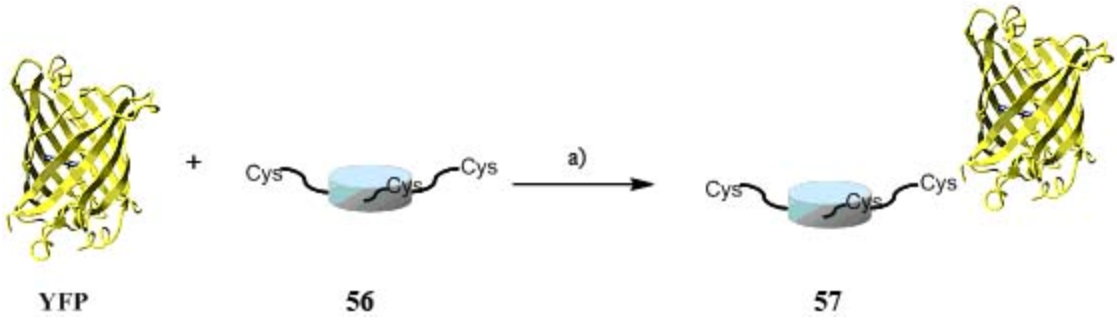

Scheme 17. Expressed protein ligation of YFP with the cysteine discotic **56**. a) Mesna, NaPi, 2 w, rt.

YFP was expressed in *E.coli* using a plasmid, pTWIN1-EYFP, derived from a previously described procedure, and isolated.[102] The protein was coupled to the discotic **56** by expressed protein ligation using a 10-fold excess of discotic. The reaction was monitored by MALDI-TOF MS. The ligation procedure that was followed was reported to be complete within 4 h for a monovalent small molecule.[102] However, in our case the coupling proceeded extremely slowly. Within the first 3 h only a small amount of product **57** was formed and detected by MALDI-TOF MS (Figure 35). Even after three days of reaction time, only a

small part of protein reacted with the free cysteine as visualized by SDS gel (Figure 35; c). Unfortunately, an undesired side reaction took place. Under the reaction conditions the cysteine discotics started to cross-link, forming disulfide bridges. Polymerization of the discotic **56** *via* covalent disulfide bridges seemed to happen faster than the protein ligation. Though the quantity of the desired product **57** seemed to have increased after 2 d, a MALDI-TOF spectrum (Figure 35) shows that the main part of the protein is still unligated. The remaining free cysteines on the discotic of the desired product **57** apparently reacted with other discotics in solution. As the mass spectrum implies, up to five discotics cross-linked through covalent binding within the first 2 d. The protein is so far the largest ligand which was attempted to be attached to the discotic scaffold. Apparently, coupling the relatively big protein is sterically hindered. Similar to the observation made with the mannose discotics in Chapter 3.2.1, again the high degree of supramolecular polymerization under the reaction conditions in aqueous solution might result in molecular crowding (*vide infra*) of the reactive functionalities. The fact that the attachment of the large YFP proceeds slowly whereas cross-linking of the discotics occurs comparably fast is one indication for overcrowding. Sterical hindrance caused by the bulky protein could prevent further reaction of the free cysteins in the supramolecular column with another large protein. The comparably small discotics on the other hand are small enough to overcome the hindrance and cross-link with each other. Cleavage of the disulfides under mild TCEP conditions without denaturation of the protein was not possible. On the other hand, there is no evidence for two- or three-fold addition of YFP to one discotic according to mass and SDS analytic.

Thus, the trivalent discotics are - under these ligation conditions - not an appropriate scaffold for protein attachment by expressed protein ligation. The cross-linking of cysteine-discotics could be avoided by synthesis of a non-symmetrical monomeric discotic which carries only one single ligand per scaffold. In our case another protein FRET pair was chosen in order to proceed with the studies on supramolecular protein assemblies.

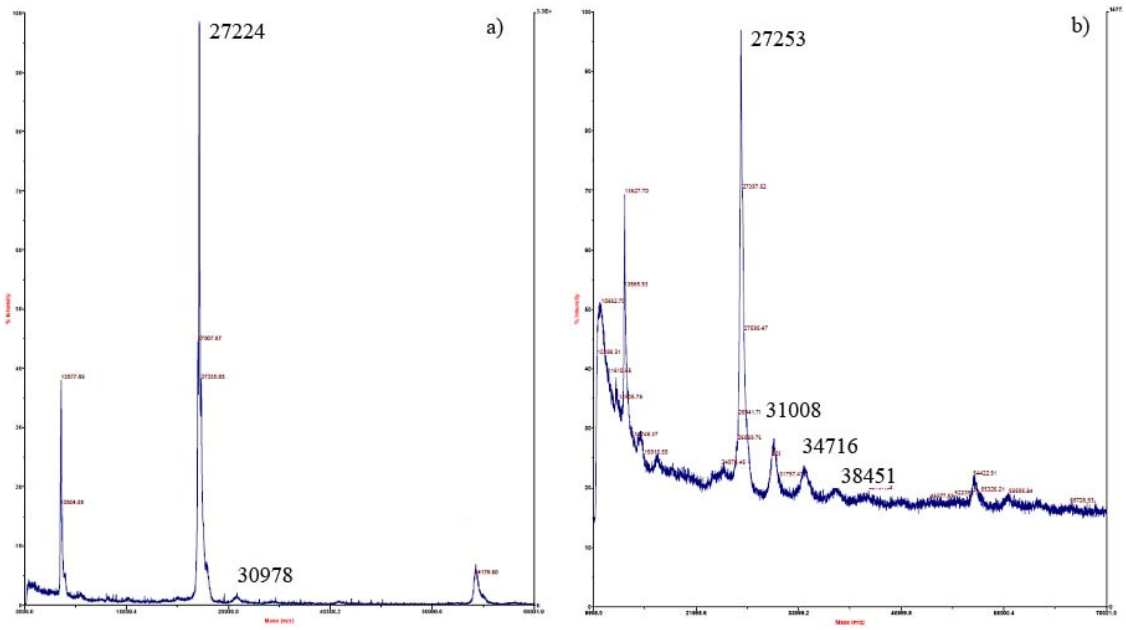

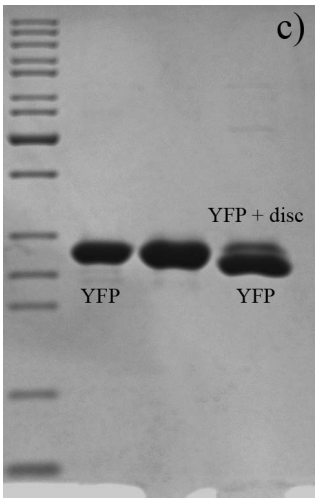

Figure 35. MALDI-TOF MS Spectra of the YFP-Disc **57** reaction mixture after a) 3 h and b) 2 d: Polymerization of cysteine discotic **56** by covalent disulfide bridges causing a cross-linkage of up to five discotics is shown. c) SDS-Gel of YFP and coupled YFP after 3 d reaction time. Still only a small amount of protein reacted with the discotic scaffold.

3.4.3 Streptavidin Binding to the Biotin Discotic

In order to get a fundamental understanding of the assembly of proteins along a supramolecular wire, the binding of proteins to the supramolecular polymers was first investigated with one type of protein only. The protein streptavidin was chosen due to its property to bind biotin strongly. Streptavidin is a tetramer formed out of four equal subunits.[105] Each of the monomers is able

to bind one biotin in a non-covalent manner exhibiting a binding strength close to a covalent bond.

Streptavidin was envisaged to bind to the biotin discotic **53** (Chapter 3.2.3). The interaction of biotin discotic **53** with streptavidin coated surfaces was previously described (Chapter 3.3.3). A fluorophor was attached to the protein that would be able to feature FRET with the discotics. To study the spatial distribution and the interaction between a protein and its attached supramolecular scaffold, titration experiments using the biotin discotic **53** and a Cy3 labeled streptavidin (SA-Cy3) were carried out. As illustrated in Figure 36 the biotin-streptavidin interaction mediates spatial proximity between the Cy3 dye on the protein and the discotic scaffold. Cy3 has its first excitation maximum at 524 nm and an emission maximum at 576 nm.[106] Thus it is an ideal FRET acceptor for the discotic scaffold serving as donor.

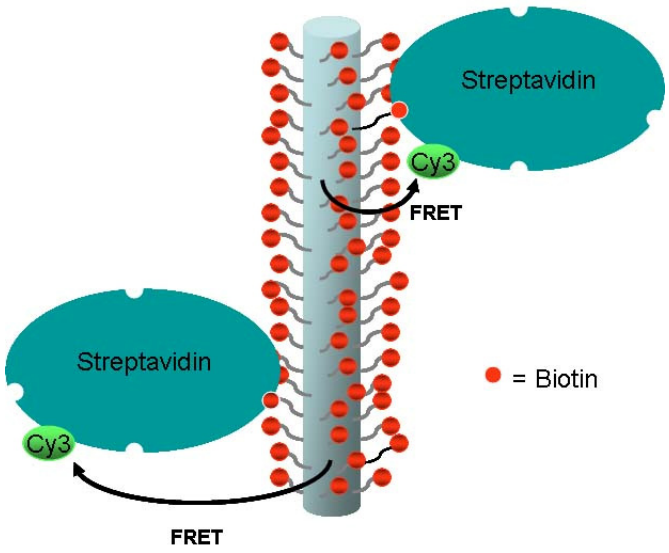

Figure 36. Cartoon demonstrating the FRET interaction with Cy3 and the discotic scaffold induced by streptavidin, binding to biotin on **53**.

3.4.4 Protein Assembly Mediated by the Biotin Discotic

Biotin discotic **53** was dissolved in water to reach a final concentration of 10^{-6} M. Cy3 labeled streptavidin was added and the mixture was stirred for 5 min after each titration step to ensure sufficient time for binding of biotin to streptavidin. The relative concentration of streptavidin-Cy3 (SA-Cy3) was

increased from 1 mol-% to 20 mol-% per discotic scaffold. Emission spectra were recorded with an excitation wavelength at 340 nm, the excitation wavelength of the discotic FRET donor. Control experiments were carried out with the inert discotic **1** to study the interaction between the discotic scaffold and streptavidin Cy3 in solution without any binding possibilities. Control studies with only water and streptavidin Cy3 showed that self-fluorescence of the Cy3 dye at the donor excitation wavelength is negligible. As shown in Figure 37, significant emission of the acceptor is achieved starting from 2 mol-% SA-Cy3. At a concentration of about 10 mol-% of SA-Cy3, the signal of the discotic FRET donor is fully quenched and only emission of acceptor is detected. Further addition of acceptor does not result in further increase of the FRET ratio (= Intensity $\lambda_{max\ acceptor\ (570\ nm)}$/ Intensity $\lambda_{max\ donor\ (524\ nm)}$) as can be seen in Figure 39.

Control studies with **1** under the same conditions show that unspecific interaction between the discotic scaffold and SA-Cy3 is negligible. As illustrated in Figure 38, only by addition of more than 9 mol-% of SA-Cy3 a first weak response of Cy3 could be seen. But even with 33 mol-% of SA-Cy3, compared to **1**, the FRET ratio does not exceed 0.5. Comparison of the highest FRET ratio achieved in both experiments shows that the ratio in presence of **53** is about 80 times higher than the ratio when compound **1** is used (Figure 39). Thus the FRET effect clearly results from the local proximity achieved by binding of biotin to streptavidin.

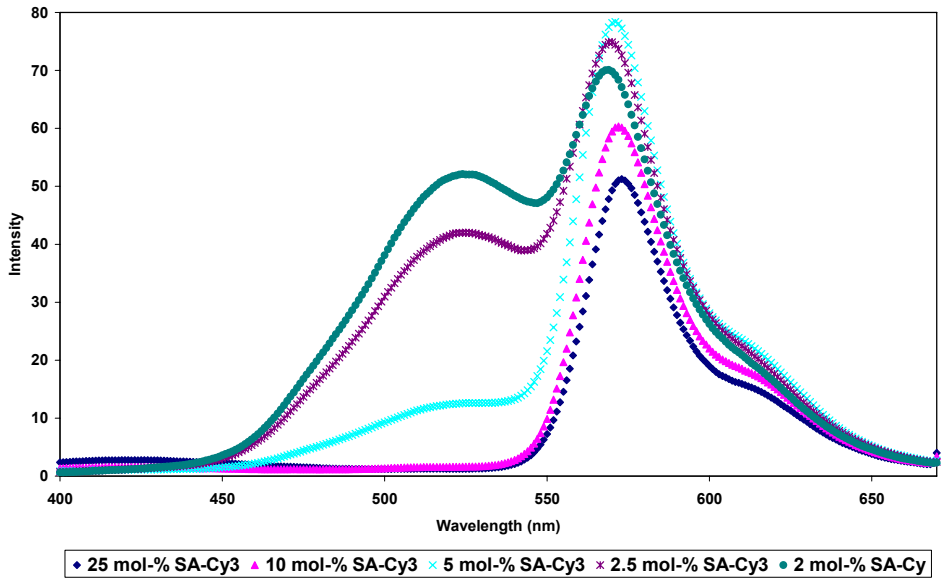

Figure 37. Titration experiment to study the FRET interaction of biotin discotic **53** with streptavidin-Cy3. Already at ratios of 1/50 of SA-Cy3/**53** (= 2 mol-% SA-Cy3) a strong excitation of the acceptor is detected at λ_{ex} = 340 nm, the excitation wavelength of the donor.

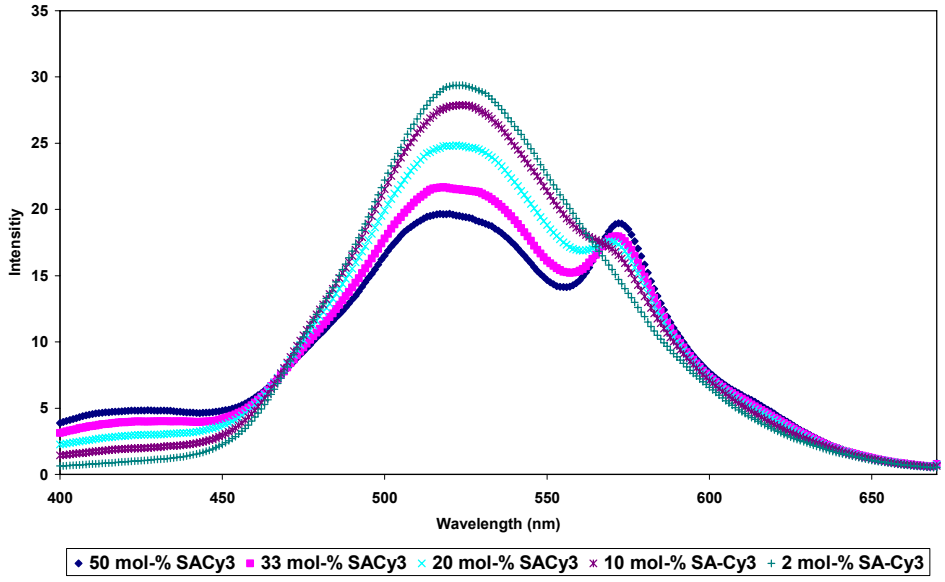

Figure 38. Control experiment at λ_{ex} = 340 nm. FRET between inert discotic **1** and streptavidinCy3. Only at ratios of higher than 1/10 of SA-Cy3/**1** (= 10 mol-% SA-Cy3) a small response of the FRET-acceptor can be seen.

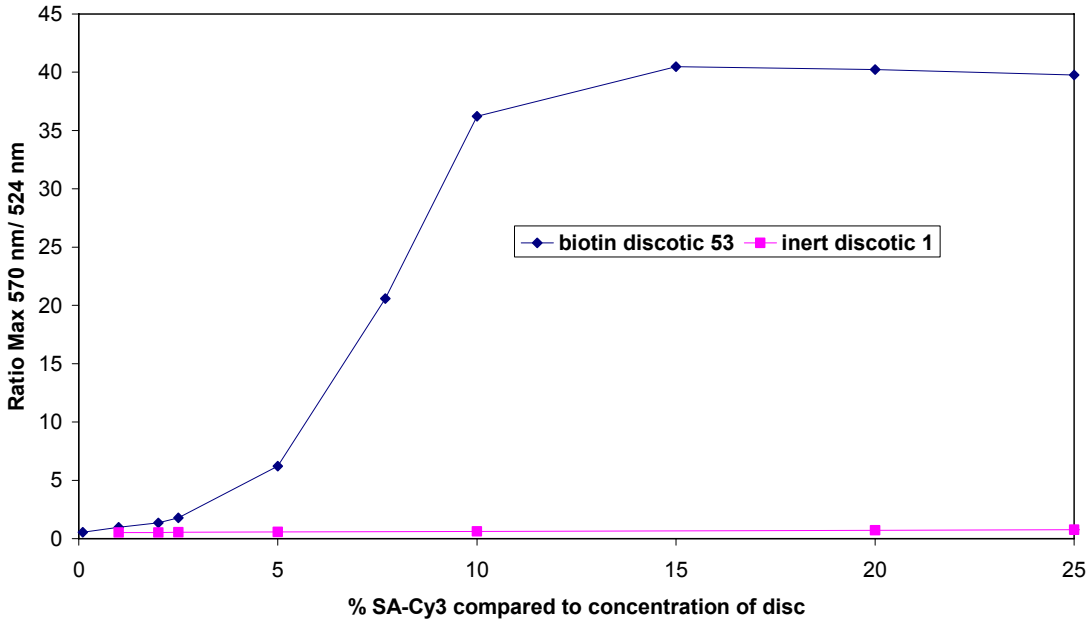

Figure 39. FRET ratio Max at 570 nm / Max at 524 nm. Biotin discotic **53** (blue plot) with 1 mol-% to 25 mol-% SA-Cy3 at λ_{ex} = 340 nm. The purple line shows the FRET ratio determined from the control experiment with **1**.

Three of the studied concentrations (2 mol-%, 5 mol-%, 7 mol-% SA-Cy3) were additionally measured at different time points (after 5 min, 10 min, 30 min, 1 h, 2h and 24h). Overlay of the corresponding spectra showed no change over time in any of the two emission maxima. Thus binding of SA-Cy3 to **53** takes place within the first five minutes after mixing.

3.4.5 Protein Modulation with Discotic Mixtures

To evaluate the effect of dilution of the biotin functionalized monomers, experiments were performed with discotic mixtures of **53** and **1**. As illustrated in Figure 36, the inert discotic **1** was envisaged to serve as spacer between the functionalized discotics **53**. By testing different ratios of **53** and **1**, the optimal amount of spacer for this type of FRET interaction between SA-Cy3 and the discotic scaffold was to be determined. Mixtures were tested ranging from a **53**/**1** ratio of 2/1 till 1/20 to evaluate the ideal spatial distribution of **53** for maximal interaction with SA-Cy3. Mixtures of the discotics were prepared twelve hours prior to the experiments to ensure complete random placement of

the two different discotics in columns. In the first experiments carried out with discotic mixtures the overall concentration of biotin discotic **53** was kept constant at 10^{-6} M. Thus the overall concentration of discotic scaffold in the higher mixtures increases significantly. The same percentage of SA-Cy3 (0.5 mol-% to 15 mol-% compared to total disc concentration) was added to all discotic mixtures. The increase in donor concentration clearly influences the FRET ratio. Due to the higher amount of overall discotic concentration (c[**53**]+c[**1**]), strong differences in the absolute values of FRET ratios of the different mixtures were determined (Figure 40). For example, the maximum FRET value for interaction of SA-Cy3 with pure biotin discotic **53** was around 37, whereas the FRET value in case of the 1I1 mixture of **53**/**1** did not exceed 17. Calculated FRET ratios for mixtures of **53**/**1** below a ratio of 1/10 did not exceed 1.3 and did not change after adding the first portion of SA-Cy3 (0.5 mol-%) and thus were not taken to account for further investigation (data not shown).

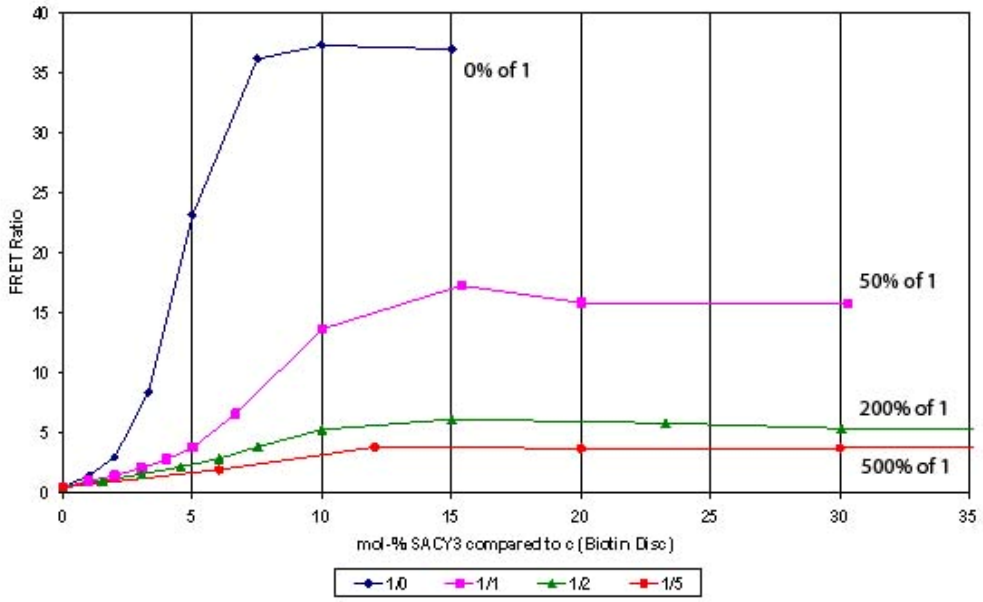

Figure 40. FRET ratio of different mixtures of **53/1** 1/0 (blue), 1/1 (purple), 1/2 (green) and 1/5 (red) plotted against c[SA-Cy3] compared to c[disc total] = c[**53**] + c[**53**].

In order to compare the actual amount of donor and acceptor in solution, the concentration of the acceptor SA-Cy3 in mol-% was related to the

concentration of FRET donor **53** only, and not to the overall concentration of discotic scaffold. The FRET ratio on the y-axis is plotted against the relative concentration of SA-Cy3 (in mol-% of the concentration of **53**). Figure 40 shows that the point of saturation, at which the plotted FRET ratios stay constant, varies in each curve. In case of pure biotin disc **53** a maximum in FRET interaction was reached after addition of 7.5 mol-% of SA-Cy3 compared to biotin disc concentration (Figure 40, blue plot). Further addition of FRET acceptor to the solution did not result in a higher FRET ratio. However, in case of the 1/1 mixture of **53**/**1** the FRET signal was still increasing after adding 7.5 mol-% of SA-Cy3. Saturation was obtained with more than 15 mol-% of SA-Cy3 (Figure 40, purple plot). A comparable value around 15 mol-% SA-Cy3 was determined for maximum FRET interaction of the SA-Cy3 dye with a 1/2 mixture of **53**/**1**, plotted in green. Addition of more than 15 mol-% did not increase the FRET ratio any more. Saturation in FRET ratio was reached slightly earlier with a 1/5 mixture of **53**/**1** at about 12 mol-% SA-Cy3 (red plot) and 13 mol-% for 1/3 mixtures (not plotted). These results can be explained as follows. In a titration series starting from 0% of FRET acceptor – while the amount of donor is kept constant – the FRET ratio increases as long as a spatial approach of donor and acceptor is possible. In our case the FRET ratio increases as long as free biotins, possible binding partners for SA-Cy3, are available. If all of these biotins are either bound or sterically blocked, no more local approximation of Cy-3 acceptor to the discotic donor is possible. Further addition of acceptor thus does not result in any further change of the fluorescent interaction. Comparison of the saturation points of pure **53** and 1/1 mixture of **53**/**1** demonstrates that the presence of **1** as spacer enhances the relative amount of streptavidines that interact with the discotic from 7.5 mol-% to over 15 mol-%. Thus the inert discotic serves as spacer and creates free space between the functionalized discotics to allow a higher percentage of biotins to bind to the protein. The ideal mixture of functionalized discotic and inert discotic seems to be about one to two inert discotics per binding scaffold. Mixtures of **53**/**1** of 1/3 and 1/5 of **53**/**1** do not enhance binding properties of the supramolecular columns any more. Mixtures of 1/10 or 1/20 of **53**/**1** are dominated by the donor fluorescence. A spacer of in average ten inert

discotics appears to be too large to obtain energy transfer from the complete scaffold to the streptavidin acceptor bound to scaffold **53**.

The influence of the order of addition of the interaction partners was investigated. In the previous experiment the discotics **53** and **1** had been mixed prior to the experiment and SA-Cy3 was added afterwards. Thus in a second experiment, the FRET pair SA-Cy3 and biotin discotic **53** was mixed in advance and the spacer **1** was added subsequently. A mixture of **53** (10^{-6} M) with 20 mol-% SA-Cy3 (2 x 10^{-7} M) was prepared 1 h prior to the experiment and split in five batches. Defined amounts of inert discotic were titrated to each batch to result final mixtures of **53**/**1** of 1/0, 1/1, 1/2, 1/3 and 1/5. Fluorescence spectra of each mixture were measured after 10 min, 30 min, 1 h, 2 h, 5 h, 24 h and 48 h. None of the fluorescence spectra changed over time. Thus, only data gained after 10 min was taken for further evaluation. As illustrated in Figure 41, addition of only one equivalent of **1** already decreases the FRET ratio significantly from 27.3 to 1.6. Higher amounts of discotic **1** decrease the FRET ratio to approximately 0.6. Values for the FRET ratio are listed in Table 2. Comparison with values obtained from the first experiment, with the same final conditions but pre-mixing of the discotic scaffold, indicates a complete loss of FRET interaction in the second study (Table 2 and Figure 41). Apparently the discotics added are not included in the pre-formed columns of **53** interacting with SA-Cy3. In the first study the discotics **53** and **1** are already mixed prior to the addition of streptavidin SA-Cy3. The protein binds to the mixed columns and Cy3 interacts with both discotics **53** and **1** included in the column. On the other hand, adding the inert discotics **1** to a pre-mixed solution of SA-Cy3 and biotin discotic **53** in fact leads to a different result. The protein SA-Cy3 immediately binds to the biotin discotic when mixed. As mentioned before streptavidin possesses four binding pockets for biotin. It seems that one SA-Cy3 binds to the biotin discotic **53** with two or more binding pockets. Firstly, multiple binding of one SA-Cy3 would lead to the linkage of two different discotics within one supramolecular column. An exchange of the supramolecules between the two linked discotics would be harder if not impossible. Several cross-linkages of discotics caused by SA-Cy3 could lead

to a complete loss of reversibility. Secondly, different supramolecular columns could be cross-linked through binding to the same SA-Cy3. In both cases cross linkage decreases the flexibility and reversibility of the supramolecules and as a result does not allow the exchange of single discotic scaffolds within one supramolecular column any more. In the previous experiments reversibility was not necessary for the outcome of the experiments. However, the subsequent addition of **1** to the pre-formed complex of SA-Cy3 and **53** heavily relies on the dynamic of the supramolecular system. Without reversibility the columns formed by **1** can not be included in the FRET interaction system of **53** and SA-Cy3. This seemed to be the case when adding **1** subsequently. Consequently, in the second experiment the fluorescent signal of the free inert columns formed by **1** is not quenched by the acceptor and the donor fluorescence dominates the comparably weak FRET signal of the rigid pre-formed columns with **53** and SA-Cy3.

Table 2. Values for the FRET ratio of mixtures of **53/1** with 20 mol-% SA-Cy3. Experiments were carried out either with pre-mixed discotics and subsequent addition of SA-Cy3 or with titration of inert discotics **1** to the pre-mixed FRET partners **53** and SA-Cy3.

Ratio of concentrations of SA-Cy3/**53**/**1**	Discotic Mixtures prepared prior to experiment – FRET ratio Intensity at 574 nm/Intensity at 524 nm	Titration of **1** to mixtures of SA-Cy3 and **53** FRET ratio Intensity at 570 nm/Intensity at 524 nm
0.2/1/0	27.3	27.3
0.2/1/1	14.3	1.6
0.2/1/2	6.2	0.9
0.2/1/3	2.9	0.7
0.2/1/5	3.5	0.6

Results are visualized in Figure 41. The values illustrated as blue and purple bars only differ in the order of compound addition not in the final composition

of the solutions. At the same concentrations of all three compounds (SA-Cy3, **53** and **1**) the FRET-ratio is significantly higher if discotics **53** and **1** are pre-formed than in case of subsequent addition of **1**. Comparison of the two experiments indicates that not only the biotin discotic scaffolds interact with the SA-Cy3 dye but also the inert discotics included in the mixed columns. Thus, in premixed supramolecular columns more inert discotics **1** transfer the energy to the acceptor. Hence, the donor signal is quenched substantially.

In all titration steps FRET ratio did not change over time. Even at time periods of 48 h the signal stayed constant. These results emphasize the assumption that the columns are blocked by the SA-Cy3 binding to biotin right at the beginning and no random exchange of the supramolecular columns **53** and **1** can take place.

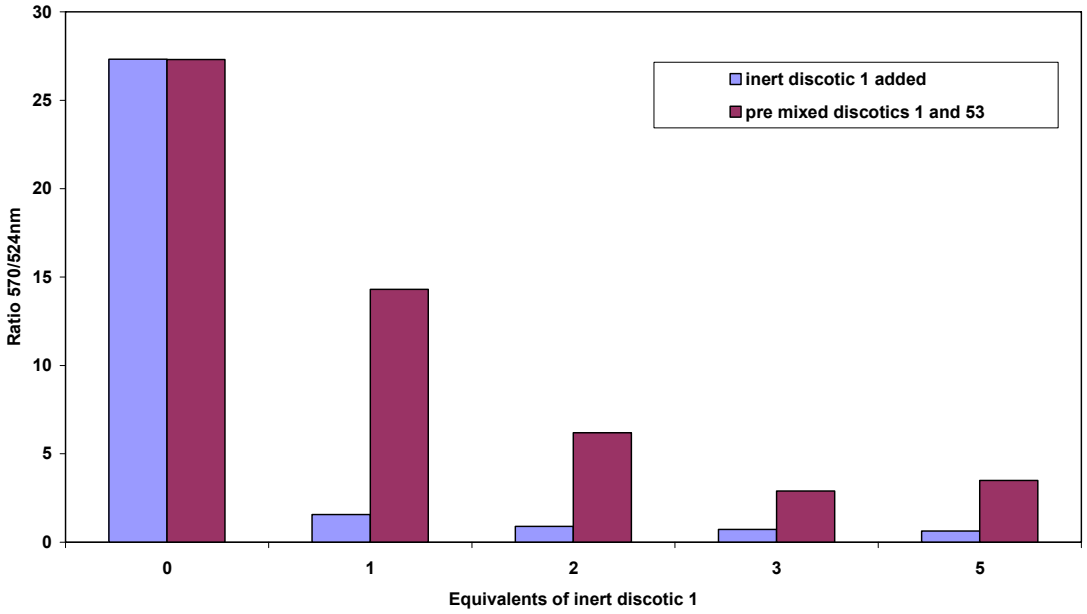

Figure 41. Plot illustrating the difference in FRET interaction depending on the order of compound addition to the FRET system. Experiments were carried out either with pre-mixed discotics and subsequent addition of SA-Cy3 (purple) or with titration of inert discotics **1** to the pre-mixed FRET partners **53** and SA-Cy3 (blue).

3.4.6 Control over Protein Assembly

To study the supramolecular control over induced protein dimerization a model system based on two differently labeled streptavidineswas studied in the presence of the biotin functionalized supramolecules **53** (Figure 42). The difference between the FRET signal of the two streptavidines with the dyes and the FRET signal of the same mixture when added to biotin discotic was to be determined. The biotin on the discotic surface binds to streptavidin as shown previously (Chapter 3.4.3). This interaction should mediate the assembly of streptavidin on the surface of the supramolecular columns and should facilitate approximation of the FRET pair. Thus, the FRET in presence of the biotin discotics **53** should increase.

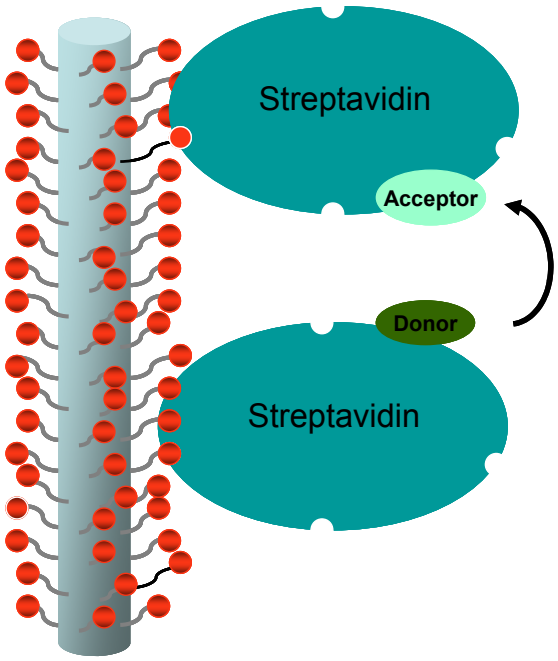

Figure 42. Cartoon demonstrating the FRET interaction of two different dyes attached to streptavidin in presence of biotin discotic **53**. The biotin discotic **53** binds to the streptavidin and leads to protein assembly on the columnar surface. The proximity of the two dyes attached to the protein can be evaluated by FRET.

The dyes used were Alexa Fluor 633 (AF-633; $\lambda_{max\ ex}$ = 633 nm; $\lambda_{max\ em}$ = 647 nm) as FRET acceptor and Texas Red (TR; $\lambda_{max\ ex}$ = 550 and 586 nm; $\lambda_{max\ em}$ = 612 nm) as FRET donor, each attached to streptavidin. The labeled

proteins are commercially available and the excitation- and emission-spectra of the two dyes as provided by the supplier are given in Figure 43.

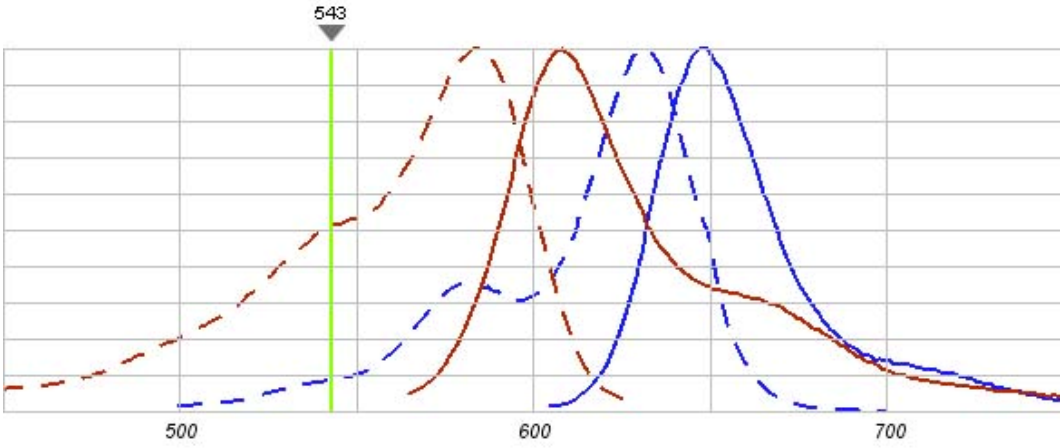

Figure 43. Excitation- (dashed) and emission- spectra (continous) of Texas Red (red) and Alexa Fluor 633 (blue) as provided by invitrogen.[107]

Streptavidin Alexa Fluor 633 (SA-AF633) and streptavidin Texas Red (SA-TR) were mixed in a 1/1 ratio (0.05 mg x mL^{-1} – 2 x 10^{-6} M of each protein) 2 h prior to the experiments, and titrated to a solution of **53** (10^{-6} M). Titration steps reached from 1 to 50 µL of protein mixture (5 x 10^{-9} M 2.5 x 10^{-7} M final concentration) which corresponds to approximately 0.5 - 25 mol-% of SA-AF633/SA-TR compared to the biotin discotic **53**. After each titration step the mixture was allowed to stir for 10 min before the fluorescence spectra was measured, to assure sufficient interaction time of the labeled proteins SA-AF633/SA-TR with the biotins of **53**. Control experiments were carried out using the same protein mixture and with inert discotic **1** (10^{-6} M), to examine unspecific interaction with the scaffold, and with the pure SA-AF633/SA-TR mixture to determine the interaction of the proteins as background. Additionally SA-AF633 was measured individually at the same final concentrations as in the mixture (5 x 10^{-9} M - 2.5 x 10^{-7} M) to determine background fluorescence of the AF633 acceptor at the TR donor excitation wavelength.

Fluorescence spectra of **53** or **1** with several concentrations of the protein mixture of SA-AF633/SA-TR are shown in Figure 44 and Figure 45. Control experiment with the pure protein mixture is shown in Figure 46. Carrying out the experiments as described results in a solution with a constant amount of

discotics **53** or **1**, to which the mixture of the protein FRET-pair is continuously added. Thus the fluorescence signal of SA-AF633 and SA-TR increases steadily with their concentration. The increase in signal can be seen in all three cases (with discotics **53** or **1** and with the pure proteins). Furthermore, in all experiments a strong fluorescence signal of the acceptor was detected. Fluorescence intensity at the SA-TR donor maximum (at $\lambda = 612$ nm) was always lower than the intensity of the SA-AF633 (at $\lambda = 647$ nm). However, the strong emission of the FRET acceptor AF633 is not merely due to a strong FRET interaction but results from direct excitation of AF633 at an excitation wavelength of 584 nm. Figure 47 shows the background signal of pure SA-AF633 as control. The strong background fluorescent of AF633 probably arises from the fact that the quantum yield of AF633 is significantly higher than the quantum yield of TR.[103] As shown in Figure 43, the excitation of AF633 at $\lambda = 612$ nm should be relatively low compared to the excitation of TR. However, the higher quantum yield of AF633, results in the strong signal of AF633, whereas the signal of TR is comparably low.

Nonetheless, comparison of the spectra gained with **53** to those gained with **1**, led to an interesting observation. In the presence of **53** the fluorescent maximum of the FRET donor SA-TR decreases substantially compared to the donor signal in presence of **1**. On the other hand spectra achieved with either **1** or pure protein mixture of SA-AF633/SA-TR yielded similar spectra and both did not result in a decrease of donor signal if compared to **53**. This result leads to the assumption that a major FRET-interaction only takes place in presence of biotin discotic **53**. Apparently, the discotic binds to both streptavidines labeled with the FRET partners SA-AF633 or SA-TR. The binding leads to protein assembly on the periphery of the supramolecular column formed by **53**. The induced proximity of the two proteins SA-AF633 and SA-TR enables non radiative energy transfer from SA-TR to SA-AF633.

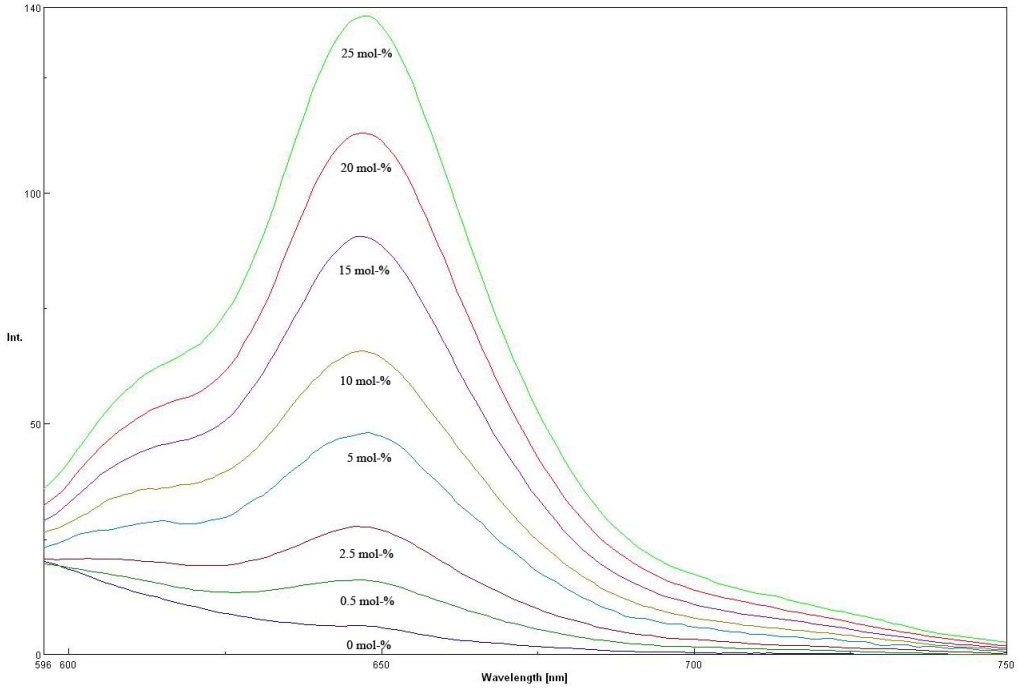

Figure 44. FRET-interaction of SA-AF633/SA-TR (5 x 10^{-9} M 2.5 x 10^{-7} M = 0.5-25 mol-%) in the presence of **53** (10^{-6} M = 100 mol-%) at an excitation wavelength of λ = 584 nm. The donors signal is quenched significantly.

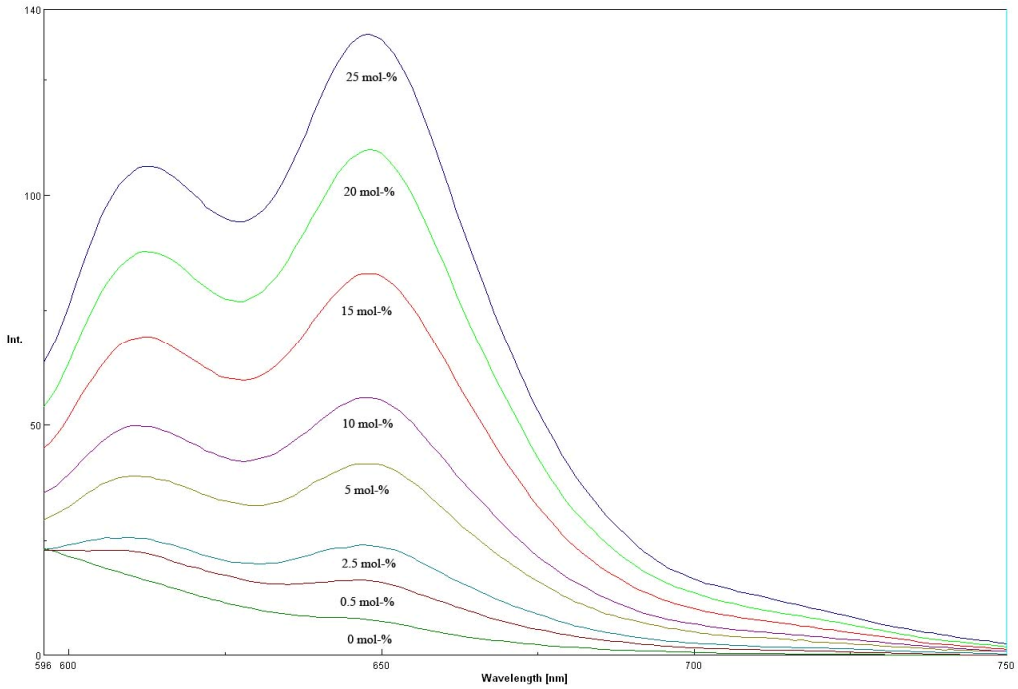

Figure 45. FRET-interaction of SA-AF633/SA-TR (5 x 10^{-9} M 2.5 x 10^{-7} M = 0.5-25 mol-%) in the presence of **1** (10^{-6} M = 100 mol-%) at an excitation wavelength of λ = 584 nm. The donors signal is high compared to the experiments with **53**.

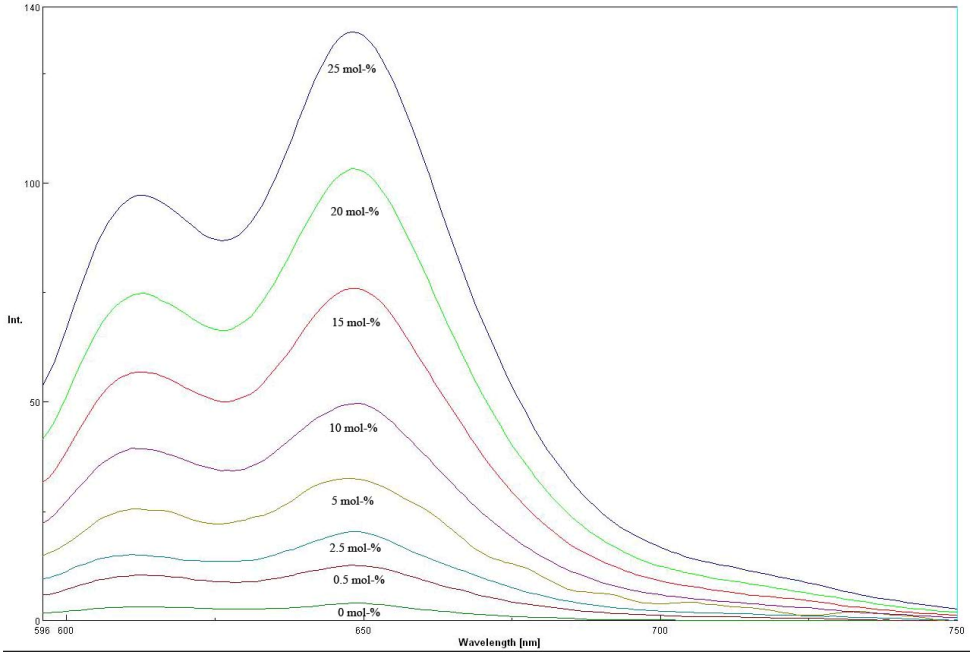

Figure 46. FRET-interaction with pure protein mixture of SA-AF633/SA-TR (5 x 10^{-9} M 2.5 x 10^{-7} M) at an excitation wavelength of λ = 584 nm. To gain a comparable value, here mole percent of protein mixture are calculated in respect to 100% discotic **53** (10^{-6} M) used in the first experiment (Figure 44). The spectra are very similar to the ones achieved in presence of **1** indicating no unspecific interaction with the scaffold.

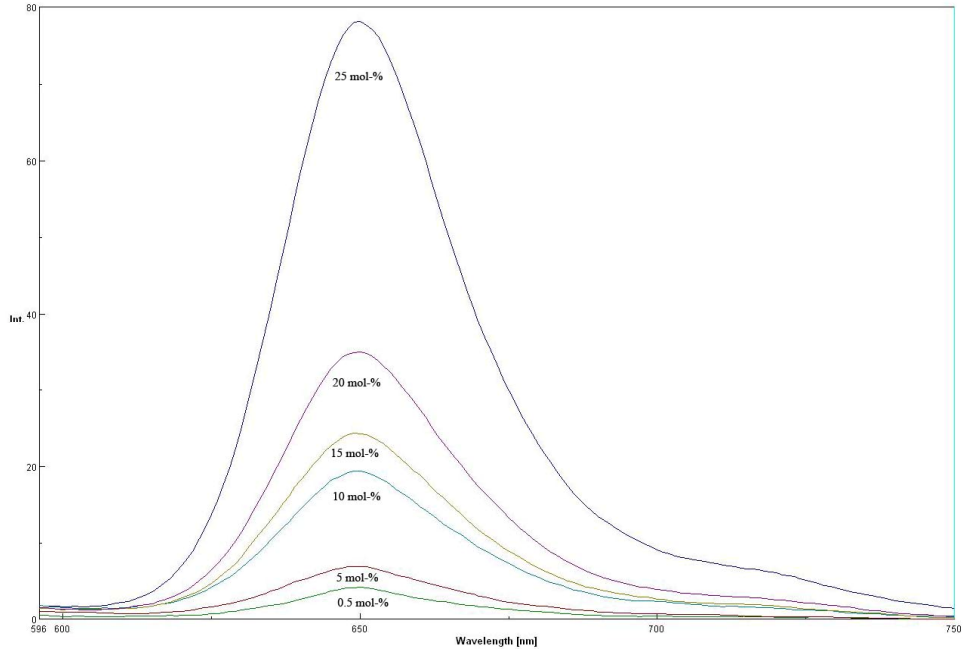

Figure 47. Fluorescence excitation of the pure FRET acceptor SA-AF633 (5 x 10^{-9} M – 2.5 x 10^{-7} M) at an excitation wavelength of λ = 584 nm. To gain a comparable value, here mole percent of protein mixture are calculated in respect to 100% discotic **53** (10^{-6} M) used in the first experiment (Figure 44). Spectra indicate that the direct excitation of the FRET acceptor SA-AF633 is relatively high.

As mentioned before, in the previous experiment the concentration of protein mixture of SA-AF633/SA-TR was steadily increased. The different concentrations make a reliable comparison of FRET ratios impossible. Therefore, subsequent experiments were carried out keeping a constant concentration of the protein mixture SA-AF633/SA-TR while **53** (or **1** as control) were added stepwise.

Streptavidin Alexa Fluor 633 (SA-AF633) and streptavidin Texas Red (SA-TR) were mixed in a 1/1 ratio (0.05 mg x mL^{-1}, 2 x 10^{-6} M of each protein) 2 h prior to the experiments and diluted to yield a final concentration of 10^{-7} M. Biotin discotic **53** or inert discotic **1** were added in steps between 0.1-20 mol-% compared to the single protein concentration. Additionally control experiments with the pure protein mixture of SA-AF633/SA-TR and with pure FRET acceptor SA-AF633 were carried out. Like the results achieved with the previous experiment, again the background fluorescence of SA-AF633 was comparably high. As before, the fluorescent signal of SA-AF633 at λ = 648 nm was higher than the signal of SA-TR at λ = 612 nm even in all the control studies. However, also in this study the obvious decrease in TR donor fluorescence indicates FRET interaction of SA-AF633/SA-TR only in presence of the biotin discotic. Figure 48 shows the overlay of spectra of the experiments in presence **53** or **1** (at 10 mol-%) with the pure protein mixture and pure acceptor SA-AF633. The spectra in presence of inert discotic **1** and of the pure protein mixture of SA-AF633/SA-TR are very similar indicating that no unspecific interaction is induced by the inert discotic scaffold **1**. For the comparison of the background fluorescence of SA-AF633 with the fluorescence maxima of SA-AF633 in presence of SA-TR it needs to be taken into account that there is an overlap of the emission spectra of TR with AR633. Thus, the maximum of AF633 at λ = 647 nm is not only caused by emission of AF633 itself but also by TR emission.

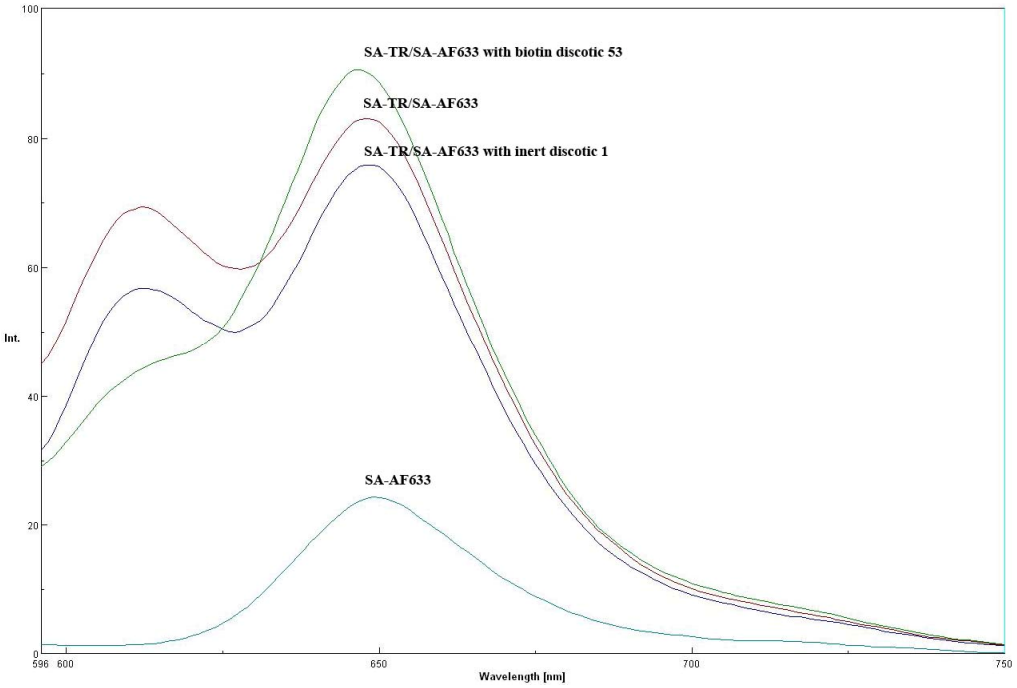

Figure 48. Overlay of the experiments with **53** (green), **1** (blue) - both 10 mol-% -, the pure protein mixture SA-AF633/SA-TR (purple) and pure acceptor SA-AF633 (light blue). Only in presence of **53** the donor signal is quenched.

The FRET ratios were calculated for the experiment in presence of **53** or **1** and for the pure protein mixture (Figure 49). FRET ratios determined with biotin discotic **53** are shown in blue, those achieved with **1** in green. Control experiments with the protein mixture SA-AF633/SA-TR without any discotic, resulted in constant FRET ratios around 1.2 at all concentrations tested. At the very low concentrations of protein (< 4 mol-% SA-AF633/SA-TR) the FRET ratio in presence of the discotic scaffold **1** or **53** was lower than that for the interaction between the pure proteins SA-AF633/SA-TR. Apparently, at these low concentrations the presence of the supramolecular polymer of **1** or **53** in solution reduces the probability of approximation of the two FRET partners SA-AF633/SA-TR and thus decreases the FRET compared to the pure protein control even in presence of **1**. In presence of **53**, SA-AF633 and SA-TR probably are kept away from each other through binding to the columns of **53**. The distance between two discotics carrying SA-AF633 and SA-TR is probably mediated by those discotics not bound to any protein. Unbound discotics **53** serve as spacer to enhance the distance between SA-AF633/SA-TR. As a result, at ratios up to 4 mol-% of SA-AF633/SA-TR, the discotic **53** is able to

decrease FRET. At concentrations above 4 mol-%, **53** increases the FRET interaction of SA-AF633/SA-TR. The FRET of the control experiment with **1** stays in the same range as the pure proteins above 4 mol-%. In presence of the supramolecular structure **53**, the FRET interaction is amplified by a factor of two, compared to the supramolecular polymer without biotin and compared to the control experiments with pure SA-AF633/SA-TR. Furthermore, the FRET interaction in presence of **53** was shown to be concentration dependent.
Evidently, the discotic, carrying ligands, is able to bind to the corresponding proteins and modulate their assembly in the periphery of the supramolecular columns in a concentration dependent manner.

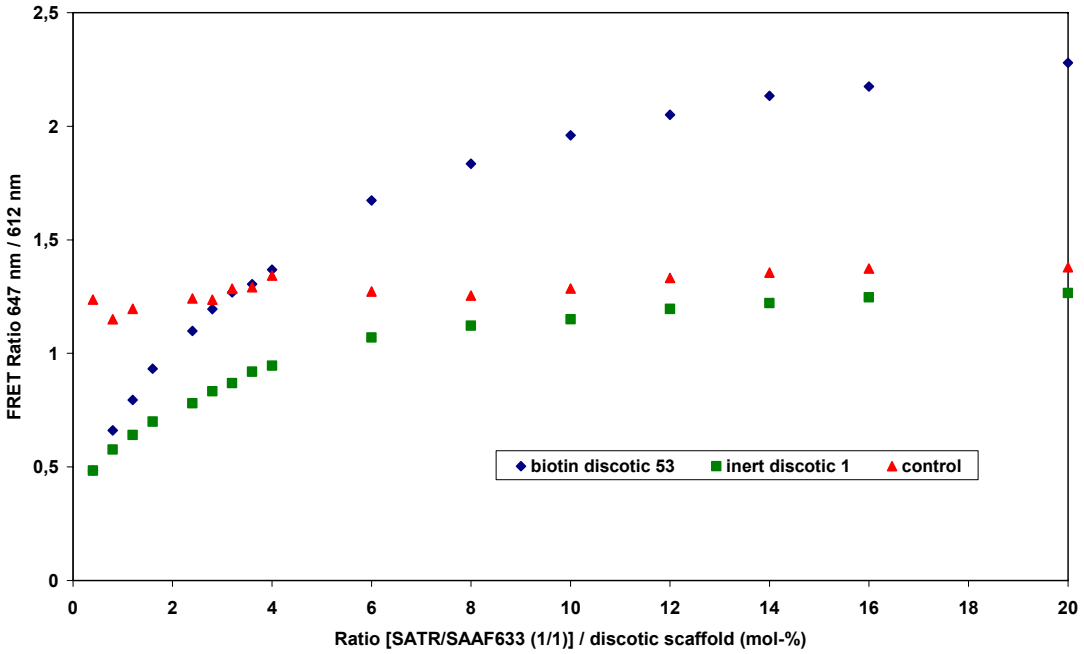

Figure 49. Plot illustrating the FRET ratio max at 647 nm / max at 612 nm. Biotin disc **53** (blue plot) with 1 to 50 µL streptavidin-Alexa Fluor 633 and streptavidin-Texas Red (1/1, 0.05 mg x mL^{-1}). The green line shows the FRET ratio determined from the control experiment with **1**. Control experiments with the protein mixture without any discotic, result in constant FRET ratios around 1.2 at all protein concentrations.

Studies with a second FRET pair Alexa Fluor 514 (AF-514) and Texas Red (TR) were carried out. The dyes used were Alexa Fluor 514 ($\lambda_{max\ ex}$ = 514 nm; $\lambda_{max\ em}$ = 541 nm) as FRET donor and TR ($\lambda_{max\ ex}$ = 550 and 586 nm; $\lambda_{max\ em}$ = 612 nm) as FRET acceptor, each attached to streptavidin. Like the

labeled proteins of the previous experiments, the streptavidin labeled with AF-514 is commercially available. The excitation- and emission-spectra of the AF-514 and TR provided by the supplier are given in Figure 50.

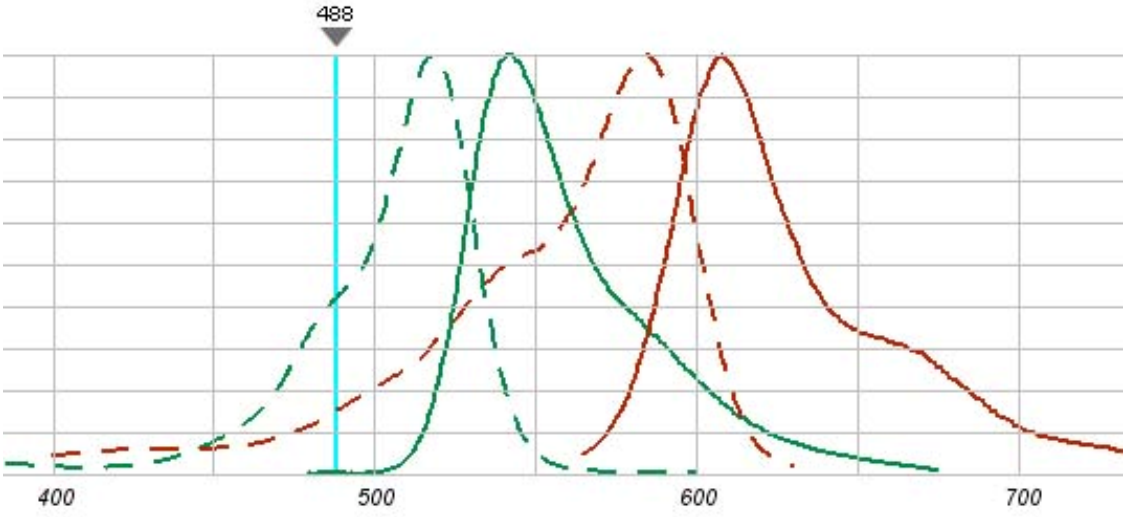

Figure 50. Excitation- (dashed) and emission- spectra (continous) of Alexa Fluor 514 (green) and Texas Red (red) as provided by invitrogen.[108]

The two proteins SA-AF514 and SA-TR were mixed (0.05 mg x mL^{-1}, 2 x 10^{-6} M of each protein) 4 h prior to the experiments. Biotin disc **53** was added in portions of 2 µL (c [**53** = 10^{-4}] final concentrations between 2 x 10^{-6} and 1 x 10^{-5} M). The resulting fluorescent spectra are shown in Figure 51. As had been the case in the previous experiment, using a different FRET pair, also this time almost no change in the maximum fluorescence intensity of the acceptor at λ = 612 nm was seen. In all spectra measured, the fluorescence intensity of the FRET acceptor SA-TR at its maximum ($\lambda_{max\ em}$ = 612 nm) stayed nearly constant. No increase of the acceptor signal could be achieved neither in presence of **53** nor in the control experiments with **1** or the pure proteins. Nevertheless, in presence of **53** a clear decrease of the fluorescence intensity of the FRET donor SA-AF514 at its maximum ($\lambda_{max(em)}$ = 541 nm) was detected.

This assumption is supported by the fact that the FRET ratio increases with the amount of biotin discotic **53** added (Figure 52). The decrease of the fluorescence intensity of the FRET donor AF514 at its maximum, in presence

of the biotin discotic **53**, while the signal of the FRET acceptor TR stayed constant, resulted in the increased FRET ratio. Control of the pure protein mixture without **53** resulted in a FRET ratio of 0.51.

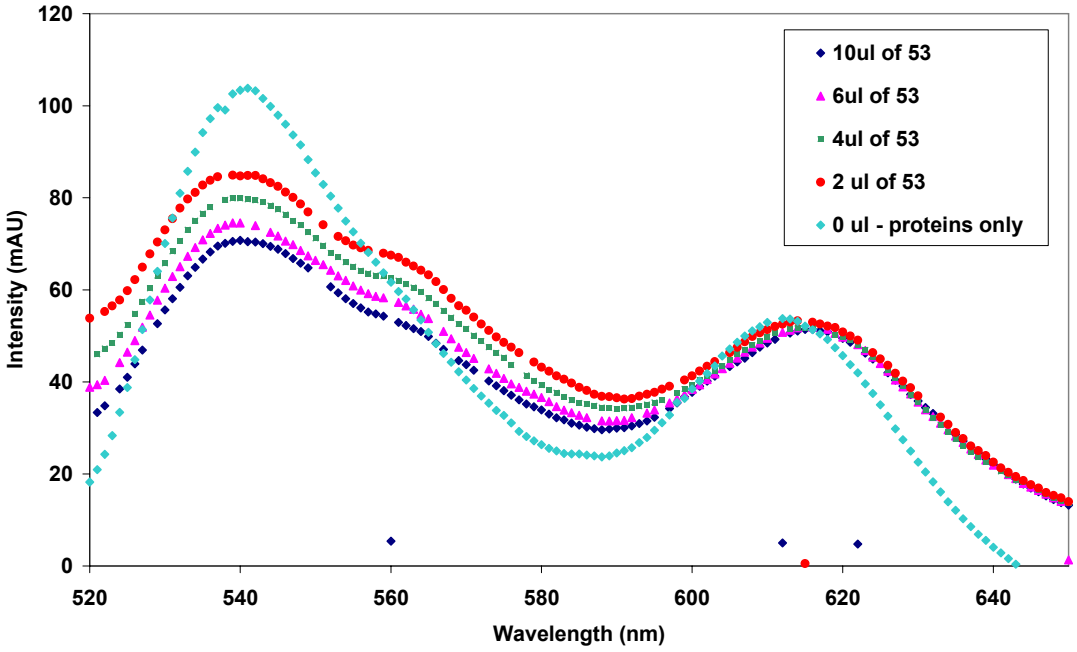

Figure 51. Titration experiment to study the control over protein assembly using biotin discotic **53** with FRET interaction of streptavidin-Alexa Fluor 514 and streptavidin-Texas Red.

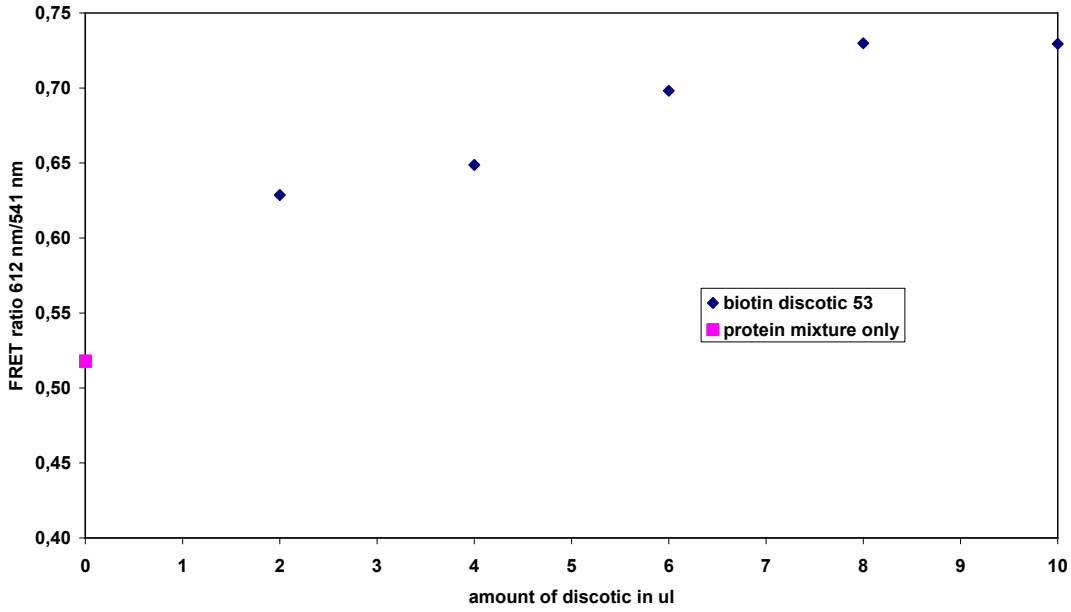

Figure 52. Plot illustrating the FRET ratio (max at 612 nm / max at 541 nm) of the streptavidin-Alexa Fluor 514 and mtreptavidin-Texas Red interaction.

Again, the difference in quantum yield of Alexa Fluorophors and TR is most probably the reason for the constant fluorescence signal of the acceptor TR at its maximum (λ = 612 nm). Additionally, the overlap in excitation wavelength of AF514 and TR seems to result in direct excitation of the FRET acceptor TR and thus causes high FRET ratios in the control studies. A change in FRET pair could overcome this problem. However, only a limited number of streptavidines carrying a fluorescent dye is commercially available. Self performed synthesis and purification of a mono-labeled streptavidin, with a desired dye would afford a tremendous effort on reaction setup and optimization. This was not within the focus of this thesis.
Nevertheless, experiments with both SA-AF514/SA-TR and SA-TR/SA-AF633 show that FRET interaction is significantly enhanced in presence of **53**. The biotin discotic **53** enables protein assembly by binding of the streptavidines to the biotins crowded on the supramolecular surface.

3.4.7 Prospective Modulation of Protein-Assembly with Discotics

Experiments with the model system consisting of biotin discotic and fluorophor labeled streptavidin demonstrated that this supramolecular polymer is able to induce protein assembly if provided with the corresponding protein-binding ligands. Mixtures with inert discotics influence the interaction only if the supramolecules have been mixed prior to the studies. In order to be able to study the influence of the order of compound addition on the magnitude of FRET interaction, a different protein than streptavidin should be chosen in future studies. Binding of different biotin discotics to several binding pockets on one streptavidin most probably resulted in cross-linkage within and between columns. For further studies a mutant streptavidin with only one binding pocked labeled with Cy3 could be used.[105] In this case cross-linkage could be avoided. On the other hand, changing the model protein from streptavidin to another fluorescently labeled protein with a well known ligand could also enable advanced studies. In that case, decoration of the discotic with the corresponding ligand would be necessary.

On the other hand, the FRET pair YFP/CFP could be considered again. Synthesis of the discotic provided with only one functional cysteine group per scaffold could enable the attachment of CFP and YFP without the co-occurrence of disulfide cross-linkages of the discotic scaffolds. This FRET pair is well studied and does not cause in any background signal arised from different quantum yield or overlay of excitation spectra.

Furthermore, experiments on protein assembly are envisaged to be transferred to the living cell. First trials using MDCK cells for microinjection have been carried out already. SA-Cy3 was injected and shown to distribute in the cells. Unfortunately, the setup for microinjection did not allow excitation at the relatively low wavelength of the discotic (340 nm) in connection with the setup for microinjection. Change of the fluorescent microscope to one with lower excitation wavelength is not feasible with the living cells, which need CO_2 atmosphere. For further studies on this challenging experiment a technical setup needs to be generated, which enables determination of FRET between the discotic scaffold and the SA-Cy3 after microinjection to the living cell.
Additionally, methods taking advantage of, for example, cell permeability should be applied. In this case cell permeation and interaction of the FRET partners takes place in the living cells. Subsequently the cells are fixed on a glass slide. FRET measurements on fixed cells allow a higher flexibility concerning the choice of fluorescent microscope and connected setup. The self-assembling discotic scaffold could provide a promising scaffold for modulation of protein interactions even for *in vivo* studies. Future investigation on this topic will lead to valuable contributions to the field of protein assembly.

4 Summary

Discotic monomers reversibly assemble into a columnar polymer at low concentrations in water and can be decorated with ligands to target carbohydrate–lectin polyvalent interactions and bind specific proteins. The ligand density in the polymer can be controlled by reversible exchange of monomers. This supramolecular polymer features strong binding to bacteria and serves as platform for protein assembly. It is easily detected by fluorescence microscopy, and the control over its ligand density allows easy optimization of adjustment to and control over biological systems.

Disc-shaped molecules **1** were built up by linking three *N*-monoacylated 2,2'-bipyridine-3,3'-diamine wedges to a central 1,3,5-benzenetricarbonyl unit. Compounds **18** and **19** were designed featuring three selectively introduced azide or amine functionalities at the periphery of the molecule, which provided a flexible platform for modifications with biological ligands in the final step of the synthesis. They were synthesized in a multistep approach in a convergent fashion, resulting in a discotic molecule provided with six inert ethylene glycol-monomethylether side chains and three azide- or amine-functionalized side chains (Scheme 18).

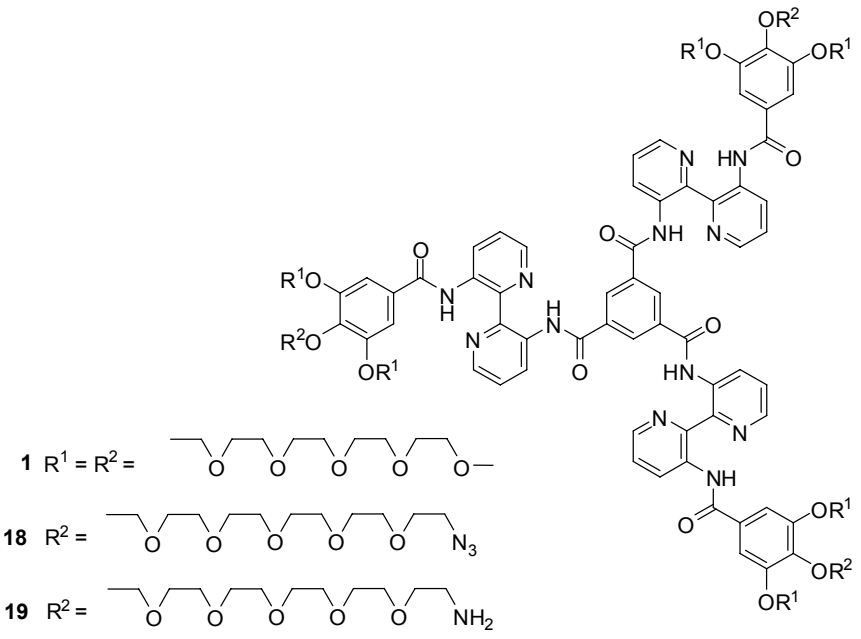

Scheme 18. The discotic scaffolds **18** and **19**, provided with functionalities for modification with ligands and the inert discotic **1**.

Discotic monomers **18** and **19** were decorated with various ligands. Propargyl-derivatives of mannose, glucose and gallactose were attached to the discotic scaffold **18** *via* Huisgen [2+3]-cycloaddition. These reactions required unusually long reaction times apparently due to ligand crowding on the periphery of the supramolecular columns. However, the dynamic rearrangement of the monomers allowed full conversion to the tri-functionalized discotic after four weeks. Compound **19** was decorated with Texas Red, biotin and cysteine. Acylation took place within four hours to three days. All discotic compounds dissolve readily in water and form supramolecular polymers (K_{ass} ~ 1 x 10^8 M^{-1}).

The binding of polyvalent supramolecular polymers built up out of **1** or mannose modified discotic **49** and mixtures thereof to bacteria was investigated by microscopy studies with the *E. coli* strain BL 21α, taking advantage of the strong auto-fluorescence of the discotic monomers when present as supramolecular polymer. Only when the bacteria were incubated with mannose discotic **49** could a strong fluorescence of the bacterial aggregates be observed, colocalizing with the brightfield image (Figure 53). Both the control experiments with nonfunctionalized scaffold **1** and with water did not show fluorescence. The specificity of the interaction of mannose modified discotic **49** with the mannose binding FimH receptors on the bacterial surface was confirmed through binding studies on two *E. coli* strains, ORN178 and ORN208. The supramolecular polymers thus bind to the bacteria through the mannose-FimH receptor interaction selectively and do not induce unspecific binding. A competition experiment between mannose discotic **49** and mannose on binding to bacteria demonstrated highly efficient polyvalent binding of the supramolecular polymers to the bacteria.

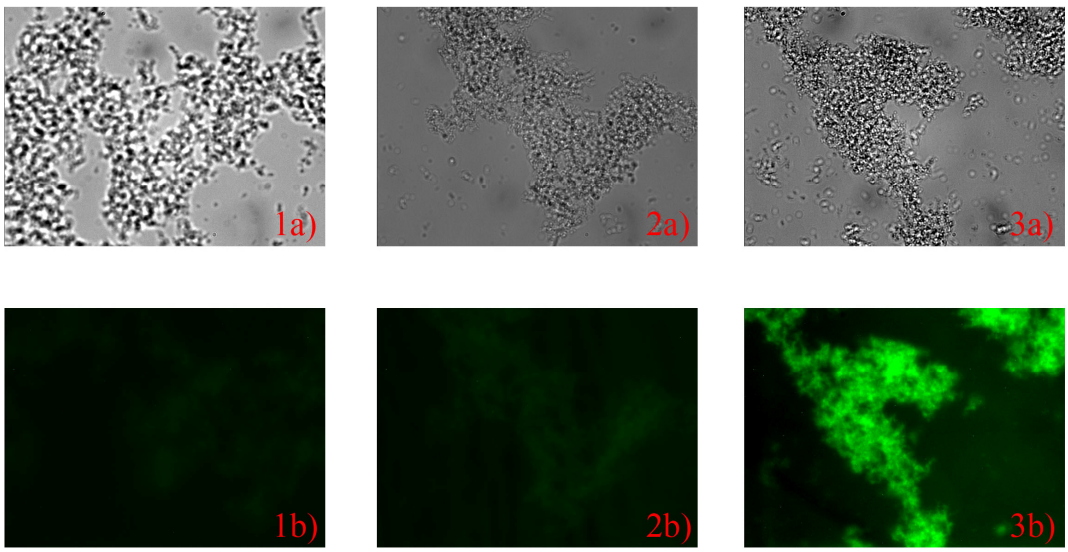

Figure 53. Microscopy pictures demonstrating binding of mannose modified discotic **49** to bacteria taken in a) brightfield and b) fluorescence (λ_{ex} = 360 nm, λ_{em} = 490 nm) mode on *E. coli* incubated with 1) water, 2) inert discotic **1**, 3) mannose discotic **49**. Only in presence of **49** a strong fluorescence of the bacterial aggregates could be observed, colocalizing with the brightfield image.

Supramolecular polymers consisting of mixtures of **1** and mannose discotic **49** were generated and similarly evaluated at dilute bacteria concentrations. These supramolecular copolymers induced bacterial aggregation at all mixture compositions evaluated. A functional-monomer percentage as low as 1% of mannose discotic **49** still resulted in the formation of bacterial aggregates. Evidently, only a limited number of mannose functionalities at the periphery of the supramolecular polymer are required to induce clustering of the bacteria around the columns. Furthermore, the supramolecular polymers are sufficiently long to bridge the distances between the few functional monomers **49** to induce bacterial cross-linking. The supramolecular nature of the polymer allows for easy adjustments and optimization of this monomer composition.

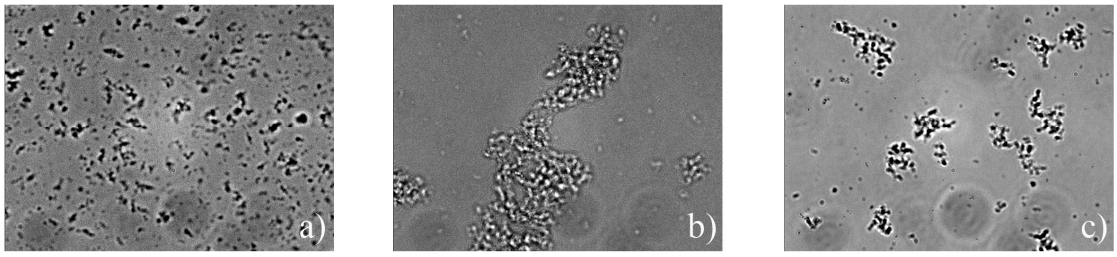

Figure 54. Microscopy pictures demonstrating aggregation of bacteria induced by mannose modified discotic **49** and by mixtures with **49** and inert discotic **1.** Microscopy pictures were taken in brightfield mode on dilute bacterial samples incubated with a) 100% **1**, b) 99/1 **1/49** and c) 100% **49**.

To quantify the polyvalent binding of the supramolecular polymers of **49**, an enzyme linked lectin assay (ELLA) was performed using horseradish peroxidase labeled Con A as the lectin and yeast mannan as the surfacefixed-ligand. The IC_{50} value for the methyl glycoside was around 3000 µM in our assay and the IC_{50} value for **49** around 120 µM (360 µM, valency corrected). The relative valency-corrected binding of **49** was 8.3 times stronger than the reference compound (24.9 per molecule **49**), showing the polyvalent inhibition of the supramolecular polymers. The supramolecular polymers formed by **49** allow effective polyvalent binding up to high valencies and show high potency per ligand. Apparently, because of the polymeric nature of **49**, the compounds are capable of spanning the distance between the mannose binding sites on Con A.

Mixtures of Texas Red discotic **52** and biotin discotic **53** were employed to assess the discotic supramolecules as heterovalent scaffold, which carries more than one functional ligand. Evaluation of the discotic mixture **52**/**53** on streptavidin coated beads showed that Texas Red discotic **52** is localized on the beads surface only in presence of the biotin discotic **53**. Apparently, the biotin discotics include the Texas Red discotics in the supramolecular columns also when they bind to the streptavidin beads. These results confirm that mixtures of different functionalized discotic monomers provide convenient access to heterovalent supramolecules featuring different ligands. Thus, the supramolecular approach gives rise to new highly flexible heterovalent substances.

Besides their ability to control multivalent interactions on bacterial assembly, the discotics were employed as platforms to control protein assembly. The discotic **53**, decorated with biotin ligands, was used to study the interaction of the discotic scaffold with streptavidin. FRET experiments were carried out, using a Cy3 labeled streptavidin (SA-Cy3). The fluorescence overlap of the discotic scaffold (FRET donor) and Cy3 (FRET acceptor) resulted in their FRET interaction. Comparison of FRET between the discotic scaffold and Cy3 in presence of **53** or **1** showed that FRET interaction clearly results from the local proximity of Cy3 with the discotic scaffold of **53** caused by binding of biotin to streptavidin. Experiments with mixtures of **53** and **1** demonstrated that the presence of **1** as spacer enhances the relative amount of streptavidines that interact with the discotic from 7.5 mol-% to over 15 mol-% (Figure 55). Thus the inert discotic serves as spacer and creates free room between the functionalized discotics to allow a higher percentage of biotins to bind to the protein. The ideal mixture of functionalized discotic and inert discotic for optimized energy transfer seems to be about one to two inert discotics per binding scaffold. However, studies to evaluate the influence of the order of compound addition demonstrated that the order in which the interaction partners (**53**, **1** and SA-Cy3) are mixed strongly influences their interaction. Supramolecular columns of the biotin discotic **53** bound to SA-Cy3 do not include inert discotic **1** into the columnar architecture, if **1** is added subsequently to premixed SACy3/**53**. Apparently, the supramolecules formed by **53** can be blocked by SA-Cy3 through cross linking of several discotic monomers to one streptavidin to result a rigid polymer carrying the proteins on the periphery.

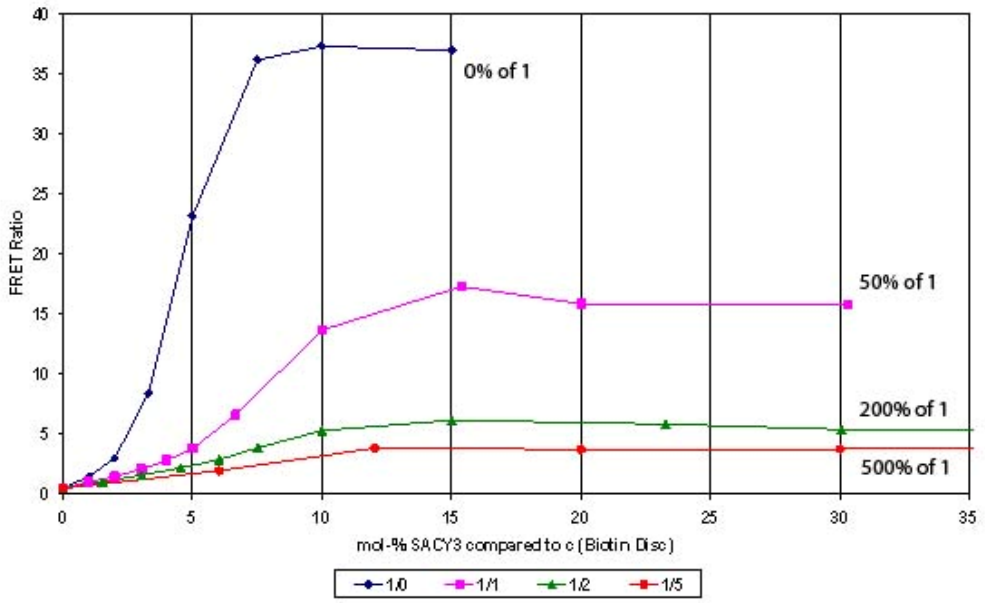

Figure 55. Studies on protein assembly of streptavidin-Cy3 (SA-Cy3) induced by the biotin discotic **53** and mixtures of **53** with inert discotic **1**. FRET interaction of the discotic scaffold and Cy3 was detected. The FRET ratio of different mixtures of **53/1** 1/0 (blue), 1/1 (purple), 1/2 (green) and 1/5 (red) plotted against c[SA-Cy3] compared to c[disc total] = c[**53**] + c[**53**]. The plot illustrates that the relative amount of SA-Cy3 that interacts with the discotic mixtures of **53**/**1** is highest in case of 1/1 and 1/2 mixtures.

The same supramolecular polymer was used to assemble two different proteins along the polymer axis. These experiments on supramolecular control over protein interaction were carried out using streptavidin Alexa Fluor 633 (SA-AF633) and streptavidin Texas Red (SA-TR), taking advantage of the overlay in fluorescence of TR and AF633. Results, summarized in Figure 56, demonstrate that the biotin discotic **53** binds to both streptavidines labeled with the FRET partners SA-AF633 and SA-TR, inducing protein assembly on the periphery of the supramolecular column formed by **53**. Experiments with SA-TR/SA-AF633 and studies with a second FRET pair SA-AF514/SA-TR evidence that the biotin discotic **53** enables protein assembly of two different proteins.

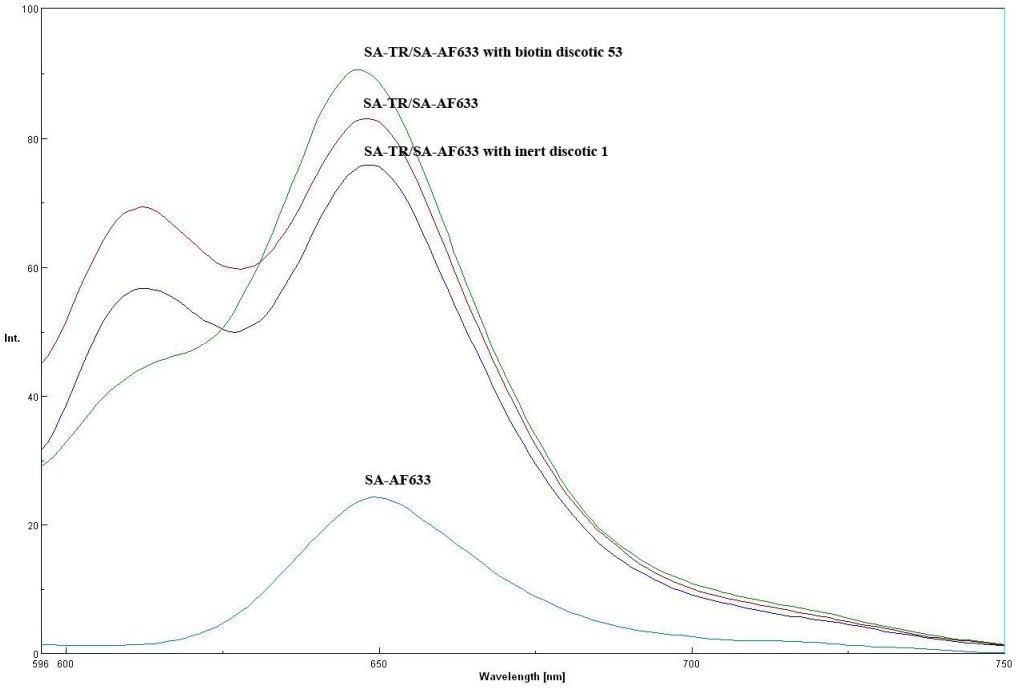

Figure 56. Studies on protein assembly induced by biotin discotic **53**. The plot shows the overlay of the experiments with biotin discotic **53** (green), inert discotic **1** (blue) (both 10 mol-% with respect to the protein mixture), the pure protein mixture SA-AF633/SA-TR (purple) and pure acceptor SA-AF633 as control (light blue). Spectra are taken at an excitation wavelength of 584 nm. Only in presence of **53** the emission of donor SATR is decreased significantly. Apparently, the proteins assemble on the periphery of the supramolecular polymers formed by **53**.

Supramolecular polymers are ideal systems to generate polyvalent architectures for binding and modulation of biological interactions. The self-assembly of monomers in reversible supramolecular polymers provides control over ligand density, polymeric architecture, and environmental response, not accessible with covalent polymeric systems. Supramolecular polymers thus have great potential for all kinds of biological applications where polyvalent effects are relevant. The self-assembling character ensures a reversible display of multiple ligands in dynamic adjustment to the biological interaction partner. The supramolecular nature additionally allows the generation of previously not accessible topologies, with possible new properties, and allows simple mixing of the required different types of monomers for the optimization of the binding event.

5 Experimental

5.1 Material and Methods

Nuclear Magnetic Resonance Spectroscopy

^{1}H and ^{13}C NMR spectra were recorded on one of the following instruments:
Varian Mercury 400 (400 MHz, ^{1}H NMR; 100.6 MHz, ^{13}C NMR)
Bruker DRX 500 (500 MHz, ^{1}H NMR; 125.8 MHz, ^{13}C NMR)
Bruker DRX 600 (600 MHz, ^{1}H NMR; 150.9 MHz, ^{13}C NMR)
with tetramethylsilane as the internal reference. The chemical shifts are provided in ppm and the coupling constants in Hz. The following abbreviations for multiplicities are used: s, singlet; d, doublet; dd, double doublet; t, triplet; q, quadruplet; m, multiplet; br, broad.

Mass Spectrometry

ESI-mass spectra were recorded on a Finnigan LCQ ESI spectrometer. The MALDI-TOF MS spectra were recorded on a Voyager-DE Pro MALDI-TOF MS and with 2,5-dihydroxybenzoic acid (DHB) as the matrix (10 mg DHB, 900 µl H_2O, 90 µl ethanol, 10 µl TFA).

Reversed-Phase High-Pressure Liquid Chromatography

Analytical HPLC was recorded on an Agilent HPLC (1100 series machine) using a 125/21 NUCLEODUR C18 Gravity, 5 µ (Macherey-Nagel) column. The standard gradient began at 10% acetonitrile and was raised to 90% over 15 min. After 3 min at 90% acetonitrile, the column was washed for 5 min with 100% acetonitrile. The column was then equilibrated for 3 min with 10% acetonitrile. Formic acid (0.1% v/v) was added to the HPLC solvents. Analytical HPLC-MS measurements were recorded on an Agilent HPLC (1100 series) coupled to a Finnigan LCQ ESI spectrometer.

Preparative Reversed-Phase High-Pressure Liquid Chromatography

Preparative MS coupled HPLC was run on an Agilent Series 1100/LC/MSD VL (ESI) using a VP50/21 Nucleodur C18 Gravity 21 µm as pre column and a

VP125/21 Nucleodur C18 Gravity 21 µm as main column (both Macherey-Nagel). Compounds were detected at 210 nm and 254 nm and with ESI-MS. The flow rate was 25 ml/min. Water was purified with a Milli-Q-System (Q-Gard 2-cardrige from Millipore). TFA (0.1% v/v) was added to the HPLC solvents.

Thin-Layer Chromatography (TLC)

Thin-layer chromatography (TLC) plates were obtained from Merck (Silica gel 60, F254). The TLCs were visualized by UV light (λ = 254 nm, 366 nm) or by staining with one of the following stains:

Stain A: 0.3 g ninhydrin, 3 mL acetic acid, 97 mL ethanol.

Stain B: 1.6 g $KMnO_4$, 10 g K_2CO_3, 2.5 mL 5% NaOH, 200 mL H_2O.

The solvent system and R_f values are noted for the synthesized compounds.

Flash Chromatography

Flash column chromatography was performed using flash silica gel (Merck, Darmstadt, 40-64 µm) with pressure ranging from 0.5 -1.0 bar. A 70-100-fold excess of silica gel to the crude product was used.

Preparative Size Exclusion Chromatography

Size Exclusion Chromatography was performed on BIO RAD Bio Beads S-X1 (200-400 mesh) in a long glass column (1.2 m) and a flow less than 1 mL/min. Chromatography was carried out using CH_2Cl_2 if not noted different.

Ultraviolet Spectroscopy

UV/VIS spectra were measured with a Cary 100 Spectrometer (Varian Inc.). Absorption spectra were recorded on a Tecan infinite M200 at a compound concentration of approximately 10^{-5} M in water or chloroform. Emission spectra were recorded on a Jasco Fluoreszenzspectrometer FP-6500 at a compound concentration of approximately 10^{-6} M in water or chloroform and excitation at 340 nm (if not stated differently).

General Microscopy

Microscopy studies on multivalency were carried out on a microscope from Axiovert 200M (Zeiss, Jena) in connection with the software Metamorph (Molecular Devices, Downingtown, USA). Pictures were taken with a CoolSnap ES camera (Roper Scientific Photometrics, Tucson, USA). Excitation and emission wavelengths are noted in the corresponding experiments.

Chemicals

Chemicals were obtained from the following suppliers and used without further purification: Acros, Aldrich, Fluka, Lancaster, Novabiochem. CH_2Cl_2 was distilled prior to use following standard protocols. Dry DMF and THF were purchased from Fluka. Additional substances were purchased as follows:

Texas Red®-X succinimidyl ester, Invitrogen (T10244)

NHS-PEO_4-Biotin, Pierce (No 21330)

NHS-PEO_{12}-Biotin, Pierce (No 21312)

Cy™3-Streptavidin, Zymed Laboratories, Invitrogen immunodetection, (43-4315)

Streptavidin Magnetic Beads (1 µm superparamagnetic beads covalently coupled to a highly pure form of streptavidin), New England Biolabs (S1420S).

Buffer

PBS stock solution (0.1 M, 10 fold):

1) 49.8 g Na_2HPO_4 x 2 H_2O in 700 mL H_2O

2) 19.3 g NaH_2PO_4 x 1 H_2O in 350 mL H_2O

3) 84.1 g NaCl

2) was added to 1) until the pH reached 7.3 and 3) was added subsequently.

PBS-Tween (0.1 %): 0.1 % Tween 20 in PBS

Citrate buffer (0.2 M)

1) 25.8 g sodium citrate in 500 mL H_2O

2) 19.2 g citric acid in 500 mL H_2O

2) was titrated to 1) until the pH reached 4.0. Finally 150 µl H_2O_2 (0.015% (v/v)) was added.

5.2 Experimental

5.2.1 Synthesis of the Glycol Side Chains

2-(2-{Benzyloxy}-ethoxy)-ethanol (6)[109]

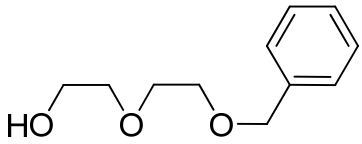

NaH (14.4 g, 0.62 mol, 60% in paraffin) was washed with THF under Argon atmosphere several times and finally suspended in THF (1000 mL). Within 2.5 h diethyleneglycol (145 mL, 1.53 mol) in THF (500 mL) was added, while the reaction mixture was mechanically stirred. Benzylbromide (38 mL, 340 mmol) was added dropwise over a period of 5 h. After stirring over night at 80 °C the reaction mixture was cooled down and poured into ice water (1000 mL). The aqueous layer was extracted with diethlyl ether (3 x 350 mL). The combined organic layers were washed with water (3 x 400 mL) and brine (3 x 300 mL), dried over $MgSO_4$ and the solvent was evaporated *in vacuo.* The crude product was purified by column chromatography (flash silica, starting with 10% ethylacetate and gradually increasing the polarity to 50% ethylacetate in cyclohexane) to yield pure **6** as a colorless oil (220.1 g, 1.13 mol, 73% in respect to NaH).

^{1}H NMR (400 MHz, *CDCl$_3$*) δ = 7.27-7.36 (m, 5H, *H*-benzyl), 4.57 (s, 2H, C*H*$_2$), 3.67-3.74 (m, 4H, OC*H*$_2$C*H*$_2$O), 3.59-3.65 (m, 4H, OC*H*$_2$C*H*$_2$O), 2.60 (br, 1H, O*H*);
^{13}C NMR (101 MHz, *CDCl$_3$*) δ = 137.9, 128.4, 127.7, 127.7, 73.3, 72.4, 70.4, 69.4, 61.8;
HPLC: R_t = 6.61 min;
MS (ESI): calcd. for $[C_{11}H_{16}O_3 + NH_4]^+$ *m/z* = 214.14 found *m/z* = 213.98.

2-(2-{2-Methoxyethoxy)-ethoxy}-ethyl p-tosylate (8)

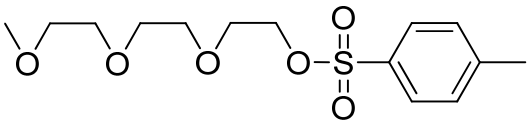

A two-phase system of NaOH (40.8 g, 1.02 mol) in water (200 mL) and 2-(2-{2-methoxy-ethoxy}-ethoxy)-ethanol (120 mL, 0.67 mol) in THF (100 mL) was cooled *via* an ice-bath with magnetic stirring. *p*-Toluenesulfonyl chloride (146.4 g, 0.76 mol) in THF (200 mL) was added dropwise to the mixture, while maintaining the temperature below 5 °C. The solution was stirred at 0 °C for another 5 h and then poured into ice-water (100 mL). The mixture was extracted with CH_2Cl_2 (3 x 150 ml) and the combined organic layers were washed with 1 N HCl (2 x 300 mL) and brine (1x 300 mL), dried over $MgSO_4$ and the solvent was evaporated *in vacuo.* The crude product was purified by column chromatography (flash silica, starting with 10% ethylacetate and gradually increasing the polarity to 50% ethylacetate in cyclohexane) to yield pure **8** as a colourless oil (151.9 g, 0.45 mol, 65%).

^{1}H NMR (400 MHz, *CDCl$_3$*) δ = 7.78 (d, *J* = 8.4 Hz, 2H, *H*-benzyl), 7.33 (d, *J* = 8.4 Hz, 2H, *H*-benzyl), 4.15 (t, 2H, OCH_2CH_2OTs), 3.69-3.65 (m, 2H, OCH_2CH_2O), 3.61-3.56 (m, 6H, OCH_2CH_2O), 3.53-3.50 (m, 2H, OCH_2CH_2OH), 3.35 (s, 3H, OCH_3), 2.43 (s, 3H, CH_3Ar);
^{13}C NMR (101 MHz, *CDCl$_3$*) δ = 144.7, 133.0, 129.8, 127.9, 71.9, 70.7, 70.5, 70.5, 69.2, 68.6, 59.0, 21.6;
HPLC: R_t = 8.50 min;
MS (ESI): calcd. for $[C_{14}H_{22}O_6S + NH_4]^+$ *m/z* = 336.14 found *m/z* = 336.00.

1-Benzyloxy-2-(2-{2-[2-(2-methoxyethoxy)-ethoxy]-ethoxy}-ethoxy)-ethane (9)

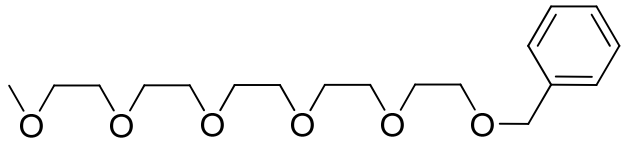

Compound **8** (123.7 g, 0.37 mol), **6** (60.0 g, 0.30 mol) and KOH (68.7 g, 1.22 mol) were heated under reflux in THF (500 mL) over night. The reaction mixture was poured in ice water and extracted with CH_2Cl_2 (3 x 400 mL). The combined organic layers were washed with brine, dried over $MgSO_4$ and evaporated *in vacuo*. The crude product was purified by column chromatography (flash silica, starting with 100% chloroform and gradually increasing the polarity to 5% methanol in chloroform) to yield pure compound **9** as a colorless oil (92.4 g, 0.27 mmol, 88%).

^{1}H NMR (400 MHz, *CDCl$_3$)* δ = 7.36-7.22 (m, 5H, *H*-benzyl), 4.55 (s, 2H, C*H*$_2$), 3.68-3.60 (m, 18H, OC*H*$_2$C*H*$_2$O), 3.55-3.50 (m, 2H, OCH$_2$C*H*$_2$OTs), 3.36 (s, 3H, OC*H*$_3$);
^{13}C NMR (101 MHz, *CDCl$_3$*) δ = 138.5, 128.5, 127.9, 127.8, 73.4, 72.1, 70.9, 70.8-69.7, 59.2;
HPLC: R_t = 8.07 min;
MS (ESI): calcd. for $[C_{18}H_{30}O_6 + NH_4]^+$ *m/z* = 360.24 found *m/z* = 360.19.

2-(2-{2-[2-(2-Methoxyethoxy)-ethoxy]-ethoxy}-ethoxy)-ethan-1-ol (10)

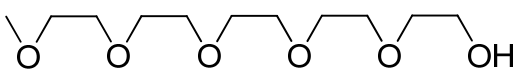

To a solution of **9** (55.13 g, 0.16 mol) in ethanol/water (50 mL/5 mL) and conc. HCl (0.5 mL) a catalytic amount of Pd/C (10%) (2 mmol) was added. The suspension was stirred for 12 h under an H_2-atmosphere of 50 bar in an

autoclave and then filtered through celite®. The filtrate was evaporated *in vacuo* to yield the product as a colorless oil (40.3 g, 0.16 mol, quant.).

^{1}H NMR (400 MHz, *CDCl$_3$)* δ = 3.78-3.70 (m, 2H, OC*H*$_2$C*H*$_2$O), 3.70-3.59 (m, 16H, OC*H*$_2$C*H*$_2$O), 3.55 (dd, *J* = 5.8 and 3.5 Hz, 2H, OCH$_2$C*H*$_2$OH), 3.38 (s, 3H, OC*H*$_3$), 2.93 (s, 1H, O*H*);
^{13}C NMR (101 MHz, *CDCl$_3$*) δ = 72.4, 71.8, 70.5-70.2, 61.6, 59.0;
HPLC: R_t = 6.85 min;
MS (ESI): calcd. for $[C_{11}H_{24}O_6 + NH_4]^+$ *m/z* = 270.19 found *m/z* = 270.05.

2-(2-{2-[2-(2-Methoxyethoxy)-ethoxy]-ethoxy}-ethoxy)-ethyl-1-p-tosylate (11)

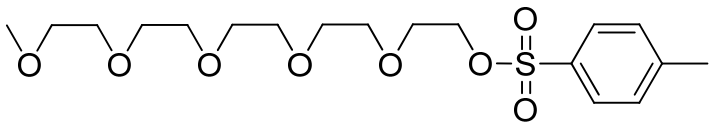

To a solution of **10** (40.0 g, 0.16 mol) and triethylamine (25 ml, 0.19 mol) in CH_2Cl_2 (200 mL) *p*-toluenesulfonyl chloride (35.0 g, 0.18 mol) in CH_2Cl_2 (300 mL) was added dropwise. The reaction was stirred over night and then washed with 1 N HCl (3 x 100 mL) and brine (100 mL). Drying over $MgSO_4$ and evaporating the solvent *in vacuo* yielded the crude product. Purification by column chromatography (flash-silica, starting with 100% CH_2Cl_2 and increasing the polarity to 5% methanol in CH_2Cl_2) yielded pure compound **11** as a colorless oil (46.80 g, 0.11 mol, 72%).

^{1}H NMR (400 MHz, *CDCl$_3$)* δ = 7.77 (d, *J* = 8.6 Hz, 2H, *H*-benzyl), 7.32 (d, *J* = 8.6 Hz, 2H, *H*-benzyl), 4.13 (t, 2H, OCH$_2$C*H*$_2$OTs), 3.69-3.64 (m, 2H, OC*H*$_2$C*H*$_2$O), 3.64-3.54 (m, 14H, OC*H*$_2$C*H*$_2$O), 3.54-3.50 (m, 2H, OCH$_2$C*H*$_2$OH), 3.35 (s, 3H, OC*H*$_3$), 2.42 (s, 3H, C*H*$_3$Ar);
^{13}C NMR (101 MHz, *CDCl$_3$*) = 144.6, 132.9, 129.6, 127.8, 71.7, 70.6-70.3, 69.0, 68.5, 58.8. 21.4;
HPLC: R_t = 7.96 min;

MS (ESI): calcd. for $[C_{18}H_{30}O_8S + NH_4]^+$ *m/z* = 424.20 found *m/z* = 424.12.

2[-2-(2-{2-[2-(2-Hydroxyethoxy)-ethoxy]-ethoxy}-ethoxy)-ethoxy]- ethyl p-tosylate (21)

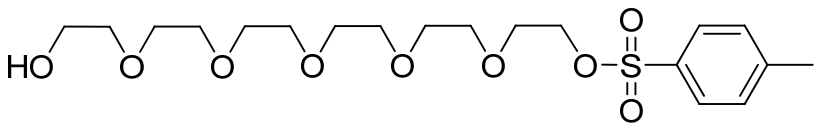

To a solution of hexaethyleneglycol (50 g, 177 mmol) and triethylamine (14 mL, 100 mmol) in THF (250 mL) *p*-toluenesulfonyl chloride (13 g, 70 mmol) in THF (250 mL) was added and stirred over night. The solution was diluted with CH_2Cl_2 (200 mL) washed with 1N HCl (3 x 150 mL) and brine (150 mL) and dried over $MgSO_4$. After evaporating the solvents *in vacuo* the residue was purified by column chromatography (silica, 2% methanol in CH_2Cl_2) to give **21** (24.4 g, 56 mmol, 80% compared to *p*-toluenesulfonyl chloride) as a colorless oil.

^{1}H NMR (400 MHz, *$CDCl_3$)* δ = 7.79 (d, *J*=8.1, 2H, Ar-C*H*), 7.33 (d, *J* = 8.0, 2H, *H*-benzyl), 4.15 (dd, 2H, $OCH_2CH_2OSO_2$-Ar), 3.74-3.56 (m, 22H, OCH_2CH_2O), 2.93 (br, 1H, O*H*), 2.44 (s, 3H, CH_3Ar);
^{13}C NMR (101 MHz, *$CDCl_3$*) δ = 145.0, 133.3, 130.0, 128.2, 72.7, 70.9-70.5, 69.5, 68.9, 61.9, 21.8;
HPLC: R_t = 7.14 min;
TLC (5 % methanol in CH_2Cl_2): R_f = 0.32;
MS (ESI): calcd. for [C19H32O9S + NH4]$^+$ *m/z* = 454.21 found *m/z* = 454.08.

2[-2-(2-{2-[2-(2-Hydroxyethoxy)-ethoxy]-ethoxy}-ethoxy)-ethoxy]- ethyl azide (22)

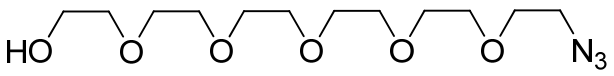

Compound **21** (24.4 g, 56 mmol) and NaN_3 (3.7 g, 57 mmol) in DMF (150 mL) were stirred over night. Subsequently the solvent was evaporated *in vacuo*. The residue was resolved in ethylacetate, filtrated over Celite® and the solvent was again evaporated *in vacuo* to yield pure **22** (14.6 g, 48 mmol, 85%).

^{1}H NMR (400 MHz, *CDCl$_3$*) δ = 3.72-3.57 (m, 22H, OCH_2CH_2O), 3.37 (t, 2H, CH_2N_3), 2.80 (s, 1H, O*H*);
^{13}C NMR (101 MHz, *CDCl3*) δ = 72.8, 70.7-70.1, 61.8, 50.7;
HPLC: R_t = 6.05 min;
TLC (6 % methanol in CH_2Cl_2): R_f = 0.38;
MS (ESI): calcd. for $[C_{12}H_{25}N_3O_6 + NH_4]^+$ *m/z* = 325.20 found *m/z* = 325.07.

2[-2-(2-{2-[2-(2-Azido-ethoxy)-ethoxy]-ethoxy}-ethoxy)-ethoxy]- ethyl p-tosylate (23)

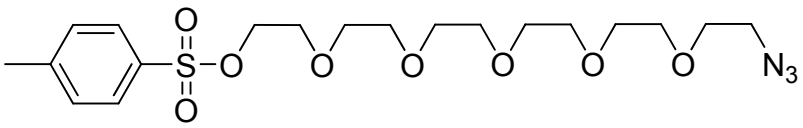

To a solution of **22** (14.6 g, 48 mmol) and triethylamine (13.4 mL, 100 mmol) in CH_2Cl_2 (80 mL) *p*-toluenesulfonyl chloride (11.9 g, 63 mmol) in CH_2Cl_2 (100 mL) was added dropwise at roomtemperature. The reaction was stirred over night and then washed with 1N HCl (3 x 100 mL) and brine (100 mL). Drying over $MgSO_4$ and evaporating the solvent *in vacuo* gave the crude product. Purification by column chromatography (flash-silica, starting with 100% CH_2Cl_2 and increasing the polarity to 4% methanol in CH_2Cl_2) yielded the pure compound as a colorless oil (14.6 g, 32 mmol, 66%).

^{1}H NMR (400 MHz, *CDCl$_3$*) δ = 7.79 (d, *J* = 7.9, 2H, *H*-benzyl), 7.33 (d, *J*=8.0, 2H, *H*-benzyl), 4.15 (t, 2H, $OCH_2CH_2OSO_2$-Ar), 3.74-3.54 (m, 20H, OCH_2CH_2O), 3.37 (t, 2H, CH_2N_3), 2.44 (s, 3H, CH_3Ar);
^{13}C NMR (101 MHz, *CDCl$_3$*) δ = 144.9, 133.2, 130.0, 128.1, 70.9-68.8, 50.8, 21.8;

HPLC: R_t = 9.45 min;
TLC (5 % methanol in CH_2Cl_2): R_f = 0.36;
MS (ESI): calcd. for $[C_{19}H_{31}N_3O_8S + NH_4]^+$ *m/z* = 479.22 found *m/z* = 479.12.

2[-2-(2-{2-[2-(2-Hydroxyethoxy)-ethoxy]-ethoxy}-ethoxy)-ethoxy]- ethyl amine (24)

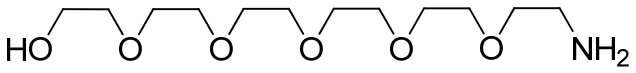

22 (7.2 g, 23 mmol) was dissolved in ethanol (20 mL) and water (5 mL) and Pd/C (10%, 0.3 g) was added. The suspension was stirred for 48 h under an H_2-atmosphere (10 bar) in an autoclave and subsequently filtered through celite®. The solvents were evaporated *in vacuo* to yield **24** (6.2 g, 22 mmol, 96%).

^{1}H NMR (400 MHz, *CDCl$_3$)* δ = 3.74-3.50 (m, 22H, OC*H*$_2$C*H*$_2$O), 2.93 (s, 2H, N*H*$_2$), 2.87 (t, *J*=5.1, 2H, C*H*$_2$N*H*$_2$);
^{13}C NMR (101 MHz, *CDCl$_3$*) δ = 77.54, 77.22, 76.90, 72.92-70.34, 61.79, 58.64, 19.87;
HPLC: R_t = 1.91 min;
MS (ESI): calcd. for $[C_{12}H_{27}NO_6 + H]^+$ *m/z* = 282.18 found *m/z* = 282.13.

2[-2-(2-{2-[2-(2-Hydroxyethoxy)-ethoxy]-ethoxy}-ethoxy)-ethoxy]- ethyl-tert-butylcarbamat (25)

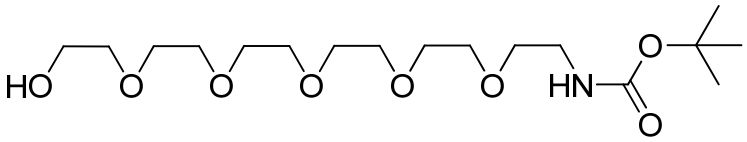

To a solution of **24** (6.2 g, 22 mmol) in dioxane (30 mL) di-*tert*-butyldicarbonat (6.0 g, 27 mmol) was added at 0 °C and stirred for 3 h. Subsequently

triethylamine (4 mL, 30 mmol) was given to the mixture and stirred over night at rt. The solvent was evaporated *in vacuo* and the crude product was purified by column chromatography (silica, 3% methanol in CH_2Cl_2) to yield **25** (5.1 g, 13 mmol, 59%).

^{1}H NMR (400 MHz, *CDCl*$_3$) δ = 3.70-3.51 (m, 20H, OC*H*$_2$C*H*$_2$O), 3.47 (t, *J* = 5.2, 2H, OC*H*$_2$CH$_2$NHboc), 3.24 (dd, *J* = 10.1 and 5.2, 2H, OCH$_2$C*H*$_2$NHboc), 1.37 (s, 9H, OC(C*H*$_3$)$_3$);
^{13}C NMR (101 MHz, *CDCl3*) δ = 155.6, 72.67-70.4, 61.8, 53.6, 40.5, 28.6.
HPLC: R_t = 6.38 min;
MS (ESI): calcd. for $[C_{17}H_{35}NO_8 + H]^+$ *m/z* = 382.16 found *m/z* = 382.02.

2[-2-(2-{2-[2-(2-tert-butoxycarbonylamino)-ethoxy)-ethoxy]-ethoxy}-ethoxy)-ethoxy]- ethyl p-tosylate (26)

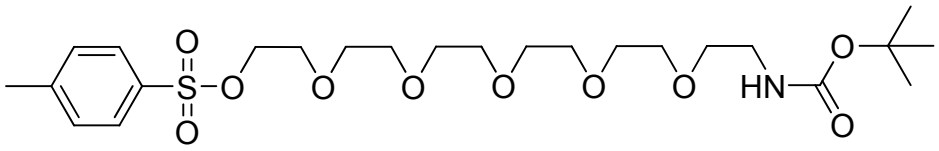

To a solution of **25** (5.06 g, 13.3 mmol) and triethylamine (5.0 mL, 38.0 mmol) in THF (50 mL) *p*-toluenesulfonyl chloride (3.04 g, 16.1 mmol) in THF (50 mL) was added dropwise. The reaction was stirred over night and then washed with 1N HCl (3 x 50 mL) and brine (50 mL). Drying over $MgSO_4$ and evaporating the solvent *in vacuo* gave the crude product. Purification by column chromatography (silica, 3% methanol in CH_2Cl_2) yielded the pure compound as a colourless oil (4.41 g, 8.2 mmol, 62%).

^{1}H NMR (400 MHz, *CDCl*$_3$) δ = 7.79 (d, *J* = 8.1, 2H, *H*-benzyl), 7.33 (d, *J* = 8.1, 2H, *H*-benzyl), 5.01 (br, 1H, N*H*), 4.15 (t, 2H, C*H*$_2$OSO$_2$-Ar), 3.71-3.49 (m, 20H, OC*H*$_2$C*H*$_2$O), 3.29 (d, *J* = 4.4, 2H, C*H*$_2$NHboc), 2.44 (s, 3H, C*H*$_3$Ar), 1.43 (s, 9H, OC(C*H*$_3$)$_3$);
HPLC: R_t = 8.97 min;

MS (ESI): calcd. for $[C_{24}H_{41}NO_{10}S + Na]^+$ *m/z* = 558.23 found *m/z* = 558.06.

5.2.2 Synthesis of the Bipyridine Core

3,3'-Dinitro-2,2'-bipyridine (3)[73]

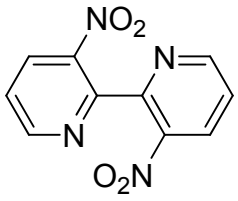

To a solution 2-chloro-3-nitropyridin (24.9 g, 158 mmol) in DMF (125 mL) Cu powder (12.6 g, 200 mmol) was added in small portions. The suspension was stirred under argon atmosphere for 3 h at 110 °C. Subsequently the hot reaction mixture was filtered over Celite®. The filtrate was diluted with ammonia (5% in water, 100 mL), the solid was filtered immediately and washed. Recrystallisation from ethanol gave the bipyridine **3** (8.5 g, 34 mmol, 21%) as a yellow solid.

^{1}H NMR (400 MHz, *DMSO-D6*) δ = 8.92 (dd, *J* = 4.8 and 1.4, 2H, *H*-6 and *H*-6'), 8.70 (dd, *J* = 8.3 and 1.4, 2H, *H*-4 and *H*-4'), 7.87 (dd, *J* = 8.3 and 4.8, 2H, *H*-5 and *H*-5');
^{13}C NMR (101 MHz, *DMSO-D6*) δ = 153.0, 149.2, 144.6, 133.7, 125.4;
HPLC: R_t = 7.67 min;
MS (ESI): calcd. for $[C_{10}H_6N_4O_4 + H]^+$ *m/z* = 247.05 found *m/z* = 247.10.

2,2'-Bipyridyl-3,3'-diamine (4)[73]

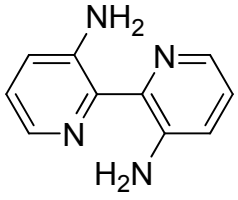

Tin(II) chloride (47.3 g, 243 mmol) was dissolved in HCl (17%, 190 mL) and **3** (6.5 g, 27 mmol) was added in portions. The resulting mixture was stirred for 2.5 h under reflux. The reaction mixture was cooled to rt and the pH was adjusted to 14 using NaOH (4 N). The aqueous layer was extracted with chloroform (3 x 350 mL). The combined organic layers were dried over $MgSO_4$ and the solvent was evaporated *in vacuo* to yield **4** (3.6 g, 19 mmol, 72%) as yellow crystals.

^{1}H NMR (400 MHz, *DMSO-D$_6$*) δ = 7.85 (d, *J* = 4.4, 2H, *H*-6 and *H*-6'), 7.15 (d, *J* = 8.2, 2H, *H*-4 and *H*-4'), 7.09 (s, 4H, N*H*$_2$), 7.06 (dd, *J*=8.2 and 4.4, 2H, *H*-5 and *H*-5');
^{13}C NMR (101 MHz, *DMSO-D$_6$*) δ = 144.6, 139.2, 133.9, 123.0, 122.8;
HPLC: R_t = 1.25 min;
MS (ESI): calcd. for $[C_{10}H_{10}N_4 + H]^+$ *m/z* = 187.10 found *m/z* = 187.24.

5.2.3 Synthesis of the Inert Discotic

Methyl- 3,4,5-tris[2-(2-{2-[2-(2-methoxyethoxy)-ethoxy]-ethoxy}-ethoxy)-ethoxy]-benzoate (13)

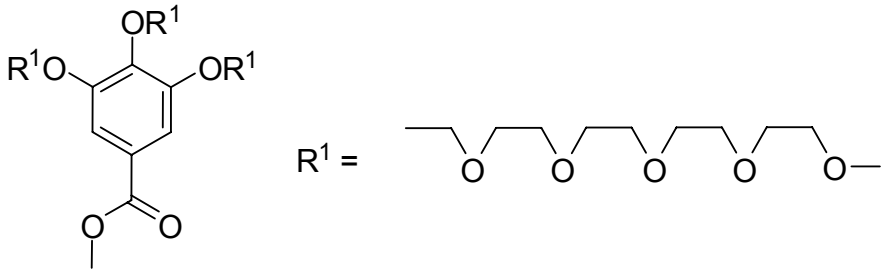

A mixture of **11** (3.6 g, 8.8 mmol), methyl 3,4,5-trihydroxybenzoate (0.48 g, 2.6 mmol) and K_2CO_3 (4.4 g, 32.0 mmol) was stirred over night at 70 °C in dry DMF (20 mL). The reaction mixture was poured in water (50 mL) and extracted with CH_2Cl_2 (3 x 50 mL). The combined organic layers were washed with brine (2 x 20 mL), dried over $MgSO_4$ and evaporated *in vacuo*. The crude product

was purified by column chromatography (alumina, 1% ethanol in chloroform) affording the pure compound **13** (1.86 g, 2.0 mmol, 81%).

^{1}H NMR (400 MHz, *CDCl$_3$)* δ = 7.27 (s, 2H, *H*-benzoyl), 4.20 (t, 4H, *m*-OC*H*$_2$CH$_2$O), 4.17 (t, 2H, *p*-OC*H*$_2$CH$_2$O), 3.86 (s, 3H, COOC*H*$_3$), 3.83 (t, 4H, *m*-OCH$_2$C*H*$_2$O), 3.77 (t, 2H, *p*-OCH$_2$C*H*$_2$O), 3.72-3.59 (m, 48H, OC*H*$_2$C*H*$_2$O), 3.35 (s, 9H, OC*H*$_3$);
^{13}C NMR (101 MHz, *CDCl$_3$*) δ = 166.5, 152.2, 142.5, 124.9, 108.9, 72.3-68.8, 58.9, 52.1.

3,4,5-Tris[2-(2-{2-[2-(2-methoxyethoxy)-ethoxy]-ethoxy}-ethoxy)-ethoxy]-benzoic acid (14)

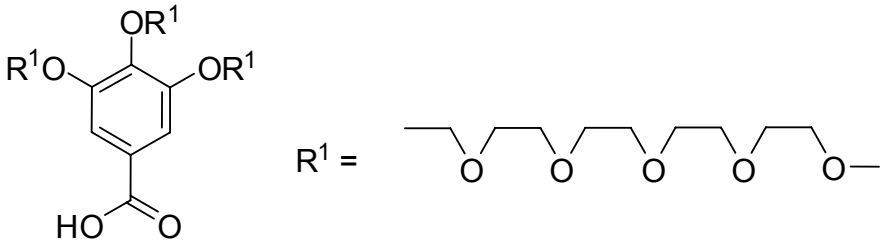

A solution of **13** (1.86 g, 2.0 mmol) and KOH (0.40 g, 7.1 mmol) in ethanol (15 mL) and water (15 mL) was heated under reflux overnight. Subsequently, the solution was cooled, acidified to pH = 2 and extracted with CH_2Cl_2 (3 x 30 mL). The CH_2Cl_2 layer was washed with brine. Drying over $MgSO_4$, evaporating *in vacuo* and drying over P_2O_5 afforded the pure compound **14** (1.43 g, 1.6 mmol, 82%).

^{1}H NMR (400 MHz, *CDCl$_3$)* δ = 7.34 (s, 2H, *H*-benzoyl), 4.23 (t, 4H, *m*-OC*H*$_2$CH$_2$O), 4.21 (t, 2H, *p*-OC*H*$_2$CH$_2$O), 3.84 (t, 4H, *m*-OCH$_2$C*H*$_2$O), 3.87 (t, 2H, *p*-OCH$_2$C*H*$_2$O), 3.73-3.50 (m, 48H, OC*H*$_2$C*H*$_2$O), 3.36 (s, 9H, *m*-OC*H*$_3$ and *p*-OC*H*$_3$);
^{13}C NMR (101 MHz, *CDCl$_3$*) δ = 168.9, 152.2, 142.9, 124.6, 109.3, 72.5-68.8, 58.9;

HPLC: R_t = 6.59 min;

MS (ESI): calcd. for $[C_{40}H_{74}O_{20} + NH_4]^+$ *m/z* = 890.50 found *m/z* = 890.76.

3'-{3,4,5-Tris[2-(2-{2-[2-(2-methoxyethoxy)-ethoxy]-ethoxy}-ethoxy)-ethoxy]- benzoylamino}-2,2'-bipyridine-3-amine (16)

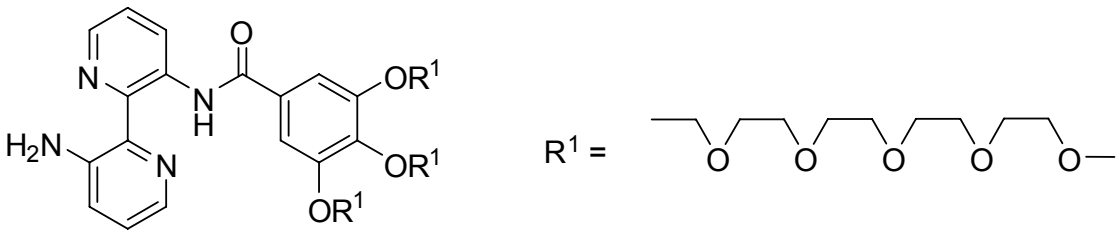

A solution of oxalyl chloride (0.23 g, 1.8 mmol) in dry CH_2Cl_2 (5 ml) containing a catalytic amount of DMF was added dropwise to a solution of **14** (1.43 g, 1.6 mmol) in dry CH_2Cl_2 (10 mL). The reaction mixture was stirred overnight at rt in the absence of light. Evaporating the solvent *in vacuo* afforded the crude product **15** (1.33 g, 1.5 mmol, 94%). This product was dissolved in dry CH_2Cl_2 (20 mL) and added dropwise to a stirred solution of 2,2'-bipyridyl-3,3'-diamine **4** (0.31 g, 1.7 mmol) and triethylamine (0.25 mL, 1.7 mmol) in dry CH_2Cl_2 (20 mL), while the temperature was kept below 5 °C. After stirring for 3 h the solution was diluted with CH_2Cl_2, washed with water (3 x 20 mL) and brine (1 x 20 mL) and dried over $MgSO_4$. After evaporation of the solvents *in vacuo* the crude product was purified by column chromatography (silica, ethylacetate followed by 5% methanol in chloroform) and size exclusion chromatography. Drying over P_2O_5 gave compound **16** (1.03 g, 1.0 mmol, 62%).

^{1}H NMR (400 MHz, *$CDCl_3$)* δ = 14.40 (s, 1H, N*H*CO), 9.21 (dd, *J* = 8.4 and 1.8 Hz, 1H, *H*-4'), 8.34 (dd, *J* = 4.5 and 1.5 Hz, 1H, *H*-6'), 8.04 (dd, *J* = 2.9 and 2.7 Hz, 1H, *H*-6), 7.33 (s, 2H, *H*-benzoyl), 7.31 (dd, *J* = 9.0 and 4.2 Hz, 1H, *H*-5'), 7.15 (m, 2H, *H*-4 and *H*-5), 6.59 (s, 2H, N*H_2*), 4.25 (m, 6H, benzoyl-OC*H_2*), 3.89 (t, 4H, *m*-OCH_2CH_2O), 3.82 (t, 2H, *p*-OCH_2CH_2), 3.75-3.52 (m, 48H, OCH_2CH_2O), 3.37 (s, 6H, *m*-OC*H_3*), 3.36 (s, 3H, *p*-OC*H_3*);

^{13}C NMR (101 MHz, *CDCl$_3$*) δ = 165.7, 152.6, 145.1, 143.6, 142.0, 140.8, 138.5, 136.1, 135.0, 130.8, 128.6, 125.3, 124.3, 122.7, 107.8, 72.4-69.2, 59.0;
HPLC: R_t = 7.18 min;
MS (ESI): calcd. for $[C_{50}H_{80}N_4O_{19} + H]^+$ *m/z* = 1041.55 found *m/z* = 1041.89.

N,N',N''-Tris{3[3'-(3,4,5-tris{2-(2-{2-[2-(2-methoxyethoxy)-ethoxy]-ethoxy}-ethoxy)-ethoxy})-benzoylamino]-2,2'-bipyridyl}benzene-1,3,5-tricarboxamide (1)

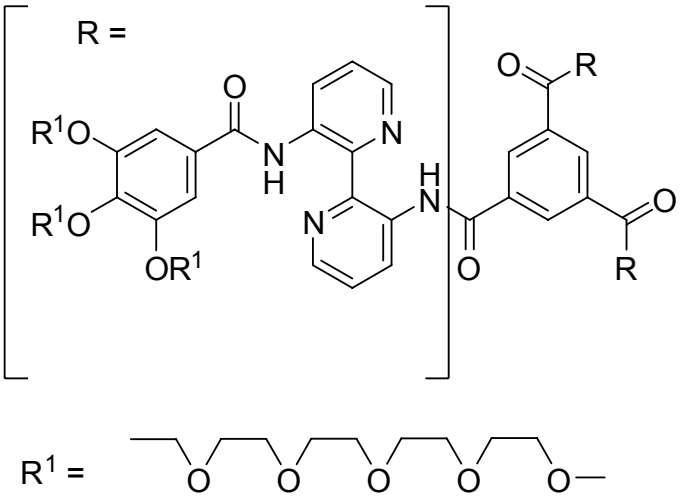

To a solution of **16** (1.00 g, 0.96 mmol) and triethylamine (0.14 mL) in dry CH_2Cl_2 (10 mL), a solution of trimesic chloride (80 mg, 0.3 mmol) in dry CH_2Cl_2 (5 mL) was added dropwise at room temperature. Stirring was continued overnight, after which the solution was diluted with CH_2Cl_2 and washed with water (2 x 25 mL). The combined water layers were extracted with CH_2Cl_2 (4 x 25 mL). The combined dichloromethane layers were washed with brine (1 x 20 mL), dried over $MgSO_4$ and evaporated *in vacuo*. The crude product was purified by column chromatography (silica, 2% methanol in chloroform) and size exclusion chromatography (in CH_2Cl_2). Thoroughly drying over P_2O_5 afforded **1** (0.58 g, 0.18 mmol, 59%).

^{1}H NMR (400 MHz, *CDCl$_3$)* δ = 15.61 (s, 3H, N*H*CO), 14.33 (s, 3H, N*H'*CO), 9.55 (br, 3H, *H*-4), 9.36 (d, 3H, *H*-4'), 9.24 (s, 3H, *o*-*H*), 9.01 (d, 3H, *H*-6'), 8.52

(dd, 3H, *H*-6), 7.57 (dd, 6H, *H*-5 and *H*-5'), 7.34 (s, 6H, *H*-benzoyl), 4.26 (t, 12H, *m*-OC*H*$_2$CH$_2$O), 4.22 (t, 6H, *p*-OC*H*$_2$CH$_2$O), 3.91 (t, 12H, *m*-OCH$_2$C*H*$_2$O), 3.88 (t, 6H, *p*-OCH$_2$C*H*$_2$O), 3.76-3.58 (m, 147H, OC*H*$_2$C*H*$_2$O), 3.36 (s, 9H, *p*-OC*H*$_3$), 3.34 (s, 18H, *m*-OC*H*$_3$);
^{13}C NMR (101 MHz, *CDCl*$_3$) δ = 166.0, 163.8, 153.0, 142.6, 142.3, 141.7, 141.0, 137.6, 137.6, 136.2, 130.7, 130.6, 130.0, 129.8, 125.1, 124.9, 108.2, 72.7-69.6, 59.2;
MS (MALDI-TOF): calcd. for $[C_{159}H_{240}N_{12}O_{60} + Na]^+$ *m/z* = 3300.6 found *m/z* = 3300.1.

5.2.4 Synthesis of the Azide Modified Discotic Scaffold

Methyl-3,4,5-triacetoxy-benzoat (27)[75]

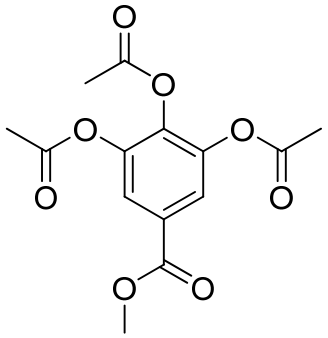

To a solution methyl-3,4,5-trihydroxybenzoate (30.0 g, 165 mmol) in pyridine (60 mL) acetic anhydride (150 mL) was added dropwise. The mixture was stirred over night, poured in CH_2Cl_2 (500 mL) and washed with brine (3 x 200 mL). The combined water layers were extracted with ethylacetate (3 x 200 mL). The combined organic layers were dried over $MgSO_4$ and evaporated *in vacuo*. The crude product was purified by column chromatography (silica, 30% ethylacetate in cyclohexane) affording the pure compound (41.2 g, 132 mmol, 80%) as colorless crystals.

mp: 127.8 °C;

^{1}H NMR (400 MHz, *CDCl$_3$)* δ = 7.80 (s, 2H, *H*-benzoyl), 3.90 (s, 3H, COOC*H*$_3$), 2.29 (s, 9H, OCC*H*$_3$);
^{13}C NMR (101 MHz, *CDCl$_3$*) δ = 166.0, 164.8, 162.8, 141.81, 137.1, 126.1, 120.3, 50.9, 18.8, 18.4;
HPLC: R_t = 8.41 min;
MS (ESI): calcd. for $[C_{14}H_{14}O_8 + NH_4]^+$ *m/z* = 328.10 found *m/z* = 327.97.

Methyl-3,5-diacetoxy-4-benzyloxybenzoat (28)[75]

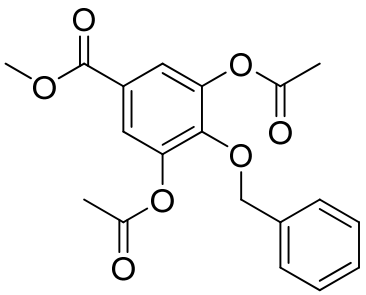

Compound **27** (41.0 g, 132 mmol), K_2CO_3 (54.3 g, 302 mmol), KI (3.5 g, 24 mmol) and benzyl bromide (18.8 g, 150 mmol, 16.8 mL) in acetone (dry, 1000 mL) were stirred over night under reflux, after which the reaction mixture was cooled to rt and water (1000 mL) was added. The mixture was extracted with ethylacetate (3 x 500 mL). The combined organic layers were washed with brine (2 x 500 mL), dried over $MgSO_4$ and evaporated *in vacuo*. The crude product was re-crystallized from ethanol affording the pure compound **28** (26.9 g, 75 mmol, 57%) as yellow crystals.

mp: 109.6 °C;
^{1}H NMR (400 MHz, *CDCl$_3$)* δ = 7.69 (s, 2H, *H*-benzoyl), 7.40-7.31 (m, 5H, *H*-benzyl), 5.05 (s, 2H, C*H*$_2$Ar), 3.89 (s, 3H, COOC*H*$_3$), 2.19 (s, 6H, *m*-OCC*H*$_3$);
^{13}C NMR (101 MHz, *CDCl$_3$*) δ = 168.4, 165.1, 147.4, 144.1, 136.6, 128.5, 128.3, 127.6, 125.5, 122.6, 75.6, 52.3, 20.5;
HPLC: R_t = 9.75 min;
MS (ESI): calcd. for $[C_{19}H_{18}O_7 + NH_4]^+$ *m/z* = 376.14 found *m/z* = 376.00.

Methyl-4-benzyloxy-3,5-dihydroxybenzoat (29)[75]

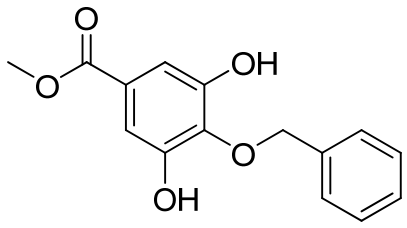

To a solution of **28** (18.5 g, 49 mmol) in methanol (300 mL) a solution of K_2CO_3 (50.8 g, 368 mmol) in water (300 mL) was added and stirred for 2 h under reflux. The solution was acidified to pH=2, cooled and extracted with ethylacetate (3 x 200 mL). The combined organic layers were washed with brine (2 x 200 mL) and water (200 mL), dried over $MgSO_4$ and evaporated *in vacuo*. Re-crystallization from chloroform afforded pure compound **29** (10.1 g, 37 mmol, 70%) as orange crystals.

mp: 135.2 °C;
^{1}H NMR (400 MHz, *CDCl$_3$)* δ = 7.39 (s, 5H, *H*-benzyl), 7.24 (s, 2H, *H*-benzoyl), 5.15 (s, 2H, C*H*$_2$Ar), 3.89 (s, 3H, COOC*H*$_3$);
^{13}C NMR (101 MHz, *CDCl$_3$*) δ = 166.8, 149.1, 137.5, 136.4, 129.4, 128.9, 126.0, 110.0, 75.9, 52.6;
HPLC: R_t = 7.78 min;
MS (ESI): calcd. for $[C_{15}H_{14}O_5 + NH_4]^+$ *m/z* = 292.12 found *m/z* = 292.29.

Methyl-4-benzyloxy-3,5-bis[2-(2-{2-[2-(2-methoxyethoxy)-ethoxy]-ethoxy}-ethoxy)-ethoxy]-benzoate (30)

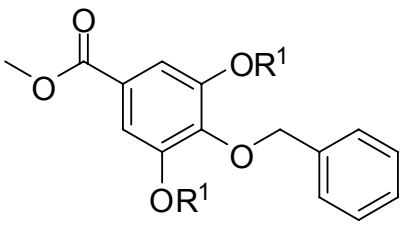

R^1 =

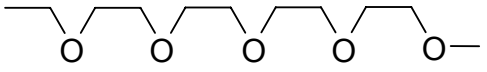

A mixture of **11** (27.8 g, 69 mmol), **29** (9.4 g, 34 mmol) and K_2CO_3 (17.0 g, 123 mmol) was stirred over night at 70 °C in dry DMF (100 mL). The reaction mixture was poured into water (150 mL) and extracted with CH_2Cl_2 (4 x 150 mL). The combined organic layers were washed with brine (100 mL), dried over $MgSO_4$ and evaporated *in vacuo*. The crude product was purified by column chromatography (alumina, 2% methanol in CH_2Cl_2) affording the pure compound (20.00 g, 27 mmol, 61%).

^{1}H NMR (400 MHz, *CDCl$_3$)* δ = 7.47 (d, 2H, *H*-benzyl), 7.35-7.26 (m, 3H, *H*-benzyl), 7.27 (s, 2H, *H*-benzoyl), 5.10 (s, 2H, C*H*$_2$Ar), 4.16 (t, 4H, *m*-OC*H*$_2$CH$_2$O), 3.87 (s, 3H, COOC*H*$_3$), 3.84 (t, 4H, *m*-OCH$_2$C*H*$_2$O), 3.73-3.58 (m, 28H, OC*H*$_2$C*H*$_2$O), 3.55-3.50 (m, 4H, OC*H*$_2$C*H*$_2$O), 3.35 (s, 6H, OC*H*$_3$);
^{13}C NMR (101 MHz, *CDCl$_3$*) δ = 166.7, 163.5, 152.7, 142.2, 137.9, 128.5, 128.3, 128.0, 125.3, 108.8, 75.0, 72.0-70.6, 69.8, 68.9, 59.1, 52.3;
HPLC: R_t = 8.65 min;
MS (ESI): calcd. for $[C_{37}H_{58}O_{15} + NH_4]^+$ *m/z* = 760.41 found *m/z* = 760.25.

Methyl-3,5-bis[2-(2-{2-[2-(2-methoxyethoxy)-ethoxy]-ethoxy}-ethoxy)-ethoxy]- 4-hydroxybenzoate (31)

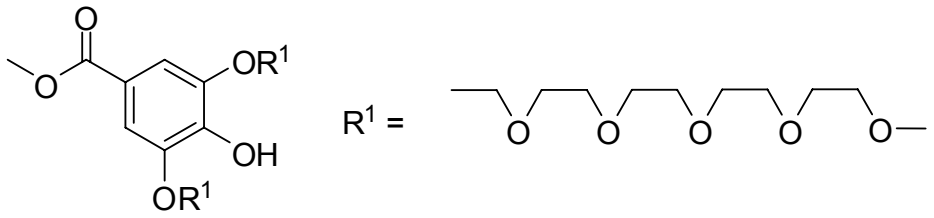

A suspension of **30** (20.0 g, 27 mmol) and Pd/C (1 g) in H_2O (5 mL) and ethanol (80 mL) with a catalytic amount of conc. HCl (0.1 mL) was stirred for 3 d under hydrogen atmosphere (50 bar) in an autoclave. The mixture was then filtered through celite® and the solvents were removed *in vacuo* to yield pure **31** (16.6 g, 25 mmol, 94%).

^{1}H NMR (400 MHz, *CDCl$_3$)* δ = 7.32 (s, 2H, *H*-benzoyl), 4.23 (t, 4H, *m*-OC*H$_2$*CH$_2$O), 3.84 (t, 4H, *m*-OCH$_2$C*H$_2$*O), 3.83 (s, 3H, COOC*H$_3$*), 3.71-3.59 (m, 28H, OC*H$_2$*C*H$_2$*O), 3.51 (dd, 4H, OC*H$_2$*C*H$_2$*O), 3.34 (s, 6H, OC*H$_3$*);
^{13}C NMR (101 MHz, *CDCl$_3$*) δ = 166.6, 146.3, 142.1, 120.4, 110.4, 71.8, 70.6-69.4, 58.90, 51.86;
HPLC: R_t = 7.32 min;
MS (ESI): calcd. for $[C_{30}H_{52}O_{15} + NH_4]^+$ *m/z* = 670.36 found *m/z* = 670.23.

Methyl-4-{2[-2-(2-{2-[2-(2-Azido-ethoxy)-ethoxy]-ethoxy}-ethoxy)-ethoxy]-ethyl}-3,5-bis[2-(2-{2-[2-(2-methoxyethoxy)-ethoxy]-ethoxy}-ethoxy)-ethoxy]-benzoat (32)

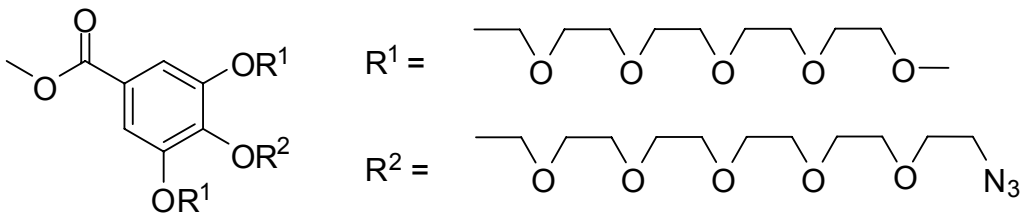

A mixture of **31** (5.76 g, 12.5 mmol), **23** (9.05 g, 9.6 mmol) and K_2CO_3 (17.0 g, 123 mmol) was stirred over night at 70 °C in dry DMF (100 mL). The reaction mixture was poured into water (150 mL) and extracted with CH_2Cl_2 (3 x 100 mL). The combined organic layers were washed with brine (80 mL), dried over MgSO4 and evaporated *in vacuo*. The crude product was purified by column chromatography (alumina, 1% ethanol in chloroform) affording pure compound **32** (6.3 g, 6.7 mmol, 70%).

^{1}H NMR (400 MHz, *CDCl$_3$)* δ = 7.23 (s, 2H, *H*-benzoyl), 4.16 (t, 4H, *m*-OC*H$_2$*CH$_2$O), 4.13 (t, 2H, *p*-OC*H$_2$*CH$_2$O), 3.82 (s, 3H, COOC*H$_3$*), 3.80 (t, 4H, *m*-OCH$_2$C*H$_2$*O), 3.73 (m, 2H, *p*-OCH$_2$C*H$_2$*O), 3.62 (m, 46H, OC*H$_2$*C*H$_2$*O), 3.48 (dd, 4H, OCH$_2$C*H$_2$*OCH$_3$), 3.32 (d, 2H, OCH$_2$C*H$_2$*N$_3$), 3.31 (s, 6H, OC*H$_3$*);
^{13}C NMR (101 MHz, *CDCl$_3$*) δ = 166.7, 152.5, 142.8, 125.1, 109.3, 72.6, 72.1, 71.0-69.1, 61.9, 59.2, 52.3, 50.9;
HPLC: R_t = 7.95 min;

MS (ESI): calcd. for $[C_{42}H_{75}N_3O_{20} + NH_4]^+$ *m/z* = 959.52 found *m/z* = 959.43.

4-{2[-2-(2-{2-[2-(2-Azido-ethoxy)-ethoxy]-ethoxy}-ethoxy)-ethoxy]-ethyl}-3,5-bis[2-(2-{2-[2-(2-methoxyethoxy)-ethoxy]-ethoxy}-ethoxy)-ethoxy]-benzoic acid (34)

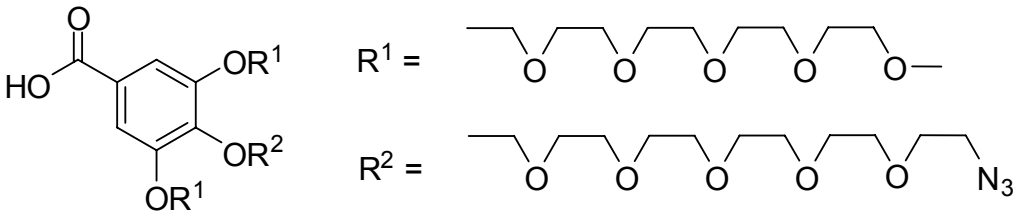

A solution of **32** (6.3 g, 6.7 mmol) and KOH (1.1 g, 20.1 mmol) in ethanol (40 mL) and water (40 mL) was heated under reflux overnight. Subsequently, the solution was acidified to pH = 2, cooled and extracted with CH_2Cl_2 (3 x 50 mL). The CH_2Cl_2 layer was washed with brine. Drying over $MgSO_4$, evaporating *in vacuo* and drying over P_2O_5 afforded the pure compound **34** (6.3 g, 6.7 mmol, quant.).

^{1}H NMR (400 MHz, *CDCl$_3$*) δ = 7.36 (s, 2H, *H*-benzoyl), 4.20 (t, 4H, *m*-OC*H*$_2$CH$_2$O), 4.22 (t, 2H, *p*-OC*H*$_2$CH$_2$O), 3.84 (t, *J* = 4.9, 4H, *m*-OCH$_2$C*H*$_2$O), 3.78 (t, *J* = 5.0, 2H, *p*-OCH$_2$C*H*$_2$O), 3.75-3.51 (m, 56H, OC*H*$_2$C*H*$_2$O), 3.39 (d, 2H, OCH$_2$C*H*$_2$N$_3$), 3.38 (s, 6H, OC*H*$_3$);
^{13}C NMR (101 MHz, *CDCl$_3$*) δ = 169.1, 152.5, 143.3, 110.2, 72.6-69.2, 59.2, 50.9;
HPLC: R_t = 7.25 min;
MS (ESI): calcd. for $[C_{41}H_{73}N_3O_{20} + NH_4]^+$ *m/z* = 945.51 found *m/z* = 945.37.

3'-(4-{2[-2-(2-{2-[2-(2-Azido-ethoxy)-ethoxy]-ethoxy}-ethoxy)-ethoxy]-ethyl}-3,5-bis[2-(2-{2-[2-(2-methoxyethoxy)-ethoxy]-ethoxy}-ethoxy)-ethoxy]-benzoylamino)-2,2'-bipyridine-3-amine (38)

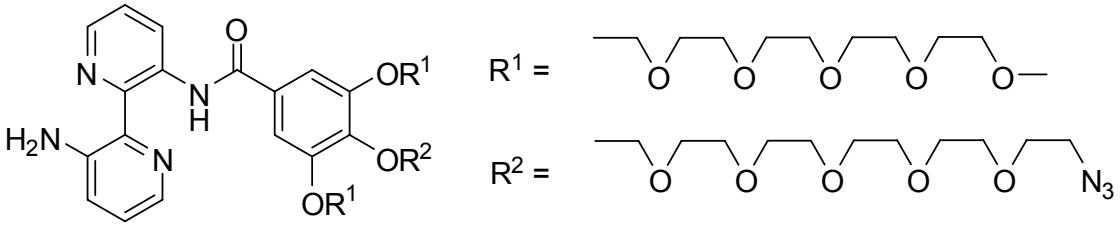

A solution of oxalyl chloride (132 mg, 1.10 mmol, 0.1 mL) in dry CH_2Cl_2 (2 mL) containing a catalytic amount of DMF was added dropwise to a solution of **34** (852 mg, 0.92 mmol) in dry CH_2Cl_2 (3 mL) at 0 °C. The reaction mixture was stirred overnight at rt in the absence of light. Evaporating the solvent *in vacuo* afforded the crude product **36** (1.33 g, 1.5 mmol, 94%). This product was dissolved in dry CH_2Cl_2 (8 mL) and added dropwise to a stirred solution of 2,2'-bipyridyl-3,3'-diamine **4** (258 mg, 1.43 mmol) and triethylamine (0.17 mL, 1.22 mmol) in dry CH_2Cl_2 (8 mL), while the temperature was kept below 5 °C. After stirring for 3 h the solvent was evaporated *in vacuo*. The crude product was purified by column chromatography (silica, ethylacetate followed by 5% methanol in chloroform) and size exclusion chromatography. Drying over P_2O_5 gave compound **38** (753 mg, 0.69 mmol, 62%).

^{1}H NMR (400 MHz, *CDCl$_3$)* δ = 9.01 (d, 1H, *H*-4'), 8.35 (d, 1H, *H*-6'), 8.00 (dd, *J* = 1.5, 4.4, 1H, *H*-6), 7.32 (d, 1H, *H*-5'), 7.31 (s, 2H, *H*-benzoyl), 7.19 (m, 2H, *H*-4 and *H*-5), 4.23 (t, 4H, *m*-OC*H$_2$*CH$_2$O), 4.21 (t, 2H, *p*-OC*H$_2$*CH$_2$O), 3.85 (t, 4H, *m*-OCH$_2$C*H$_2$*O), 3.78 (t, 2H, *p*-OCH$_2$C*H$_2$*O), 3.73-3.56 (m, 46H, OC*H$_2$*C*H$_2$*O), 3.50 (dd, 4H, OC*H$_2$*C*H$_2$*O), 3.35 (t, 2H, *p*- OCH$_2$C*H$_2$*N$_3$), 3.32 (s, 6H, *m*-OC*H$_3$*);

^{13}C NMR (101 MHz, *CDCl$_3$*) δ = 165.6, 152.8, 152.5, 145.0, 144.0, 141.9, 141.7, 135.7, 134.0, 130.2, 126.2, 125.3, 124.5, 123.1, 107.7, 72.3, 71.8, 70.7-70.4, 69.9, 69.6, 69.2, 58.9, 50.6;

HPLC: R_t = 8.34 min;

MS (ESI): calcd. for $[C_{51}H_{81}N_7O_{19} + H]^+$ *m/z* = 1096.56 found *m/z* = 1096.47.

N,N',N''-Tris{3[3'-(4-{2[-2-(2-{2-[2-(2-Azido-ethoxy)-ethoxy]-ethoxy}-ethoxy)-ethoxy]-ethyl}-3,5-bis[2-(2-{2-[2-(2-methoxyethoxy)-ethoxy]-ethoxy}-ethoxy)-ethoxy]-benzoylamino]-2,2'-bipyridyl}benzene-1,3,5-tricarboxamide (18)

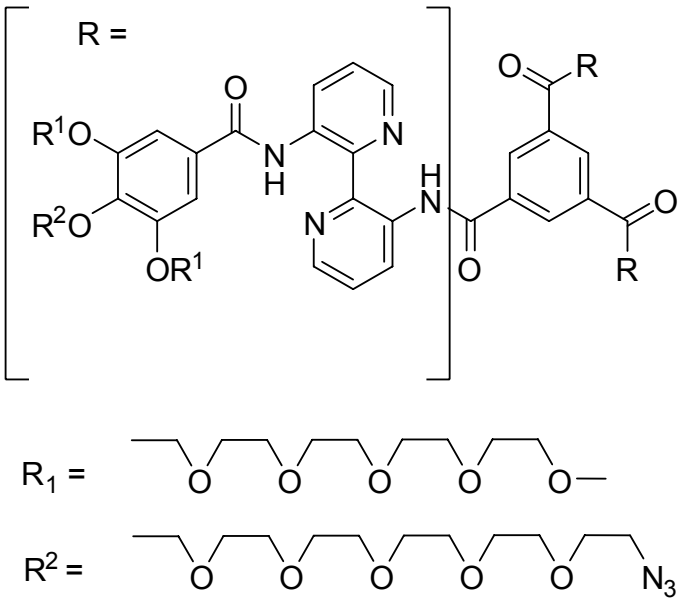

To a solution of **38** (0.7 g, 0.64 mmol) and triethylamine (0.1 mL, 0.8 mmol) in dry CH_2Cl_2 (8 mL), a solution of trimesic chloride (53 mg, 0.19 mmol) in dry CH_2Cl_2 (4 mL) was added dropwise at room temperature. Stirring was continued overnight, after which the solvent was evaporated *in vacuo*. The crude product was purified by column chromatography (silica, 5% methanol in chloroform) and size exclusion chromatography (in CH_2Cl_2). Drying over P_2O_5 afforded 0.25 g of **18** (0.07 mmol, 39%).

^{1}H NMR (600 MHz, *$CDCl_3$)* δ = 15.41 (s, 3H, N*H*CO), 14.36 (s, 3H, N*H'*CO), 9.57 (br, 3H, *H*-4), 9.36 (d, *J* = 7.8, 3H, *H*-4'), 9.25 (s, 3H, *o*-*H*), 9.03 (br, 3H, *H*- 6'), 8.52 (br, 3H, *H*-6), 7.57 (br, 6H, *H*-5 and *H*-5'), 7.35 (s, 6H, *H*-benzoyl), 4.26 (t, 12H, *m*-OC*H*$_2$CH$_2$O), 4.26 (t, 6H, *p*-OC*H*$_2$CH$_2$O), 3.90 (t, *J* = 4.8, 12H, *m*-OCH$_2$C*H*$_2$O), 3.82 (t, 6H, *p*-OCH$_2$C*H*$_2$O), 3.79-3.47 (m, 150H, OC*H*$_2$C*H*$_2$O), 3.37 (t, 6H, *p*- OCH$_2$C*H*$_2$N$_3$), 3.34 (s, 18H, *m*-OC*H*$_3$);

^{13}C NMR (151 MHz, *CDCl$_3$*) δ = 165.9, 164.4, 152.7, 142.6, 142.3, 141.7, 141.5, 137.7, 137.6, 135.8, 130.7, 130.5, 130.0 129.9, 124.9, 124.7, 108.3, 72.7-69.6, 59.5, 50.3, 29.9;
MS (MALDI-TOF): calcd. for $[C_{162}H_{243}N_{21}O_{60} + Na]^+$ *m/z* = 3465.7, found *m/z* = 3464.9.

5.2.5 Synthesis of the Amine Modified Discotic Scaffold

Methyl-4-{2[-2-(2-{2-[2-(2-tert-butoxycarbonylamino-ethoxy)-ethoxy]-ethoxy}-ethoxy)-ethoxy]-ethyl}-3,5-bis[2-(2-{2-[2-(2-methoxyethoxy)-ethoxy]-ethoxy}-ethoxy)-ethoxy]-benzoat (33)

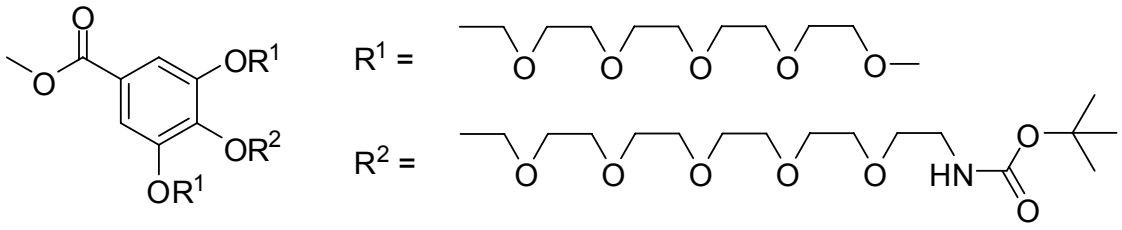

A mixture of **26** (5.60 g, 10.5 mmol), **31** (6.52 g, 10.0 mmol) and K_2CO_3 (17.11 g, 124 mmol) was stirred 4 h at 100 °C in dry DMF (100 mL). The reaction mixture was poured into water (150 mL) and extracted with CH_2Cl_2 (3 x 150 mL). The combined organic layers were washed with brine (100 mL), dried over $MgSO_4$ and evaporated *in vacuo*. The crude product was purified by column chromatography (alumina, 1% ethanol in chloroform) affording pure compound **33** (9.57 g, 9.4 mmol, 90%).

^{1}H NMR (400 MHz, *CDCl$_3$*) δ = 7.26 (s, 2H, *H*-benzoyl), 5.01 (br, 1H, N*H*), 4.18 (t, 4H, *m*-OC*H$_2$*CH$_2$O), 4.16 (t, 2H, *p*-OC*H$_2$*CH$_2$O), 4.07 (t, 2H, *m*-OCH$_2$C*H$_2$*O), 3.85 (s, 3H, COOC*H$_3$*), 3.83 (t, 4H, *p*-OCH$_2$C*H$_2$*O), 3.79-3.45 (m, 46H, OC*H$_2$*C*H$_2$*O), 3.34 (s, 6H, OC*H$_3$*), 3.27 (d, 2H, OCH$_2$C*H$_2$*NHboc), 1.41 (s, 9H, OC(C*H$_3$*)$_3$);

^{13}C NMR (101 MHz, *CDCl$_3$*) δ = 171.3, 152.3, 144.6, 127.0, 109.1, 71.9, 70.8-70.2, 69.6, 68.9, 59.0, 28.4;
HPLC: R_t = 8.16 min;
MS (ESI): calcd. for $[C_{47}H_{85}NO_{22} + NH_4]^+$ *m/z* = 1033.59 found *m/z* = 1033.33.

4-{2[-2-(2-{2-[2-(2-tert-butoxycarbonylamino-ethoxy)-ethoxy]-ethoxy}-ethoxy)-ethoxy]-ethyl}-3,5-bis[2-(2-{2-[2-(2-methoxyethoxy)-ethoxy]-ethoxy}-ethoxy)-ethoxy]-benzoic acid (35)

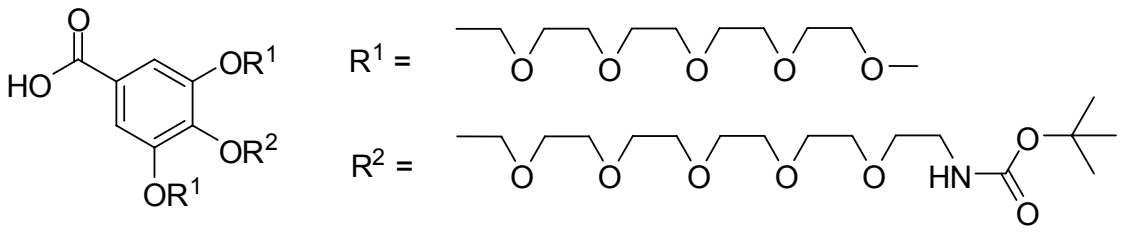

A solution of **33** (9.57 g, 9.4 mmol) and KOH (5.4 g, 28.1 mmol) in ethanol (40 mL) and water (40 mL) was heated under reflux overnight. Subsequently, the solution was acidified to pH = 2, cooled and extracted with CH_2Cl_2 (4 x 100 mL). The CH_2Cl_2 layer was washed with brine (70 mL). Drying over $MgSO_4$, evaporating *in vacuo* and drying over P_2O_5 afforded the pure compound **35** (8.81 g, 8.8 mmol, 94%).

^{1}H NMR (400 MHz, *CDCl$_3$*) δ = 7.35 (s, 2H, *H*-benzoyl), 4.23 (t, 4H, *m*-OC*H$_2$*CH$_2$O), 4.19 (t, 2H, *p*-OC*H$_2$*CH$_2$O), 3.85 (t, 4H, *m*-OCH$_2$C*H$_2$*O), 3.82 (t, 2H, *p*-OCH$_2$C*H$_2$*O), 3.79-3.49 (m, 90H, OC*H$_2$*C*H$_2$*O), 3.36 (s, 6H, OC*H$_3$*), 3.30 (d, 2H, OCH$_2$C*H$_2$*NHboc), 1.43 (s, 9H, OC(C*H$_3$*)$_3$);
^{13}C NMR (101 MHz, *CDCl$_3$*) δ = 161.5, 156.3, 142.8, 124.6, 98.3, 72.0, 70.9-69.8, 59.0, 28.4;
HPLC: R_t = 7.41 min;
MS (ESI): calcd. for $[C_{46}H_{83}NO_{22} + NH_4]^+$ *m/z* = 1019.57 found *m/z* = 1019.31.

3'-(4-{2[-2-(2-{2-[2-(2-tert-butoxycarbonylamino-ethoxy)-ethoxy]-ethoxy}-ethoxy)-ethoxy]-ethyl}-3,5-bis[2-(2-{2-[2-(2-methoxyethoxy)-ethoxy]-ethoxy}-ethoxy)-ethoxy]-benzoylamino)-2,2'-bipyridine-3-amine (39)

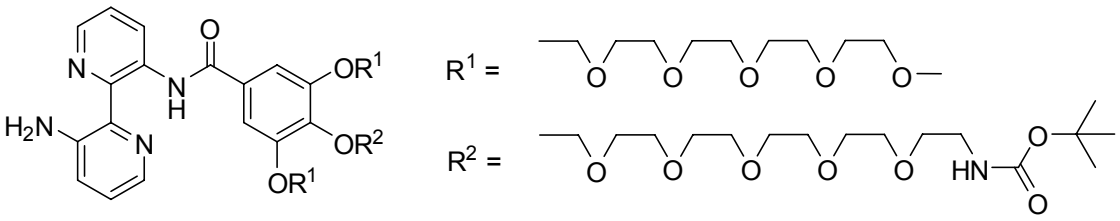

A solution of oxalyl chloride (330 mg, 2.6 mmol, 0.22 mL) in dry CH_2Cl_2 (5 mL) containing a catalytic amount of DMF (3 drops) was added dropwise to a solution of **35** (2.17 g, 2.17 mmol) in dry CH_2Cl_2 (5 mL). The reaction mixture was stirred overnight at rt in the absence of light. Evaporating the solvent *in vacuo* afforded the crude product **37** (2.38 g, 2.17 mmol, quant.). This product was dissolved in dry CH_2Cl_2 (25 mL) and added dropwise to a stirred solution of 2,2'-bipyridyl-3,3'-diamine **4** (504 mg, 2.7 mmol) and triethylamine (0.17 mL, 1.22 mmol) in dry CH_2Cl_2 (25 mL) within 1.5 h, while the temperature was kept below 5 °C. After stirring for 2 h the solvent was evaporated *in vacuo*. The crude product was purified by column chromatography (silica, ethylacetate followed by 5% methanol in chloroform) and size exclusion chromatography to yield **39** (1.34 g, 1.14 mmol, 52%) containing an impurification. Some amount (500 mg) of the crude was purified by preparative HPLC (10-50% acetonitrile in water) resulting pure **39**.

^{1}H NMR (400 MHz, *CDCl$_3$*) δ = 9.19 (dd, *J* = 8.4 and 1.4, 1H, *H*-4'), 8.31 (dd, *J* = 4.5 and 1.4, 1H, *H*-6'), 8.02 (t, *J* = 2.9, 1H, *H*-6), 7.30 (s, 2H, *H*-benzoyl), 7.28 (m, 1H, *H*-5'), 7.13 (d, *J* = 2.9, 2H, *H*-4 and *H*-5), 5.05 (s, 1H, N*H*), 4.24 (t, 4H, *m*-OC*H$_2$*CH$_2$O), 4.23 (t, 4H, *p*-OC*H$_2$*CH$_2$O), 3.86 (t, 4H, *m*-OCH$_2$C*H$_2$*O), 3.80 (t, 2H, *p*-OCH$_2$C*H$_2$*O), 3.72-3.50 (m, 46H, OC*H$_2$*C*H$_2$*O), 3.34 (s, 6H, *m*-OC*H$_3$*), 3.28 (d, 2H, OCH$_2$C*H$_2$*NHboc), 1.42 (s, 9H, OC(C*H$_3$*)$_3$);
HPLC: R_t = 7.92 min;
MS (ESI): calcd. for $[C_{56}H_{91}NO_{21} + H]^+$ *m/z* = 1170.63 found *m/z* = 1170.37.

N,N',N''-Tris{3[3'-(4-{2[-2-(2-{2-[2-(2-tert-butoxycarbonylamino-ethoxy)-ethoxy]-ethoxy}-ethoxy)-ethoxy]-ethyl}-3,5-bis[2-(2-{2-[2-(2-methoxyethoxy)-ethoxy]-ethoxy}-ethoxy)-ethoxy]-benzoylamino]-2,2'-bipyridyl}benzene-1,3,5-tricarboxamide (19a)

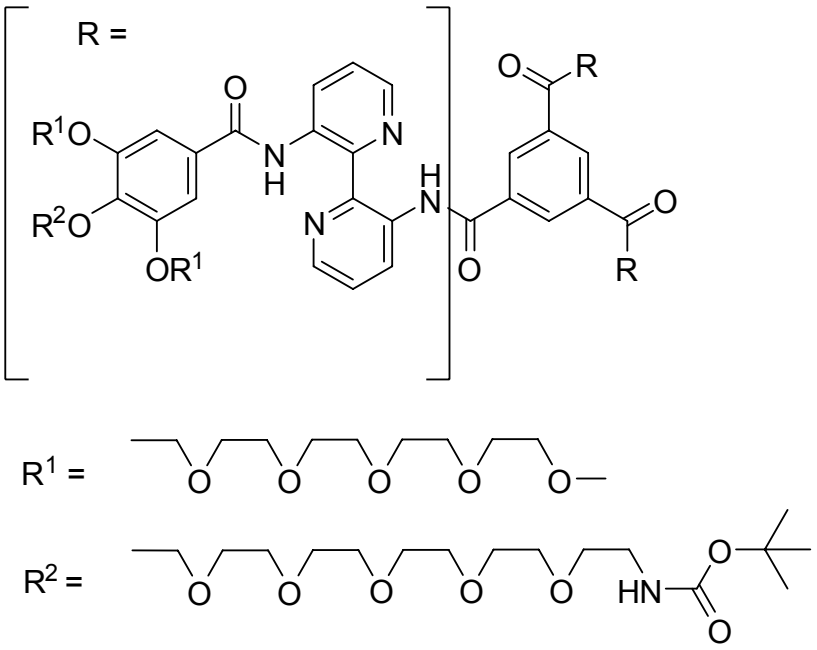

To a solution of **39** (375 mg, 0.32 mmol) and triethylamine (55 µL, 0.4 mmol) in dry CH_2Cl_2 (6 mL), a solution of trimesic chloride (26.5 mg, 0.10 mmol) in dry CH_2Cl_2 (4 mL) was added dropwise at room temperature. Stirring was continued overnight, after which the solution was diluted with CH_2Cl_2 (10 mL) and washed with water (2 x 10 mL). The combined water layers were extracted with CH_2Cl_2 (4 x 15 mL). The combined dichloromethane layers were washed with brine (10 mL), dried over $MgSO_4$ and evaporated *in vacuo*. The crude product was purified by size exclusion chromatography (in CH_2Cl_2), column chromatography (silica, 10% methanol with 1% triethylamine in chloroform) and size exclusion chromatography (in CH_2Cl_2). Drying over P_2O_5 afforded **19a** (210 mg, 57 µmol, 57%).

^{1}H NMR (400 MHz, *CDCl$_3$*) δ = 15.52 (s, 3H, N*H*CO), 14.35 (s, 3H, N*H'*CO), 9.60 (dd, *J* = 8.5 and 1.4, 3H, *H*-4), 9.40 (dd, *J* = 8.6 and 1.5, 3H, *H*-4'), 9.29 (s, 3H, *o-H*), 9.06 (dd, *J* = 4.6 and 1.4, 3H, *H*-6'), 8.52 (dd, *J* = 4.6 and 1.5, 3H,

H-6), 7.57 (dd, *J* = 8.6 and 4.6, 6H, *H*-5 and *H*-5'), 7.36 (s, 6H, *H*-benzoyl), 4.29 (t, 12H, *m*-OC*H*$_2$CH$_2$O), 4.27 (t, 6H, *p*-OC*H*$_2$CH$_2$O), 3.91 (t, *J* = 4.9, 12H, *m*-OCH$_2$C*H*$_2$O), 3.91 (m, 6H, *p*-OCH$_2$C*H*$_2$O), 3.74-3.48 (m, 150H, OC*H*$_2$C*H*$_2$O), 3.35 (s, 18H, *m*-OC*H*$_3$), 3.31 (d, 6H, *p*- OCH$_2$C*H*$_2$NHboc), 1.44 (s, 27H, OC(C*H*$_3$)$_3$).

^{13}C NMR (151 MHz, *CDCl*$_3$) δ = 169.1, 166.0, 164.9, 153.0, 142.6, 142.0, 141.8, 141.7, 137.8, 135.2, 132.0, 131.8, 130.2, 128.8, 128.7, 124.9, 124.6, 108.3, 72.7-69.6, 59.2, 46.0, 28.7, 8.8.

MS (MALDI-TOF): calcd. for [$C_{177}H_{273}N_{15}O_{66}$ + Na]$^+$ *m/z* = 3688.9, found *m/z* = 3689.0.

N,N',N''-Tris{3[3'-(4-{2[-2-(2-{2-[2-(2-amino-ethoxy)-ethoxy]-ethoxy}-ethoxy)-ethoxy]-ethyl}-3,5-bis[2-(2-{2-[2-(2-methoxyethoxy)-ethoxy]-ethoxy}-ethoxy)-ethoxy]-benzoylamino]-2,2'-bipyridyl}benzene-1,3,5-tricarboxamide (19)

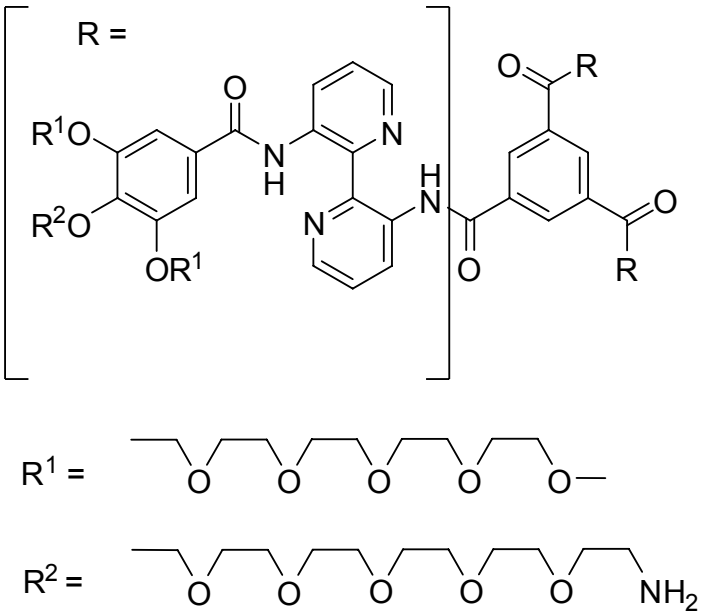

19a (200 mg, 54 µmol) and trifluoracetic acid (1 mL) in CH_2Cl_2 (3 mL) were stirred for 3 h. Toluene (3 mL) was added and the solvents were evaporated *in vacuo*. The crude product was purified by size exclusion chromatography (in CH_2Cl_2) affording **19** (186 mg, 54 µmol, quant.).

^{1}H NMR (400 MHz, *CDCl$_3$*) δ = 15.43 (s, 3H, N*H*CO), 14.45 (s, 3H, N*H'*CO), 9.57 (d, *J* = 8.4, 3H, *H*-4), 9.32 (d, *J* = 8.4, 3H, *H*-4'), 9.19 (s, 3H, *o*-*H*), 9.03 (d, *J* = 4.1, 3H, *H*-6'), 8.45 (s, 3H, *H*-6), 7.55 (br, 6H, *H*-5 and *H*-5'), 7.30 (s, 6H, *H*-benzoyl), 4.27 (br, 12H, *m*-OC*H$_2$*CH$_2$O), 4.26 (br, 6H, *p*-OC*H$_2$*CH$_2$O), 3.91 (br, 12H, *m*-OCH$_2$C*H$_2$*O), 3.84 (br, 6H, *p*-OCH$_2$C*H$_2$*O), 3.77-3.49 (m, 150H, OC*H$_2$*C*H$_2$*O), 3.33 (s, 18H, *m*-OC*H$_3$*), 3.21 (br, 6H, *p*- OCH$_2$C*H$_2$*NH$_2$);
^{13}C NMR (151 MHz, *CDCl$_3$*) δ = 169.1, 164.7, 152.8, 141.8, 141.7, 141.1, 140.7, 139.5, 137.7, 135.2, 131.4, 131.2, 130.2, 129.7, 127.5, 124.9, 124.7, 107.5, 89.5, 72.7-69.3, 67.2, 59.2, 40.4, 29.9.
MS (MALDI-TOF): calcd. for $[C_{162}H_{249}N_{15}O_{60} + H]^+$ *m/z* = 3387.63, found *m/z* = 3388.71.

5.2.6 Synthesis of the Glycosidic Ligands (Chapter 3.2.1)

1,2,3,4,6-Penta-O-acetyl-α-D-mannopyranosid (40)

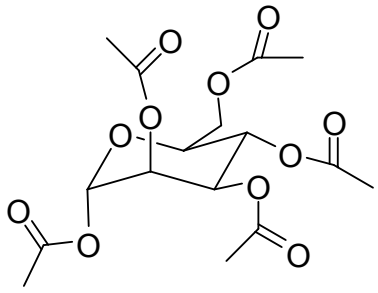

To a solution of D(+)-mannose (2.05 g, 11.1 mmol) in pyridine (20 mL) acetic anhydride (40 mL, 420 mmol) was added tropwise at 0 °C. The mixture was stirred overnight at rt and the solvent was co-evaporated *in vacuo* using toluene. Purification by column chromatography (silica, 20% ethylacetate in cyclohexane) yielded **40** (4.04 g, 10.4 mmol, 93%).

^{1}H NMR (400 MHz, *CDCl$_3$*) δ = 6.06 (d, *J* = 1.9, 1H), 5.35-5.30 (m, 2H), 5.24 (t, *J* = 2.2, 1H), 4.33-4.19 (m, 1H), 4.16-3.97 (m, 3H), 2.15 (d, *J* = 3.2, 6H), 2.07 (s, 3H), 2.03 (s, 3H), 1.98 (s, 3H);
^{13}C NMR (101 MHz, *CDCl$_3$*) δ = 170.8, 170.2, 169.9, 169.7, 168.3, 90.8, 70.8, 69.0, 68.6, 65.8, 62.3, 21.1, 21.0, 20.9, 20.9, 20.8;
HPLC: R_t = 8.05 min;
MS (ESI): calcd. for $[C_{16}H_{22}O_{11} + NH_4]^+$ *m/z* = 408.12 found *m/z* = 407.89.

1-Propargyl-2,3,4,6-tetra-*O*-acetyl-α-D-mannopyranosid (41)[76]

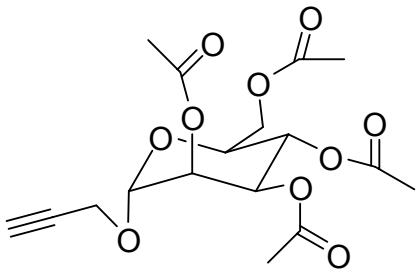

A solution of **40** (4.02 g, 10.3 mmol) and $SnCl_4$ (1.2 ml, 10.3 mmol) in CH_2Cl_2 (17 mL) was stirred for 30 min. Subsequently 2-propargylalcohol (0.9 mL, 15.4 mmol) was added and stirred for another 4 h. The reaction mixture was washed with $NaHCO_3$ (5% in water, 25 mL). The aqueous layer was extracted with CH_2Cl_2 (3 x 25 mL). The combined organic layers were washed with 1N HCl (50 mL) and brine (50 mL), dried over $MgSO_4$ and evaporated *in vacuo*. Purification by column chromatography (silica, 30% ethylacetate in cyclohexane) yielded **41** (2.15 g, 5.6 mmol, 54 %).

^{1}H NMR (400 MHz, *CDCl$_3$)* δ = 5.36-5.24 (m, 3H), 5.02 (d, *J* = 1.8, 1H), 4.30-4.23 (m, 3H), 4.10 (dd, *J* = 2.5, 12.2, 1H), 4.01 (ddd, *J* = 2.4, 5.2, 9.2, 1H), 2.46 (q, *J* = 2.8, $OCH_2CC\mathit{H}$, 1H), 2.15 (s, 3H, $COC\mathit{H_3}$), 2.09 (s, 3H, $COC\mathit{H_3}$), 2.03 (s, 3H, $COC\mathit{H_3}$), 1.98 (s, 3H, $COC\mathit{H_3}$);
^{13}C NMR (101 MHz, *CDCl$_3$*) δ = 170.9, 170.2, 170.1, 169.9, 96.5, 78.1, 77.4, 75.8, 69.6, 69.2, 69.2, 66.3, 55.2, 21.1, 21.0, 20.9, 20.9;
HPLC: R_t = 8.93 min;
MS (ESI): calcd. for $[C_{17}H_{22}O_{10} + NH_4]^+$ *m/z* = 404.15 found *m/z* = 404.00.

1-Propargyl-α-D-mannopyranosid (42)[76]

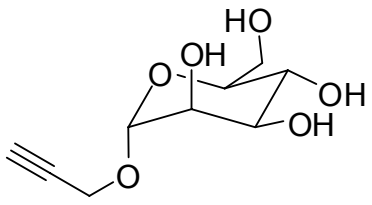

To a solution of **41** (2 g, 5.18 mmol) in methanol (10 mL) a catalytic amount of sodium-methanolat was added. The reaction was stirred for 3 h at rt. Subsequently the solution was filtered through celite®. The solvent was evaporated *in vacuo* to yield 1.13 g (5.18 mmol, quant.) of crude **42**. A small amount (200 mg) of the crude was purified by preparative HPLC (10-50% acetonitrile in water) resulting compound **42.**

^{1}H NMR (400 MHz, D_2O) δ = 4.90 (d, *J* = 1.8, 1H, *H*-1α), 4.20 (dq, *J* = 15.9 and 2.4, 2H, OCH_2CCH), 3.82 (dd, *J* = 3.4 and 1.8, 1H, *H*-2), 3.75 (dd, *J* = 12.2 and 1.9, 1H, *H*-4), 3.68 -3.60 (m, 2H, *H*-3 and *H*-5), 3.58-3.49 (m, 2H, CH_2OH), 2.79 (t, *J* = 2.4, 1H, OCH_2CCH);
^{13}C NMR (101 MHz, $CDCl_3$) δ = 98.9, 79.0, 76.3, 73.3, 70.6, 70.1, 66.8, 61.0, 54.7;
HPLC: R_t = 2.39 min;
MS (ESI): calcd. for $[C_9H_{14}O_6 + NH_4]^+$ *m/z* = 236.11 found *m/z* = 235.95.

1,2,3,4,6-Penta-O-acetyl-α,β-D-galactopyranosid (43)

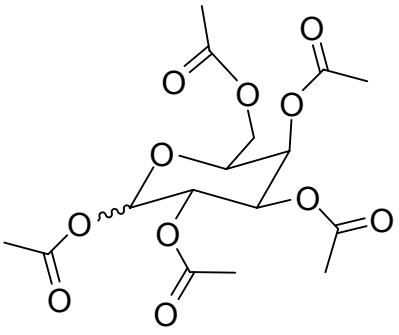

To a solution of D(+)-galactose (21 g, 117 mmol) in pyridine (105 mL) acetic anhydride (150 mL, 1.6 mol) was added tropwise at 0 °C. The mixture was stirred overnight at rt and the solvent was co-evaporated *in vacuo* using toluene. Purification by column chromatography (silica, 20% ethylacetate in cyclohexane) yielded the pure compound as colorless oil (41.13 g, 105 mmol, 90%).

^{1}H NMR (400 MHz, *CDCl$_3$*) δ = 6.37 (d, 1H, *J* = 2.0, *H*-1α), 5.69 (d,1H, *J* = 8.0, *H*-1β), 5.49 (dd, 1H, *J* = 2.8 and 1.2, *H*-3), 5.34 (m, 2H, *H*-2 and *H*-4), 4.32-4.35 (m, 1H, *H*-5), 4.07-4.13 (m, 2H, *H*-6a and *H*-6b), 2.15 (d, *J* = 3.2, 6H, COC*H$_3$*), 2.03 (s, 3H, COC*H$_3$*), 2.01 (s, 3H, COC*H$_3$*), 2.00 (s, 3H, COC*H$_3$*);
^{13}C NMR (101 MHz, *CDCl$_3$*) δ = 170.3, 170.1, 170.1, 169.8, 168.9, 89.7, 68.7, 67.4, 67.3, 66.4, 61.2, 20.8, 20.6, 20.6, 20.5, 20.5;
TLC (25 % ethylacetate in cyclohexane): R_f = 0.77;
HPLC: R_t = 8.12 min;
MS (ESI): calcd. for $[C_{16}H_{22}O_{11} + NH_4]^+$ *m/z* = 408.12 found *m/z* = 407.93.

1-Propargyl-2,3,4,6-tetra-*O*-acetyl-β-D-galactopyranosid (44)[76]

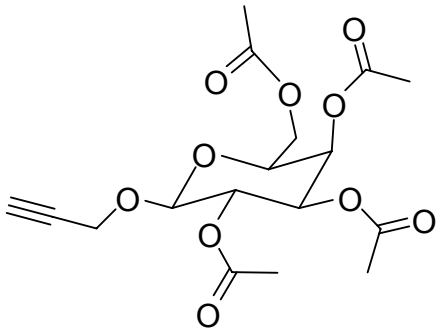

A solution of **43** (5.0 g, 13 mmol) and $SnCl_4$ (1.4 ml, 13 mmol) in CH_2Cl_2 (20 mL) was stirred for 1 h. Subsequently 2-propargylalcohol (1.5 mL, 20 mmol) was added and stirred for another 12 h. The reaction mixture was washed with $NaHCO_3$ (5% in water, 25 mL). The aqueous layer was extracted with CH_2Cl_2 (3 x 75 mL). The combined organic layers were washed with 1N HCl (50 mL) and brine (50 mL), dried over $MgSO_4$ and evaporated *in vacuo*.

Purification by column chromatography (silica, 30% ethylacetate in cyclohexane) yielded **44** (2.17 g, 5.6 mmol, 46%).

^{1}H NMR (400 MHz, *CDCl$_3$)* δ = 5.40 (d, *J* = 3.2, 1H, *H*-4), 5.22 (d, *J* = 7.7, 1H, *H*-2), 5.06 (dd, *J* = 10.0 und 3.2, 1H, *H*-3), 4.73 (d, *J* = 7.6, 1H, *H*-1β), 4.38 (d, *J* = 2.4, 2H, OC*H*$_2$CCH), 4.16 (m, 2H, *H*-6b and *H*-5), 3.94 (t, *J* = 6.4, 1H, *H*-6a), 2.46 (q, *J* = 2.4, OCH$_2$CC*H*, 1H), 2.16 (s, 3H, COC*H$_3$*), 2.08 (s, 3H, COC*H$_3$*), 2.06 (s, 3H, COC*H$_3$*), 1.99 (s, 3H, COC*H$_3$*);
^{13}C NMR (101 MHz, *CDCl$_3$*) δ = 170.9, 170.7, 170.5, 170.1, 98.9, 75.6, 71.1, 71.0, 68.8, 67.3, 61.5, 56.1, 21.0, 20.9, 20.8, 20.7;
TLC (30 % ethylacetate in cyclohexane): R_f = 0.3;
HPLC: R_t = 9.04 min;
MS (ESI): calcd. for $[C_{17}H_{22}O_{10} + NH_4]^+$ *m/z* = 404.15 found *m/z* = 404.06.

1-Propargyl-β-D-galactopyranosid (45)[76]

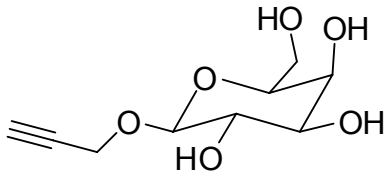

To a solution of **44** (375 mg, 0.97 mmol) in methanol (abs., 3.5 mL) a catalytic amount of sodium-methanolat was added. The reaction was stirred for 12 h at rt. Subsequently the solution was filtered through celite®. The solvent was evaporated *in vacuo* to yield 209.4 mg (0.96 mmol, 98%) of crude **45**. A small amount (100 mg) of the crude was purified by preparative HPLC (10-50% acetonitrile in water) resulting pure compound **45.**

^{1}H NMR (400 MHz, *CDCl$_3$)* δ = 4.46 (d, *J* = 8.0, 1H, *H*-1β), 3.97 (dd, *J* = 9.6 and 3.2, 1H, *H*-3), 3.82 (dd, *J* = 3.2 and 0.8, 1H, *H*-4), 3.66 (d, *J* = 12.4 and 4.0, 1H, *H*-6b), 4.38 (d, *J* = 1.8, 2H, OC*H*$_2$CCH), 3.57-3.61 (m, 1H, *H*-5), 3.54 (m, *J* = 12.4 and 7.2, 1H, *H*-6a), 3.51-3.44 (m, 2H, C*H*$_2$OH), 3.42 (t, *J* = 9.6 and 8.0, 1H, *H*-2), 2.79 (t, *J* = 2.4, 1H, OCH$_2$CC*H*);

TLC (30 % ethylacetate in cyclohexane): R_f = 0.0;
HPLC: R_t = 2.21 min;
MS (ESI): calcd. for $[C_9H_{14}O_6 + NH_4]^+$ *m/z* = 236.11 found *m/z* = 235.98.

1,2,3,4,6-Penta-O-acetyl-α,β-D-glucopyranosid (46)

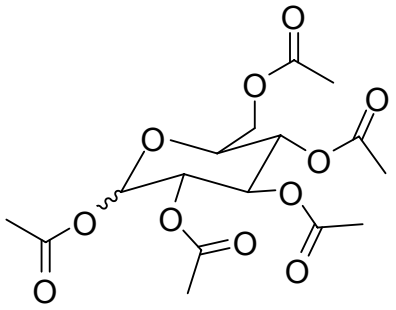

To a solution of D(+)-glucose (20.0 g, 111 mmol) in pyridine (100 mL) acetic anhydride (140 mL, 1.5 mol) was added tropwise at 0 °C. The mixture was stirred overnight at rt and the solvent was co-evaporated *in vacuo* using toluene. The crude compound was recrystallized (10% ethylacetate in cyclohexane) to yield pure **46** as colorless crystalls (42.0 g, 108 mmol, 97%).

^{1}H NMR (400 MHz, *CDCl$_3$*) δ = 6.32 (d, 1H, *J* = 3.6, *H*-1α), 5.70 (d, 1H, *J* = 8.0, *H*-1β), 5.46 (t, 1H, *J* = 10.0, *H*-3), 5.12-5.15 (m, 1H, *H*-4), 5.09 (dd, 1H, *J* = 10.0 and 3.6, *H*-2), 4.25 (dd, 1H, *J* = 12.4 and 4.0, *H*-6b), 4.08 (dd, 1H, *J* = 12.4 and 2.0, *H*-6a), 3.38 (ddd, 1H, *J* = 10.0, 4.0 and 2.0, *H*-5), 2.15 (s, 3H, COC*H$_3$*), 2.08 (s, 3H, COC*H$_3$*), 2.03 (s, 3H, COC*H$_3$*), 2.02 (s, 3H, COC*H$_3$*), 2.00 (s, 3H, COC*H$_3$*);
^{13}C NMR (101 MHz, *CDCl$_3$*) δ = 170.8, 170.4, 169.8, 169.6, 168.9, 89.3, 70.0, 70.0, 69.4, 68.1, 61.7, 21.1, 20.9, 20.9, 20.8, 20.6;
TLC (25 % ethylacetate in cyclohexane): R_f = 0.75;
HPLC: R_t = 8.06 min;
MS (ESI): calcd. for $[C_{16}H_{22}O_{11} + NH_4]^+$ *m/z* = 408.12 found *m/z* = 407.97.

1-Propargyl-2,3,4,6-tetra-*O*-acetyl-β-D-glucopyranosid (47)[76]

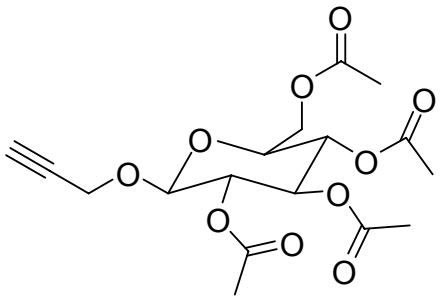

A solution of **46** (5.0 g, 13 mmol) and $SnCl_4$ (1.4 ml, 13 mmol) in CH_2Cl_2 (20 mL) was stirred for 1 h. Subsequently 2-propargylalcohol (1.5 mL, 20 mmol) was added and stirred for another 12 h. The reaction mixture was washed with $NaHCO_3$ (5% in water, 25 mL). The aqueous layer was extracted with CH_2Cl_2 (3 x 75 mL). The combined organic layers were washed with 1N HCl (50 mL) and brine (50 mL), dried over $MgSO_4$ and evaporated *in vacuo*. Purification by column chromatography (silica, 30% ethylacetate in cyclohexane) yielded **47** (2.6 g, 7.0 mmol, 54%).

^{1}H NMR (400 MHz, *CDCl$_3$)* δ = 5.24 (t, *J* = 9.6, 1H, *H*-3), 5.08-5.16 (m, 1H, *H*-4), 5.01 (dd, *J* = 9.6 and 8.0, 1H, *H*-2), 4.77 (d, *J* = 8.0, 1H, *H*-1β), 4.37 (d, *J* = 2.4, 2H, OC*H$_2$*CCH), 4.24-4.29 (m, 1H, *H*-6b), 4.14 (dd, 1H, *J* = 12.0 and 2.4, *H*-6a), 3.72 (ddd, *J* = 10.0, 4.4 and 2.4, 1H, *H*-5), 2.46 (t, *J* = 2.4, 1H, OCH$_2$CC*H*), 2.09 (s, 3H, COC*H$_3$*), 2.03 (s, 3H, COC*H$_3$*), 2.02 (s, 3H, COC*H$_3$*), 2.01 (s, 3H, COC*H$_3$*);
^{13}C NMR (101 MHz, *CDCl$_3$*) δ = 170.6, 170.2, 169.6, 168.7, 98.1, 89.0, 75.4, 69.8, 69.1, 67.9, 61.4, 55.9, 29.8, 20.6, 20.5, 20.4;
TLC (30 % ethylacetate in cyclohexane): R_f = 0.36;
HPLC: R_t = 9.11 min;
MS (ESI): calcd. for $[C_{17}H_{22}O_{10} + NH_4]^+$ *m/z* = 404.15 found *m/z* = 404.11.

1-Propargyl-β-D-glucopyranosid (48)[76]

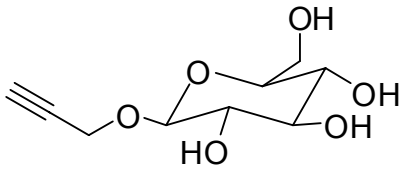

To a solution of **47** (2.0 g, 5.2 mmol) in methanol (abs., 19 mL) a catalytic amount of sodium-methanolat was added. The reaction was stirred for 4 h at rt. Subsequently the solution was filtered through celite®. The solvent was evaporated *in vacuo* to yield 1.1 g (5 mmol, 96%) of crude **48**. A small amount (200 mg) of the crude was purified by preparative HPLC (10-50% acetonitrile in water) resulting pure compound **48.**

^{1}H NMR (400 MHz, *CDCl$_3$)* δ = 4.53 (d, *J* = 8.0, 1H, *H*-1β), 4.36 (d, *J* = 2.4, 2H, OC*H*$_2$CCH), 3.81 (d, *J* = 12.4 and 2.0, 1H, *H*-6b), 3.61 (dd, *J* = 12.4 and 6.0, 1H, *H*-6a), 3.39 (t, *J* = 9.0, 1H, *H*-4), 3.34-3.38 (m, 1H, *H*-5), 3.28 (t, *J* = 9.0, 1H, *H*-3), 3.42 (dd, *J* = 9.0 and 8.0, 1H, *H*-2), 2.81 (t, *J* = 2.4, 1H, OCH$_2$CC*H*);
^{13}C NMR (101 MHz, *CDCl$_3$*) δ = 101.8, 76.5, 76.2, 73.1, 69.8, 69.6, 62.3, 60.9, 56.7;
TLC (30 % ethylacetate in cyclohexane): R_f = 0.0;
HPLC: R_t = 2.21 min;
MS (ESI): calcd. for $[C_9H_{14}O_6 + NH_4]^+$ *m/z* = 236.11 found *m/z* = 236.07.

5.2.7 Synthesis of Functionalized Discotics (3.2)

Mannose Discotic (49) (Chapter 3.2.1)

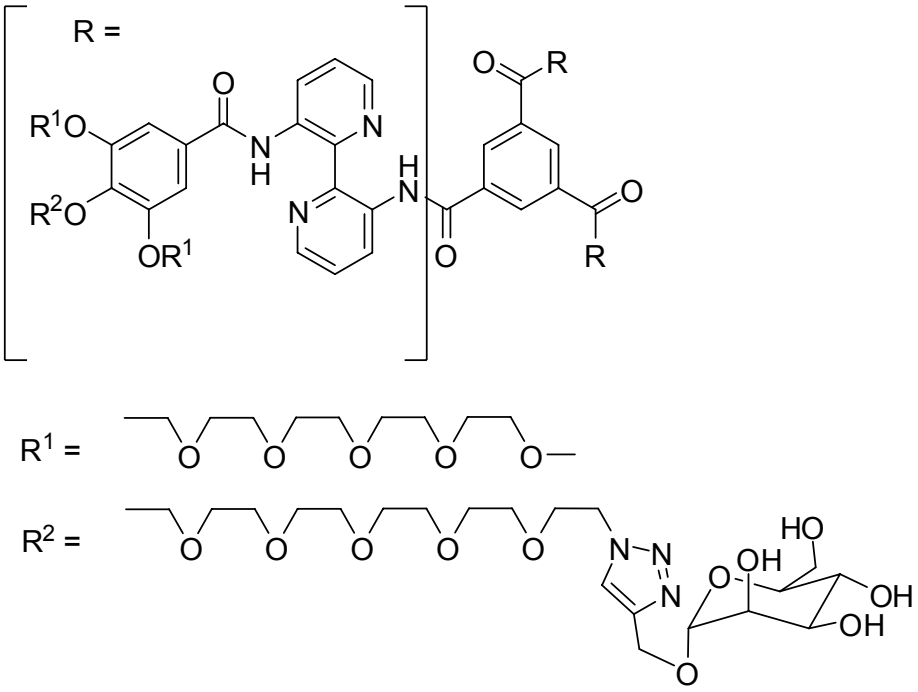

A solution of **18** (10 mg, 3 µmol) and **42** (30 mg, 140 µmol) in water (50 µL) and t-butanol (50 µl) with catalytic amounts of sodium-ascorbate (5 mol-%) and $CuSO_4$ (2 mol-%) was stirred at rt for 4 weeks. The crude product was purified by size exclusion chromatography (in CH_2Cl_2) followed by repeated size exclusion chromatography (in DMF). Drying over P_2O_5 afforded of **49** (12 mg, 2.5 µmol, 80%).

^{1}H NMR (400 MHz, *CDCl$_3$*) δ = 14.56 (s, 3H, N*H*CO), 13.56 (s, 3H, N*H'*CO), 8.74 (br, 3H, *H*-4), 8.48 (br, 3H, *H*-4'), 8.22 (s, 3H, *o*-*H*), 8.07 (br, 3H, *H*-6'), 7.65 (br, 3H, *H*-6), 7.39 (s, 6H, *H*-5 and *H*-5'), 7.2 (s, 6H, *H*-benzoyl), 4.13 (m, 12H, *m*-OC*H$_2$*CH$_2$O), 4.02 (m, 6H, *p*-OC*H$_2$*CH$_2$O), 3.85 (m, 12H, *m*-OCH$_2$C*H$_2$*), 3.75 (m, 6H, mannose-*H*), 3.61-3.38 (m, 21H, mannose-*H* and *p*-OCH$_2$C*H$_2$*), 3.26-2.57 (m, 183H, OC*H$_2$*C*H$_2$*O), 2.50 (s, 18H, *m*-OC*H$_3$*);
MS (MALDI-TOF): calcd. for $[C_{189}H_{285}N_{21}O_{78} + H]^+$ *m/z* = 4096.9, found *m/z* = 4098.1.

Galactose Discotic (50) (Chapter 3.2.1)

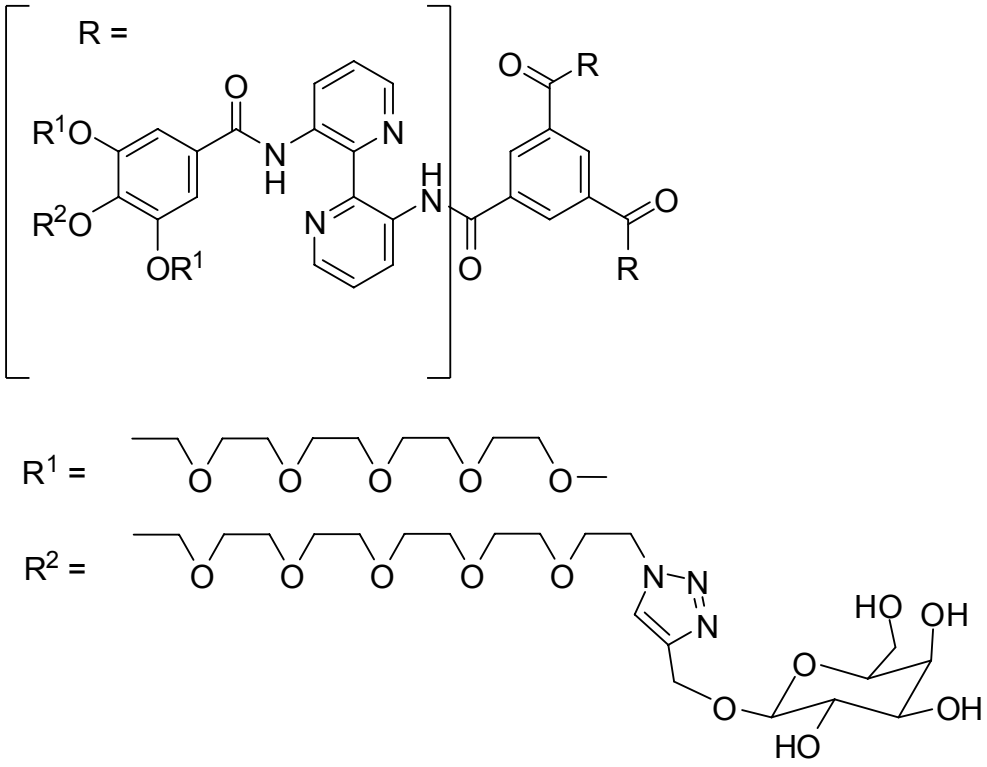

A solution of **18** (2.1 mg, 0.6 µmol) and **45** (10 mg, 46 µmol) in water (50 µL) and t-butanol (50 µl) with catalytic amounts of sodium-ascorbate (5 mol-%) and $CuSO_4$ (2 mol-%) was stirred at rt for 4 weeks. The crude product was purified by size exclusion chromatography (in CH_2Cl_2) followed by repeated size exclusion chromatography (in DMF). Drying over P_2O_5 afforded of **50** (1.9 mg, 0.5 µmol, 78%).

MS (MALDI-TOF): calcd. for $[C_{189}H_{285}N_{21}O_{78} + NH_4]^+$ *m/z* = 4118.6, found *m/z* = 4116.7.

Glucose Discotic (51) (Chapter 3.2.1)

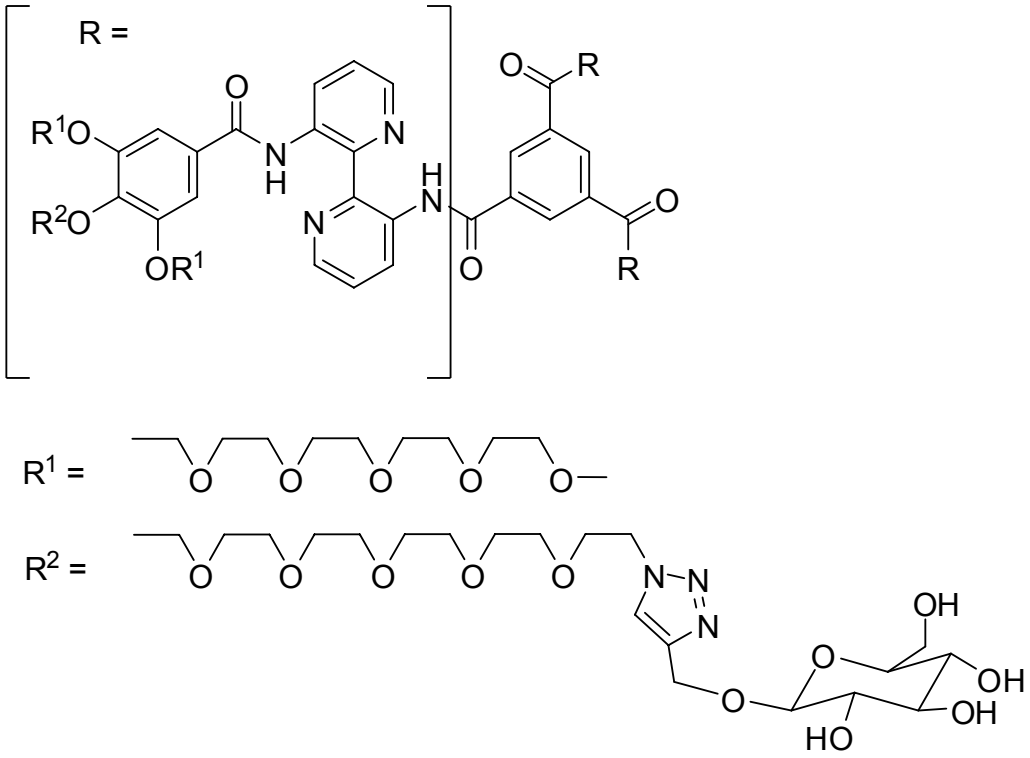

A solution of **18** (1.9 mg, 0.6 µmol) and **48** (10 mg, 46 µmol) in water (50 µL) and t-butanol (50 µl) with catalytic amounts of sodium-ascorbate (5 mol-%) and $CuSO_4$ (2 mol-%) was stirred at rt for 4 weeks. The crude product was purified by size exclusion chromatography (in CH_2Cl_2) followed by repeated size exclusion chromatography (in DMF). Drying over P_2O_5 afforded of **51** (1.5 mg, 0.4 µmol, 61%).

MS (MALDI-TOF): calcd. for $[C_{189}H_{285}N_{21}O_{78} + H]^+$ *m/z* = 4096.9, found *m/z* = 4098.1.

Texas Red Discotic (52) (Chapter 3.2.2)

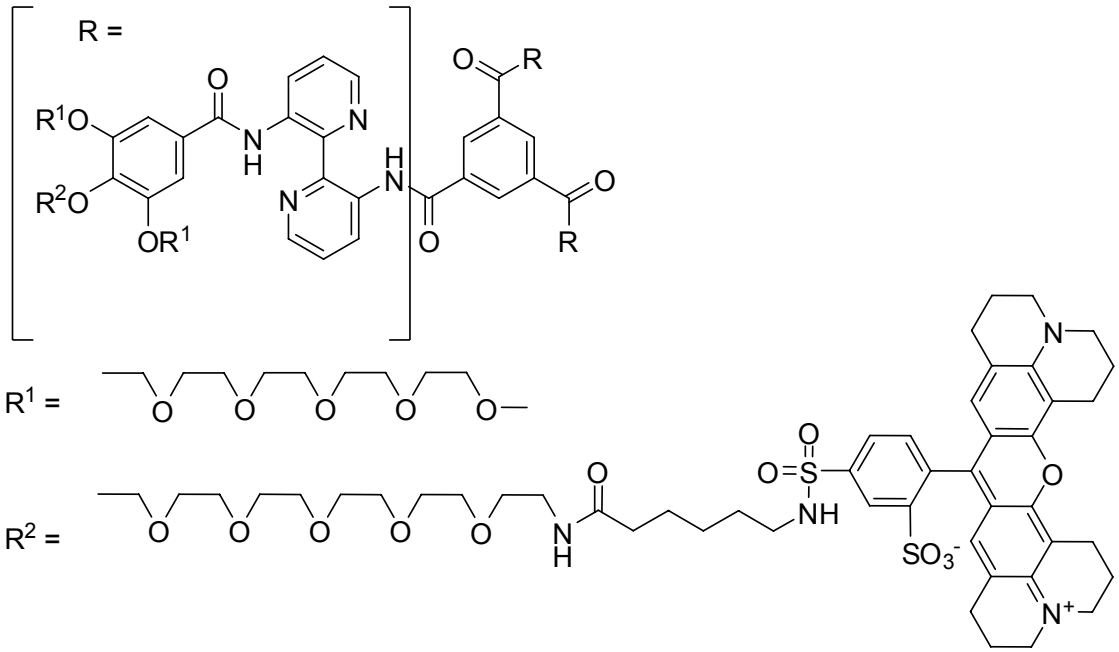

To a solution of **19** (2.5mg, 0.8 µmol) in CH_2Cl_2 (0.3 mL) Texas Red®-X succinimidyl ester (2.5 mg, 3 µmol) was slowly added. After stirring for 30 min, triethylamine (5 µL) was added to the mixture and stirring was continued. The reaction was monitored by MALDI-TOF MS. After 4 days additional Texas Red®-X succinimidyl ester (2 mg, 2.5 µmol) and triethylamine (8 µL) was added. After 2 weeks no further conversion of intermediates could be observed. The solvent was evaporated *in vacuo* and the crude product was purified by size exclusion chromatography (in CH_2Cl_2) affording **52** with its side products.

Triacylated compound: Exact Mass: 5468.4
MS (MALDI-TOF): calcd. for $[C_{273}H_{366}N_{24}O_{81}S_6 + K]^+$ *m/z* = 5508.3 found *m/z* = 5509.4;
Diacylated compound: Exact Mass: 4767.1
MS (MALDI-TOF): calcd. for $[C_{236}H_{327}N_{21}O_{74}S_4 + Na]^+$ *m/z* = 4790.1 found *m/z* = 4790.6;
Monoacylated compound: Exact Mass: 4065.9

MS (MALDI-TOF): calcd. for $[C_{199}H_{288}N_{18}O_{67}S_2 + Na]^+$ *m/z* = 4088.9 found *m/z* = 4090.0.

Biotin Discotic (53) (Chapter 3.2.3)

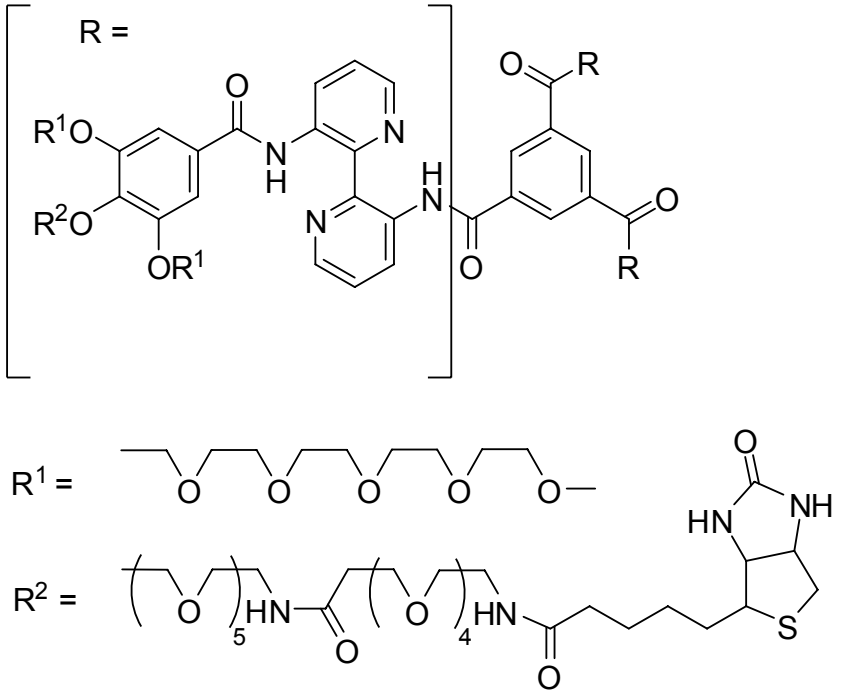

To a solution of **19** (5 mg, 1.5 µmol) in CH_2Cl_2 (0.3 mL) BiotinPEO_4-NHS (8 mg, 13.5 µmol) was slowly added. After stirring for 1 h, triethylamine (8 µL) was given dropwise to the mixture and stirred for another 4 h. The reaction was monitored by MALDI-TOF MS. After 4 h only traces of mono- and double-acylated side products were left. After adding more BiotinPEO_4-NHS (3 mg, 5.0 µmol) and stirring for another 24 h no change could be observed. The solvent was evaporated *in vacuo* and the crude product was purified by size exclusion chromatography (in DMF) affording **53** (4.6 mg, 1 µmol, 65%).

^{1}H NMR (500 MHz, *CDCl$_3$*) δ = 15.32 (s, 3H, N*H*CO), 14.28 (s, 3H, N*H'*CO), 9.60 (d, *J* = 8.0, 3H, *H*-4), 9.39 (d, *J* = 8.8, 3H, *H*-4'), 9.29 (s, 3H, *o*-*H*), 9.06 (d, *J* = 3.7, 3H, *H*-6'), 8.53 (d, *J* = 4.8, 3H, *H*-6), 7.57 (dd, *J* = 2.7, 7.2, 6H, *H*-5 and *H*-5'), 7.36 (s, 6H, *H*-benzoyl), 4.50 (m, 3H, biotin-NHC*H*), 4.30 (t, 12H,

m-OC*H*$_2$CH$_2$O), 4.29 (m, 3H, biotin-NHC*H*), 4.28 (t, 6H, *p*-OC*H*$_2$CH$_2$O), 3.91 (t, 12H, *m*-OCH$_2$C*H*$_2$O), 3.83 (t, 6H, *p*-OCH$_2$C*H*$_2$O), 3.79-3.50 (m, 216H, OC*H*$_2$C*H*$_2$O), 3.46-3.39 (m, 12H, biotin-SC*H*$_2$), 3.36 (s, 18H, *m*-OC*H*$_3$), 3.19-3.09 (m, 3H, biotin-SC*H*$_2$), 2.55-2.41 (m, 6H, *H*-Alkyl), 2.27-2.14 (m, 6H, *H*-Alkyl), 1.51-1.38 (m, 6H, *H*-Alkyl), 1.27-1.22 (m, 6H, *H*-Alkyl);
MS (MALDI-TOF): calcd. for $[C_{225}H_{354}N_{24}O_{81}S_3 + Na]^+$ *m/z* = 4807.34, found *m/z* = 4810.33.

Biotin Discotic (54) (Chapter 3.2.3)

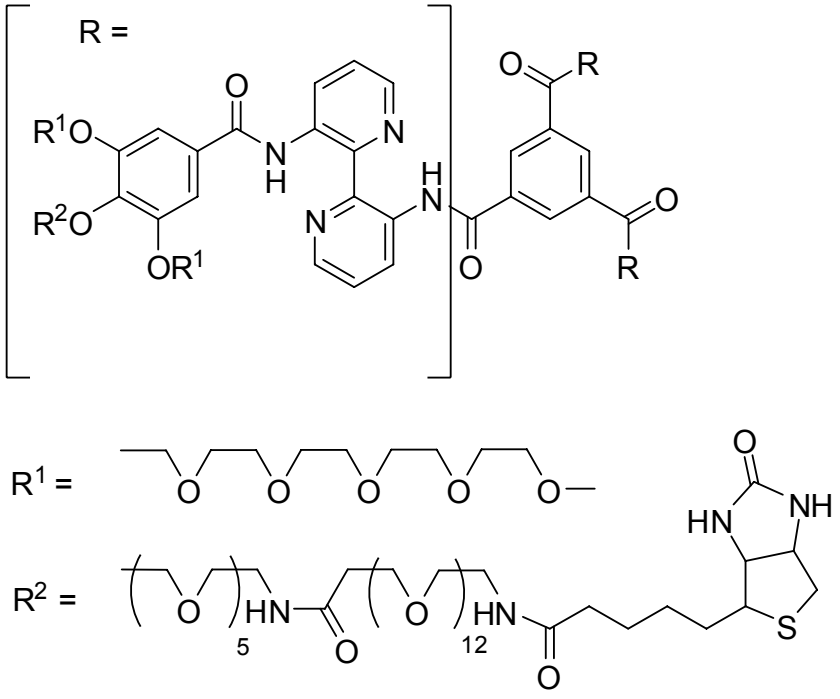

To a solution of **19** (5 mg, 1.5 µmol) in CH_2Cl_2 (0.3 mL) BiotinPEO$_{12}$-NHS (13 mg, 13.5 µmol) was slowly added. After stirring for 1 h, triethylamine (10 µL) was added dropwise to the mixture and stirred for another 4 h. The reaction was monitored by MALDI-TOF MS. After 4 h the starting material had reacted completely and mono-, double- and triacylated side products could be found. After adding more BiotinPEO$_{12}$-NHS (3 mg, 3.1 µmol) and stirring for another 48 h no change could be observed. The solvent was evaporated *in*

vacuo and the crude product was purified by size exclusion chromatography (in DMF) affording **54** with traces of side products.

54 triacylated compound: Exact Mass: 5840.98
MS (MALDI-TOF): calcd. for $[C_{199}H_{316}N_{18}O_{75}S + Na]^+$ *m/z* =, found *m/z* = 5846.18.
Diacylated compound: Exact Mass: 5015.55
MS (MALDI-TOF): calcd. for $[C_{236}H_{383}N_{21}O_{90}S_2 + K]^+$ *m/z* = 5055.4, found *m/z* = 5055.2.
Monoacylated compound: Exact Mass: 4190.12
MS (MALDI-TOF): calcd. for $[C_{273}H_{450}N_{24}O_{105}S_3 + Na]^+$ *m/z* = 4213.1, found *m/z* = 4211.3.

Boc-Cys(Trt) Discotic (55) (Chapter 3.2.4)

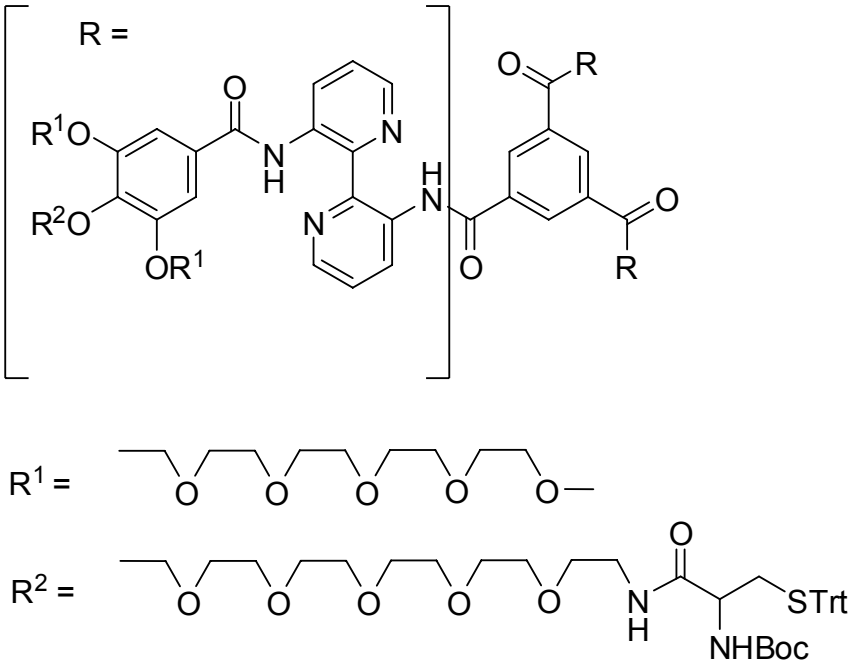

To a solution of **19** (10 mg, 3 µmol) in CH_2Cl_2 (0.3 mL) Boc-Cys(Trt)-NHS (10 mg, 25 µmol) was slowly added. After stirring for 30 min, triethylamine (8.4 µL) was added dropwise to the mixture and stirred over night. The reaction was monitored by MALDI-TOF MS. The solvent was evaporated *in*

vacuo and the crude product was purified by size exclusion chromatography (in CH_2Cl_2) affording **55** (12 mg, 2.5 µmol, 85%).

^{1}H NMR (400 MHz, *CDCl$_3$*) δ = 15.52 (s, 3H, N*H*CO), 14.49 (s, 3H, N*H'*CO), 9.60 (d, *J* = 8.5, 3H, *H*-4), 9.39 (d, *J* = 8.6, 3H, *H*-4'), 9.29 (s, 3H, *o*-*H*), 9.05 (d, *J* = 4.6, 3H, *H*-6'), 8.52 (d, *J* = 3.0, 3H, *H*- *H*-46), 7.57 (dd, *J* = 4.6, 8.5, 6H, *H*-5 and *H*-5'), 7.40 (d, *J* = 7.4, 18H, *H*-trityl), 7.36 (s, 6H, *H*-benzoyl), 7.29 (d, *J* = 7.2, 18H, *H*-trityl), 7.21 (t, *J* = 7.2, 9H, *H*-trityl), 4.28 (t, 12H, *m*-OC*H*$_2$CH$_2$O), 4.26 (t, 6H, *p*-OC*H*$_2$CH$_2$O) 3.90 (t, 12H, *m*-OCH$_2$C*H*$_2$O), 3.83 (t, 6H, *p*-OCH$_2$C*H*$_2$O), 3.77-3.47 (m, 182H), 3.39 (t, *J* = 5.3, 6H, *p*-OCH$_2$C*H*$_2$NHCys), 3.35 (s, 18H, *m*-OC*H*$_3$), 2.74-2.53 (m, 6H, *H*-Cys), 1.41 (s, 27H, OC(C*H*$_3$)$_3$).
MS (MALDI-TOF): calcd. for $[C_{243}H_{330}N_{18}O_{69}S_3 + Na]^+$ *m/z* = 4723.19, found *m/z* = 4727.09.

Cysteine-Discotic (56) (Chapter 3.2.4)

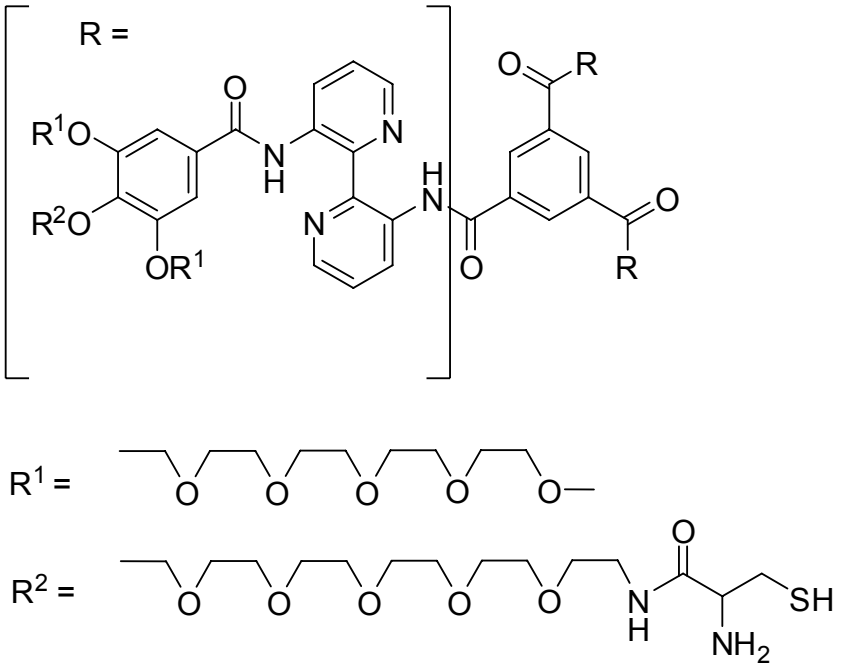

A solution of **55** (6 mg, 1.3 µmol) in CH_2Cl_2 (0.4 mL) with TFA (0.1 mL) and triethylsilane (10 µL) was stirred for 2 h. The reaction was monitored by

MALDI-TOF MS. The solvent was co-evaporated with toluene (3 x 2 mL) *in vacuo* and the crude product was purified by size exclusion chromatography (in CH_2Cl_2) affording **56** (4.5 mg, 1.2 µmol, 98%).

^{1}H NMR (400 MHz, *CDCl$_3$*) δ = 15.52 (s, 3H, N*H*CO), 14.49 (s, 3H, N*H'*CO), 9.60 (d, *J* = 8.5, 3H, *H*-4), 9.39 (d, *J* = 8.6, 3H, *H*-4'), 9.29 (s, 3H, *o*-*H*), 9.05 (d, *J* = 4.6, 3H, *H*-6'), 8.52 (d, *J* = 3.0, 3H, *H*- *H*-46), 7.57 (dd, *J* = 4.6 and 8.5, 6H, *H*-5 and *H*-5'), 7.36 (s, 6H, *H*-benzoyl), 4.28 (t, 12H, *m*-OC*H$_2$*CH$_2$O), 4.26 (t, 6H, *p*-OC*H$_2$*CH$_2$O) 3.90 (t, 12H, *m*-OCH$_2$C*H$_2$*O), 3.83 (t, 6H, *p*-OCH$_2$C*H$_2$*O), 3.77-3.47 (m, 182H), 3.39 (t, *J* = 5.3, 6H, *p*-OCH$_2$C*H$_2$*NHCys), 3.35 (s, 18H, *m*-OC*H$_3$*), 2.74-2.53 (m, 6H, *H*-Cys), 1.41 (s, 27H, OC(C*H$_3$*)$_3$).
MS (MALDI-TOF): calcd. for $[C_{171}H_{264}N_{18}O_{63}S_3 + Na]^+$ *m/z* = 3695.12, found *m/z* = 3692.94.

Ligation of 56 to YFP (57) (Chapter 3.4.2)

A solution of **56** (4.5 mg, 1.2 µmol) and TCEP (400 mM, pH 7) in ligation buffer (30 mM Na_2HPO_4, pH 7.5, 50 mM NaCl degassed by bubbling argon through the buffer) was stirred over night in order to reduce disulfide bridges of **56**. This solution was diluted (1.5 mM **56**) and 100 µL (0.15 µmol) of **56** were added to a solution of YFP (0.014 µmol, 50 µL in 30 mM Na_2HPO_4, 50 mM NaCl, 0.1 m MEDTA, 0.04 % NaN_3,) in ligation buffer (400 µL) with MESNA (50 µL). The reaction mixture was incubated on a rotating wheel at rt over several days. The mixture was analyzed by SDS-PAGE and MALDI-TOF MS spectrometry.

MS (MALDI-TOF): calcd. for $[YFP + C_{171}H_{264}N_{18}O_{63}S_3 + Na]^+$ *m/z* = 30981, found *m/z* = 31008.

5.2.8 Bacterial Assays (Chapter 3.3.1)

5.2.8.1 General Bacterial Microscopy Experiments (Chapter 3.3.1.1)

100 µL frozen culture of *E. coli* strain BL 21 α were grown overnight in 4 ml LB media with Ampicilin (0.1 mg/mL) in a shaker at 37 °C. The OD_{600} was measured and the culture was diluted to reach an OD_{600} of 1. The bacterial culture was split in portions of 200 µL and centrifuged for 5 min at 3000 rpm. The liquid was removed and the pellet was re-suspended in 200 µL of PBS buffer and washed three times with this buffer. Finally the pellet was re-suspended in 200 µL PBS containing $MnCl_2$ and $CaCl_2$ (1 mM). The bacteria were incubated with either compound **1** or **49**, at a total overall concentration of **1** of 10^{-7} M, for 1 h at rt. Incubation with water was carried out as a control. Subsequently, the bacteria were washed with PBS buffer as described. The pellet was re-suspended in 50 µL PBS. 20 µL of this suspension were fixed on microscope slides using Aqua Poly Mount, covered with glass slides and left to dry over night at 5 °C.

Microscopic observation was carried out on a Zeiss fluorescent microscope using brightfield and an optical filter corresponding to the spectroscopic profile of compounds **1** and **49** (λ_{ex} = 360 nm, λ_{em} = 490 nm).

5.2.8.2 Bacterial Microscopy Experiments with Fluorescent E. coli (Chapter 3.3.1.2)

The assay was performed as described in 5.2.8.1, however using *E. coli* strain BL 21 α pECFP, for exact fluorescence colocalization studies of the bacteria with compound **49**. Microscopic observation was carried out on a Zeiss fluorescent microscope using brightfield and an optical filter corresponding to the spectroscopic profile of compounds **1** and **49** (λ_{ex} = 360 nm, λ_{em} = 490 nm) or of CFP expressed in the bacteria (CFP optical filter).

5.2.8.3 Bacterial Microscopy Experiments with ORN178 and ORN208 (Chapter 3.3.1.3)

The assay was performed using *E. coli* strains ORN178 (overexpressing FimH) and ORN 208 (not expressing FimH). The strains were a kind gift from Prof. Paul Orndorff (North Carolina State University).

100 µL frozen culture of *E. coli* strain ORN178 and ORN208 were grown overnight in 4 mL LB media in a shaker at 37 °C. ORN178 does not carry any plasmid encoding for any antibiotic resistance. Therefore only ORN208 was grown in presence of with Ampicilin (0.1 mg/mL). The OD_{600} was measured and the culture was diluted to reach an OD_{600} of 1. The bacterial culture was split in portions of 200 µL and centrifuged for 5 min at 3000 rpm. The liquid was removed and the pellet was re-suspended in 200 µL of PBS buffer and washed three times with this buffer. Finally the pellet was re-suspended in 200 µL PBS containing $MnCl_2$ and $CaCl_2$ (1 mM). The bacteria were incubated with either compound **1** or **49** as described under 5.2.8.1, and fixed on microscope slides using Aqua Poly Mount. Microscopic observation was carried out on a Zeiss fluorescent microscope using brightfield and an optical filter corresponding to the spectroscopic profile of compounds **1** and **49** (λ_{ex} = 360 nm, λ_{em} = 490 nm).

5.2.8.4 Bacterial Experiments with Mixtures of 1 and 49 (Chapter 3.3.1.4)

E. coli strain BL 21 α was cultured as described in 5.2.8.1. Discotic mixtures of **1** and **49** with ratios of 1/1, 2/1, 3/1, 5/1, 10/1, 20/1 and 99/1 were prepared 12 h prior to the incubation with bacteria to ensure complete mixing of the individual compounds. The bacteria were incubated with the different mixtures of **1** and **49** at rt for 1 h. The overall concentration of discotics (c[**1**] + c[**49**] = 10^{-7} M) was kept constant. After washing as described, the pellet was re-suspended in 200 µL PBS. 10 µL of this suspension were fixed on microscope slides using Aqua Poly Mount, covered with glass slides and left to dry over night at 5 °C. Microscopic observation was carried out on a Zeiss fluorescent microscope using brightfield and an optical filter corresponding to the spectroscopic profile of compounds **1** and **49** (λ_{ex} = 360 nm, λ_{em} = 490 nm).

5.2.8.5 Bacterial Mannose Competition Experiments (Chapter 3.3.1.5)

E. coli strain BL 21 α was cultured as described in 5.2.8.1. The bacteria were pre-incubated with different concentrations of methyl-α-D-mannopyranoside ranging from 3 x 10^{-1} M to 3 x 10^{-7} M for 10 min at rt. Compound **49** was then added to each vial to reach a final concentration of 10^{-7} M and incubated for 1 h at rt. Subsequently, the suspension was centrifuged for 5 min at 3000 rpm. The liquid was removed and the pellet was re-suspended in 200 µL of PBS buffer and washed three times with this buffer. The pellet was re-suspended in 50 µL PBS. 20 µL of this suspension were fixed on microscope slides using Aqua Poly Mount, covered with glass slides and left to dry over night at 5 °C. Controls were performed with pure methyl-α-D-mannopyranoside, water, and **49**. Mounting and microscopic observation was performed as described.

5.2.8.6 Bacterial growth control (Chapter 3.3.1.6)

E. coli strain BL 21 α was cultured as described under 5.2.8.1. 200 µl of cell culture per vial were washed and re-suspended in LB medium to reach an OD_{600} of 0.5. **49** or **1**, at final concentrations of 10^{-7} M, or water were added to three vials each and incubated for 4 h at 37 °C. Subsequently the bacteria were washed and the OD_{600} was measured again.

5.2.8.7 Colocalization studies with 52 (Chapter 3.3.3)

E. coli strain BL 21 α was cultured as described under 5.2.8.1. Discotic mixtures of **1** and **52** with ratios of 1/1, 9/1 and 99/1 were prepared 12 h prior to the incubation with bacteria to ensure complete mixing of the individual compounds. The bacteria were incubated with the different mixtures of **1** and **52** and with compound **52** at room temperature. The overall concentration of discotics (c[**1**] + c[**52**] = 10^{-7} M) was kept constant. After washing as described, the pellet was re-suspended in 200 µL PBS. 10 µL of this suspension were fixed on microscope slides using Aqua Poly Mount, covered with glass slides and left to dry over night at 5 °C. Microscopic observation was carried out on a Zeiss fluorescent microscope using brightfield and an optical filter corresponding to the spectroscopic profile of compounds **1** and **52** (λ_{ex} = 360

nm, λ_{em} = 490 nm) and to the spectroscopic profile of Texas Red (λ_{ex} = 569 nm, λ_{em} = 620 nm).

5.2.9 Experiments with Streptavidin Beads

5.2.9.1 Binding to Streptavidin Beads (Chapter 3.3.3.1)

Streptavidin Magnetic Beads were washed with PBS buffer. A magnet was used to gather the beads on the bottom of the vial. The liquid was removed and the pellet was re-suspended in 200 µL of PBS buffer and washed three times with this buffer. The beads were incubated with either compound **1** or **53** at a total overall concentration of **1** of 10^{-7} M, for 1 h at rt. Incubation with water was carried out as control. Subsequently, the bacteria were washed with PBS buffer as described. The pellet was re-suspended in 50 µL PBS. 20 µL of this suspension were fixed on microscope slides using Aqua Poly Mount, covered with glass slides and left to dry over night at 5 °C. Microscopic observation was carried out on a Zeiss fluorescent microscope using brightfield and an optical filter corresponding to the spectroscopic profile of compounds **1** and **53** (λ_{ex} = 360 nm, λ_{em} = 490 nm).

5.2.9.2 Streptavidin Beads with 52 and 1 (Chapter 3.3.3.1)

Discotic mixtures of **52** and **53** with ratios of 1/1, 9/1 and 99/1 were prepared 12 h prior to the incubation with bacteria to ensure complete mixing of the individual compounds. The beads were incubated with the different mixtures of **52** and **53** at room temperature. The overall concentration of discotics (c[**52**] + c[**53**] = 10^{-7} M) was kept constant. The beads were washed as described. Subsequently the beads were washed with PBS buffer as described. The pellet was re-suspended in 50 µL PBS. 20 µL of this suspension were fixed on microscope slides using Aqua Poly Mount, covered with glass slides and left to dry over night at 5 °C.

Microscopic observation was carried out on a Zeiss fluorescent microscope using brightfield and an optical filter corresponding to the spectroscopic profile

of compounds **52** and **53** (λ_{ex} = 360 nm, λ_{em} = 490 nm) and to the spectroscopic profile of Texas Red (λ_{ex} = 569 nm, λ_{em} = 620 nm).

5.2.10 Enzyme Linked Lectine Assay (Chapter 3.3.2)[90]

5.2.10.1 Determination of Enzyme concentration

Nunc Immuno Maxi-Sorp™ plates were incubated with 100 µL/well mannan (10 µg/ml in 0.01 M PBS, pH = 7.3 with 0.1 mM Mn^{2+} and Ca^{2+}) overnight at room temperature. Subsequently each well was washed three times with 300 µL washing buffer (PBS with 0.05 % (v/v) Tween). The wells were then blocked for 1 h at 37 °C using 150 µL/well BSA (1% in PBS). Washing was repeated as described. Afterwards the plates were incubated for 1 h at 37 °C with different dilutions of Horseradish Peroxidase labeled Con A in buffer, ranging from 10^{-1} to 10^{-5} mg/mL. The washing step was repeated and 50 µL/well ABTS (0.25 mg/mL citrate buffer 0.2 M, pH = 4.0 with 0.015 % (v/v) H_2O_2) were added. Color development was stopped after 20 min by adding 50 µL/well 1M H_2SO_4. Light absorption was measured at 415 nm. The concentration of Con A-HRP with the readout between 0.8 and 1 was used for inhibition studies (Figure 57).

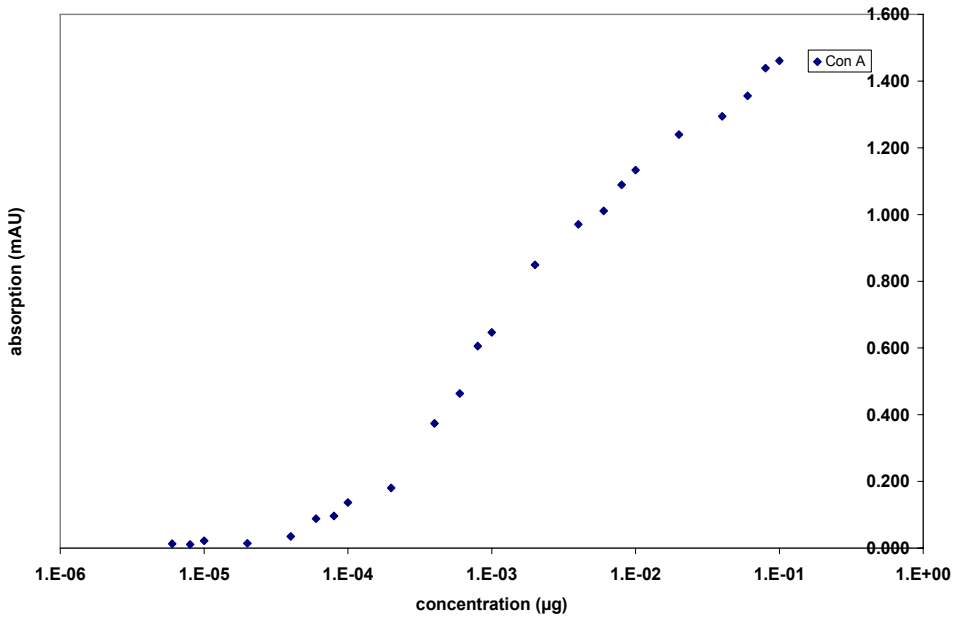

Figure 57. Determination of Con A concentration for assay procedure.

5.2.10.2 Inhibition Experiments

Nunc Immuno Maxi-Sorp^{TM} plates were coated, washed and blocked as described above. Independently, 60 µL/well of serial dilutions of inhibitor (either methyl-α-D-mannopyranoside or **49**) were made in a Nunclon 96 well plate. To each of these wells 60 µL of Con-A HRP was added and incubated for 1 h at 37 °C. 100 µL/well of these inhibitor-lectin mixtures were transferred to the mannan coated plate and incubated for 1 h at 37 °C. The wells were washed and treated with ABTS. The reaction was stopped after 20 min. Absorption was measured at 415 nm and the % inhibition was calculated as follows:

$$\% \text{ Inhibition} = \{[A_{(\text{no inhibitor})} - A_{(\text{with inhibitor})}] / A_{(\text{no inhibitor})}\} \times 100$$

The calculated IC_{50} values were 3020 µM in case of methyl-α-$_D$-mannopyranoside and 120 µM for **49**. The valency corrected value (360 µM) was obtained multiplying the calculated IC_{50} by the amount of mannose per single discotic scaffold (= 3).

5.2.11 Foerster Resonance Energy Transfer Experiments (Chapter 3.4)

5.2.11.1 Interaction of SA-Cy3 and 53 (Chapter 3.4.4)

Cy3 labeled streptavidin (10^{-5} M in PBS) was titrated to **53** or **1** (each 10^{-6} M in PBS) or water in serial concentrations from 10^{-7} to 0.5 10^{-6} M (ratio **53**/SA-Cy3 from 100/1 till 2/1) at 20 °C and stirred for 5 min after each titration step. Fluorescence- (λ_{ex} = 340 nm, λ_{em} = 350 till 770 nm) and UV- (200 till 750 nm) spectra were measured after each titration step. FRET-ratios were determined as follows: FRET-ratio = (Emission at $\lambda_{max\ Cy3}$ / Emission at $\lambda_{max\ Discotic}$) = (Emission at 570 nm / Emission at 524 nm).

5.2.11.2 Titration of SA-Cy3 to mixtures of 1/53 (Chapter 3.4.5)

Stock solutions (10^{-5} M) of **53** and **1** in PBS (0.01 M, pH = 7.3) were prepared and diluted until the emission was approximately the same. Different ratios of **53** and **1** (1/0, 1/1, 1/2, 1/3, 1/5, 1/10 and 1/20) were mixed and left overnight at room temperature to assure equilibration of the discotic columns. Each mixture was diluted in PBS to reach a final concentration of **53** of 10^{-6} M. Cy3 labeled streptavidin was added in serial concentrations from 10^{-7} to 0.5 10^{-6} M at 20 °C and stirred for 5 min. Fluorescence- (λ_{ex} = 340 nm, λ_{em} = 350 till 770 nm) and UV- (200 till 750 nm) spectra were measured after each titration step. FRET-ratios were determined as follows: Emission at ($\lambda_{max\ Cy3}$ / Emission at $\lambda_{max\ Discotic}$) = Emission at (570 nm / Emission at 524 nm).

5.2.11.3 Titration of 1 to mixtures of SA-Cy3/53 (Chapter 3.4.5)

Cy3 labeled streptavidin (10^{-5} M in PBS) and **53** were mixed 1 h prior to the experiment with a ratio of 5/1 **53**/SA-Cy3 at 20 °C. Each mixture was diluted in PBS to reach a final concentration of **53** of 10^{-6} M. **1** was added to each mixture in serial concentrations to yield final ratios of **53**/**1** (1/0, 1/1, 1/2, 1/3, 1/5, 1/10 and 1/20). Fluorescence- (λ_{ex} = 340 nm, λ_{em} = 350 till 770 nm) and

UV- (200 till 750 nm) spectra were measured after 5 min, 30 min, 1 h, 2 h, 1 day and 2 days. FRET-ratios were determined as follows: (Emission at $\lambda_{max\ Cy3}$ / Emission at $\lambda_{max\ Discotic}$) = Emission at (570 nm / Emission at 524 nm).

5.2.11.4 Titration of SA-TR and SA-AF633 to 53 (Chapter 3.4.6)

Texas Red labeled streptavidin (SA-TR) and Alexa Fluor 633 labeled streptavidin (SA-AF633) were mixed 2 h prior to the experiments to reach a final concentration of 0.05 mg/mL^{-1} of each protein. This protein mixture was titrated to **53** or **1** (each 10^{-6} M in PBS) or water in serial volumes ranging from 1 to 50 µL at 20 °C and stirred for 10 min after each titration step. Fluorescence- (λ_{ex} = 340 nm, λ_{em} = 350 till 770 nm) and UV- (200 till 750 nm) spectra were measured after each titration step. FRET-ratios were determined as follows: FRET-ratio = (Emission at $\lambda_{max\ Alexa\ Fluor\ 633}$ / Emission at $\lambda_{max\ Texas\ Red}$) = (Emission at 647 nm / Emission at 612 nm).

5.2.11.5 Titration of 53 to SA-TR and SA-AF633 (Chapter 3.4.6)

Texas Red labeled streptavidin (SA-TR) and Alexa Fluor 633 labeled streptavidin (SA-AF633) were mixed 4 h prior to the experiments to reach a final concentration of 0.05 mg/mL^{-1} of each protein. From a stock solution of **53** (c [**53** = 10^{-4}]) portions of 1-5 µL were added to reach final concentrations between 2 x 10^{-6} M and 1 x 10^{-5} M (0.5-25 mol-% compared to the single protein concentration). Resulting mixtures were stirred for 10 min after each titration step. Fluorescence- (λ_{ex} = 340 nm, λ_{em} = 350 till 770 nm) and UV- (200 till 750 nm) spectra were measured after each titration step. FRET-ratios were determined as follows: FRET-ratio = (Emission at $\lambda_{max\ Alexa\ Fluor\ 633}$ / Emission at $\lambda_{max\ Texas\ Red}$) = (Emission at 647 nm / Emission at 612 nm).

5.2.11.6 Titration of 53 to SA-TR and SA-AF514 (Chapter 3.4.6)

Texas Red labeled streptavidin (SA-TR) and Alexa Fluor 514 labeled streptavidin (SA-AF514) were mixed 4 h prior to the experiments to reach a final concentration of 0.05 mg/mL^{-1} of each protein. From a stock solution of **53** (c [**53** = 10^{-4}]) portions of 2 µL were added to reach final concentrations between 2 x 10^{-6} M and 1 x 10^{-5} M. Resulting mixtures were stirred for 10 min after each titration step. Fluorescence- (λ_{ex} = 340 nm, λ_{em} = 350 till 770 nm) and UV- (200 till 750 nm) spectra were measured after each titration step. FRET-ratios were determined as follows: FRET-ratio = Emission at ($\lambda_{max\ Texas\ Red}$ / Emission at $\lambda_{max\ Alexa\ Fuor\ 514}$) = (Emission at 612 nm / Emission at 541 nm).

6 Abbreviations

Å	Angstroem
ABTS	2,2'-azinobis-(3-ethylbenzothiazoline-6-sulfonic acid)diammonium salt
ar	aromatic
BIACORE	surface plasmon resonance based biosensors
Boc	*tert*-butoxy-carbonyl
br	broad
calcd.	calculated
CFP	cyan fluorescent protein
Con A	concanavalin A (lectin)
d	doublet
dd	doublet of a doublet
δ	ppm parts per million
DHB	2,5-dihydroxybenzoic acid
DIC	diisopropylcarbodiimide
DIPEA	*N*,*N*-diisopropylethylamine
DMAP	4-dimethylaminopyridine
DMF	dimethylformamide
DP	Degree of polymerization
E. Coli	Escherischia Coli
EDTA	ethylenediaminetetraacetic acid
ELISA	Enzyme linked immunosorbent assay
ELLA	Enzyme linked lectin assay
equiv.	equivalent
ESI	electron spray ionization
et al.	et alii
FimH	fimbrae H - receptors of *E. coli* that recognize mannose
FRET	Foerster resonance energy transfer
g	gram
gCOSY	gradient enhanced Correlation Spectroscopy

HATU	2-(1*H*-7-Azabenzotriazol-1-yl)-1,1,3,3-tetramethyl uronium hexafluorophosphate
HIA	hemagglutination assay
HPLC	high pressure liquid chromatography
HRP	Horseradish-peroxidase
IC_{50}	half maximal inhibitory concentration
ITC	isothermal titration calorimetry
J	coupling constant
K_{ass}	association constant
λ	wavelength in nm
L	liter
LB	lysogenic broth - nutrient solution to grow *E. coli*
LC/MS	liquid chromatography followed by mass spectroscopy
M	molar
m	meter
m/z	mass per charge
MALDI-TOF	matrix-assisted laser desorption/ionization time of flight
Max	maximum
MDCK	Madin Darby canine kidney from dog
mg	milligram
MHz	megahertz
min	minute
mL	milliliter
mM	millimolar
mmol	millimole
mol	mole
mol-%	mole percent
mp	melting point
nm	nanometer
NMR	nuclear magnetic resonance
OD_{600}	optical density at 600 nm

ORN178	*E. coli* strain with overexpressed FimH
ORN208	*E. coli* strain with supressed FimH
PBS	phosphate buffer saline
PBS-T	phosphate buffer saline with 5% Tween
Pd/C	palladium on charcoal
pECFP	plasmid encoding CFP
pTWIN1-EYFP	plasmid encoding YFP
quant.	quantitative
R_f	retention factor
rpm	revolutions per minute
rt	room temperature
R_t	retention time
s	singlet
SA	streptavidin
SA-AF514	streptavidin labeled with Alexa Fluor 514
SA-AF633	streptavidin labeled with Alexa Fluor 633
SA-Cy_3	streptavidin labeled with Cy3
SA-TR	streptavidin labeled with Texas Red
TES	triethylsilane
TFA	trifluoric acid
THF	tetrahydrofuran
µ	micro
µg	microgram
µM	micro molar
µm	micromole
UV	ultra violet
UV-Vis	ultra violet-visible spectroscopy
v/v	percent volume
YFP	yellow fluorescent protein

7 Literature

[1] M. Mammen, S. K. Choi, G. M. Whitesides, *Angewandte Chemie-International Edition* 1998, *37*, 2755.
[2] A. Varki, *Glycobiology* 1993, *3*, 97.
[3] N. Sharon, *Febs Letters* 1987, *217*, 145.
[4] S. J. Williams, G. J. Davies, *Trends in Biotechnology* 2001, *19*, 356.
[5] M. Mammen, G. Dahmann, G. M. Whitesides, *Journal of Medicinal Chemistry* 1995, *38*, 4179.
[6] H. Connell, W. Agace, P. Klemm, M. Schembri, S. Marild, C. Svanborg, *Proceedings of the National Academy of Sciences of the United States of America* 1996, *93*, 9827.
[7] M. A. Gimbrone, T. Nagel, J. N. Topper, *Journal of Clinical Investigation* 1997, *99*, 1809.
[8] T. K. Lindhorst, C. Kieburg, U. Krallmann-Wenzel, *Glycoconjugate Journal* 1998, *15*, 605.
[9] W. P. Jencks, *Proceedings of the National Academy of Sciences of the United States of America-Biological Sciences* 1981, *78*, 4046.
[10] L. L. Kiessling, J. E. Gestwicki, L. E. Strong, *Angewandte Chemie-International Edition* 2006, *45*, 2348.
[11] A. L. Banerjee, D. Eiler, B. C. Roy, X. Jia, M. K. Haldar, S. Mallik, D. K. Srivastava, *Biochemistry* 2005, *44*, 3211.
[12] C. A. Macken, A. S. Perelson, *Journal of Mathematical Biology* 1982, *14*, 365.
[13] G. Ercolani, *Journal of the American Chemical Society* 2003, *125*, 16097.
[14] J. D. Badjic, A. Nelson, S. J. Cantrill, W. B. Turnbull, J. F. Stoddart, *Accounts of Chemical Research* 2005, *38*, 723.
[15] L. Baldini, A. Casnati, F. Sansone, R. Ungaro, *Chemical Society Reviews* 2007, *36*, 254.
[16] L. L. Kiessling, J. E. Gestwicki, L. E. Strong, *Current Opinion in Chemical Biology* 2000, *4*, 696.
[17] L. L. Kiessling, L. E. Strong, J. E. Gestwicki, in *Annual Reports in Medicinal Chemistry, Vol 35, Vol. 35*, 2000, pp. 321.
[18] P. I. Kitov, D. R. Bundle, *Journal of the American Chemical Society* 2003, *125*, 16271.
[19] V. Martos, P. Castreno, J. Valero, J. de Mendoza, *Current Opinion in Chemical Biology* 2008, *12*, 698.
[20] A. Mulder, J. Huskens, D. N. Reinhoudt, *Organic & Biomolecular Chemistry* 2004, *2*, 3409.
[21] J. M. Lehn, *Chemical Society Reviews* 2007, *36*, 151.
[22] Y. C. Lee, R. T. Lee, *Accounts of Chemical Research* 1995, *28*, 321.
[23] J. Huskens, *Current Opinion in Chemical Biology* 2006, *10*, 537.
[24] R. Abidi, I. Oueslati, H. Amri, P. Thuery, M. Nierlich, Z. Asfari, J. Vicens, *Tetrahedron Letters* 2001, *42*, 1685.
[25] I. Oueslati, R. Abidi, Z. Asfari, J. Vicens, B. Masci, P. Thuery, M. Nierlich, *Journal of Inclusion Phenomena and Macrocyclic Chemistry* 2001, *39*, 353.
[26] G. M. L. Consoli, F. Cunsolo, C. Geraci, V. Sgarlata, *Organic Letters* 2004, *6*, 4163.
[27] L. L. Kiessling, N. L. Pohl, *Chemistry & Biology* 1996, *3*, 71.
[28] J. J. Lundquist, E. J. Toone, *Chemical Reviews* 2002, *102*, 555.
[29] K. Drickamer, *Nature Structural Biology* 1995, *2*, 437.
[30] C. H. Xue, S. P. Jog, P. Murthy, H. Y. Liu, *Biomacromolecules* 2006, *7*, 2470.
[31] T. L. Kelly, M. C. W. Lam, M. O. Wolf, *Bioconjugate Chemistry* 2006, *17*, 575.
[32] P. R. Ashton, S. E. Boyd, C. L. Brown, N. Jayaraman, J. F. Stoddart, *Angewandte Chemie-International Edition in English* 1997, *36*, 732.
[33] P. R. Ashton, S. E. Boyd, C. L. Brown, S. A. Nepogodiev, E. W. Meijer, H. W. I. Peerlings, J. F. Stoddart, *Chemistry-a European Journal* 1997, *3*, 974.
[34] B. Colonna, V. D. Harding, S. A. Nepogodiev, F. M. Raymo, N. Spencer, J. F. Stoddart, *Chemistry-a European Journal* 1998, *4*, 1244.
[35] S. M. Rele, W. X. Cui, L. C. Wang, S. J. Hou, G. Barr-Zarse, D. Tatton, Y. Gnanou, J. D. Esko, E. L. Chaikof, *Journal of the American Chemical Society* 2005, *127*, 10132.

[36] D. A. Tomalia, A. M. Naylor, W. A. Goddard, *Angewandte Chemie-International Edition in English* 1990, *29*, 138.
[37] T. Toyokuni, A. K. Singhal, *Chemical Society Reviews* 1995, *24*, 231.
[38] M. L. Wolfenden, M. J. Cloninger, *Journal of the American Chemical Society* 2005, *127*, 12168.
[39] M. L. Wolfenden, M. J. Cloninger, *Bioconjugate Chemistry* 2006, *17*, 958.
[40] E. K. Woller, M. J. Cloninger, *Organic Letters* 2002, *4*, 7.
[41] E. K. Woller, E. D. Walter, J. R. Morgan, D. J. Singel, M. J. Cloninger, *Journal of the American Chemical Society* 2003, *125*, 8820.
[42] M. D. Disney, J. Zheng, T. M. Swager, P. H. Seeberger, *Journal of the American Chemical Society* 2004, *126*, 13343.
[43] J. G. Rudick, V. Percec, *Accounts of Chemical Research* 2008, *41*, 1641.
[44] W. J. Lees, A. Spaltenstein, J. E. Kingerywood, G. M. Whitesides, *Journal of Medicinal Chemistry* 1994, *37*, 3419.
[45] S. Yagai, A. Kitamura, *Chemical Society Reviews* 2008, *37*, 1520.
[46] O. Ikkala, G. ten Brinke, *Chemical Communications* 2004, 2131.
[47] P. R. Ashton, R. Ballardini, V. Balzani, S. E. Boyd, A. Credi, M. T. Gandolfi, M. GomezLopez, S. Iqbal, D. Philp, J. A. Preece, L. Prodi, H. G. Ricketts, J. F. Stoddart, M. S. Tolley, M. Venturi, A. J. P. White, D. J. Williams, *Chemistry-a European Journal* 1997, *3*, 152.
[48] M. Lazzari, C. Rodriguez-Abreu, J. Rivas, M. A. Lopez-Quintela, *Journal of Nanoscience and Nanotechnology* 2006, *6*, 892.
[49] W. H. Binder, R. Zirbs, in *Hydrogen Bonded Polymers, Vol. 207*, 2007, pp. 1.
[50] T. Rehm, C. Schmuck, *Chemical Communications* 2008, 801.
[51] P. Y. W. Dankers, E. W. Meijer, *Bulletin of the Chemical Society of Japan* 2007, *80*, 2047.
[52] L. Brunsveld, B. J. B. Folmer, E. W. Meijer, R. P. Sijbesma, *Chemical Reviews* 2001, *101*, 4071.
[53] M. Fujita, *Journal of Synthetic Organic Chemistry Japan* 1995, *53*, 432.
[54] J. M. Lehn, *Proceedings of the National Academy of Sciences of the United States of America* 2002, *99*, 4763.
[55] A. Scarso, J. J. Rebek, in *Supramolecular Chirality, Vol. 265*, 2006, pp. 1.
[56] F. H. Huang, H. W. Gibson, *Progress in Polymer Science* 2005, *30*, 982.
[57] A. Nelson, J. M. Belitsky, S. Vidal, C. S. Joiner, L. G. Baum, J. F. Stoddart, *Journal of the American Chemical Society* 2004, *126*, 11914.
[58] J. N. Lowe, D. A. Fulton, S. H. Chiu, A. M. Elizarov, S. J. Cantrill, S. J. Rowan, J. F. Stoddart, *Journal of Organic Chemistry* 2004, *69*, 4390.
[59] D. A. Fulton, S. J. Cantrill, J. F. Stoddart, *Journal of Organic Chemistry* 2002, *67*, 7968.
[60] R. Langer, J. P. Vacanti, *Science* 1993, *260*, 920.
[61] L. C. Palmer, S. I. Stupp, *Accounts of Chemical Research* 2008, *41*, 1674.
[62] K. Rajangam, M. S. Arnold, M. A. Rocco, S. I. Stupp, *Biomaterials* 2008, *29*, 3298.
[63] J. H. Ryu, E. Lee, Y. B. Lim, M. Lee, *Journal of the American Chemical Society* 2007, *129*, 4808.
[64] B. S. Kim, D. J. Hong, J. Bae, M. Lee, *Journal of the American Chemical Society* 2005, *127*, 16333.
[65] G. C. L. Wong, J. X. Tang, A. Lin, Y. L. Li, P. A. Janmey, C. R. Safinya, *Science* 2000, *288*, 2035.
[66] G. Thoma, A. G. Katopodis, N. Voelcker, R. O. Duthaler, M. B. Streiff, *Angewandte Chemie-International Edition* 2002, *41*, 3195.
[67] G. A. Silva, C. Czeisler, K. L. Niece, E. Beniash, D. A. Harrington, J. A. Kessler, S. I. Stupp, *Science* 2004, *303*, 1352.
[68] L. Brunsveld, H. Zhang, M. Glasbeek, J. Vekemans, E. W. Meijer, *Journal of the American Chemical Society* 2000, *122*, 6175.
[69] V. V. Rostovtsev, L. G. Green, V. V. Fokin, K. B. Sharpless, *Angewandte Chemie-International Edition* 2002, *41*, 2596.
[70] P. Wu, V. V. Fokin, *Aldrichimica Acta* 2007, *40*, 7.
[71] R. J. Pieters, D. T. S. Rijkers, R. M. J. Liskamp, *Qsar & Combinatorial Science* 2007, *26*, 1181.

[72] A. R. A. Palmans, J. Vekemans, H. Fischer, R. A. Hikmet, E. W. Meijer, *Chemistry-a European Journal* 1997, *3*, 300.
[73] C. R. Rice, S. Onions, N. Vidal, J. D. Wallis, M. C. Senna, M. Pilkington, H. Stoeckli-Evans, *European Journal of Inorganic Chemistry* 2002, 1985.
[74] L. Kaczinarek, P. Nantka-Namirski, *Acta Polon. Pharm.* 1979, *6*, 629.
[75] A. J. Pearson, P. R. Bruhn, *Journal of Organic Chemistry* 1991, *56*, 7092.
[76] R. J. Kaufman, R. S. Sidhu, *Journal of Organic Chemistry* 1982, *47*, 4941.
[77] W. D. Sharpless, P. Wu, T. V. Hansen, J. G. Lindberg, *Journal of Chemical Education* 2005, *82*, 1833.
[78] O. H. Laitinen, V. P. Hytonen, H. R. Nordlund, M. S. Kulomaa, *Cellular and Molecular Life Sciences* 2006, *63*, 2992.
[79] L. Brunsveld, B. G. G. Lohmeijer, J. Vekemans, E. W. Meijer, *Chemical Communications* 2000, 2305.
[80] S. Hong, P. R. Leroueil, I. J. Majoros, B. G. Orr, J. R. Baker, M. M. B. Holl, *Chemistry & Biology* 2007, *14*, 107.
[81] N. Smiljanic, V. Moreau, D. Yockot, J. M. Benito, J. M. G. Fernandez, F. Djedaini-Pilard, *Angewandte Chemie-International Edition* 2006, *45*, 5465.
[82] S. L. Harris, P. A. Spears, E. A. Havell, T. S. Hamrick, J. R. Horton, P. E. Orndorff, *Journal of Bacteriology* 2001, *183*, 4099.
[83] K. Landsteiner, *The specificity of serological reaction* 1962, Rev. ed. xviii+330p.
[84] J. P. McCoy, J. Varani, I. J. Goldstein, *Federation Proceedings* 1983, *42*, 933.
[85] E. Freire, O. L. Mayorga, M. Straume, *Analytical Chemistry* 1990, *62*, A950.
[86] R. L. Rich, D. G. Myszka, *Current Opinion in Biotechnology* 2000, *11*, 54.
[87] R. L. Rich, D. G. Myszka, *Journal of Molecular Recognition* 2000, *13*, 388.
[88] J. H. Naismith, C. Emmerich, J. Habash, S. J. Harrop, J. R. Helliwell, W. N. Hunter, J. Raftery, A. J. Kalb, J. Yariv, *Acta Crystallographica Section D-Biological Crystallography* 1994, *50*, 847.
[89] J. B. Corbell, J. J. Lundquist, E. J. Toone, *Tetrahedron-Asymmetry* 2000, *11*, 95.
[90] S. G. Gouin, E. Vanquelef, J. M. G. Fernaandez, C. O. Mellet, F. Y. Dupradeau, J. Kovensky, *Journal of Organic Chemistry* 2007, *72*, 9032.
[91] *for information on the beads see: http://www.neb.com/nebecomm/products/productS1420.asp*.
[92] D. M. Spencer, T. J. Wandless, S. L. Schreiber, G. R. Crabtree, *Science* 1993, *262*, 1019.
[93] P. J. Belshaw, D. M. Spencer, G. R. Crabtree, S. L. Schreiber, *Chemistry & Biology* 1996, *3*, 731.
[94] K. C. Nicolaou, F. Roschangar, D. Vourloumis, *Angewandte Chemie-International Edition* 1998, *37*, 2015.
[95] A. R. Minter, B. B. Brennan, A. K. Mapp, *Journal of the American Chemical Society* 2004, *126*, 10504.
[96] Y. Kwonj, H. D. Arndt, M. Qian, Y. Choi, Y. Kawazoe, P. B. Dervan, M. Uesugi, *Journal of the American Chemical Society* 2004, *126*, 15940.
[97] B. Liu, P. G. Alluri, P. Yu, T. Kodadek, *Journal of the American Chemical Society* 2005, *127*, 8254.
[98] M. Ueno, A. Murakami, K. Makino, T. Morii, *Journal of the American Chemical Society* 1993, *115*, 12575.
[99] M. E. Bush, N. D. Bouley, A. R. Urbach, *Journal of the American Chemical Society* 2005, *127*, 14511.
[100] T. Nguyen, N. S. Joshi, M. B. Francis, *Bioconjugate Chemistry* 2006, *17*, 869.
[101] C. Renner, J. Piehler, T. Schrader, *Journal of the American Chemical Society* 2006, *128*, 620.
[102] L. Zhang, Y. W. Wu, L. Brunsveld, *Angewandte Chemie-International Edition* 2007, *46*, 1798.
[103] C. A. Royer, S. F. Scarlata, in *Fluorescence Spectroscopy, Vol. 450*, Elsevier Academic Press Inc, San Diego, 2008, pp. 79.
[104] R. Y. Tsien, *Annual Review of Biochemistry* 1998, *67*, 509.
[105] M. Howarth, D. J. F. Chinnapen, K. Gerrow, P. C. Dorrestein, M. R. Grandy, N. L. Kelleher, A. El-Husseini, A. Y. Ting, *Nature Methods* 2006, *3*, 267.

[106] J. E. Berlier, A. Rothe, G. Buller, J. Bradford, D. R. Gray, B. J. Filanoski, W. G. Telford, S. Yue, J. X. Liu, C. Y. Cheung, W. Chang, J. D. Hirsch, J. M. Beechem, R. P. Haugland, *Journal of Histochemistry & Cytochemistry* 2003, *51*, 1699.
[107] http://www.invitrogen.com/site/us/en/home/support/Research-Tools/Fluorescence-SpectraViewer.html
[108] http://www.invitrogen.com/site/us/en/home/support/Research-Tools/Fluorescence-SpectraViewer.html
[109] J. A. Marshall, J. D. Trometer, B. E. Blough, T. D. Crute, *Journal of Organic Chemistry* -1988, *53*, 4274.

Zusammenfassung

der Dissertation von

Marion K. Müller

aus Mainz

Supramolekulare Multivalenz

Diskotische Monomere assemblieren schon bei geringen Konzentrationen in Wasser reversibel zu säulenartigen Polymeren. Mit den entprechenden Liganden ausgestattet, können diese Supramoleküle gezielt Kohlenhydrat-Rezeptor-Wechselwirkungen beeinflussen und Proteine spezifisch binden. Die Ligandendichte des Polymers kann dabei durch den reversiblen Austausch einzelner Monomere gesteuert werden. Dieses supramolekulare Polymer bindet an Bakterien und dient als Plattform zur Steuerung von Protein-Aggregationen.

Die discotischen Moleküle **1** wurden durch Verlinkung von drei *N*-monoacylierten 2,2'-Bipyridin-3,3'-diamin-Flügeln zu einer zentralen 1,3,5-Benzoltricarbonyl-Einheit aufgebaut. Durch selektiv eingeführte Azid- oder Amin-Funktionalitäten dienten die diskotischen Grundgerüste **2** und **3** als flexible Plattform zur Modifikation mit biologisch aktiven Liganden im letzten Schritt der Synthese. Der konvergente Aufbau der Monomere führte zu diskotischen Molekülen, die je mit sechs inerten Ethylenglycol-Monomethylether-Seitenketten und mit drei Azid- oder Amin-funktionalisierten Seitenketten ausgestattet waren (Abb. 1).

Des Weiteren wurden die diskotischen Monomere **2** und **3** mit unterschiedlichen Liganden dekoriert. Propargyl-Derivate von Mannose, Glucose und Gallactose wurden mittels Huisgen-[2+3]-Zykloaddition an das diskotische Grundgerüst **2** angebracht. Die Zykloaddition beanspruchte ungewöhnlich lange Reaktionszeiten, was durch die hohe Ligandendichte, die sich um die supramolekularen Säulen generierte, erklärt wurde. Nach vier Wochen ermöglichte der dynamische, reversible Austausch der Monomere die volle Umsetzung zum trifunktionalisierten diskotischen Molekül. Die

Acylierung des Grundgerüsts **3** mit Texas Red-, Biotin- und Cystein-Derivaten benötigte Reaktionszeiten zwischen vier Stunden und drei Tagen. Alle diskotischen Verbindungen sind gut in Wasser löslich und bilden supramolekulare Säulen (K_{ass} ~ 1 x 10^8 M^{-1}).

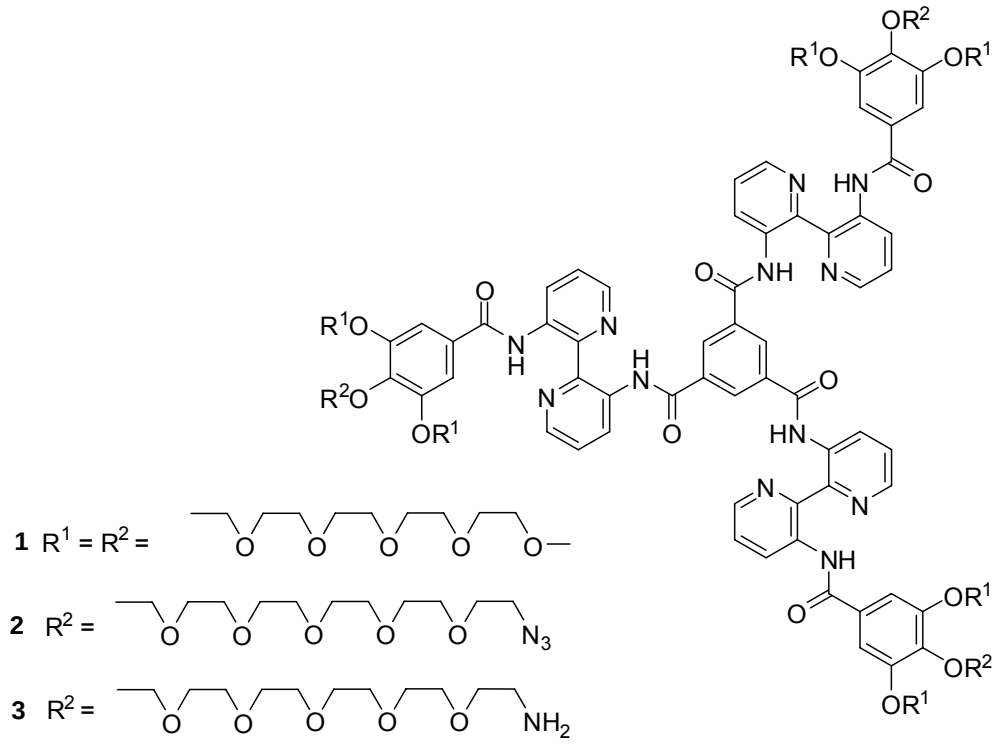

Abb. 1.: Die diskotischen Grundgerüste **2** und **3**, ausgestattet mit funktionellen Gruppen für weitere synthetische Modifikationen.

Die Eigenschaft der Mannose-modifizierten Diskoten, der inerten Diskoten **1** und Mischungen beider an Bakterien zu binden, wurde durch mikroskopische Studien mit dem *E. coli* BL 21α Stamm verifiziert. Hierbei wurde die starke Fluoreszenz des diskotischen Kerns zur Autodetektion der Supramoleküle genutzt. Nur wenn die Bakterien mit dem Mannose-modifizierten Diskoten inkubiert wurden, konnte eine starke Fluoreszenz der Bakterien-Aggregate detektiert werden, die mit dem Durchlichtbild kolokalisierte (Abb. 2). Beide Kontrollexperimente, Bakterien ohne Substrat und in Anwesenheit des inerten Diskoten, zeigten keinerlei Fluoreszenz. Die Spezifität der Interaktion zwischen dem Mannose-modifizierten Diskoten und dem FimH-Rezeptor auf der Bakterienoberfläche wurde durch Bindungsstudien mit den Bakterienstämmen ORN208 und ORN178 bestätigt. Die Experimente ergaben, dass die

supramolekularen Diskoten selektiv über die Interaktion von Mannose an den FimH-Rezeptoren binden und zeigen, dass keine unspezifische Wechselwirkung vorliegt. Die Durchführung eines Konkurrenz Experiments zwischen dem Mannose-modifizierten Diskoten und Mannose bezüglich ihrer Bindungsstärke zu den Bakterien zeigte, dass die multivalenten Diskoten hocheffizient an Bakterien binden. Selbst bei einem 10^6-fachen Überschuss, wurden die Diskoten nicht von der freien Mannose verdrängt.

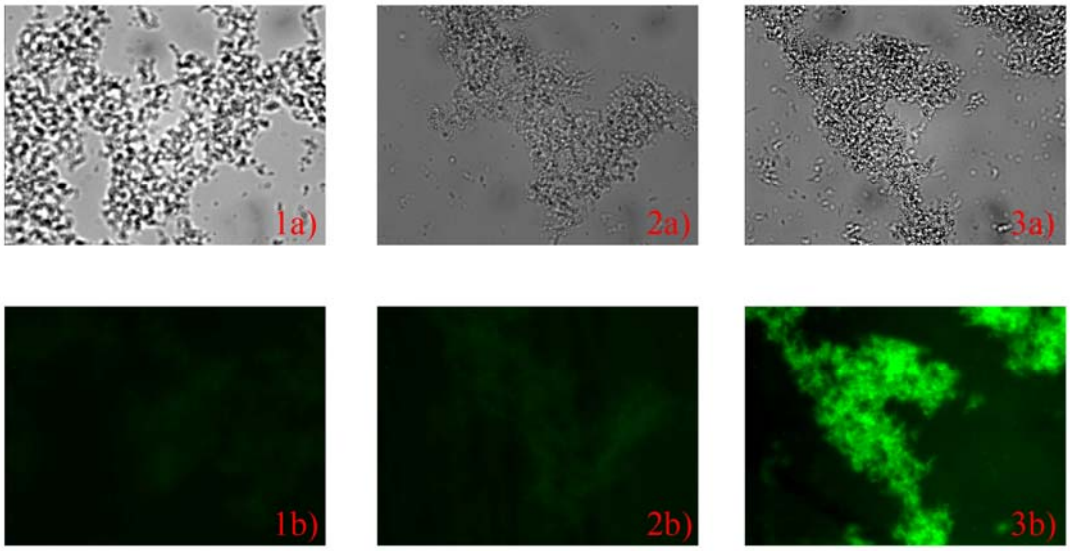

Abb. 2.: Mikroskopbilder im a) Durchlicht und b) Fluoreszenz (λ_{ex} = 360 nm, λ_{em} = 490 nm) Modus von *E. coli*, die mit 1) Wasser, 2) inertem Diskoten **1** oder 3) Mannose-modifiziertem Diskoten inkubiert wurden. Nur in Anwesenheit des Mannose-modifizierten Diskoten wurde die starke Fluoreszenz des diskotischen Grundgerüsts auf den Bakterien detektiert.

Mischungen der Supramoleküle aus den Mannose-modifizierten Diskoten und den inerten Diskoten **1** wurden generiert und auf verdünnten Bakterienproben evaluiert. Alle getesteten supramolekularen Mischungen induzierten Aggregation der Bakterien. Selbst eine Verdünnung mit nur 1% funktionellem Monomer führte noch zur Ausbildung bakterieller Aggregate. Offensichtlich wird nur eine begrenzte Anzahl an Mannose Einheiten auf der Oberfläche der supramolekularen Säulen benötigt, um die Cluster-Bildung der Bakterien um die Säule herum hervorzurufen. Des Weiteren scheinen die supramolekularen Strukturen groß genug zu sein, um die Distanzen zwischen den Mannose fuktionalisierten Monomeren zu überbrücken und die Bakterien zu verlinken. Die supramolekularen Eigenschaften des Moleküls ermöglichen offensichtlich

eine unkomplizierte Adaption und Optimierung der Zusammensetzung aus Monomeren.

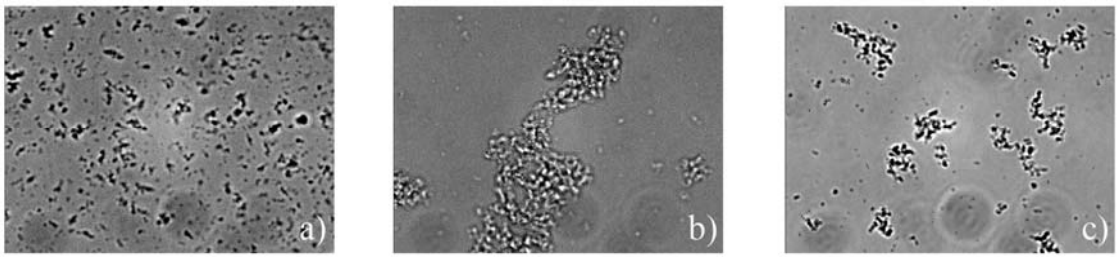

Abb. 3.: Mikroskopbilder zur Veranschaulichung der Bakterienaggregation in Anwesenheit des Mannose-modifizierten Diskoten und Mischungen des Mannose-modifizierten Diskoten mit dem inerten Diskoten **1**. Die Bilder wurden im Durchlicht Modus mit verdünnten Bakterienproben, die mit a) 100% inerten-Diskoten **1**, b) 99/1 inerten Diskoten **1/**Mannose-modifizierten Diskoten and c) 100% Mannose-modifizierten Diskoten inkubiert worden waren, aufgenommen.

Um die polyvalenten Eigenschaften der supramolekularen Polymere zu quantifizieren wurden Enzym-gekoppelte Lektin Studien (enzyme linked lectin assay, ELLA) mit Hilfe von Meerrettich-Peroxidase-markiertem Concanavalin A und immobilisiertem Mannan durchgeführt. In unseren Studien wurde ein IC_{50}-Wert für die Methylglykosid Kontrolle um 3000 µM erhalten. Der IC_{50}-Wert der Mannose-modifizierten Diskoten lag bei 120 µM (360 µM, valenzkorrigiert). Die relative valenzkorrigierte Bindungstärke des Mannose-modifizierten Diskoten war damit 8.3 fach höher als die der Referenzverbindung (dies entspricht einer 24.9 fachen Erhöhung pro Mannose-Diskot) und unterstreicht die polyvalente Bindungsstärke der Diskoten. Die Mannose-modifizierten, supramolekularen Dikoten ermöglichen effiziente, polyvalente Bindungen mit hohen Valenzen und entwickeln ein starkes Bindungspotential pro Mannoseligand. Aufgrund seiner polymeren Eigenschaften, ist der Mannose-modifizierte Diskot scheinbar in der Lage, die Distanz zwischen den verschiedenen Bindungsstellen des Concanavalin A zu überbrücken und multivalent zu binden.

Mischungen des Texas-Red-modifizierten Diskoten und des Biotin-modifizierten Diskoten wurden eingesetzt, um Zugang zu heterovalenten Verbindungen, die mehr als eine Art Ligand tragen, zu erhalten. Die

Evaluierung dieser diskotischen Mischungen zeigte, dass Texas-Red-modifizierte-Diskoten in Anwesenheit von Biotin-modifizierten Diskoten auf der Oberfläche von Straptavidin-beschichteten Kugeln lokalisiert werden können. Offensichtlich integrieren die Biotin-modifizierten Diskoten die Texas-Red-modifizierten Diskoten in ihre Säulen und halten so die Texas-Red-modifizierten Diskoten in der supramolekularen Struktur, wenn Biotin an Streptavidin bindet. Diese Resultate zeigen, dass die supramolekularen Diskoten einen unkomplizierten Zugang zu heterovalenten Grundgerüsten durch einfaches Mischen von fuktionalisierten Diskoten ermöglichen. Dieser supramolekulare Ansatz erlaubt den Aufbau hochflexibler, heterovalenter Substanzen.

Zusätzlich zu Ihrer Fähigkeit multivalente Interaktionen mit bakteriellen Aggregaten zu kontrollieren, wurden die Diskoten als Plattform für Protein-Zusammenlagerungen verwendet. Biotin-modifizierte Diskoten wurden eingesetzt, um die Interaktion des diskotischen Grundgerüsts mit Streptavidin zu evaluieren. FRET-Experimente mit Cy3-markiertem Streptavidin (SA-Cy3) wurden duchgeführt. Hierbei führte die Überlappung des Fluoreszenzsignals des diskotischen Grundgerüsts (FRET-Donor) mit Cy3 (FRET-Akzeptor) zu der FRET-Interaktion. Der Vergleich des FRET-Signals in Gegenwart des Biotin-modifizierten Diskoten mit dem FRET-Signal in Gegenwart des inerten Diskoten zeigte, dass das FRET-Signal aus der räumlichen Annäherung der fluoreszierenden Partner durch Bindung von Biotin an Straptavidin hervorgerufen wird. Experimente mit Mischungen des inerten Diskoten und des Biotin-modifizierten Diskoten ergaben, dass in Anwesenheit des inerten Diskoten als Platzhalter die relative Menge an Streptavidin Cy3, das mit den Supramolekülen agiert von 7.5 mol-% auf 15 mol-% angehoben wird (Abb. 4). Der inerte Diskot schafft somit Raum zwischen den funktionalisierten Diskoten und ermöglicht es, einem größeren prozentualen Anteil an Biotinen an Straptavidin zu binden. Das beste Mischungsverhältniss an inerten Diskoten zu Biotin-modifizierten Diskoten für optimalen FRET-Austausch scheint bei etwa einer bis zwei inerten Diskoten pro Biotin-modifiziertem Diskot zu liegen. In weiteren Studien wurde untersucht, ob die Reihenfolge der Zugabe der Interaktionspartner einen Einfluss auf den Aufbau der Säulen hat. Hierbei

zeigte sich, dass supramolekulare Säulen aus Biotin-modifizierten Diskoten, die mit SA-Cy3 inkubiert wurden, nachträglich keine inerten Diskoten mehr in die supramolekularen Säulen aufnehmen. Scheinbar werden die Supramoleküle aus Biotin-modifizierten Diskoten durch die Bindung an Streptavidin blockiert und ergeben undynamische polymere Strukturen, die das Protein auf der Oberfläche tragen.

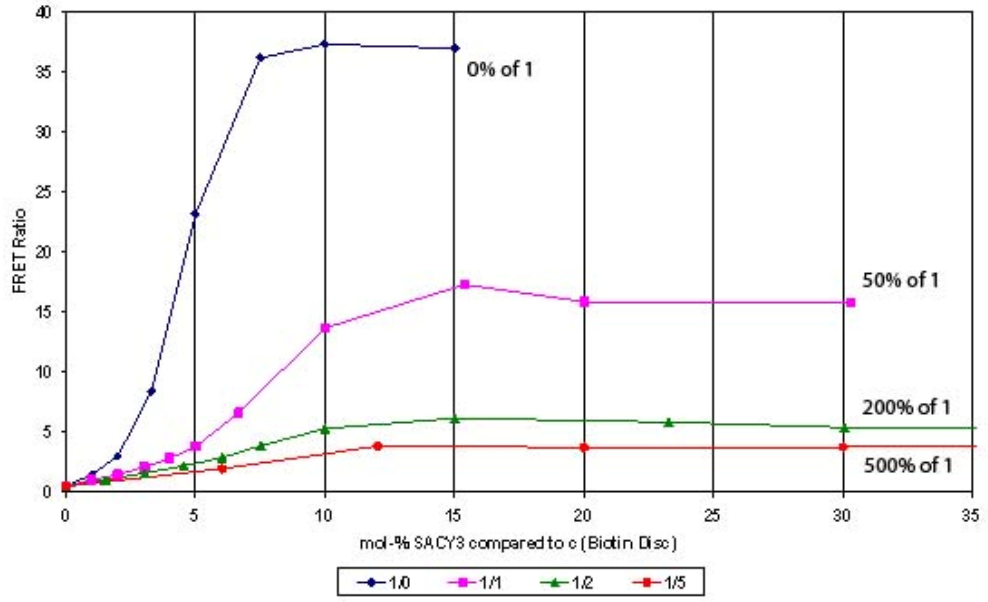

Abb. 4.: Experimente zur Protein-Aggregation mit Streptavidin-Cy3 (SA-Cy3) und Mischungen aus Biotin-modifizierte Diskoten und inerten Diskoten. FRET-Interaktion des diskotischen Grundgerüsts mit Cy3 wurde detektiert. Das FRET-Verhältnis von verschiedenen Mischungen von Biotin-modifizierten Diskoten/inerten Diskoten bei 1/0 (blau), 1/1 (lila), 1/2 (grün) und 1/5 (rot) aufgetragen gegen c[SA-Cy3] im Vergleich zu c[disc total] (= c[**53**] + c[**53**]). Der Graf zeigt, dass die prozentuale Menge an SA-Cy3, das mit den diskotischen Säulen interagiert, im Fall von 1/1- und 1/2-Mischungen am höchsten ist.

Dasselbe supramolekulare Polymer wurde verwendet, um die Zusammenlagerung zweier unterschiedlicher Proteine zu untersuchen. Diese Experimente zur supramolekularen Steuerung von Protein-Interaktionen wurden mit Alexa-Fluor-633-markiertem Streptavidin (SA-AF633) und mit Texas-Red-markiertem Streptavidin (SA-TR) durchgeführt Dabei wurde die Überlappung des Fluoreszenzsignals von TR und AF633 genutzt. Die Ergebnisse zeigen, dass der Biotin-modifizierte Diskot beide Proteine bindet und die Zusammenlagerung der beiden Streptavidine von SA-AF633 und SA-

TR bewirkt. Dies kann durch die resultierende FRET-Interaktion belegt werden. Diese Experimente mit SA-TR/SA-AF633 und Studien mit einem weiteren FRET-Paar SA-AF514/SA-TR zeigen, dass die Anwesenheit des Biotin-modifizierten Diskoten die Zusammenlagerung von zwei verschiedenen Proteinen auslöst.

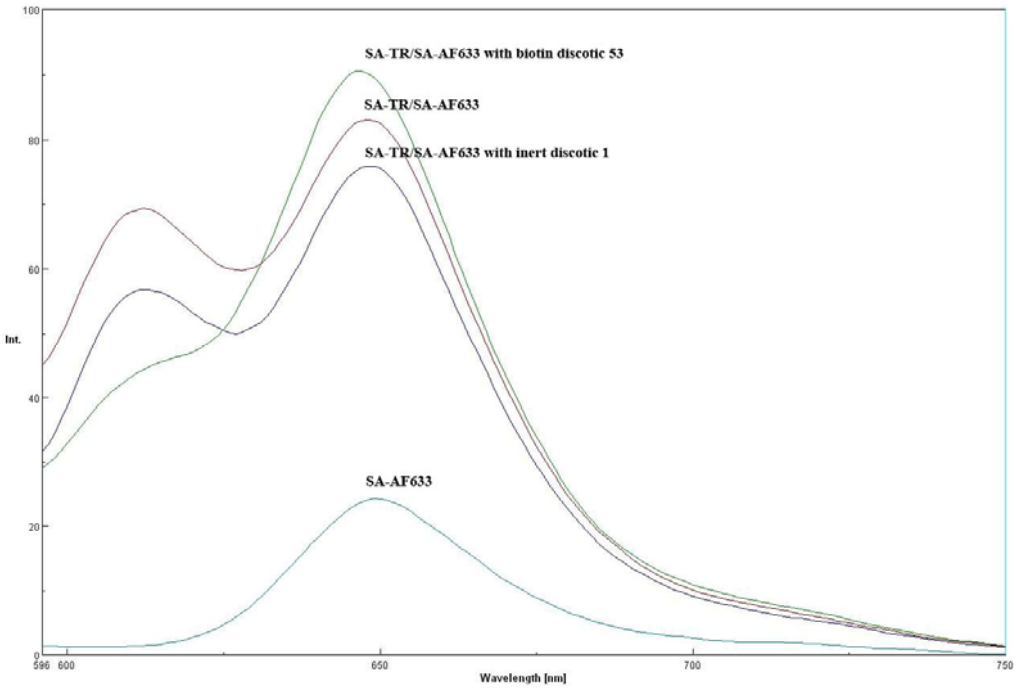

Abb. 5.: Studien zur Beeinflussung von Protein-Aggregation durch den Biotin-modifizierten Diskoten. Der Graph zeigt die Experimente in Anwesenheit des Biotin-modifizierten Diskoten (grün), mit dem inerten Diskoten (blau), mit dem reinen Proteingemisch SA-TR/SA-AF633 (lila) und mit dem reinen FRET Akzeptor SA-AF633 (hellblau). Die Spektren wurden bei einer Anregungswellenlänge von 584 nm aufgenommen. Nur in Gegenwart der Biotin-modifizierten Diskoten geht das Emissionssignal des FRET-Donors SA-TR signifikant zurück. Offensichtlich lagern sich die Proteine auf der Oberfläche der Supramoleküle aus Biotin-modifizierten Diskoten zusammen.

Supramolekulare Polymere stellen ideale Grundgerüste zur Generierung polyvalenter Strukturen dar, die zur Bindung und Modulierung biologischer Interaktionen genuzt werden können. Die Eigenschaft der Monomere durch eigenständige Aggregation reversible, supramolekulare Polymere zu bilden, ermöglicht es, Kontrolle über die Ligandendichte, die Reaktion auf äußere Einflüsse und den polymeren Aufbau zu erhalten. Dies ist mit kovalenten polymeren Systemen nicht möglich. Die Flexibilität trägt dazu bei, dass

supramolekulare Polymere ein hohes Potential als polyvalente Grundgerüste zur Beeinflussung unterschiedlicher biologischer Wechselwirkungen besitzen, in denen polyvalente Effekte eine Rolle spielen. Die Eigenschaft der selbst-Aggregation zu polymeren Säulen ermöglicht die reversible Ausstattung mit Liganden und die dynamische Anpassung des Systems an den Interaktionspartner. Nicht zuletzt erlaubt es die supramolekulare Natur des Systems, bislang noch nicht zugängliche Topologien mit neuen Eigenschaften zu generieren. Dies kann durch einfaches Mischen unterschiedlich funktionalisierter diskotischer Monomere erreicht werden und ermöglicht es, Bindungsvorgänge zu optimieren.

Danksagungen

Zunächst gilt mein größter Dank Herrn Prof. Dr. Luc Brunsveld für die interessante, innovative Themenstellung und die hervorragende Betreuung und Unterstützung während meiner Promotion. Es war eine inspirierende und lehrreiche Zeit für mich, die ich immer in guter Erinnerung behalten werde.
Herrn Prof. Dr. Herbert Waldmann danke ich herzlich für die Bereitstellung hervorragender Arbeitsbedingungen.
Ein herzlicher Dank gilt allen Mitarbeitern am Max-Planck-Institut für Molekulare Physiologie, dem Chemical Genomics Center, der Technischen Universität Dortmund und der Technischen Universität Eindhoven, die zum Gelingen dieser Arbeit beigetragen haben. Hervorzuheben sind hier Andreas Rumpf für die synthetische Unterstützung während seiner Ausbildung zum Chemielaboranten, Bernhard Ellinger, Sascha Menninger, Dr. Maelle Carraz und Sabine Möcklinghoff für die Einweisung in biologische Methoden, Dr. Dorothee Wasserberg für die Unterstützung bei der Durchführung der spektrometrischen Experimente, Dr. Petra Janning und Joost van Dongen für Hilfe in allen analytischen Fragestellungen, Stefan Wetzel für die Geduld bei der Lösung computerbezogener Probleme und Nicola Bisek als Anlaufstelle für alle fachbezogenen wie fachfremden Fragestellungen.
Allen Mitarbeitern in der Abteilung Chemische Biologie am Max-Planck-Institut Dortmund und der gesamten Arbeitsgruppe Brunsveld möchte ich für die freundschaftlich-kollegiale Arbeitsatmosphäre danken. Dieser Dank gilt ganz besonders meinen Laborkolleg(inn)en Dana Uhlenheuer, Dr. Belen Vaz Araujo und Andreas Rumpf, die mir viele heitere Stunden in wissenschaftlicher Atmosphäre bereitet haben. Außerdem danke ich meinen Bürokolleg(inn)en Sebastian Koch, Sebastian Schoof, Katrin Wittstein, Jinyong Lu, Torben Lessmann und Tobias Voigt für anregende Diskussionen in eingeschränkter Räumlichkeit.
Für das zügige Korrigieren des Manuskripts danke ich meinen Korrekturlesern Dr. Robin Bon, Wolfram Wilk, Tanja Knoth, Sebastian Koch, Dana Uhlenheuer, Katja Petkau und Prof. Dr. Rolf Breinbauer.

Ein besonders großes Dankeschön gilt Tanja Knoth für die Aufrechterhaltung meines seelischen und physischen Gleichgewichts und die andauernde Unterstützung während der gesamten Zeit meiner Promotion.
Besonders waren mir Tanja Knoth, Sebastian Koch, Wolfram Wilk, Robin Bon, Maelle Carraz, Jerome Clerc, Rolf Breinbauer, Esther und Belen Vaz Araujo und Üffes wichtige Freunde, denen ich für bleibende Erinnerungen an gemeinsame Unternehmungen, Kletter-, Kicker- und Spiele-Abende in Dortmund dankbar bin.
Schließlich danke ich ganz besonders meinen Eltern, meinen Geschwistern Martin und Mareike so wie Nuria für die liebevolle Unterstützung während all der Jahre der Promotion und des Studiums.

Eidesstattliche Erklärung

Hiermit erkläre ich an Eides statt, dass ich diese Arbeit selbständig und nur mit den angegebenen Hilfsmitteln angefertigt habe.

Dortmund, April 2009